To the Graduate Council:

I am submitting herewith a dissertation written by Frank Holger Försterling entitled " Synthesis and Fluxional Behavior of Mixed Metal Trinuclear Cluster Complexes of the Cobalt Group Containing Carbene, Carbyne or Alkyne Ligands." I have examined the final copy of this dissertation for form and content and recommend that it be accepted in partial fulfillment of the requirements for the degree of Doctor of Philosophy, with a major in Chemistry.

Craig E Barnes

Craig E. Barnes, Major Professor

We have read this dissertation
and recommend its acceptance:

James L. Adcock

K S Dae

Ergin Sorgunu

Accepted for the Council:

Carl Minkel

Associate Vice Chancellor and
Dean of The Graduate School

Synthesis and Fluxional Behavior of Mixed Metal Trinuclear Clusters of the Cobalt Group Containing Carbene, Carbyne and Alkyne Ligands

A Dissertation

Presented for the

Doctor of Philosophy Degree

The University of Tennessee, Knoxville

Frank Holger Försterling

August 1996

DEDICATION

This dissertation is dedicated to my parents, Ingeborg and Horst-Dieter Försterling. Without their financial and continued moral support this work would have been impossible. I will be forever in their debt.

ACKNOWLEDGMENTS

There is a number of individuals who have contributed to the success of this work. First of all, I would like to express my thanks to my advisor Dr. Craig Barnes. His enthusiasm for research is exceptional. He was very motivating and inspiring throughout my research and taught me a lot about conducting high quality research. His advice and friendship were and always will be of great value for me. I would also like to thank Dr. James Adcock, Dr. Engin Serpersu and Dr. Ziling Xue for serving on my Ph.D. committee and for many helpful discussions. Further thanks go to all my previous teachers of chemistry, especially to Prof. Stefan Berger, who introduced me to the exiting field of NMR spectroscopy.

My work was also made enjoyable by the good comradeship within our group. In particular with my labmates and friends Stephanie Vierkötter, Bill King and Michael Player I did not only share many late hours in lab and underwent many enlightening discussions about our research. We also spent numerous memorable hours, whether it was barbecuing or hiking in the mountains. I would also like to thank all other former and current members of the Barnes group, Jane Doll, Martina Ralle, Suree Sangkerdsub and Yongsoon Shin. I will miss you all.

The help of the support staff in the Chemistry Department has been essential for the success of this thesis. In particular I would like to thank Bill

Gurley from the electronic shop for numerous repairs performed on the departemental NMR spectrometers, without which this thesis would have been impossible. Whenever the instrument broke down we knew we could rely on his skills to get it back up, and over and over he proved as a miraclemaker. Further thanks go to the members of the glassblowing shop, Elder Mellon and Arthur Pratt. They have been very helpful, and I have learned to appreciate their skills. Also thanks to the members of the mass spectrometry lab, Al Tuinman and Martin Haddix, for the measurement of numerous mass spectra.

Finally, I would like to thank my friends Andreas Boller, Stefan Kreitmeier, Reinhard Festag, Peter Sajonz, Marek Galecki, Slawomir Kolodynski, Jennifer Murray, Susan Nadig, Ludger Wirtz, Jens Pannekamp, Peter Ferdus and everybody whom I might have forgotten to mention. Whether we were exploring the backcountry of the Appalachians, playing volleyball or hanging out at Sam and Andy's, you made my time here in Knoxville an enjoyable one.

ABSTRACT

The addition of diazoalkanes and alkynes to a series of unsaturated heteronuclear metal cluster complexes of the general formula L-M$(CpCo)_2(\mu_3$-$CO)_2$ has been described. One focus of the investigation was to study the kinetics and thermodynamics of ligand reorientation about the metal triangle. The nature of the metal fragment L-M was found to influence both the rate of reorientation as well as the preference for a certain positional isomer. The differences in energy for different orientations of the ligand with respect to the different metal-metal edges were found to be relatively small, and in many cases two or more isomers with ligands bridging different edges were observed in equilibrium with each other.

Reaction of the trinuclear complexes diazoalkanes can result in two types of adduct, one containing a carbene and one with a hydrazone ligand. The carbene ligands are mobile about the different edges of the metal triangle. In the Cp^*Rh complex **7**, an intermediate involving a triply bridging carbene ligand was observed for this process, a coordination mode which was not known for carbene ligands so far. In the case of the Cp^*Ir complex **8** refluxing in toluene resulted in loss of a CO ligand resulting in the carbyne hydride complex **18**. The hydride ligand exchanges with the hydrogen of the carbyne ligand at a rate observable by magnetization transfer techniques. The addition of alkynes R-C≡C-R′ to the unsaturated complexes L-M$(CpCo)_2(\mu_3$-$CO)_2$ results in the formation of the alkyne

adducts L-M$(CpCo)_2(\mu_3\text{-}CO)(\eta^2,\mu_2\text{-}R\text{-}C{\equiv}C\text{-}R')$ (R = R′ = H, Tol, Ph; R = Tol, R′ = H). In all complexes, the alkyne coordinates in a μ_3-$\parallel$ fashion with the C≡C bond parallel to a metal edge. Fast interconversion of the different positional isomers takes place at room temperature, but at -100 °C the rate of interchange is frozen out on the NMR time scale. In addition, the rotation of the tolyl substituents of the alkynes is locked at low temperature due to steric interaction with the Cp^* and Cp ligands.

Furthermore, ^{13}C NMR relaxation times were used to study the rotational reorientation of phenyl substituents in several single and linked bis-carbyne cluster complexes of the general form $(CpCo)_3(\mu_3\text{-}CR)_2$. The rate of phenyl group rotation was found to be determined predominantly by steric interaction with the Cp ligands of the $(CpCo)_3$ units.

TABLE OF CONTENTS

CHAPTER 1: Introduction ..... - 1 -

References : ..... - 12 -

CHAPTER 2: Reactions of Trinuclear Cluster Complexes with Diazoalkanes: Carbene and Carbyne Ligands in Trinuclear Cluster Complexes of the Cobalt Group ..... - 13 -

2.1. Introduction ..... - 13 -

2.2. Reaction of the All-CpCo cluster $(CpCo)_3(\mu_3\text{-}CO)_2$ (5) with Diazomethane ..... - 19 -

2.2.1. Carbene Adduct $(CpCo)_3(\mu_2\text{-}CO)_2(\mu_2\text{-}CH_2)$ (6) ..... - 19 -

2.2.1.1. Crystal Structure ..... - 19 -

2.2.1.2. Spectroscopic Data of Carbene Adduct 6 ..... - 22 -

2.2.2. Diazomethane Adduct $(CpCo)_3(\mu_3\text{-}CO)(\mu_3\text{-}NNCH_2)$ (9) . - 24 -

2.2.2.1. Crystal Structure ..... - 24 -

2.2.2.2. Spectroscopic Data ..... - 27 -

2.3. Reaction of the Heteronuclear Complexes $Cp^*M(CpCo)_2(\mu_3\text{-}CO)_2$ and $Cp^{\ddagger}Co(CpCo)_2(\mu_3\text{-}CO)_2$ with Diazomethane ..... - 32 -

2.3.1. Crystal Structure of $Cp^*Rh(CpCo)_2(\mu\text{-}CO)_2(\mu\text{-}CH_2)$ .... - 33 -

2.3.2. Spectroscopic Data ..... - 35 -

2.4. Reaction with Diazoethane ..... - 41 -

2.5. Carbene Mobility on the Cluster Surface ..... - 43 -

2.5.1. Rh-Co to Co-Co edge Isomerization in

$Cp^*Rh(CpCo)_2(\mu_2\text{-}CO)(CH_2)$ ..... - 44 -

2.5.2. Carbene Exchange Between Rh-Co Edges ..... - 49 -

2.5.3. The Nature of the Intermediate **7c** ..... - 57 -

2.6. Formation of a Carbyne Hydride Complex ..... - 68 -

2.6.1. General Scheme : ..... - 68 -

2.6.2. Crystal Structure of $Ir^*Co_2(CH)(\mu\text{-}H)$ (18) ..... - 69 -

2.6.3. Spectroscopic Properties of $Cp^*Ir(CpCo)_2(CH)(H)$: ... - 74 -

2.6.4. Hydride Mobility About Metal Triangle ..... - 76 -

2.6.5. Carbyne-Hydride Exchange ..... - 78 -

2.6.6. Mechanism of Carbyne Hydride Fluxionality ..... - 84 -

2.6.7. Reactivity Towards Donor Ligands ..... - 86 -

2.6.8 CpCo and Cp^*Rh Analogues ..... - 90 -

2.7. Summarizing Discussion about Carbene Chemistry ..... - 91 -

2.8 References ..... - 96 -

CHAPTER 3: Alkyne Adducts of Mixed Metal Trinuclear Clusters of the Cobalt Group: Synthesis and Fluxional Behavior ..... - 101 -

3.1. Introduction ..... - 101 -

3.2. Acetylene Adducts ..... - 106 -

3.2.1. Crystal Structure . . . . . - 106 -

3.2.2. IR and MS Data . . . . . - 112 -

3.2.3. Variable Temperature NMR Spectroscopy and

Fluxional Behavior of $Cp^*Ir(CpCo)_2(CO)(HC{\equiv}CH)$ . . - 113 -

3.2.3.1. General . . . . . - 113 -

3.2.3.2. Lineshape Analysis . . . . . - 118 -

3.2.4. NMR Spectra of $Cp^*Rh(CpCo)_2(\mu_3\text{-}CO)(HC{\equiv}CH)$ (20) - 123 -

3.2.5. $Cp^*Co(CpCo)_2(CO)(HC{\equiv}CH)$ (21) and Trends . . . . . - 127 -

3.2.6. Dinuclear Side Product Obtained from

$Cp^*Ir(CpCo)_2(CO)_2$ + $HC{\equiv}CH$ . . . . . - 127 -

3.3. Phenyl- and Tolylacetylene Adducts . . . . . - 130 -

3.3.1. Crystal Structure . . . . . - 131 -

3.3.2. Variable Temperature NMR Spectra of

$Cp^*Ir(CpCo)_2(CO)$(Tol-C≡C-H) . . . . . - 136 -

3.3.3. Cp^*Rh- and Cp^*Co Containing Complexes 24, 25 and

26 . . . . . - 146 -

3.3.4. $Cp^{\ddagger}Co(CpCo)_2(CO)$(Tol-C≡CH) (27) and

$(CpCo)_3(CO)$(Ph-C≡CH) (28) . . . . . - 151 -

3.3.5. Hindered Phenyl Ring Rotation: Evidence for

Correlated Motion: . . . . . - 154 -

3.4. Diphenyl- and Bistolylacetylene Adducts . . . . . - 162 -

3.4.1. General. . . . . - 162 -

3.4.2. Low Temperature Structure . . . . . - 165 -

3.5. Discussion of Thermodynamics and Kinetics of Alkyne Rotation - 168 -

3.6. Scission Reactions . . . . . - 175 -

3.7. Summary . . . . . - 178 -

3.8. References: . . . . . - 180 -

CHAPTER 4: Diffusional and Internal Rotation in Single and Linked Trinuclear Bis-carbyne Cluster Complexes Determined by Carbon-13 NMR Relaxation Times . . . . . - 183 -

4.1. Introduction . . . . . - 183 -

4.2. Experimental . . . . . - 187 -

4.3. Determination of Diffusion Coefficients . . . . . - 188 -

4.3.1. Phenyl Ring Rotation . . . . . - 190 -

4.3.2. Cp Ring Rotation . . . . . - 192 -

4.4. Results and Discussion . . . . . - 193 -

4.4.1. Direct Evaluation of T_1 Values . . . . . - 194 -

4.4.2. Hydrodynamic Models . . . . . - 202 -

4.4.3. Steric versus Electronic Interactions . . . . . - 207 -

4.5. Conclusions . . . . . - 211 -

4.6. References . . . . . - 212 -

CHAPTER 5: Addition of Oxygen to Mixed Metal Trinuclear Cluster Complexes: Formation of Oxo Adducts ..... - 215 -

5.1 Introduction ..... - 215 -

5.2 Formation of oxo adducts ..... - 217 -

5.3. Spectroscopic Data ..... - 218 -

5.4. Crystal Structure ..... - 220 -

5.5. Summary ..... - 223 -

5.6. References ..... - 223 -

CHAPTER 6: Summary ..... - 224 -

CHAPTER 7: Experimental Part ..... - 228 -

7.1. Spectroscopic and Analytical Methods ..... - 228 -

7.2. Lineshape Analysis ..... - 230 -

7.3. General Techniques ..... - 230 -

7.4. Literature Procedures ..... - 231 -

6.5. Diazomethane ..... - 232 -

7.6. Diazoethane ..... - 233 -

7.7. Mono- and Dinuclear Precursors ..... - 234 -

7.7.1. Cobalt(II)-hexamine Chloride $[Co(NH_3)_6]Cl_2$ ..... - 234 -

7.7.2. Cobaltocene ..... - 234 -

7.7.3. Cyclopentadienyl-cobalt(I)-bis-ethylene, $CpCo(C_2H_4)_2$. - 235 -

7.7.4. Bis(pentamethylcyclopentadienyl-rhodium(III)-dichloride, $(Cp^*RhCl)_2Cl_2$ . . . . . - 235 -

7.7.5. Bis(pentamethylcyclopentadienyl-iridium(III)-dichloride, $(Cp^*IrCl)_2Cl_2$ . . . . . - 236 -

7.7.6. Activated Zinc . . . . . - 237 -

7.7.7. Pentamethylcyclopentadienyl-rhodium(I)-dicarbonyl, $Cp^*Rh(CO)_2$ . . . . . - 237 -

7.7.8. Pentamethylcyclopentadienyl-iridium(I)-dicarbonyl, $Cp^*Rh(CO)_2$, Method 1 . . . . . - 238 -

7.7.9. Pentamethylcyclopentadienyl-iridium(I)-dicarbonyl, $Cp^*Rh(CO)_2$, Method 2 . . . . . - 238 -

7.7.10. Carbon-13 Labled Pentamethylcyclopentadienyl-rhodium(I)-dicarbonyl, $Cp^*Rh(^{13}CO)_2$ . . . . . - 239 -

7.8. Unsaturated Trinuclear 46e$^-$ complexes . . . . . - 240 -

7.8.1. Pentamethylcyclopentadienyl-rhodium(I)-bis(cyclopentadienyl-cobalt(I))-di-μ_3-carbonyl, $Cp^*Rh(CpCo)_2(\mu_3\text{-}CO)_2$ . . . - 240 -

7.8.2. Pentamethylcyclopentadienyl-iridium(I)-bis(cyclopentadienyl-cobalt(I))-di-μ_3-carbonyl, $Cp^*Ir(CpCo)_2(\mu_3\text{-}CO)$ . . . . . - 240 -

7.8.3. Tris(cyclopentadienyl-cobalt(I))-di-μ_3-carbonyl, $(CpCo)_3(\mu_3\text{-}CO)_2$ . . . . . - 241 -

7.8.4. (Trifluoromethyl-tetramethyl)cyclopentadienyl-cobalt(I)-bis(cyclopentadienyl-cobalt(I))-di-μ_3-carbonyl,

$Cp^{‡}Co(CpCo)_2(\mu_3\text{-}CO)_2$ . . . . . - 241 -

7.9. General procedures for Diazoalkane reactions . . . . . - 242 -

7.9.1. Cp^* Containing Cluster Complexes . . . . . - 242 -

7.9.2. All CpCo and $Cp^{‡}$ Containing Complexes . . . . . - 242 -

7.9.3. Reaction of $(CpCo)_3(\mu_3\text{-}CO)_2$ with Diazomethane . . . . - 243 -

7.9.4. Reaction of $(CpCo)_3(\mu_3\text{-}CO)_2$ with Diazoethane . . . . . - 243 -

7.9.5. Reaction of $Cp^*Co(CpCo)_2(\mu_3\text{-}CO)_2$ with Diazomethane - 244 -

7.9.6. Reaction of $Cp^{‡}Co(CpCo)_2(\mu_3\text{-}CO)_2$ with Diazomethane - 244 -

7.9.7. Reaction of $Cp^*Rh(CpCo)_2(\mu_3\text{-}CO)_2$ with Diazomethane - 245 -

7.9.8. Reaction of $Cp^*Rh(CpCo)_2(\mu_3\text{-}CO)_2$ with Diazoethane - 245 -

7.9.9. Reaction of $Cp^*Ir(CpCo)_2(\mu_3\text{-}CO)_2$ with Diazomethane - 246 -

7.9.10. Reaction of $Cp^*Ir(CpCo)_2(\mu_3\text{-}CO)_2$ with Diazoethane . - 246 -

7.10. Pentamethyl-cyclopentadienyliridium(I)-bis-(cyclopentadienyl-cobalt(I))(μ_3-methylidyne)-(μ_3-carbonyl)(μ_2-hydride), $Cp^*Ir(CpCo)_2(\mu_3\text{-}CO)(\mu_3\text{-}CH)(\mu_2\text{-}H)$ **(18)** . . . . . - 246 -

7.11. Reaction of $Cp^*Ir(CpCo)_2(\mu_3\text{-}CH)(\mu_2\text{-}H)$ **(18)** with tolyacetylene: Formation of 1,3,4- and 1,3,5-tristolylbenzene . - 247 -

7.12. Reaction of $Cp.Rh(CpCo)_2(\mu_3\text{-}CO)_2$ and $Cp^*Ir(CpCo)_2(\mu_3\text{-}CO)_2$ with acetylene . . . . . - 248 -

7.12.1. Pentamethylcyclopentadienyl-iridium(I)-bis(cyclopentadienyl-cobalt(I))-μ_3-carbonyl-μ_3-acetylene, $Cp^*Ir(CpCo)_2\text{-}\mu_3\text{-}CO\text{-}\mu_3,\eta^2\text{-}(HC{\equiv}CH)$ . . . . . - 248 -

7.12.2. Pentamethylcyclopentadienyl-rhodium(I)-bis(cyclopentadienyl-cobalt(I))-μ_3-carbonyl-μ_3-acetylene, $Cp^*Rh(CpCo)_2\mu_3$-CO-μ_3,η^2-(HC≡CH) ..... - 249 -

7.13. Reaction of $Cp^*Co(CpCo)_2(\mu_3\text{-}CO)_2$ (3), $Cp^*Rh(CpCo)_2(\mu_3\text{-}CO)_2$ (2) and $Cp^*Ir(CpCo)_2$ (1) with Tolylacetylene ..... - 249 -

7.13.1. Pentamethylcyclopentadienyl-iridium(I)-bis(cyclopentadienyl-cobalt(I))-μ_3-carbonyl-μ_3-tolylacetylene, $Cp^*Ir(CpCo)_2$-μ_3-CO-μ_3,η^2-(Tol-C≡CH) (23) ..... - 249 -

7.13.2. Pentamethylcyclopentadienyl-rhodium(I)-bis(cyclopentadienyl-cobalt(I))-μ_3-carbonyl-μ_3-tolylacetylene, $Cp^*Rh(CpCo)_2$-μ_3-CO-μ_3,η^2-(Tol-C≡CH) ..... - 250 -

7.13.3. Pentamethylcyclopentadienyl-cobalt(I)-bis(cyclopentadienyl-cobalt(I))-μ_3-carbonyl-μ_3-tolylacetylene, $Cp^*Co(CpCo)_2$-μ_3-CO-μ_3,η^2-(Tol-C≡CH) ..... - 250 -

7.13.4. (Trifluoromethyl-tetramethyl)cyclopentadienyl-cobalt(I)-bis(cyclopentadienyl-cobalt(I))-μ_3-carbonyl-μ_3-tolylacetylene, $Cp^‡Co(CpCo)_2$-μ_3-CO-μ_3,η^2-(Tol-C≡CH) ..... - 251 -

7.14. Reaction of $Cp^*Rh(CpCo)_2(CO)_2$ (2) and $Cp^*Ir(CpCo)_2(CO)_2$ with Diphenylacetylene (Bistolan) and Bistolylacetylene .... - 251 -

7.14.1. Pentamethylcyclopentadienyl-iridium(I)-bis(cyclopentadienyl-cobalt(I))-μ_3-carbonyl-μ_3-diphenylacetylene, $Cp^*Ir(CpCo)_2$-μ_3-CO-μ_3,η^2-(PhC≡CPh) (29) ..... - 251 -

7.14.2. Pentamethylcyclopentadienyl-iridium(I)-bis(cyclopentadienyl-cobalt(I))-μ_3-carbonyl-μ_3-bistolylacetylene, $Cp^*Ir(CpCo)_2\mu_3$-CO-μ_3,η^2-(TolC≡CTol) (**30**) . . . . . - 252 -

7.14.3. Pentamethylcyclopentadienyl-rhodium(I)-bis(cyclopentadienyl-cobalt(I))-μ_3-carbonyl-μ_3-diphenylacetylene, $Cp^*Rh(CpCo)_2$-μ_3-CO-μ_3,η^2-(PhC≡CPh) (**31**) . . . . . - 252 -

7.14.4. Pentamethylcyclopentadienyl-rhodium(I)-bis(cyclopentadienyl-cobalt(I))-μ_3-carbonyl-μ_3-bistolylacetylene, $Cp^*Rh(CpCo)_2$-μ_3-CO-μ_3,η^2-(TolC≡CTol) (**32**) . . . . . - 252 -

7.15. Formation of μ_3-oxo adducts: . . . . . - 253 -

7.15.1. Pentamethylcyclopentadienyl-iridium(I)-bis(cyclopentadienyl-cobalt(I))-μ_3-carbonyl-μ_3-oxo, $Cp^*Ir(CpCo)_2(\mu_3\text{-CO})(\mu_3\text{-O})$ . . . . . - 253 -

7.15.2. Pentamethylcyclopentadienyl-rhodium(I)-bis(cyclopentadienyl-cobalt(I))-μ_3-carbonyl-μ_3-oxo, $Cp^*Rh(CpCo)_2(\mu_3\text{-CO})(\mu_3\text{-O})$ . . . . . - 253 -

7.16. Scission reactions . . . . . - 253 -

7.16.1. Tris(cyclopentadienyl-cobalt(I)-μ_3-methylidyne-μ_3-phenylmethylidyne, $(\mu_3\text{-PhC})(CpCo)_3(\mu_3\text{-CH})$ (**35**) . . . - 254 -

7.17. References . . . . . - 255 -

APPENDIXES . . . . . - 256 -

APPENDIX 1: Description of NMR Pulse Programs . . . . . - 257 -

APPENDIX 2: Input Format for DNMR5 . . . . . - 267 -

APPENDIX 3: Relaxation Times of Bis-Carbyne Complexes **35** - **37** and Bistolan **38** . . . . . - 271 -

APPENDIX 4: Crystal Structure of $(CpCo)_3(\mu_2\text{-}CO)_2(\mu_2\text{-}CH_2)$ . . . . - 273 -

APPENDIX 5: Crystal Structure of $(CpCo)_3(\mu_3\text{-}CO)_3(\mu_3\text{-}NNCH_2)$ . . - 278 -

APPENDIX 6: Crystal Structure of $Cp^*Rh(CpCo)_2(\mu_2\text{-}CO)_2(\mu_2\text{-}CH_2)$ - 284 -

APPENDIX 7: Crystal Structure of $Cp^*Ir(CpCo)_2(\mu_3\text{-}CO)(\mu_3\text{-}CH)(\mu_2\text{-}H)$ . . . . . - 292 -

APPENDIX 8: Crystal Structure of $Cp^*Rh(CpCo)_2(CpCo)_2(\mu_3\text{-}CO)(\mu_3\text{-}HC{\equiv}CH)$ . . . . . - 298 -

APPENDIX 9: Crystal Structure of $Cp^*Rh(CpCo)_2(CpCo)_2(\mu_3\text{-}CO)(\mu_3\text{-}HC{\equiv}CH)$ . . . . . - 304 -

APPENDIX 10: Crystal Structure of $Cp^*Ir(CpCo)_2(CpCo)_2(\mu_3\text{-}CO)(\mu_3\text{-}HC{\equiv}CH)$ . . . . . - 312 -

APPENDIX 11: Crystal Structure of $Cp^*Rh(CpCo)_2(CpCo)_2(\mu_3\text{-}CO)(\mu_3\text{-}O)$ . . . . . - 320 -

APPENDIX 12: Crystal Structure of $Cp^*Ir(CpCo)_2(CpCo)_2(\mu_3\text{-}CO)(\mu_3\text{-}O)$ . . . . . - 326 -

VITA . . . . . - 332 -

LIST OF FIGURES

FIGURE

1.1 Synthesis of 46e⁻ cluster complexes shown for **2**. . . . . - 8 -

1.2 Reaction of 46e⁻ Complexes with donor ligands. . . . . - 10 -

2.1 Reaction of unsaturated trinuclear complexes **1** - **5** with diazoalkanes illustrating the formation of carbene and diazoalkane adducts. . . . . - 18 -

2.2 Crystal structure of **6** . . . . . - 20 -

2.3 ^{1}H NMR spectrum of carbene complex **6**. . . . . - 23 -

2.4 Crystal structure of **9**. . . . . - 26 -

2.5 ^{1}H NMR spectrum of the hydrazone complex **9**. . . . . - 27 -

2.6 Methylene region of the proton coupled ^{13}C NMR spectrum of **9** (top); ^{13}C satellite peaks in the ^{1}H NMR spectrum (bottom). . . . . - 29 -

2.7 Assignment of methylene protons in **9** by C-H coupling constants and NOE measurements. . . . . - 31 -

2.8 Crystal structure of **7**. . . . . - 34 -

2.9 ^{1}H NMR spectrum of the carbene complex **7**. . . . . - 37 -

2.10 NOESY spectrum of the Rh complex **7** at room temperature. . . . . - 38 -

2.11 Carbene region of the ^{1}H NMR spectrum of **7a** . . . . . - 39 -

2.12 ^{13}C NMR spectrum of the carbene complex **7**. . . . . - 40 -

2.13 Methylene and Cp regions of the ^{1}H NMR spectrum of **7** showing the appearance of isomer **b**. . . . . - 46 -

2.14 Kinetics of isomerization **7a** → **7b**. . . . . - 46 -

2.15 Semilogarithmic plots of the rate constant (left) and the equilibrium constants (right) versus 1/T for **7a** → **7b**. . . . . - 48 -

2.16 Carbene region of the NOESY spectrum of a mixture of isomers **a**, **b** and **c** at 365 K. . . . . - 50 -

2.17 NOESY spectrum of the Cp region of **7** at 300 K (top) and 355 K (bottom) indicating exchange between the CpCo edges at high temperature. . . - 51 -

2.18 Carbene migration between RhCo edges showing two possible coordination modes for the carbene ligand in the intermediate **7c**. . . - 54 -

2.19 Cross peak intensities of methylene protons in **7** versus mixing time for isomers **a** and **b**. . . . . - 55 -

2.20 Identification of Cp and Cp^* signal of **7c** against the background of ^{13}C satellite peaks . . . . . - 60 -

2.21 Portion of the NOESY spectrum of **7** showing the cross peak between methylene and Cp^* protons of **c**. . . . . - 61 -

2.22 Carbene region of a HMQC spectrum of **7** using a sample with the carbene carbon enriched in ^{13}C. . . . . - 63 -

2.23 Possible pathways for carbonyl migration in the case of a triply bridging carbene ligand. . . . . - 65 -

2.24 Terminal/bridging to all bridging isomerization in the tricarbonyl $Cp^*Ir(CpCo)_2(CO)_3$ (left) and one structure of $(CpCo)_3(CO)_3$. . . . . - 67 -

2.25 Formation of carbyne-hydride complex **18** from the carbene complex **8**. . . . . - 69 -

2.26 Crystal structure of carbyne hydride complex **18**. . . . . - 70 -

2.27 Electron Density Difference map of the carbyne-hydride complex **18** indicating the possible position of the hydride ligand. . . . . - 73 -

2.28 ^{1}H NMR spectra of **18** . . . . . - 75 -

2.29 Experimental and calculated lineshapes of the Cp proton signals of **18** at variable temperatures. . . . . - 77 -

2.30 Pulse sequence for selective inversion transfer (top), hydride (middle) and carbyne signal (bottom) with increasing τ. . . . . - 80 -

2.31 Experimental data from selective inversion experiment at 275K (triangles) and fit through the data according to (2(8) and (2(9). . . . . - 83 -

2.32 Proposed mechanism for exchange of the carbyne and hydride hydrogens involving agostic hydrogens. . . . . - 85 -

2.33 Reactions attempted with the carbyne hydride complex **18**; only addition of CO lead to clean addition. . . . . - 88 -

2.34 Frontier orbitals of $[CpMn(CO)_2]_2$. . . . . - 91 -

2.35 Possible intermediate in the formation of hydrazone and carbene adducts. . . . . - 94 -

3.1 Formation of the alkyne adducts from 46 e$^-$ complexes. . . . . - 105 -

3.2 Crystal structure of **20**. In the side view, a Cp ligand has been omitted for clarity. . . . . - 108 -

3.3 Side view visualizing the almost planer geometry around the alkyne carbons. . . . . - 111 -

3.4 Bonding of the alkyne in **20**. . . . . - 111 -

3.5 ^1H NMR spectra of **19** in toluene-d_8 at 300 K (top) and 170 K (bottom). . . . . - 114 -

3.6 Full NOESY spectrum of **19** . . . . . - 115 -

3.7 Alkyne region of NOESY spectrum of **19**. . . . . - 116 -

3.8 Mobility of the alkyne ligands between the two possible positions parallel to the Ir-Co and Co-Co edge. . . . . - 118 -

3.9 Variable temperature ^1H spectra of the alkyne region of **19** . . . . . - 119 -

3.10 Eyring plot for exchange between positional isomers **19A** and **19B**. - 122 -

3.11 Alkyne region of the NOESY spectrum of **20** at 170 K. . . . . - 124 -

3.12 Variable temperature spectra of the alkyne region of **20**. . . . . - 125 -

3.13 Temperature dependence of the equilibrium constant for **A** → **B** in the rhodium complex **20**. . . . . - 126 -

3.14 Comparism of the low temperature spectra of **19** - **21** showing the change in the preferred orientational isomer. . . . . - 128 -

3.15 Crystal structure of the tolylacetylene adducts $Cp^*Rh(CpCo)_2(CO)(TolC{\equiv}CH)$ (top) and $Cp^*Ir(CpCo)_2(CO)(TolC{\equiv}CH)$ (bottom). . . . . - 133 -

3.16 Vertical and horizontal tilt of the Cp and Cp^* rings in the crystal structure of **23** and **24**. . . . . - 137 -

3.17 Proton NMR spectrum of **23** at 181 K showing three different isomers. . . . . - 139 -

3.18 Possible structures for the tolylacetylene adducts showing the three pairs of enantiomers. . . . . - 140 -

3.19 Downfield part of the NOESY spectrum of **23** at 175 K. . . . . - 141 -

3.20 Cp region of the experimental (left) and simulated (right) ^{1}H NMR spectra of **23** at variable temperatures. . . . . - 145 -

3.21 Low temperature ^{1}H NMR spectrum of **24**. T = 170K . . . . . - 148 -

3.22 Experimental (left) and simulated (right) spectra for the Cp region of **25**. . . . . - 150 -

3.23 Low temperature ^{1}H NMR spectrum of tolylacetylene complex **27**. . - 152 -

3.24 Temperature dependent ^{1}H NMR spectra showing the phenyl region of **25**. . . . . - 154 -

3.25 NOESY spectrum of **25** at 170 K . . . . . - 157 -

2.26 Phenyl region of the NOESY spectrum of **23** at 170 K. . . . . - 160 -

3.27 View along the rotation axis of the tolyl substituent in **24**. . . . . - 163 -

3.28 Low Temperature spectrum of the ditolylacetylene adduct **30** . . . . . - 166 -

3.29 Proposed mechanism of alkyne rotation between different μ-$\parallel$ orientations through a μ-$\perp$ transition state. . . . . - 172 -

3.30 Energy profile for alkyne rotation in **23** . . . . . - 173 -

3.31 Illustration of unhindered rotation of the phenyl ring in the transition state. . . . . - 176 -

3.32 Mechanism of alkyne scission in a trinuclear cluster complex ..... - 177 -

4.1 Summary of complexes investigated in this study ..... - 186 -

4.2 $^{13}C\{^1H\}$ correlation spectrum of the linked cluster complex **36** illustrating the assignment of the ^{13}C resonances ..... - 188 -

4.3 $D_\perp$: Motion of molecule perpendicular to main axis, $D_\parallel$: motion of entire molecule about main axis, R: internal rotation of phenyl substituents - 189 -

4.4 (a) Calculated NOE values (b) T_1 values calculated with general equations (solid) and for extreme narrowing limit ..... - 196 -

4.5 Experimental and calculated diffusion coefficients versus inverse temperature ..... - 199 -

4.6 Rotational cones of the hydrogens in the phenyl and Cp rings .... - 208 -

4.7 Top view of crystal structure of **34** illustrating interaction of the phenyl ring with only two of the three Cp rings ..... - 210 -

5.1 Different possible pathways for addition of dioxygen to trinuclear cluster complexes. ..... - 216 -

5.2 Formation of oxo-adducts **41**, **42** and **43** in the solid state (top) versus cluster fragmentation in solution (bottom). ..... - 218 -

5.3 Crystal structure of $Cp^*Ir(CpCo)_2(\mu_3\text{-}CO)(\mu_3\text{-}O)$ (**43**) ..... - 221 -

LIST OF TABLES

TABLE

1.1 NMR methods used to study of fluxional processes. . . . . - 5 -

2.1 Selected bond distances in **6**. . . . . - 21 -

2.2 Spectroscopic data for carbene and diazomethane adducts of $(CpCo)_3(\mu_3\text{-}CO)_2$, **6** and **9**. . . . . - 25 -

2.3 Selected bond distances and -angles in the diazomethane complex **9**. - 26 -

2.4 Spectroscopic data of the carbene and hydrazone adducts **7,8, 10** - **12**. . . . . - 36 -

2.5 Spectroscopic data of diazoethane adducts $LM(CpCo)(\mu_3\text{-}CO)(\mu_3\text{-}NNCHMe)$. . . . . - 42 -

2.6 Spectroscopic data of the different positional isomers of **7** . . . . . - 45 -

2.7 T_1 and NOE values of the carbene protons of **7a** and rate constants calculated for carbene migration. . . . . - 57 -

2.8 Free energies of activation $\Delta G^{\ddagger}$ for carbene migration in **8** - **6** . . . . . - 58 -

2.9 Selected bond distances and -angles in **18** . . . . . - 71 -

2.10 Spectroscopic data for the carbyne-hydride complex **18**. . . . . - 74 -

2.11 Activation barriers for carbyne hydride exchange and hydride scrambling in **18**. . . . . - 83 -

3.1 Spectroscopic data for acetylene adducts $Cp^*M(CpCo)_2(CO)(HC{\equiv}CH)$ at 300K. . . . . - 107 -

3.2 Selected bond distances, bond angles and interplanar angles in **20** . - 109 -

3.3 Spectroscopic data for the byproduct **33**. . . . . - 129 -

3.4 Spectroscopic data for tolylacetylene adducts $LM(CpCo)_2(\mu_3$-CO)(Tol-C≡CH) **23** - **27** at 300 K. . . . . - 133 -

3.5 Selected bond distances and -angles for $Cp^*Ir(CpCo)_2(CO)$(Tol-C≡CH) (**23**). . . . . - 134 -

3.6 Selected bond distances and -angles in $Cp^*Rh(CpCo)_2(CO)$(Tol-C≡CH) (**24**). . . . . - 135 -

3.7 Activation parameters for the interconversion of isomers **A**, **B** and **C** of the alkyne complex **23**. . . . . - 147 -

3.8 Spectroscopic data of diphenylacetylene adducts $Cp^*M(CpCo)_2(\mu_3$-CO)(RC≡CR). . . . . - 164 -

3.9 Kinetic and thermodynamic parameters determined for interconversion **A** → **B** in acetylene and tolyl acetylene adducts . . . . - 169 -

4.1 T_1 carbon-13 relaxation times obtained for **34** . . . . . - 194 -

4.2 Diffusion parameters at 298 K . . . . . - 201 -

4.3 Diffusion coefficients $D_\perp$ at T=298 K and comparison with calculated values using hydrodynamic stick and slip models . . . . . - 204 -

5.1 Spectroscopic data of the μ_3-oxo adducts **41** - **43**. . . . . - 219 -

5.2 Selected bond distances in the oxo cluster complexes $Cp^*M(CpCo)_2(\mu_3$-CO)(μ_3-O), **42** and **43**. . . . . - 222 -

A-3.1 Carbon-13 relaxation times in **35** . . . . . - 272 -

A-3.2 Carbon-13 relaxation times in **36** . . . . . - 272 -

A-3.3 Carbon-13 relaxation times in **37** . . . . . - 272 -

A-3.4 Carbon-13 relaxation times in **38** . . . . . - 272 -

LIST OF ABBREVIATIONS

2D	Two dimensional
APT	Attached proton test
Cp	Cyclopentadienyl
Cp^*	Pentamethylcyclopentadienyl
$Cp^‡$	Trifluoromethyl-tetramethylcyclopentadienyl
COSY	Homonuclear *co*rrelation *s*pectroscop*y*
DEPT	*D*istortionless *e*nhancement by *p*olarisation *t*ransfer
FT	Fourier transform
HMQC	*H*eteronuclear *m*ultiple *q*uantum *c*oherence
HOMO	*H*ighest *o*ccupied *m*olecular *o*rbital
HRMS	*H*igh *r*esolution *m*ass *s*pectroscopy
IR	Infrared spectroscopy
LUMO	*L*owest *u*noccupied *m*olecular *o*rbital
Me	Methyl
MS	Mass spectrometry
NMR	Nuclear magnetic resonance
NOE	*N*uclear *O*verhauser *e*ffect
NOESY	Two dimensional *N*uclear *O*verhauser *e*ffect *s*pectroscop*y*
Ph	Phenyl
ROESY	*R*otational frame *O*verhauser *e*ffect *s*pectroscop*y*
Tol	Tolyl

SYMBOLS AND CONSTANTS

γ_C	gyromagnetic ratio of ^{13}C, $0.6726 \cdot 10^8$ s A rad kg^{-1}
γ_H	gyromagnetic ratio of ^{1}H, $1.6752 \cdot 10^8$ s A rad kg^{-1}
δ	chemical shift [ppm]
η	viscosity
π	3.14159265
τ	mixing time [s or ms]
τ_c	correlation time [ps]
a,b	length
D_ϑ, $D_\parallel$, $D_\perp$	Diffusion coefficient about different axes of the molecule [s^{-1}]
e	2.7182818
ΔG^0	free energy of a reaction [kJ mol^{-1}]
$\Delta G^\ddagger$	free energy of activation [kJ mol^{-1}]
h	Planck's constant, $6.626 \cdot 10^{-34}$ J s^{-1}
$\hbar$	$h/2\pi$
$\Delta H^\ddagger$	enthalphy of activation [kJ mol^{-1}]
J	scalar coupling [s^{-1}, Hz]
k, k_{AB}	rate constant for interconversion A → B [s^{-1}]
k_B	Boltzmann's constant, $1.3805 \cdot 10^{-23}$ J K^{-1}
K, K_c	Equilibrium constant
N_A	Avogadro's constant, $6.022 \cdot 10^{23}$ mol^{-1}
r	radius [Å]

R, R_{Ph}	Internal rotation rate [s^{-1}, Hz]
R_G	Gas constant, 8.314 J K^{-1} mol^{-1}
$\Delta S^{\ddagger}$	entropy of activation [J K^{-1} mol^{-1}]
T	Temperature [K, °C]
T_1	NMR relaxation time [s]
T_c	Coalescence temperature [K]

CHAPTER 1

Introduction

In this thesis, the chemistry and mobility of carbene, carbyne and alkyne ligands on a variety of heteronuclear cluster complexes will be discussed. In recent years, metal cluster complexes have attracted considerable attention. One reason for such interest is the fact that cluster complexes resemble a metal surface[1] and therefore can be used as models when studying intermediates in heterogeneous catalysis reactions taking place on metal surfaces. Understanding the mechanism of such reactions is essential in order to systematically improve existing processes and to develop new catalysts. For that purpose, the identity and structure of the reaction intermediates on the metal surface have to be established. Furthermore, mobility of the organic fragments on the surface is thought to be of importance in order for the initial C_1 fragments to couple with each other to form carbon chains. Understanding of such processes is of importance if, for example, one wants to control the chain length of the desired hydrocarbon product.

Solid state methods like Low Energy Electron Diffraction (LEED)[2] or reflection-adsorption infrared spectroscopy[3] have been used to investigate simple organic fragments; one recent example is coadsorbed CO and benzene[4] on a Rh (111) surface. However, most of these methods are limited by experimental difficulties such as the requirement of defined single crystal faces and ultra high vacuum conditions. Structural information, on the other hand, is often quite limited. Information about the dynamics of the coordinated fragments on metal surfaces is especially scarce. For these reasons, molecular metal cluster complexes have been used to mimic metal surfaces on a molecular level. The advantage of this approach is several fold. First, molecular complexes can be characterized using spectroscopic techniques which are routine methods in molecular chemistry. These include not only solution methods such as IR and NMR spectroscopy, but also single crystal x-ray diffraction, one of the most powerful methods of structure determination. For the study of dynamic processes, spectroscopic methods applied to systems in solution are much more informative than the methods commonly used to characterize metal surfaces. A second advantage of studying systems in solution is the availability of several well established methods of separation and purification. These readily allow one to study well defined systems and determine the "surface" geometry of such systems in detail.

Another area in which metal cluster complexes are currently gaining interest is the use of such complexes as building blocks for new materials. For example such substances containing linked metal clusters are thought to have

interesting properties which are different from purely organic based materials. Metal complexes often show facile redox behavior and their electronic structure often involves partially filled molecular orbitals. These properties make metal clusters promising precursors for electrically conducting materials. Even though the development of such materials still lies in the future, several linked cluster systems have been described in the recent literature.[5] One focus of the investigations described here is the study of the interaction between different cluster units. These interactions are important in order to understand the properties of the material on the basis of its building blocks. Cyclovoltametry is one method that has been used in order to investigate the electrochemical behavior of such materials and to study electronic interactions between the building blocks. Another property sensitive to interactions between the building blocks is the relative mobility of the individual groups with respect to each other. In polymers, *microscopic* processes such as internal rotation and flexibility of single groups often have pronounced effects on *macroscopic* properties like glass transition temperatures and the elasticity of the material. Barriers to such rotations can arise from both steric and electronic interactions of the monomeric groups with each other. In order to fully predict the properties of a material one therefore must understand the influence of these contributions on the mobility of single groups in the building blocks.

The above examples show that study of dynamic processes taking place in cluster complexes can be of great importance in both catalysis and materials

science. Organometallic complexes are known to exhibit many different types of dynamic processes. Some of these processes involve metal to carbon bonds like the rotation of π-bound ligands (Cp, ethylene, alkynes) about the metal-ligand bonding axis or migration of σ-bound species like CO, carbene or hydride ligands between different metal centers. Another class of processes involves C-C and C-H bonds within the ligands which are activated due to coordination of the ligand to the metal.

One of the most versatile methods to study fluxional processes in solution is nuclear magnetic resonance (NMR) spectroscopy. A variety of NMR spectroscopic techniques is known which allow for the investigation of reactions and fluxional processes with time scales ranging from hours to nanoseconds. Table 1.1 summarizes appropriate NMR methods applied to dynamic processes with different time scales. Several examples mentioned in this thesis are also listed as examples, illustrating the variety of processes investigated.

Conventional one-dimensional spectroscopy can be used to study the kinetics of reactions involving reactants with lifetimes of hours or minutes by monitoring the decay or appearance of a set of signals. For this approach it is of importance that initially the reactants are present in non-equilibrium concentrations. Equilibria in which interchange takes place on a timescale of seconds can be investigated using magnetization transfer techniques. In this type of experiment ono set of spins is selectively labeled without affecting the other spins. The reestablishment of equilibrium between both sets of spins is then monitored and

Table 1.1: NMR methods used to study of fluxional processes.

Technique	accessible rate constants k / s^{-1}	Dynamic process investigated with that method
conventional 1D NMR	< 0.1	carbene migration from Rh-Co to Co-Co edge (CHAPTER 2)
magnetization transfer techniques, NOESY	0.01 - 10	carbene migration between Rh-Co edges (CHAPTER 2) carbyne-hydride interconversion (CHAPTER 2)
coalescence broadening	$1 - 10^3$	hydride migration in $Cp^*Ir(CpCo)_2(CO)(CH)(H)$ (CHAPTER 2) alkyne rotation (CHAPTER 3)
$T_{1,\rho}$ measurements	10^4	Ethylene ligand rotation in the solid state (Reference 8)
T_1 measurements	$10^8 - 10^{10}$	Phenyl ring rotation in bis-carbyne complexes (CHAPTER 4)

can be evaluated on a quantitative basis. Labeling can be achieved by either selective saturation or inversion of the signal of one of the exchanging species. A two dimensional version of this method is the NOESY experiment which, in addition to extraction of rate constants, allows for a straightforward determination of the exchange pathway. One example of such a process is the exchange of a hydrogen atom between a terminal carbyne and a hydride position in $Cp^*Ir(CpCo)_2(\mu_3\text{-}CO)(\mu_3\text{-}CH)(\mu_2\text{-}H)$ as described in Chapter 2 of this thesis.

Dynamic processes on the timescale of 10^{-1} to 10^{-3} s fall in the range of so-called coalescence broadening. On this timescale the rate of exchange becomes

comparable to the chemical shift difference between the signals of the exchanging species measured in Hz. At this point the two signals broaden and finally coalesce into one. A quantitative analysis of the lineshape of the exchanging signals allows for an extraction of rate constants. Such an analysis has been perfomed in order to investigate the rotation of alkyne ligands about the face of a trinuclear cluster complex described in Chapter 3.

Motions faster than the ones studied by coalescence methods can be investigated using relaxation time measurements. Relaxation becomes most efficient if the overall rotation rate of a group becomes comparable to the Larmor frequency. In the solid state, motions in the kilohertz range (lifetime of 10^{-4} s) may be studied by measuring the relaxation under spin lock conditions (relaxation in rotating frame, $T_{1,\rho}$). One example is the rotation of ethylene ligands taking place in $Rh(acac)(C_2H_4)_2$ in the solid state.[6] The proton atoms of the rotating ethylene ligand were found to have $T_{1,\rho(proton)}$ values considerably shorter than the ones in the rigid cyclooctadiene ligand in Rh(acac)(cod).

In solution at room temperature, molecular tumbling causes correlation times to be in the nanosecond range which corresponds to diffusion coefficients of several hundred to several thousand megahertz which is the approximate Larmor frequency of ^1H or ^{13}C on modern spectrometers with superconducting magnets. Such processes therefore can be studied by measuring T_1 relaxation times, preferably of ^{13}C in the molecule or complex. Fast internal rotation of substituents like methyl or phenyl groups about carbon-carbon single bonds will

shorten the correlation times further, thus increasing the overall rotation rate away from the match with the Larmor frequency. Such groups will therefore exhibit longer relaxation times. An example discussed in this thesis is the rotation of phenyl substituents in several bis-carbyne complexes. This study is the subject of Chapter 4.

In our group, we have developed a synthetic route for the preparation of a series of unsaturated clusters containing cobalt group metals which are based on Cp and Cp^* ligands. These complexes have the general formula $Cp'M(CpCo)_2(\mu_2\text{-}CO)_2$, where Cp'-M = CpCo, $Cp^{\ddagger}Co$ ($Cp^{\ddagger} \equiv C_5(CH_3)_4(CF_3)$), Cp^*Co, Cp^*Rh or Cp^*Ir. The synthesis of heteronuclear complexes is achieved in a few steps starting from the metal chlorides. The assembly of the cluster core takes place in the last step involving a high yield reaction of Jonas reagent, $CpCo(C_2H_4)_2$,[7] with the corresponding dicarbonyl $Cp'M(CO)_2$. Figure 1.1 outlines the synthesis using the complex $Cp^*Rh(CpCo)_2(\mu_3\text{-}CO)_2$ (**2**) as an example.

According to the 18 electron rule, the number of valence electrons in a saturated transition metal cluster complex can be calculated from the number of metal atoms (n) and the number of metal-metal bonds (m) as 18 n - 2 m. For a trinuclear complex, n = m = 3 and 48 cluster valence electrons are expected. The number of valence electrons in a cluster is determined by counting the electrons of the metal atoms plus the electrons donated by the ligands. If all ligands are considered neutral, then each metal in the complexes $Cp'M(CpCo)_2(\mu_3\text{-}CO)_2$ (M = Co, Rh, Ir) contributes nine electrons; each Cp or

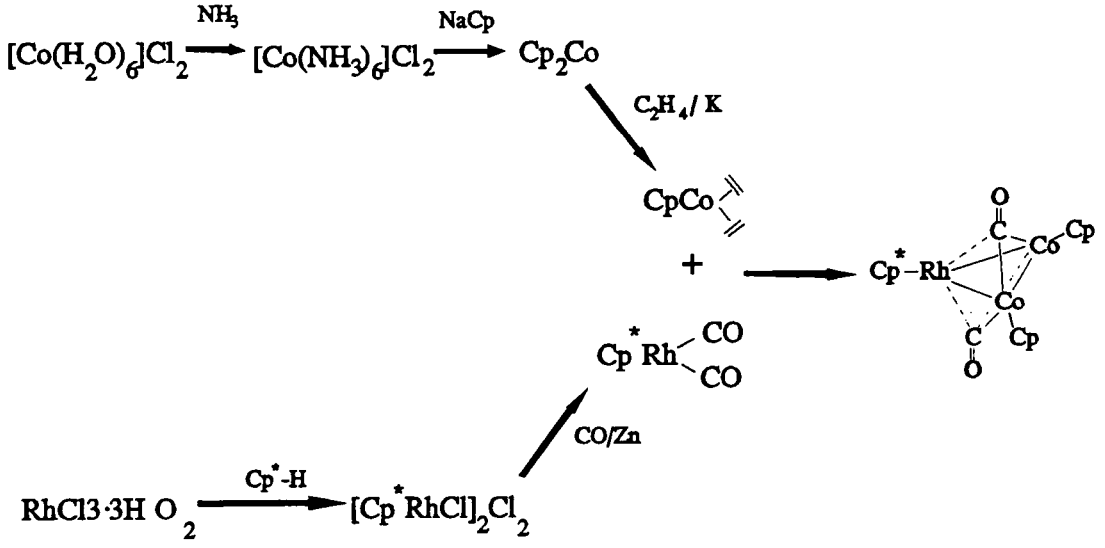

Figure 1.1: Synthesis of 46e⁻ cluster complexes shown for **2**. The other complexes are synthesized in an analogous manner.

3 d -M:[9]	3 x 9	= 27
3 Cp:	3 x 5	= 15
2 CO:	2 x 2	= 4
total:		46

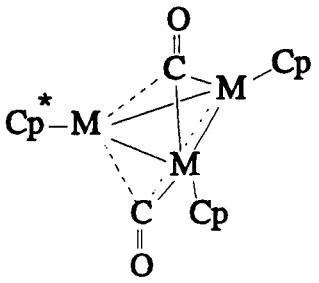

Cp^* ligand five electrons and each carbonyl ligand 2 electrons to the cluster electron count. This results in a count of (3 × 9) + (3 × 5) + (2 × 2) = 46 cluster valence electrons. This is two electrons short of the number of 48 electrons expected for a saturated metal cluster. The above complexes are therefore

electronically unsaturated and readily add donor ligands in order to achieve a saturated shell of 48 cluster valence electrons. This property makes them ideal precursors for the introduction of a variety of simple organic ligands into this cluster type. Figure 1.2 summarizes the different ligands that have been added to these complexes. Two electron donor ligands like carbon monoxide or carbenes generated from diazoalkanes simply add to the cluster complex, whereas four electron donor ligands like alkynes, oxygen or diazoalkanes displace one of the two carbonyl ligands. In both cases, the final adduct contains 48 cluster valence electrons. With this strategy, metal cluster complexes containing a variety of organic fragments become available. In particular a general procedure for the synthesis of a family of heteronuclear cluster complexes is introduced. This allows one to create systems containing different metal edges in a controlled manner thus mimicking binary metal catalyst systems.

This thesis will focus on the study of the fluxionality of carbene, carbyne and alkyne ligands attached to a metal cluster. In Chapter Two the reaction of a family of unsaturated trinuclear cluster complexes of the general structure $Cp^*M(CpCo)_2(\mu_3\text{-}CO)_2$ with diazoalkanes will be discussed. The formation of two types of adducts is observed. One is a carbene adduct; the other one is best described as hydrazone adduct. The formation of carbene versus hydrazone depends on the hetero metal as well as on the substituent on the diazomethane. Characterization of these complexes is presented using spectroscopy and single crystal x-ray diffraction. Two dimensional NMR spectroscopy is used to study the

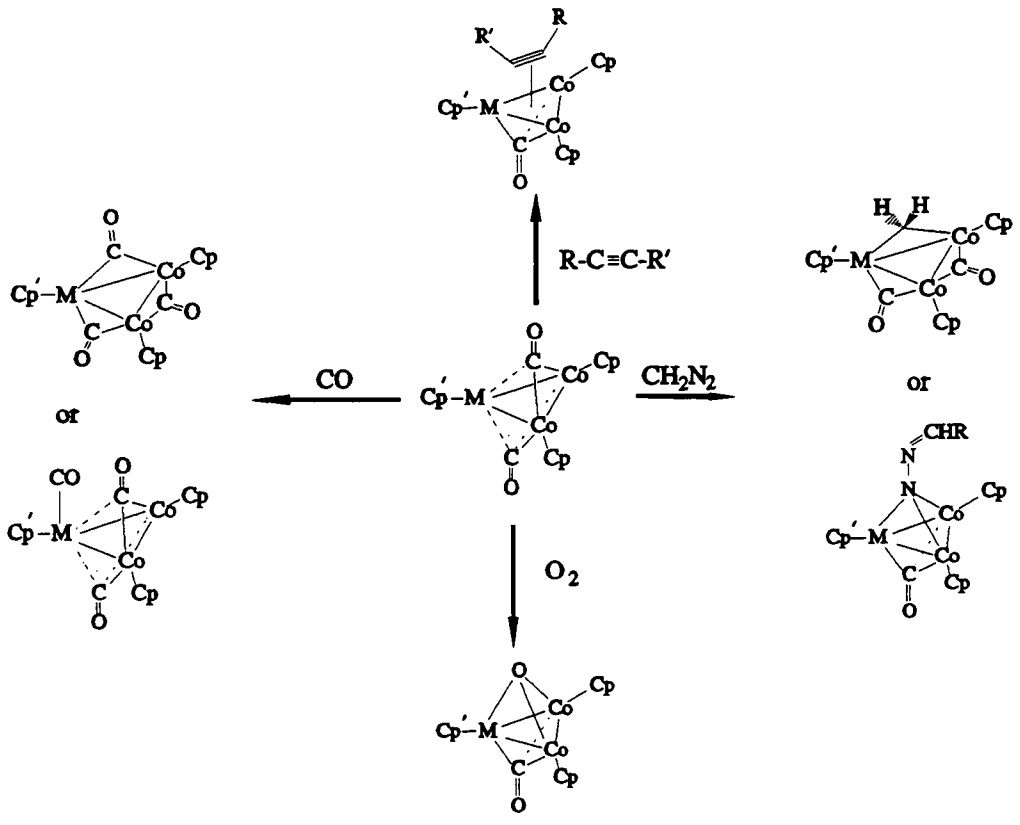

Figure 1.2: Reaction of 46e⁻ complexes with donor ligands.

migration of the carbene ligand around the metal triangle. In the case of the Ir containing cluster complex, formation of a carbyne hydride complex is observed upon heating under reflux in toluene. This carbyne hydride complex exhibits exchange between the hydride ligand and the terminal carbyne ligand.

Chapter Three describes the addition of alkynes to a series of mixed metal cluster complexes $Cp^*M(CpCo)_2(CO)_2$, M = Co, Rh, Ir. At room temperature the coordinated alkyne is fluxional about the metal triangle, but at low temperature this motion may be frozen out and different positional isomers can be distinguished. In all cases the alkyne is parallel to a metal-metal edge as expected for

48 e^- complexes. For M = Ir the preferred orientation of the alkyne is parallel to an Cp^*Ir-CpCo edge, whereas for M = Co the alkyne is parallel to the CpCo-CpCo edge. In the case of M = Rh both possible orientations of the alkyne are found in comparable amounts. The kinetics and thermodynamics of the equilibration of the different positional isomers are investigated in some detail using line shape analysis.

Chapter Four presents a study of internal phenyl substituent rotation in some single and linked bis-carbyne cluster complexes. Carbon-13 NMR relaxation times are used to investigate the rotation of the phenyl substituents on a nanosecond timescale. The rotation rates for phenyl rings differ considerably depending on the position and the environment of the phenyl substituent in the molecule. Phenyl groups located on the periphery of the molecule rotate faster than the ones linking two clusters, and phenyl rings substituted with an alkyne are faster than the ones with a $(CpCo)_3$-carbyne substituent. It appears that the most important factor determining the barrier to rotation of the phenyl groups is steric interactions between the hydrogens of the phenyl ring and the ones of the Cp ligands on the cluster.

Finally, Chapter Five will give a brief report on the formation of oxo adducts which are formed when the unsaturated cluster complexes $Cp^*M(CpCo)_2(\mu_3\text{-}CO)$ are exposed to air in the solid state.

References :

1. Muetterties, E. L.; Rhodin, T. N.; Band, E.; Brucker, C. F.; Pretzer, W. R.; *Chem. Rev.* **1979**, *79*, 91-136.

2. Ertl, G.; Küppers, J.; "Low Energy Electrons and Surface Chemistry", *Verlag Chemie*, Weinheim **1974**.

3. Chester, M. J.; Prichard, J.; Sims, M. L.; *Adsorbtion-Desorbtion Phenomena*, Academic Press, New York, 1972.

4. Van Hove, M. A.; Lin, R. F.; Somorjai, G. A.; *J. Am. Chem. Soc.* **1986**, *108*, 2532.

5. a) Hoskins, B. F.; Robson, R.; *J. Am. Chem. Soc.* **1992**, *114*, 1546. b) Stein, A.; Keller, S. W.; Mallouk, T. E.; *Science* **1993**, *259*, 1558.

6. Vierkötter, S. A.; *Ph. D. Thesis*, University of Tennessee, Knoxville; **1994**.

7. Jonas, K.; Deffense, E.; Haberman, J.; *Angew. Chem.* **1983**, *95*, 729.

CHAPTER 2:

Reactions of Trinuclear Cluster Complexes with Diazoalkanes: Carbene and Carbyne Ligands in Trinuclear Cluster Complexes of the Cobalt Group

2.1. Introduction

The formation and breaking of carbon-hydrogen and carbon-carbon bonds are the basic steps in the build up of complex organic compounds from simple precursors. One industrial process of great importance involving such reactions is Fischer-Tropsch synthesis; the reductive hydration and oligomerization of carbon monoxide using a heterogeneous metal catalyst.[1] In order to elucidate the mechanism of such reactions, interest has focused on the study of the various C_1 fragments which occur as intermediates bound to metal surfaces. One important question in this context concerns the mobility of these fragments on the surface. In order for several fragments to couple and form hydrocarbon chains it is believed that they must be able to move about on a metal surface. Recently, Hoffmann et. al. published a theoretical study of the bonding and mobility of CH_3,

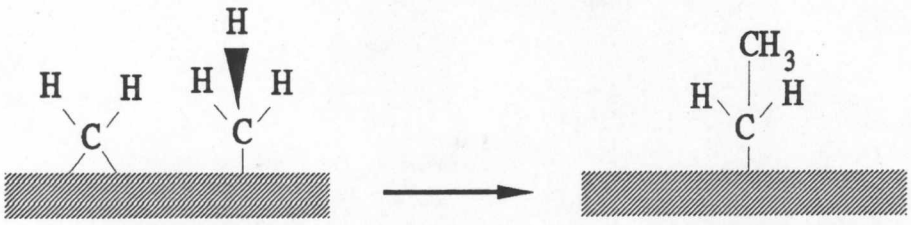

CH_2 and CH groups on Ti, Cr and Co surfaces.[2] Several groups reported experimental evidence of these ligands on various metal surfaces,[3] however studies on bulk metals are limited by experimental difficulties and so far, little information is available about migration of C_1 fragments on a metal surface.

Molecular cluster complexes have been used to model some of the hypothesized steps involved in the Fischer-Tropsch synthesis on a molecular level.[4] To date, most efforts in this area have focused on cluster systems based on carbonyl[5, 6, 7] or Cp and Cp^* ligands[8, 9, 10, 11] It was found that, consistent with the calculations performed by Hoffmann for metal surfaces, in multinuclear complexes a carbene ligand exhibits an edge-bridging coordination mode whereas carbyne ligands prefer face-bridging coordination modes:

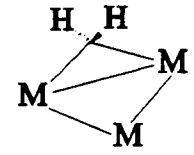

μ_2-carbene

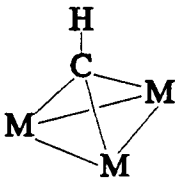

μ_3-carbyne

Cluster complexes have also been used to model a variety of processes which are believed to take place during heterogeneous catalysis reactions. One example is the stepwise hydrogenation of a CO ligand, initially converting it a to formyl group,[12] then a carbene ligand and eventually releasing CH_4.[7, 13] C-H activation steps have been observed by studying agostic hydrogens,[5b, 6c, 14] dehydrogenation of methyl or carbene ligands to yield carbene- hydride and carbyne-hydride complexes[5a] and exchange of C-H hydrogens with hydride ligands.[15, 16] Finally, the movement of a carbene ligand about the different edges of a metal cluster has been reported.[5]

The study of carbene and carbyne ligands in molecular transition metal complexes has therefore generated considerable interest in recent years. Some highlights in general carbene chemistry are the synthesis of the first terminal transition metal carbene[17] and carbyne[18] complexes by E. O. Fisher in 1964 and 1973 and the first methylidene complex without a hetero substituent ("Schrock type carbene") reported by Schrock in 1975[19]. Hetero-substituted bridging carbene complexes were first reported by the groups of Sternberg and Albanesi in the late 1950s.[20, 21] Another 15 years were required before the first

unsubstituted bridging methylene complex $[CpMn(CO)_2]_2(\mu_2\text{-}CH_2)$ was synthesized by addition of diazomethane to $CpMn(CO)_2 \cdot THF$.[22] Several methods for the incorporation of a methylene ligand in a polynuclear complex have since been developed.[23] For example, Wittigs reagent $Ph_3P{=}CH_2$ [24] reacts with $(CpFe)_2(CO)_4$ to yield $(CpFeCO)_2(\mu\text{-}CO)(\mu\text{-}CH_2)$[25], and di-iodomethane reacts with $[Fe_2(CO)_8]^{2-}$ and $[(CpCo)_2(\mu\text{-}CO)_2]^-$ to yield the corresponding neutral carbene complexes $Fe_2(CO)_8(\mu\text{-}CH_2)$ and $(CpCo)_2(CO)_2(\mu\text{-}CH_2)$.[26, 27] The most versatile and general method for the preparation of Schrock type carbene complexes, however, still appears to be the addition of diazoalkanes to a suitable precursor.[23] This method has yielded a large variety of dinuclear and trinuclear complexes containing bridging carbene ligands. One limitation of this method is the possibility of the formation of diazoalkane complexes which has been observed in a number of cases.[28]

Efforts in our group have been focused on the reactivity of the Cp based, unsaturated $46e^-$ trinuclear clusters of the type $Cp^*M(CpCo)_2(CO)_2$ (M = Co, Rh, Ir).[29] These cluster complexes are unsaturated and readily add donor ligands. This makes them promising candidates for the preparation of carbene complexes by reaction with diazoalkanes. Some preliminary work in that area has shown that this might be true only in some cases. In the cases of the complexes $Cp^*Ir(CpCo)_2(\mu_3\text{-}CO)_2$ (**1**) and $Cp^*Rh(CpCo)_2(\mu_3\text{-}CO)_2$ formation of a carbene adduct has reported upon addition of diazomethane.[11, 30] On the other hand, reaction of the complex $Cp^*Co(CpCo)_2(\mu_3\text{-}CO)_2$ with diazomethane and

diazoethane does not yield a carbene adduct but instead results in a diazoalkane adduct[31, 30] in which the terminal nitrogen displaces one of the carbonyl ligands and coordinates to the cluster in a triply bridging fashion.

In this chapter, the reaction of the entire series of clusters $LM(CpCo)_2(\mu_3\text{-}CO)_2$ (LM = Cp^*Co, Cp^*Rh, Cp^*Ir, CpCo, $Cp^{\ddagger}Co$) with diazomethane and diazoethane is presented (Figure 2.1). It appears that the course of the reaction depends on the nature of the metal fragment LM and the specific diazoalkane, yielding carbene and/or diazomethane adduct. In the case of diaz*omethane*, when LM ≡ Cp^*Ir only carbene adduct is formed, whereas when LM ≡ Cp^*Rh and CpCo yield equal amounts of carbene and diazomethane adduct are formed. For LM ≡ Cp^*Co and $Cp^{\ddagger}Co$ only diazomethane adduct is observed. In the case of diazoethane, no carbene adduct is observed for any of the complexes, but only the diazoethane adduct. In the first part of this chapter, the full characterization of the carbene and diazomethane adducts will be described. Following this, the mobility of the carbene ligand on the cluster surface will be discussed and evidence for the presence of a triply carbene ligand as a minor isomer of $Cp^*Rh(CpCo)_2(\mu_2\text{-}CO)_2(\mu_2\text{-}CH_2)_2$ will be presented. Finally, the formation of the carbyne hydride complex $Cp^*Ir(CpCo)_2(\mu_3\text{-}CO)(\mu_3\text{-}CH)(\mu_2\text{-}H)$ from the corresponding carbene complex and a study of its interesting properties will be described.

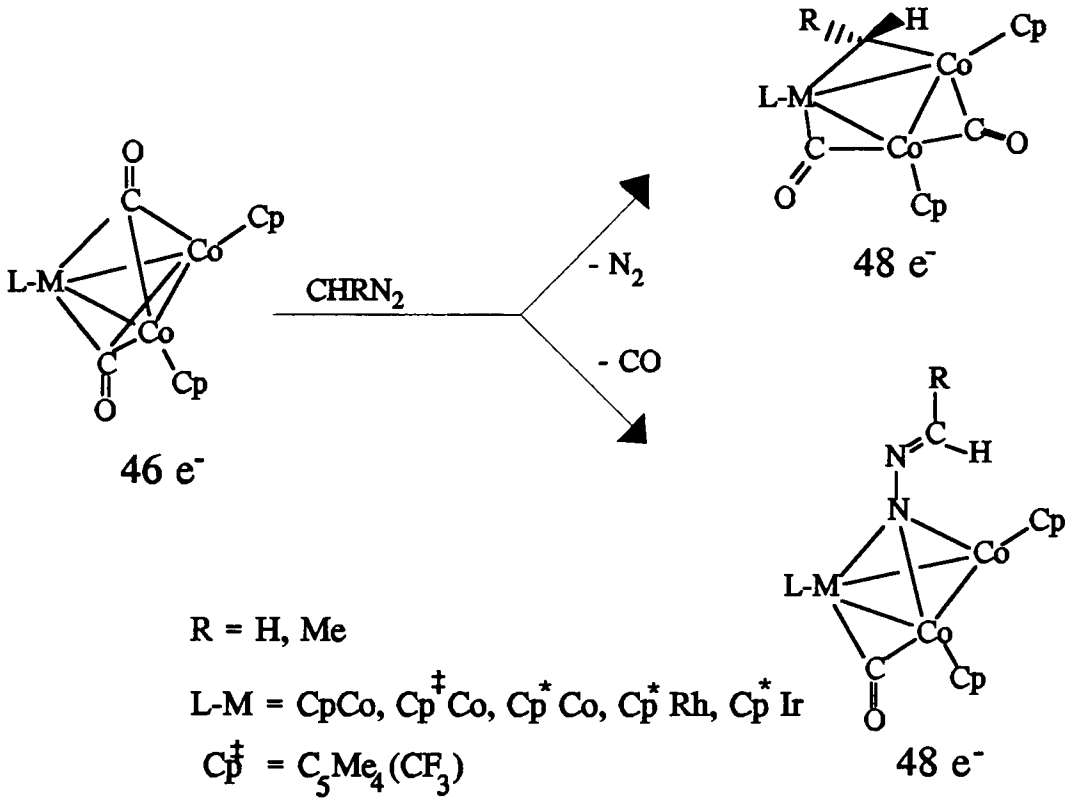

Figure 2.1: Reaction of the unsaturated trinuclear cluster complexes **1** - **5** with diazoalkanes illustrating the formation of carbene and diazoalkane adducts.

2.2. Reaction of the All-CpCo Cluster Complex $(CpCo)_3(\mu_3\text{-}CO)_2$ (5) with Diazomethane

The cluster complex $(CpCo)_3(\mu_3\text{-}CO)_2$ (**5**) is the most reactive one in the series and spontaneously decomposes in solution.[32] The reaction was therefore performed by adding a solution of diazomethane to the solid compound. As products, both the carbene and diazomethane adduct are obtained in about equal amounts. Chromatography achieves the separation of the two compounds, with the less polar carbene adduct eluting first.

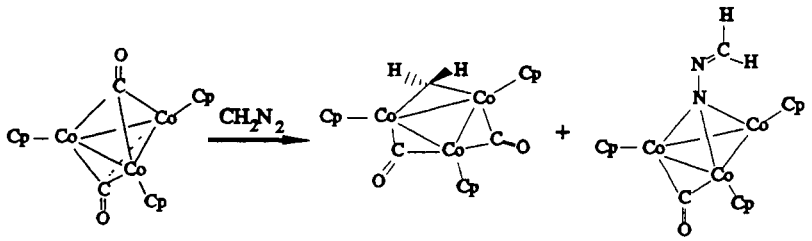

5 6 9

2.2.1. Carbene adduct $(CpCo)_3(\mu_2\text{-}CO)_2(\mu_2\text{-}CH_2)$ (6)

2.2.1.1. Crystal Structure

Figure 2.2 shows two views of the crystal structure of the carbene adduct **6**, and Table 2.1 summarizes selected bond distances. The Co-Co-Co angles are all close to 60° (60.2(1) and 59.92(5)°), with the carbonyl bridged edges slightly shorter (2.379(3) Å) than the one bridged by the carbene ligand (2.385(3) Å). A plane of symmetry perpendicular to the metal ring bisects the complex in the solid state and includes the unique cobalt atom Co(2), the CH_2 group and one carbon atom of the Cp ring bound to Co(2). The carbene and carbonyl ligands are all

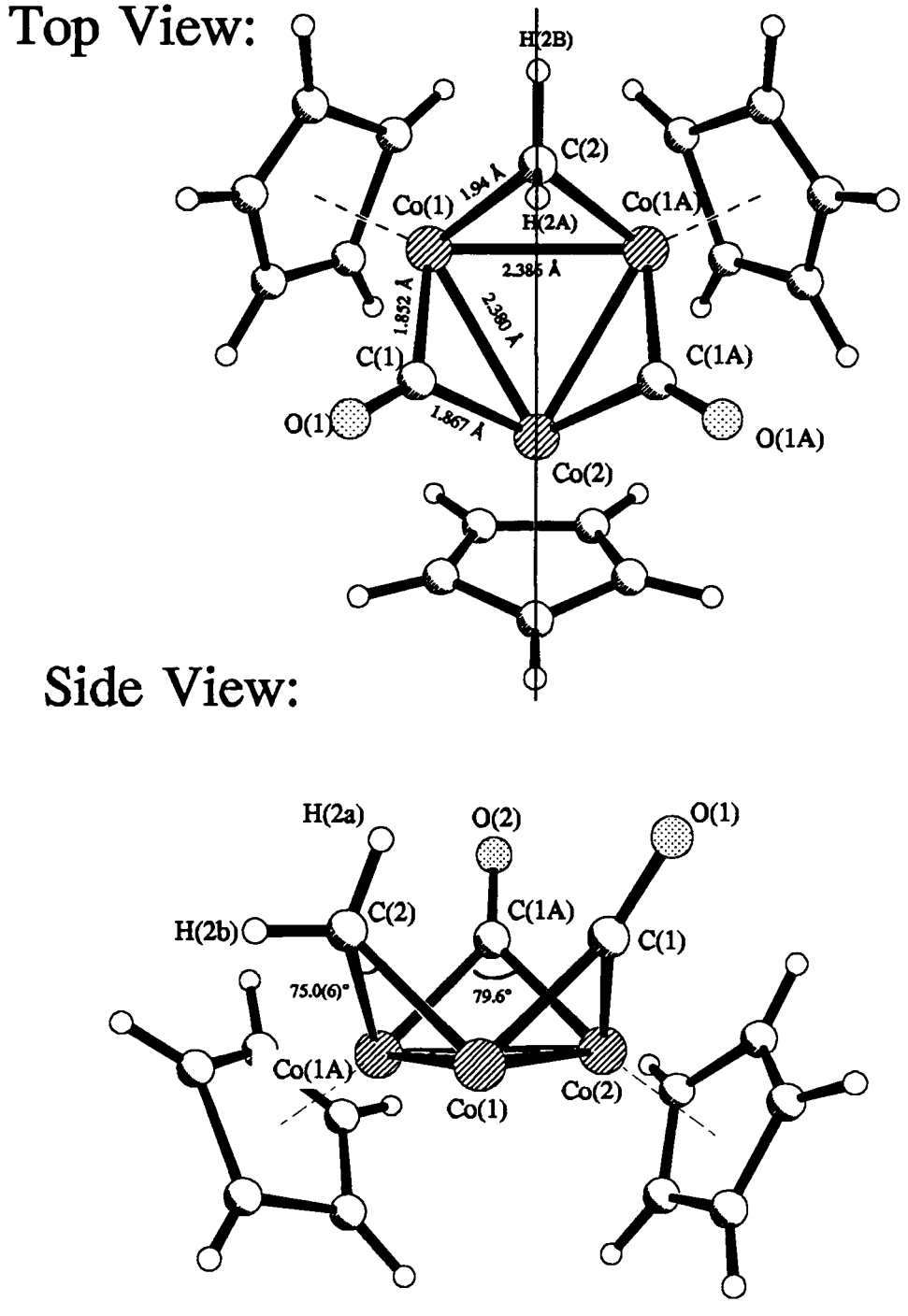

Figure 2.2: Crystal structure of **6**. The solid line indicates a mirror plane. In the side view, one Cp ligand has been omitted for clarity.

Table 2.1: Selected bond distances in **6.**

Bond Distance / Å			
Co2 C1	1.867(14)	Co2 C1	1.867(14)
Co2 Co1	2.380(3)	C2 Co1a	2.380(3)
Co1 Co1a	2.386(4)	C2 Co1	1.94(2)
Co1 C1	1.852(15)	Co1 C2	1.94(2)
Bond Angle / °			
Co1 Co2 Co1	60.16(11)	Co2 Co1 Co1	59.92(5)
Co1 C2 Co1a	75.9(7)	H2A C2 H2B	113.1
O1 C1 Co1	143.1(15)	O1 C1 Co2	137.2(14)
Co1 C1 Co2	79.6(6)		

bridging different Co-Co edges and are on the same side of the metal triangle similar to a number of tricarbonyl complexes like $Cp^*Ir(CpCo)_2(\mu_2\text{-}CO)_3$ or $(CpRh)_3(\mu_2\text{-}CO)_3$ containing three edge bridging carbonyl ligands.[33] These ligands are tilted out of the metal plane by an angle of 57.4° for the carbene and 56.8° for the carbonyl ligands. The coordination about the carbene carbon is distorted tetrahedral with a strongly reduced MCM angle of 75.0(6)°. One carbon-hydrogen bond is pointing up and is tilted towards the metal triangle (H2a), whereas the other one is directed outward horizontally away from the metal ring (H2b). The plane defined by the CH_2 moiety is perpendicular to the plane of the two carbene carbon-cobalt bonds as well as to the metal triangle and includes the plane of symmetry bisecting the molecule. The centroids of the Cp ligands are found below the metal plane by angles of 32.7 and 25.8° towards the

opposite face of the cluster resulting in an angles of 57.3 and 64.2° between the Cp ring planes and the plane of the metal triangle.

2.2.1.2. Spectroscopic Data of Carbene Adduct 6

Figure 2.3 shows the ^1H NMR spectrum of the carbene adduct **6** in CD_2Cl_2 at room temperature. The spectrum exhibits two signals for the protons of the Cp ligand with a relative intensity of 2:1. This is consistent with a static structure in which the carbene ligand is bridging one cobalt-cobalt edge causing two of the three CpCo vertices to be equivalent. Furthermore, two signals at 7.07 and 6.72 ppm are observed for the two diastereotopic methylene hydrogens of the carbene ligand as expected for a rigid group. A NOESY spectrum[34] (T = 300 K, τ = 2 s) exhibits a strong negative cross peak connecting the signals of the methylene protons with each other. The upfield methylene signal at 6.72 ppm displays a crosspeak with the signal of the two equivalent Cp rings consistent with the assignment that the upfield methylene signal is the one associated with the carbene hydrogen pointing outward towards the Cp rings on that edge (H2b) whereas the downfield signal belongs to the hydrogen pointing up (H2a). Another interesting feature of the ^1H NMR spectrum is the fact that the geminal coupling constant $^2J_{HH}$ between the two methylene protons is smaller than one Hertz. That is in contrast to similar carbonyl based trinuclear carbene complexes where a geminal coupling constants of around 5 Hz were observed.[5e, 7]

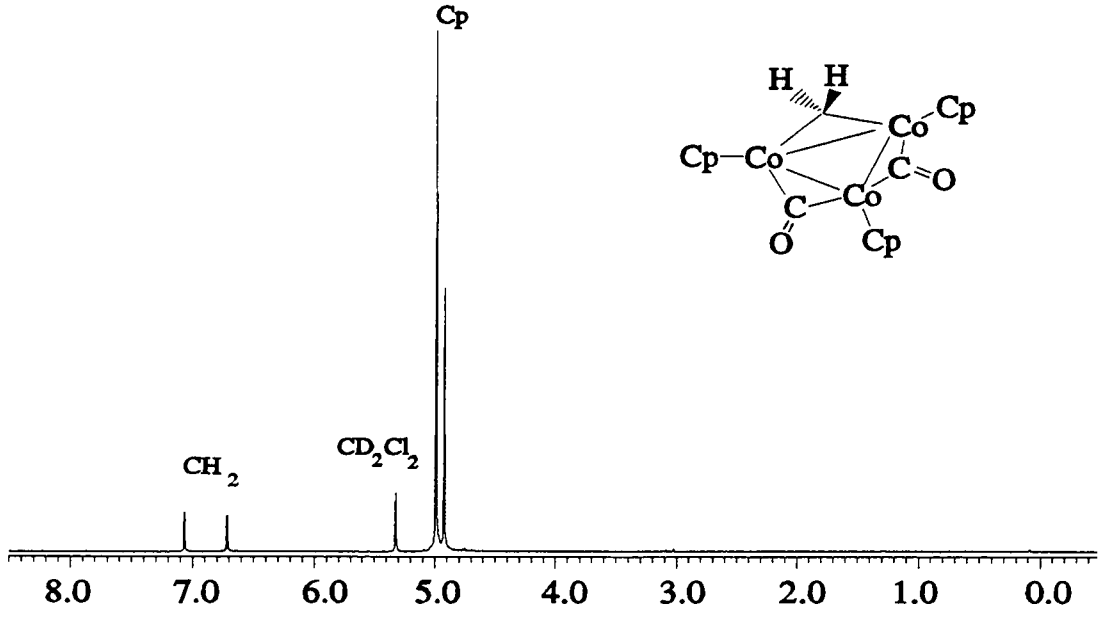

Figure 2.3: ^{1}H NMR spectrum of carbene complex **6**.

The ^{13}C-NMR spectrum is consistent with the conclusions drawn from the ^{1}H NMR spectrum. Two signals are observed in the Cp region and the signal of the carbene carbon at 139.1 ppm is consistent with an edge bridging carbene ligand.[23] In a proton coupled ^{13}C-NMR spectrum this signal is split into a triplet ($^{1}J_{CH} \approx$ 136-140 Hz) indicating equal or very similar coupling constants to the two diastereotopic protons of the CH_2 group. Additionally, a signal at 253.9 ppm is observed for the two equivalent carbonyl carbons bridging the remaining Co-Co edges. The signals of both the carbene and carbonyl carbons are significantly broadened by scalar coupling to the Co nuclei[35] thereby prohibiting a more accurate determination of the C-H coupling constant.

The IR spectrum (KBr) shows two carbonyl stretches at 1814 and 1766 cm^{-1} supporting the presence of edge bridging carbonyl ligands. The mass spectrum exhibits a very weak molecular ion peak at m/q = 442, but a strong peak for M^+- CO (relative intensity 3 : 100) indicating facile loss of CO (see chapter about carbyne-hydride formation below). No peak due to loss of two CO ligands is observed (m/q = 386 expected for M^+- 2 CO), however a fragment peak consistent with loss of one CO plus loss of H_2CO is observed (m/q = 384). The strongest fragment peak is due to the cobaltocenium cation Cp_2Co^+, m/q = 189. A summary of all NMR, IR and MS data is given in Table 2.2.

2.2.2. Diazomethane Adduct $(CpCo)_3(\mu_3\text{-}CO)(\mu_3\text{-}NNCH_2)$ (9)

2.2.2.1. Crystal Structure

Single crystals of the diazomethane adduct $(CpCo)_3(\mu_3\text{-}CO)(\mu_3\text{-}NNCH_2)$ (9) suitable for x-ray diffraction were obtained by recrystallization from methylene chloride / hexane at -20°C. A side view of the crystal structure is shown in Figure 2.4, and selected bond distances and angles are listed in Table 2.3. The three Co atoms are arranged in a triangle in which the Co-Co-Co angles are all equal to 60° within one degree. The diazoalkane coordinates to one face of the metal cluster with its terminal nitrogen atom, whereas the carbonyl ligand bridges the opposite face. The carbon-nitrogen bond distance is 1.260(6) Å, significantly shorter than in CH_2N_2 (1.34 Å)[36] and consistent with a C=N double bond (average for C=N 1.28 Å[37, 38]). The nitrogen-nitrogen bond distance of

Table 2.2: Spectroscopic data for carbene and diazomethane adducts of $(CpCo)_3(\mu_3\text{-}CO)_2$, **6** and **9**.

compound	$(CpCo)_3(\mu_2\text{-}CO)_2(\mu_2\text{-}CH_2)$ **6**	$(CpCo)_3(\mu_3\text{-}CO)(\mu_3\text{-}NNCH_2)$ **9**
^{1}H NMR	C_6D_6	C_6D_6
CH_2	7.63 d, $^2J_{HH}\approx$ 1 Hz, 1H 6.62 d, $^2J_{HH}\approx$ 1 Hz, 1H	7.95 d, J≈13 Hz, 1H 7.08 d, J≈13 Hz, 1H
Cp	4.536 s, 10H; 4.532 s, 5H	4.56 s, 15 H
^{13}C NMR	CD_2Cl_2	C_6D_6
	253.86 (CO), 139.11 (t, CH_2) 89.61 (Cp), 88.58 (Cp)	141.53 (dd, J_{CH}=162 Hz, J_{CH}=181 Hz, CH_2); 83.86 (d, Cp)
IR (KBr)	1814, 1766;	1667
MS (EI)	442 (1%, M^+); 414 (35%, M^+- CO); 384 (32%, M^+ - CO, H_2CO); 189 (100%, Cp_2Co^+)	442 (100%, M^+); 414 (6%, M^+- CO); 387 (24%, M^+- CO, HCN); 321 (100%, M^+- CO, HCN, CpH) HRMS: M^+ = 441.93261 (calc. 441.9337).

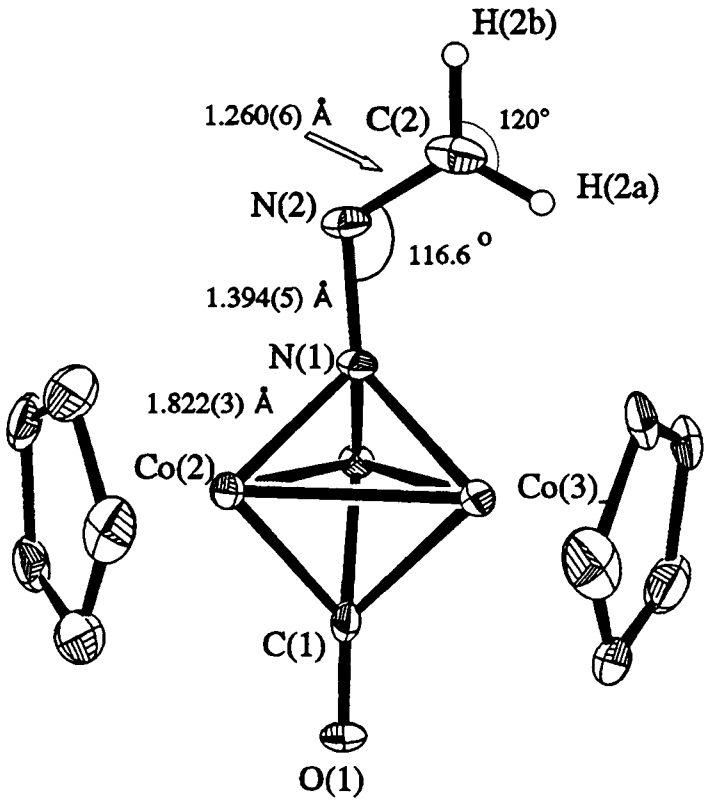

Figure 2.4: Crystal structure of **9**. One Cp ligand has been removed for clarity.

Table 2.3: Selected bond distances and -angles in the diazomethane complex **9**.

Bond distance / Å			
Co(1)-N(1)	1.821(3)	Co(1)-C(1)	1.970(5)
Co(1)-Co(3)	2.3879(8)	Co(1)-Co(2)	2.3900(9)
Co(2)-N(1)	1.822(3)	Co(2)-C(1)	1.942(4)
Co(2)-Co(3)	2.4218(8)	Co(3)-N(1)	1.832(4)
Co(3)-C(1)	1.979(4)	C(1)-O(1)	1.189(5)
C(2)-N(2)	1.260(6)	N(1)-N(2)	1.394(5)
Bond angles / °			
Co(3)-Co(1)-Co(2)	60.91(3)	Co(1)-Co(2)-Co(3)	59.50(2)
Co(1)-Co(3)-Co(2)	59.59(2)	O(1)-C(1)-Co(2)	136.4(3)
O(1)-C(1)-Co(2)	133.9(3)	O(1)=C(1)-Co(3)	135.0(3)
N(2)-N(1)-Co(1)	127.2(3)	N(2)-N(1)-Co(2)	126.8(3)
N(2)-N(1)-Co(3)	137.2(3)	C(2)-N(2)-N(1)	116.9(4)

1.394(5) Å, on the other hand, is significantly longer than in free CH_2N_2 (1.12 Å)[36] and resembles a N-N single bond (1.43 Å in $H_2N_2O_2$) rather than a N=N double bond (1.21 Å in N_2F_2).[39] The angle N(1)-N(2)-C(2) is 116.9(4)°, compared with 180° in CH_2N_2, suggesting sp^2 hybridization for N(2). Such an angle indicates that coordinated diazomethane might be better described as a hydrazone ligand. As a result, the CH_2 group is bent towards one CpCo vertex with one hydrogen pointing up and one pointing down.

2.2.2.2. Spectroscopic Data

In Table 2.2 the spectroscopic data found for the diazomethane adduct **9** are summarized. The room temperature proton NMR spectrum shown in Figure

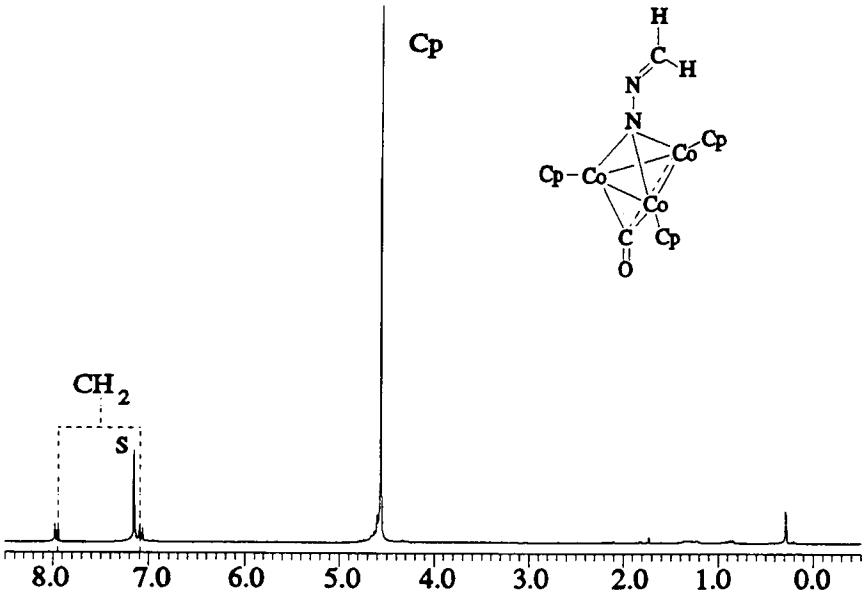

Figure 2.5: ^1H NMR spectrum of the hydrazone complex **9**.

2.5 exhibits only one signal for the Cp hydrogens indicating that all three CpCo edges are equivalent. Such an equivalency can be explained by fast rotation of the $N=CH_2$ moiety about the N-N bond. One can not rule out the possibility that the chemical shift difference induced by a static $N=CH_2$ moiety is too small to be resolved for the Cp groups. However, fast rotation about the N-N bond would be consistent with a single bond as found in the crystal structure. Two signals are observed for the two methylene hydrogens, indicating that there is no fast rotation about the C=N bond as expected for a double bond. The spectroscopic data therefore support the designation of the coordinated diazomethane as a hydrazone. The shifts of the methylene protons for the methylene group of the hydrazone ligand are in the same region as the ones for the carbene ligand in **6**. In contrast to the carbene ligand, however, a large geminal coupling is observed between the two hydrazone hydrogens, $^2J_{HH}$ = 13 Hz.

In agreement with the ^1H NMR spectrum, the ^{13}C NMR spectrum exhibits only one signal for the Cp ring carbons, and a signal for the $NNCH_2$ group at 141.5 ppm. We were not able to observe a signal for the carbonyl carbon which would be expected at 250-270 ppm.

An interesting feature concerning this complex is revealed by the proton coupled ^{13}C-NMR spectrum. As shown on top of Figure 2.6, a doublet of doublets is observed instead of the triplet found for the carbene adduct **6**. This indicates that the two diastereotopic methylene protons have different coupling constants $^1J_{CH}$ to the methylene carbon (162.6 and 180.8 Hz). In order to assign

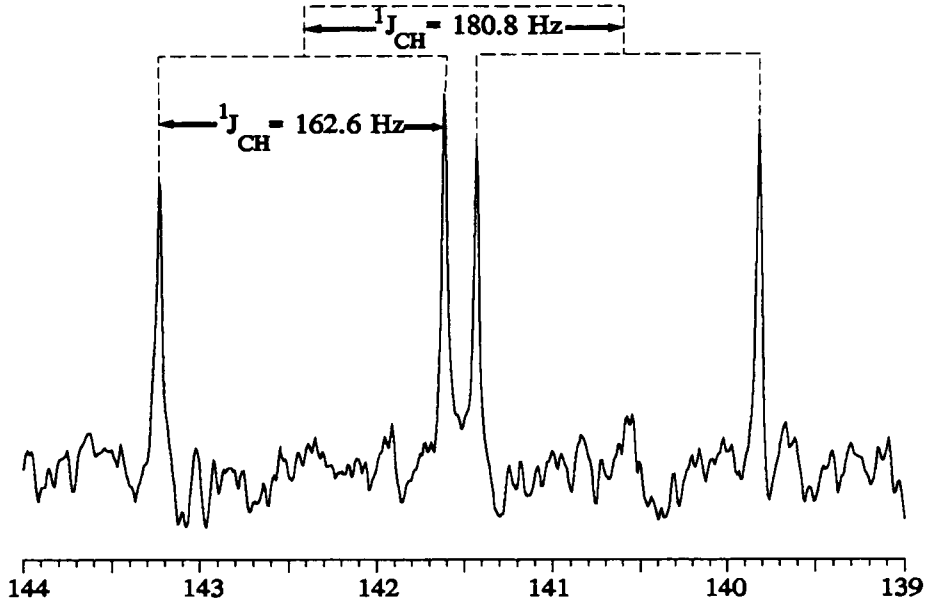

* Signal associated with solvent signal.

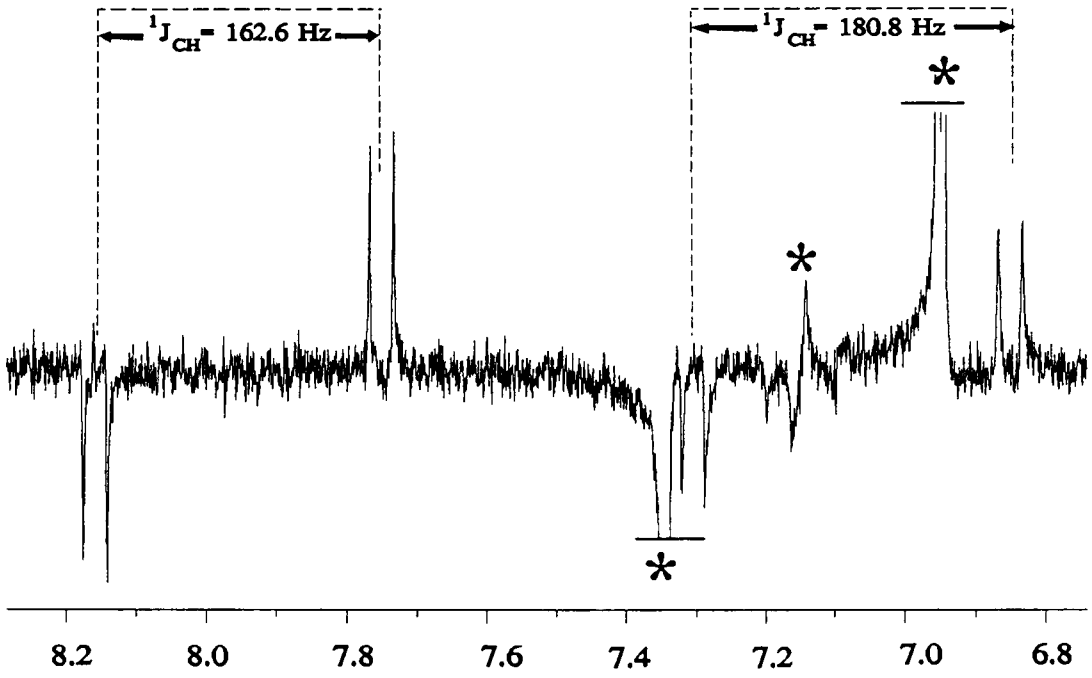

Figure 2.6: Methylene region of the proton coupled ^{13}C NMR spectrum of **9** (top); ^{13}C satelite peaks in the ^1H NMR spectrum (bottom).

the coupling constants to the two methylene proton signals, the acquisition of proton coupled carbon spectra with selective decoupling of one of the two methylene protons was attempted. However, due to the proximity of the signals in the proton spectrum it was not possible to fully decouple one carbon proton coupling without also effecting the other one. The remaining doublet therefore always showed a reduced splitting, prohibiting a clear assignment. An alternative method of assigning the two coupling constants involves observing the carbon-13 satellites in the proton spectrum. These appear as doublets with 0.55 % intensity of the main proton signal. In order to distinguish these signals from impurities or spinning sidebands, a pulse sequence employing a double quantum filter was applied which suppresses all signals arising from protons not bound to ^{13}C. Such an experiment yields the spectrum shown in the bottom of Figure 2.6 with the ^{13}C satellite peaks as an antiphase doublet revealing the carbon-proton coupling constants. One can see that the downfield proton exhibits the smaller coupling constant of 162 Hz, whereas the larger coupling of 180.8 Hz belongs to the upfield proton signal.

The difference in $^1J_{CH}$ coupling constants is due to the nitrogen lone pair. In compounds containing a N=CHR group, a proton *cis* to the nitrogen lone pair experiences a larger ^{13}C-^1H coupling than a proton *trans* to the lone pair of the nitrogen.[40] Aldoxime ($H(CH_3)C=N-OH$) for example shows a C-H coupling of 163 Hz for the E-isomer where the hydrogen is *trans* to the lone pair and 177 Hz for the Z-isomer with the hydrogen *cis* to the lone pair. Similar effects have been

studied for azirines. In the case of the $(CpCo)_3(\mu_3\text{-}CO)(\mu_3\text{-}NNCH_2)$ the proton pointing up away from the Co triangle is *cis* to the nitrogen lone pair. It is therefore expected to show the larger C-H spin-spin coupling whereas the hydrogen pointing downwards is the one with the smaller one. One can therefore assign the downfield signal at 7.93 ppm with the smaller carbon-proton coupling of 162 Hz to the C-H bond pointing down (H2a) whereas the upfield signal at 7.08 ppm exhibiting the larger C-H coupling belongs to the bond pointing up (H2b). These findings are also supported by NOE measurements; upon irradiation of the Cp proton resonance, the proton signal at 7.95 ppm exhibited twice the NOE as the signal at 7.08 ppm indicating that the downfield resonance belongs to the hydrogen closer to the metal triangle. These results are summarized in Figure 2.7.

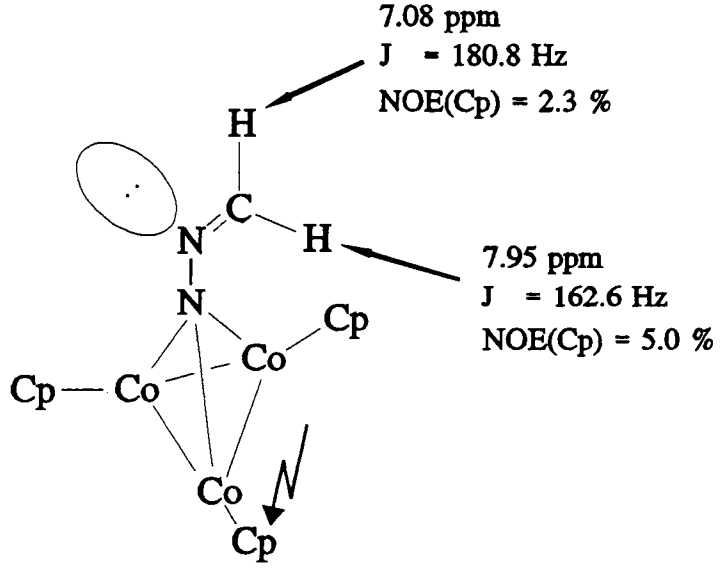

Figure 2.7: Assignment of methylene protons in **9** by C-H coupling constants and NOE measurements.

The IR spectrum of **9** exhibits one band for the CO stretching vibration at 1667 cm^{-1} consistent with one face bridging carbonyl ligand. The MS shows a strong parent ion peak with respect to the fragment peak due to loss of one CO ligand (90:5) indicating that loss of CO is less facile than in the corresponding carbene complex. Furthermore, a fragment peak due to the combined loss of CO and HCN is observed. It should be noted that the nominal mass of the parent ion of the hydrazone complex is the same as that for the carbene complex **6**. A high resolution MS and elemental analysis, however, confirm the presence of the hydrazone ligand in the structure of **9** (experimental M^+ = 441.93261, calculated for **9** 441.9337).

2.3. Reaction of the Heteronuclear Complexes $Cp^*M(CpCo)_2(\mu_3\text{-}CO)_2$ and $Cp^‡Co(CpCo)_2(\mu_3\text{-}CO)_2$ with Diazomethane

The products obtained from the reaction of the heteronuclear cluster complexes $Cp^*M(CpCo)_2(\mu_3\text{-}CO)_2$, M = Co, Rh, Ir (**1** - **3**) appears to depend mainly on the identity of the metal M. In the case of M = Co (**3**) only the hydrazone adduct **10** is observed in significant amounts, whereas for M = Ir only carbene adduct **8** is found. M = Rh yields a mixture of the carbene adduct **7** and the hydrazone adduct **11**. Reaction of the complex $Cp^‡Co(CpCo)_2(\mu_3\text{-}CO)_2$ (**4**) yields the corresponding hydrazone complex **12** only. $Cp^‡$ stands for the tetramethyl-trifluoromethyl-cyclopetadienyl ligand which sterically resembles the Cp^* ligand, but is electronically more similar to the Cp ligand.[41]

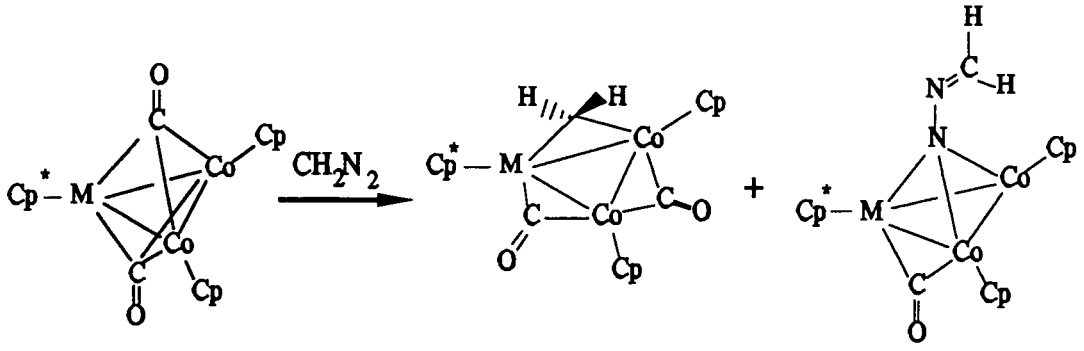

M =	Co	1	-	10
	Rh	2	7	11
	Ir	3	8	-
$Cp^{\ddagger}$	Co	4	-	12

2.3.1. Crystal Structure of $Cp^*Rh(CpCo)_2(\mu\text{-}CO)_2(\mu\text{-}CH_2)$

Two views of the crystal structure of **7** are shown in Figure 2.8. The general features are similar to the ones of the structure of $(CpCo)_3(\mu_2\text{-}CO)_2(CH_2)$. The carbene ligand bridges one Rh-Co edge, whereas the carbonyl ligands bridge the remaining Rh-Co and the Co-Co edge. The crystal exhibited some disorder between the CO ligand bridging a Rh-Co edge and the carbene ligand, caused by the fact that both enantiomers of **7** are present in the crystal lattice. Both carbonyl ligands and the carbene ligand are bent upwards out of the plane defined by the metal atoms forming a "crown" type structure analogous to the all CpCo carbene complex **6**. For the carbene ligand the angle between the Rh-Co-C plane and the metal triangle is 59.2°, whereas for the carbonyl ligands the corresponding angles are 56.4 ° and 54.4°. The Cp and Cp^* ligands, on the other hand, are all found below the metal triangle, tilted by 31.3°, 32.4° (Cp

Top Viev:

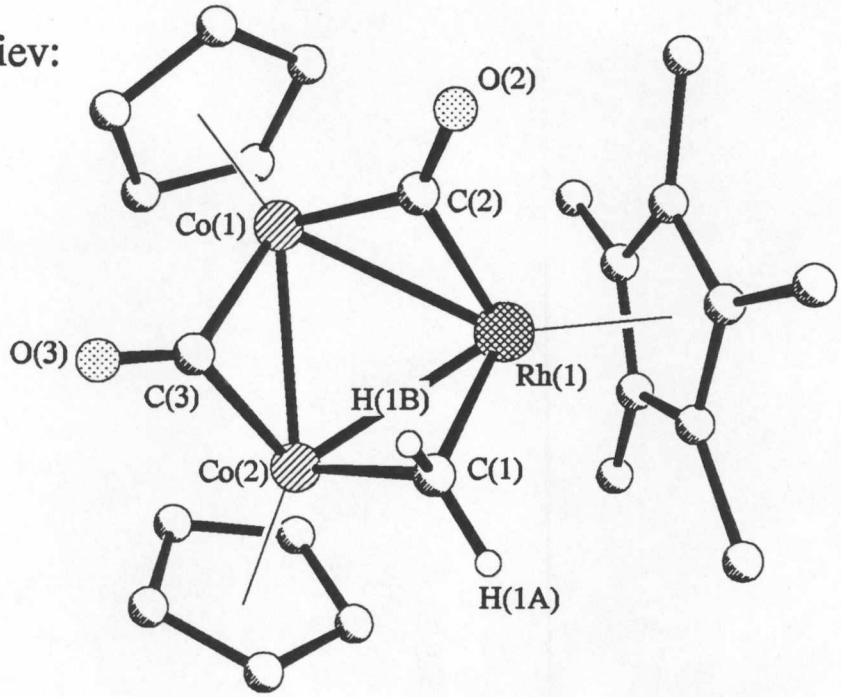

Side View:

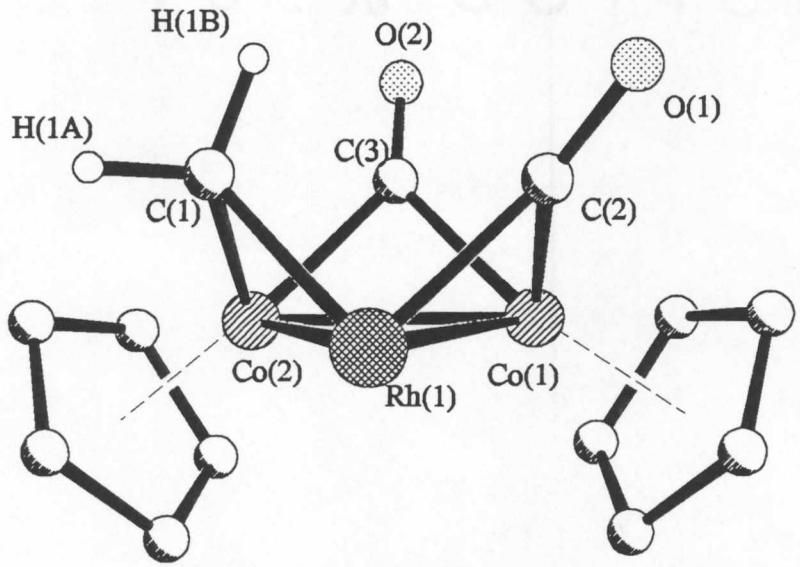

Figure 2.8: Crystal structure of **7**. In the bottom view the Cp^* ligand has been omitted for clarity.

21.7 ° (Cp^* ligand) away from the positions for a cluster with two symmetric faces. The corresponding angles between the Cp and Cp^* planes on one side and the $RhCo_2$ plane on the other are 58.7° and 57.6° for the Cp ligands and 68.3° for the Cp^* ligand. The HCH plane of the carbene ligand is perpendicular to the one defined by the Co(2)-C(1)-Rh(1) triangle. One of the carbene C-H bonds is pointing outward, horizontally away from the metal triangle, whereas the other one is pointing up and is slightly bent towards the center of the metal triangle.

2.3.2. Spectroscopic Data

The spectroscopic data for these complexes are summarized in Table 2.4. Figure 2.9 shows the ^1H NMR spectrum of the Rh complex **7** which also very closely resembles the one of the corresponding Ir complex **8**. Both carbene complexes exhibit two signals for the hydrogens of the Cp ligands. This indicates that the carbene ligand bridges the Cp^*M-CpCo edge resulting in two inequivalent CpCo edges. No evidence of the isomer containing the carbene bridging the Co-Co edge is found in the initial reaction mixture.

However, upon standing in solution, the carbene ligand in complex $Cp^*Rh(CpCo)_2(\mu_2\text{-}CO)_2(\mu\text{-}CH_2)$ is observed to move between the different edges achieving an equilibrium between the different isomers in approximately 8h at room temperature. The initially formed isomer is therefore from now on referred to as **7a**, whereas the subsequently observed isomer is isomer **7b**. The carbene migration process will be described in more detail below (subchapter 2.4).

Table 2.4: Spectroscopic data of the carbene and hydrazone adducts **7, 8, 10 - 12.**

	carbene		hydrazone		
L-M	Cp^*Rh (7a)	Cp^*Ir (8)	Cp^*Co (10)	$Cp^‡Co$ (12)	Cp^*Rh (11)
^{1}H NMR (ppm)	C_6D_6[a]	C_6D_6[b]	C_6D_6	C_6D_6	C_6D_6
CH_2	7.34 d $^2J_{HH}$=0.5 Hz 6.04 dd $^2J_{HH}$=0.5 Hz $^3J_{RhH}$=2.1 Hz	7.36 d $^2J_{HH}$=1Hz 6.05 d $^2J_{HH}$=1Hz	7.91 d $^2J_{HH}$=13.7 Hz 7.23 d $^2J_{HH}$=13.8 Hz	7.80 d, $^2J_{HH}$ =13.5Hz 7.14 d, $^2J_{HH}$ =13.5 Hz	7.57 d ^2J= 13.8 Hz 7.12 d
Cp	4.57, 4.49	4.59, 4.55	4.48 (10H)	4.481 (10H)	4.56 s (10H)
Cp^*	1.52 (15H)	1.70 (15H)	1.56 (15H)	1.89, 1.43	1.61 s (15H)
^{13}C NMR (ppm)	CD_2Cl_2, 170K	CD_2Cl_2		C_6D_6	C_6D_6
CO	262.7, 250.0 d J_{Rh-C}=50 Hz	268.3, 234.4	276.7 (s)	273.3	
CH_2	138.3 d, $^1J_{Rh-C}$= 33 Hz $^1J_{CH}$=139, 147 Hz	112.9 d	139.4 dd $^1J_{CH}$=162 Hz $^1J_{CH}$=180 Hz	140.6 dd $^1J_{CH}$ =163 Hz $^1J_{CH}$=181 Hz	139.9
Cp	87.5, 87.4	88.8, 88.3	83.1 (d)	83.69 d	83.2 (d)
Cp^*	101.8 d, J_{Rh-H} = 4 Hz; 9.8	98.6, 9.7	92.8(s), 9.5(q)	127.3, $^1J_{CF}$= 270Hz; 95.5; 94.1; 9.46; 8.98, $^4J_{CF}$ = 2 Hz	97 (s), 9.95 (q)
IR ν_{CO} (cm^{-1})	hexane:[a] 1761, 1797 KBr: 1793, 1826	KBr: 1782, 1752, 1743[b]	KBr: 1670[a]		KBr: 1657, 1680
MS (m/e)	556 (0.5, M^+) 528(100,-CO) 500(70,-2CO) 303 (72, $[Cp^*RhCp]^+$) 189 (10, Cp_2Co^+)	646 (3, M^+) 618 (58,-CO) 590(100,-2CO) 393 (14, $[Cp^*IrCp]^+$) HRMS: 590.0383 (exp) 590.0406 (cal)	512 (100, M^+); 484 (8, -CO); 457 (22, -CO, -HCN); 391 (72, -CO, -HCN, -CpH); 259 (41, $[Cp^*CoCp]^+$) 189(19, Cp_2Co^+)	566 (100, M^+) 538 (11, -CO) 511 (6, -CO, -HCN); 510 (7, -CO, $-N_2$ 414 (31, -CO, -CpCo); 313 13, $[Cp^‡CoCp]^+$ HRMS: 565.981 (exp) 565.984 (cal)	556 (100, M^+); 528 (3, -CO); 501 (24, -CO, -HCN); 500 (20, -CO, $-N_2$); 435 (88, -CO, -HCN, -CpH); 303 (81, $[Cp^*RhCp]^+$)

a) Ref. 30 b) Ref. 11

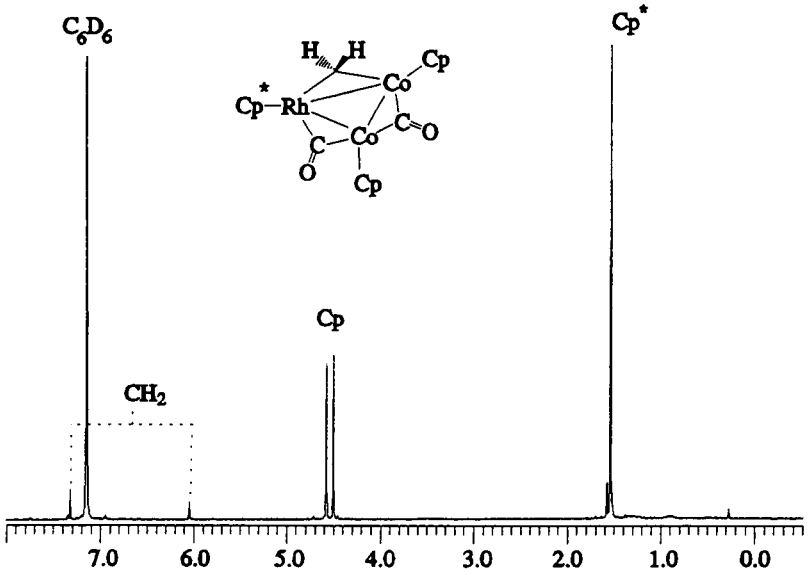

Figure 2.9: ^{1}H NMR spectrum of the carbene complex **7**.

The diastereotopic methylene protons are separated by more than one ppm and show a geminal coupling constant smaller than 1 Hz. NOESY spectra show cross peaks connecting the upfield methylene proton with one Cp and the Cp^* signal whereas the downfield methylene signal shows no cross peaks with either signal (Figure 2.10). Similar to the $(CpCo)_3$ complex **6**, the upfield carbene signal is associated with the proton directed outward. In the Rh complex **7a** the upfield methylene signal shows a significant coupling to the rhodium ($^{2}J_{RhH}$ = 2.1 Hz). Resolution enhanced spectra reveal a $^{2}J_{RhH}$ of 0.5 Hz for the downfield methylene proton as well. Homonuclear decoupling has been used to distinguish the heteronuclear coupling J_{RhH} from the homonuclear coupling J_{RhH} (Figure 2.11).

The ^{13}C NMR spectrum of the Rh complex **7a** shows two signals for the carbonyl carbons. Only one of the two carbonyl carbons shows a coupling to the

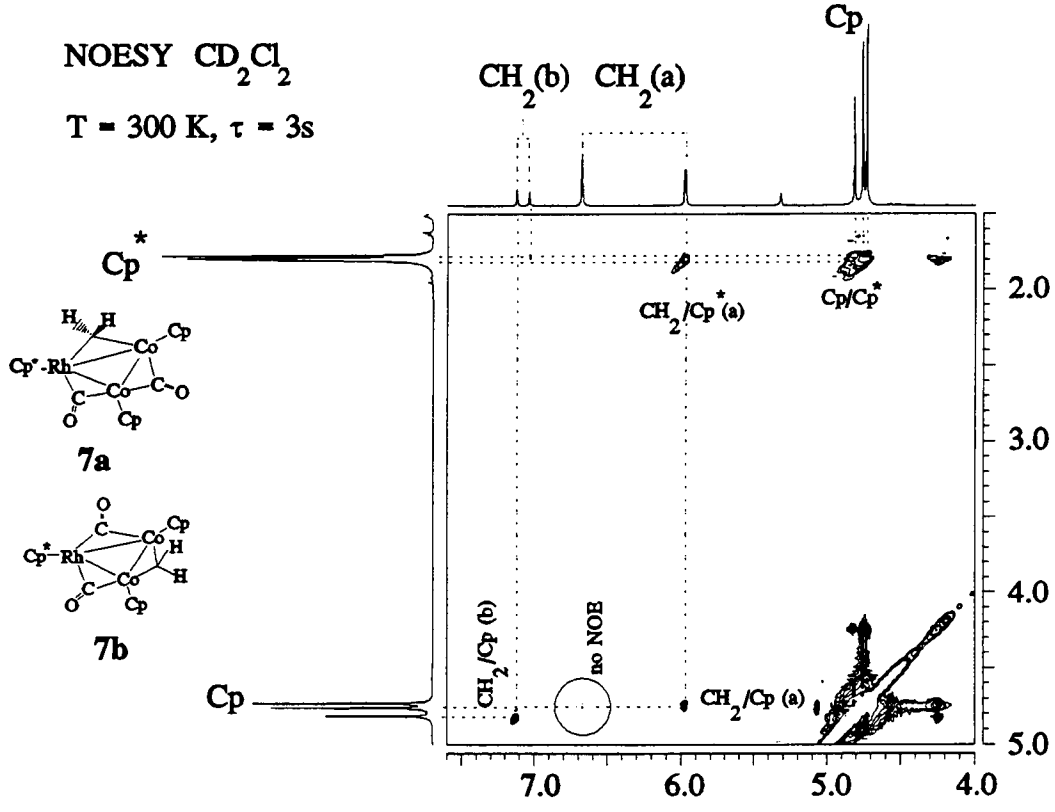

Figure 2.10: NOESY spectrum of the Rh complex **7** at room temperature. The small signals in the carbene region are due to isomer **b.**

Rh ($^1J_{RhC}$ = 50 Hz) consistent with one carbonyl ligand on the Co-Co and one on a Rh-Co edge (Figure 2.12). The methylene carbon resonance of 138.3 ppm is observed in the range consistent with an edge bridging carbene ligand (100-210 ppm).[23] The Cp*Ir containing complex **8** exhibits a similar spectrum, however one should note the upfield shift of approximate 26 ppm observed for the carbene carbon when compared with both the Rh complex **7a** or the all-CpCo complex **6.** The carbon-proton coupling constants for the carbene carbon with the two methylene protons are similar but not equal ($^1J_{CH}$= 139 and 147 Hz in the case of **7a**). The carbene carbon of the rhodium complex **7a** exhibits a carbon-rhodium

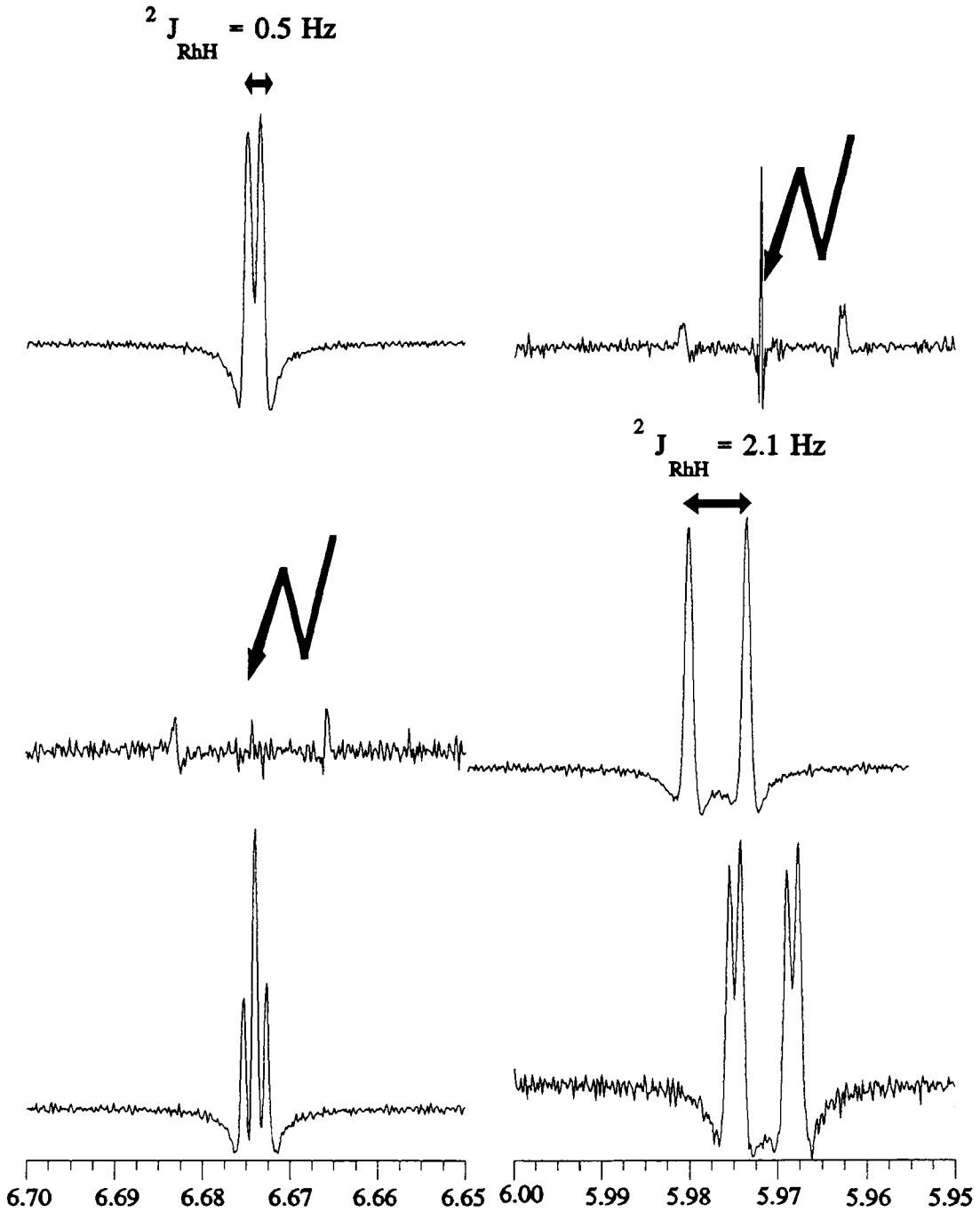

Figure 2.11: Carbene region of the ^1H NMR spectrum of **7a.** (sine window, ssb = 0). Bottom: undecoupled spectrum Middle: signal at 6.67 ppm irradiated Top: signal at 6.97 ppm irradiated.

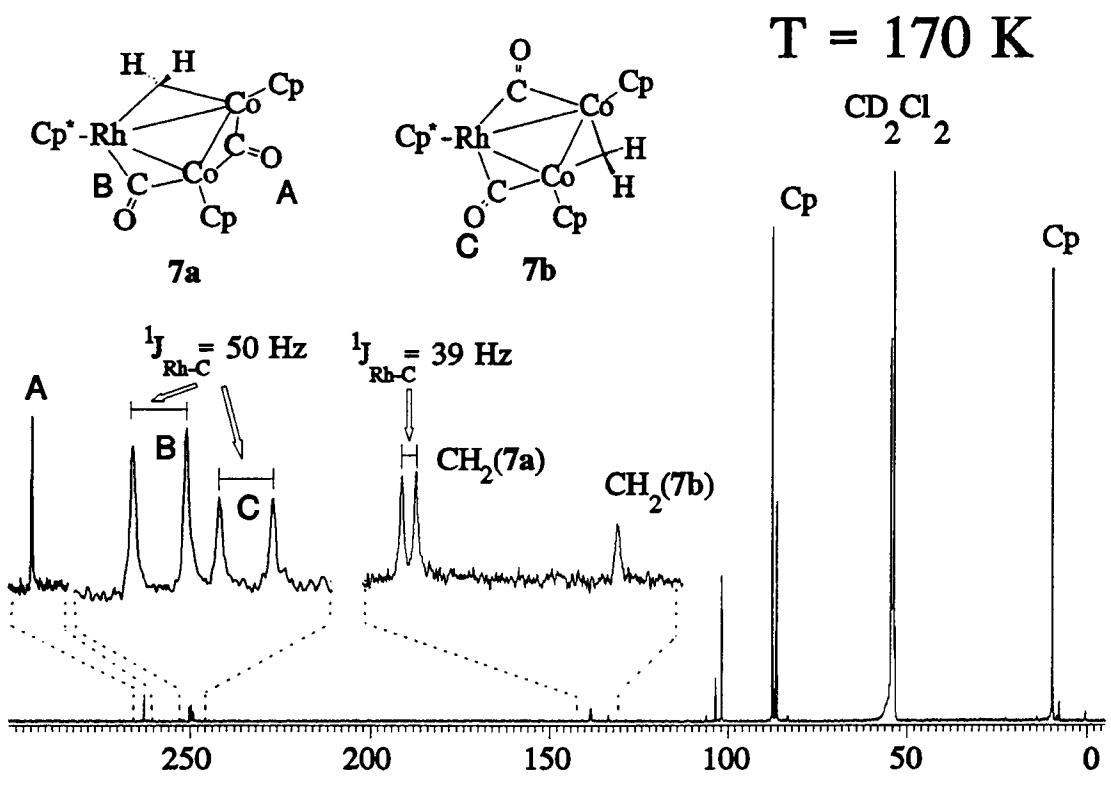

Figure 2.12: ^{13}C NMR spectrum of the carbene complex **7**.

coupling ($^1J_{RhH}$ = 30 Hz) consistent with the position of the carbene ligand on a Rh-Co edge. Similar to the all-CpCo carbene complex **6** the mass spectra of the carbene complexes **7** and **8** exhibit a very weak molecular ion peak, but shows a very strong signal due to the fragment formed by loss of one CO ligand.

The hydrazone adducts **10**, **11** and **12** exhibit spectra very similar to the ones observed for $(CpCo)_3(\mu_3\text{-}CO)(\mu_3\text{-}NNCH_2)$ (see Table 2.4). Only one signal is observed for the protons of the Cp ligands in all cases.

2.4. Reaction with Diazoethane

Reaction of the unsaturated trinuclear complexes with diazoethane yields exclusively the hydrazone adducts **13** - **15**. In the case of $Cp^*Ir(CpCo)_2(\mu_3\text{-}CO)_2(\mu_3\text{-}NNCHMe)$ (**16**) the adduct appears to be very unstable and decomposes to unknown products when purification by chromatography is attempted, even at low temperature. The Cp^*Co containing complex **14** has already been completely characterized by Finniss,[30] whereas his work mentions only partial data for the

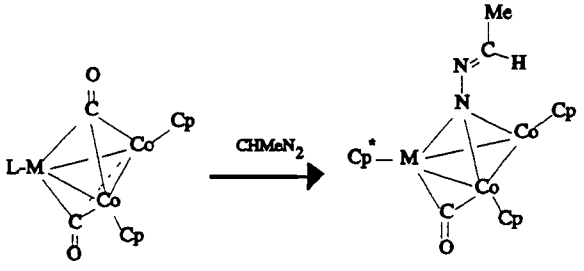

L-M =			
	CpCo	5	13
	Cp^*Co	3	14
	Cp^*Rh	2	15
	Cp^*Ir	1	16

Cp^*Rh complex **15**. The methylene carbons in both **13** and **15** exhibit a carbon-proton coupling constant of $^1J_{CH}$ = 160 Hz indicating that the hydrogen is *trans* to the lone pair on the nitrogen and pointing downwards towards the metal cluster. Accordingly, the methyl group is pointing up away from the metal triangle. These observations are consistent with the crystal structure reported for the Cp^*Co analogue **14**.[30] A summary of the spectroscopic data for all diazoethane complexes is shown in Table 2.5.

Table 2.5: Spectroscopic data of diazoethane adducts $LM(CpCo)_2(\mu_3\text{-}CO)(\mu_3\text{-}NNCHMe)$

LM	CpCo (13)	Cp*Co a/b[a)] (14)	Cp*Rh (15)	Cp*Ir (16)
^{1}H NMR	C_6D_6:	C_6D_6	CD_2Cl_2:	C_6D_6
CHMe, $CHCH_3$	8.46 (q) 1.81 (d) $^3J_{HH}$=5.5 Hz	8.46 / 7.74 1.95 / 1.81 $^3J_{HH}$=5.5 Hz	8.26 (q) 2.18 (d) $^3J_{HH}$ = 5.6 Hz	8.07 (q) 1.73 (d)
Cp Cp*	4.60 -	4.53 / 4.39 1.59 / 1.65	4.53 1.715	4.44 1.85
^{13}C NMR	CD_2Cl_2:	CD_2Cl_2	CD_2Cl_2:	
CO	277.6	257.5 / 257.5	273	
CHMe	153.7 dd $^1J_{CH}$=160.5 Hz $^2J_{CH}$=7.3 Hz	151.0 / 148.8	154.5 dq $^1J_{CH}$ = 160 Hz $^2J_{CH}$ = 7 Hz	-
$CHCH_3$	19.3 qd $^1J_{CH}$=127.9 Hz $^2J_{CH}$=11.0 Hz	19.2 / 15.5	20.7 qd $^1J_{CH}$=127.7 Hz $^2J_{CH}$ = 11 Hz	
Cp Cp*	84.1 s -	83.2 / 83.6 9.63 / 9.35	85.1 (d) 99.4 (s), 12.0 (q)	
IR	(KBr): 1697 cm^{-1}	KBr: 1671	(hexane): 1682 cm^{-1}	
MS	456 (88%, M^+) 428 (5%, -CO) 387 (22%, -CO, -MeCN) 321 (100%, -CO, -MeCN, -CpH) 189 (85%, $Cp_2Co^{\bullet +}$)	526 (M^+)	567 (100%, M^+) 542 (8%, -CO) 435 (90%, -CO, -MeCN,-Cp-H) 303 (80%, $[Cp^*RhCp]^+$) HRMS: 569.998(exp) 570.000(cal)	

a) Ref. 30: 2 isomers are mentioned for this compound (see text)

For all the cases studied in this thesis (**13**, **15**, and **16**), only this isomer is observed in which the methyl group of the hydrazone ligand is directed away from the metal triangle. On the other hand, in reference 30 mention is made of two isomers isolated in the case of **14**, the data of which are also included in Table 2.5. Isomer **14a** is the hydrazone adduct with the methyl group pointing up as found in the crystal structure mentioned above. No description of the nature of the second isomer **14b** is given, however the fact that the CHMe resonance in the ^{1}H NMR spectrum of **14b** is much further upfield than in **14a** is consistent with the methyl group in isomer **14b** pointing down:

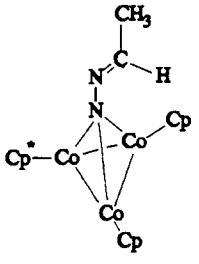

14 a

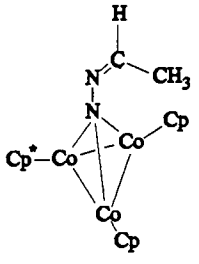

14 b

No carbon-proton coupling constants were reported which would distinguish between the two different protons pointing up and down.

2.5. Carbene Mobility on the Cluster Surface

One important property of carbene ligands on metal surfaces is their ability to move along the surface. Surface mobility is believed to play an important role in the coupling of these fragments to form hydrocarbon chains. A theoretical study by Hoffmann suggests that carbene migration on a metal surface should be

relatively facile.[2] There have been so far no experimental studies of carbene mobility on metal surfaces, but carbene migration along the edges of a molecular cluster complex has been reported.[5d] The following section describes the observation of carbene mobility in the complexes described above. The focus of this discussion will be on the Rh containing complex **7** for which this process was studied in more detail than for the other ones.

2.5.1. Rh-Co to Co-Co Edge Isomerization in $Cp^*Rh(CpCo)_2(\mu_2\text{-}CO)(CH_2)$

When the carbene complex **7a** was left in solution at room temperature for several days, a second set of signals was observed to grow in.[30] This new set still exhibited two signals for the carbene protons, but only one for the Cp protons and was therefore attributed to an isomer of this complex in which the carbene ligand bridging the Co-Co instead of the Rh-Co edge (see Table 2.6 and Figure 2.13):

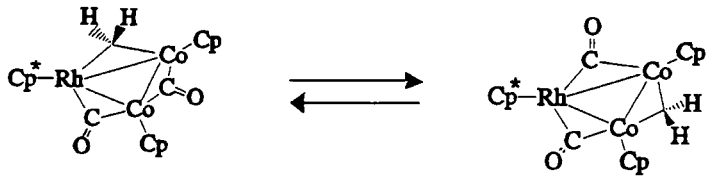

7a **7b**

Finniss proposed that the isomer with the carbene ligand on a Rh-Co edge (isomer **7a**) is the kinetic isomer whereas the second one with the carbene on the Co-Co edge (isomer **7b**) was the thermodynamic isomer.[30] A closer examination of this process, however, has revealed that the conversion **7a** → **7b** does not proceed to completion but that an equilibrium is reached in which both isomers

Table 2.6: Spectroscopic data of the different positional isomers of **7**. Solvent: CD_2Cl_2

CH_2 Bonding Mode	μ_2-(Rh-Co) **7a**	μ_2-(Co-Co) **7b**	μ_3- **7c**
^{1}H NMR			
CH_2	6.68 J_{HH} = 0.5 Hz, J_{RhH} = 0.6 Hz	7.02 J_{HH} = 0.5 Hz, J_{RhH} < 0.2 Hz	8.3 J_{RhH} = 1.4 Hz
	5.98 J_{HH} = 0.5 Hz, J_{RhH} = 2.4 Hz	7.12 J_{HH} = 0.5 Hz, J_{RhH} = 0.6 Hz	
Cp	4.73, 4.79	4.82	4.57
Cp^*	1.80 J_{RhH} = 0.5 Hz	1.77 J_{RhH} = 0.5 Hz	1.62 J_{RhH} = 0.6 Hz
^{13}C NMR			
CO	262.7	249 J_{RhC} = 50 Hz	
	250.0 J_{RhC}=50 Hz		
CH_2	140.5 J_{RhC}=33 Hz	135.1	145.3 J_{Rh-H} = 29 Hz
Cp	87.5, 87.4	86.4	89.7
Cp^*-C	101.8 J_{RhC}=4 Hz	103.3	
Cp^*-CH_3	9.8	11.4	10.6

occur in comparable amounts. Quantitative kinetic studies were performed by monitoring the intensities of the ^{1}H NMR signals at temperatures above room temperature, where equilibrium is reached within a few hours. Figure 2.14 shows a plot of the intensities of the Cp^* proton resonances versus time for a sample at 320 K. One can see the concentration of isomer **7b** increases exponentially at the expense of isomer **7a** until equilibrium is reached. At that point isomer **7b** slightly dominates the mixture (55:45), corresponding to an equilibrium constant K_c(**7a**→**7b**) = 1.2. If the energies of the two isomers were exactly equal, the ratio **7b**:**7a** would be 1:2 for statistical reasons since there are two Rh-Co edges and only one Co-Co edges in the molecule. The fact that we instead observe a small excess of isomer **7b** indicates that isomer **7b** is somewhat energetically favored, but the difference in energy between **7a** and **7b** is slight. Therefore, it does not

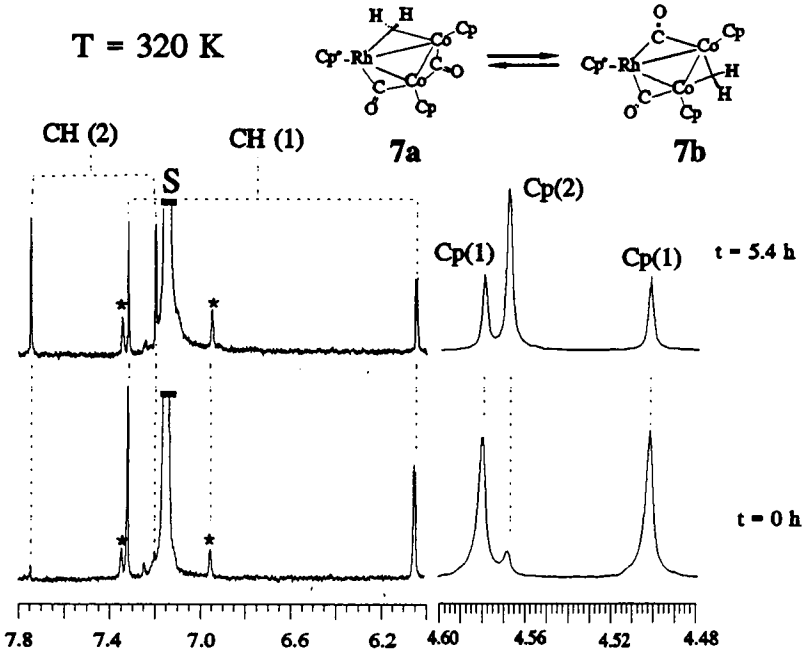

Figure 2.13: Methylene and Cp regions of the ^{1}H NMR spectrum of **7** showing the appearance of isomer **b**.

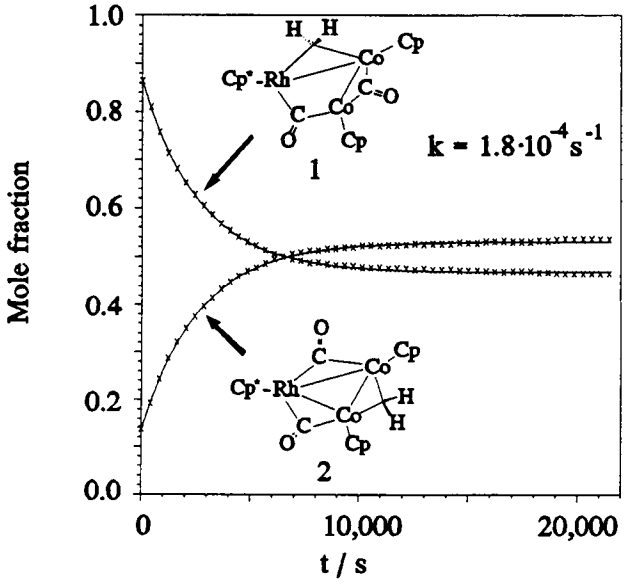

Figure 2.14: Kinetics of isomerization **7a** → **7b**. Data are normalized to the sum **a**+**b** to compensate for decomposition.

seem justified to call isomer **b** the thermodynamic isomer.

The change in concentration for the initial reactant in a reversible reaction with first order kinetics[42] is described by

$$c(a) = c_0(a)\,\frac{\frac{k}{K_c} + k\,e^{-(k+\frac{k}{K_c})t}}{k + \frac{k}{K_c}} \qquad (2.1)$$

A nonlinear fit of the data according (2.1)) yielded a rate constant k_{ab} = $1.8 \cdot 10^{-4}$ s^{-1} for the interconversion of the two isomers. The solid line through the data in Figure 2.14 illustrates the good agreement of the experimental data with this model. Kinetic experiments were conducted over a range of temperatures (310 to 335 K) and the rate constants evaluated according to the Eyring equation[43]:

$$k = \frac{k_B T}{h}\, e^{-\frac{\Delta G^{\ddagger}}{R_G T}} \qquad (2.2)$$

On the left side of Figure 2.15, $\ln(k \cdot h/k_B \cdot T)$ is plotted versus inverse temperature. Using the relationship $\Delta G = \Delta H - T\,\Delta S$ a linear fit through these data yields values of $\Delta H^{\ddagger}$ = 106(12) kJ mol^{-1}, $\Delta S^{\ddagger}$ = 4(38) J mol^{-1} K^{-1} and $\Delta G^{\ddagger}(298K)$ = 104.7 kJ mol^{-1}. The relative large errors in $\Delta H^{\ddagger}$ and $\Delta S^{\ddagger}$ are caused by the very narrow temperature range available. At higher temperatures the timescale of the reaction becomes comparable to the time it takes to

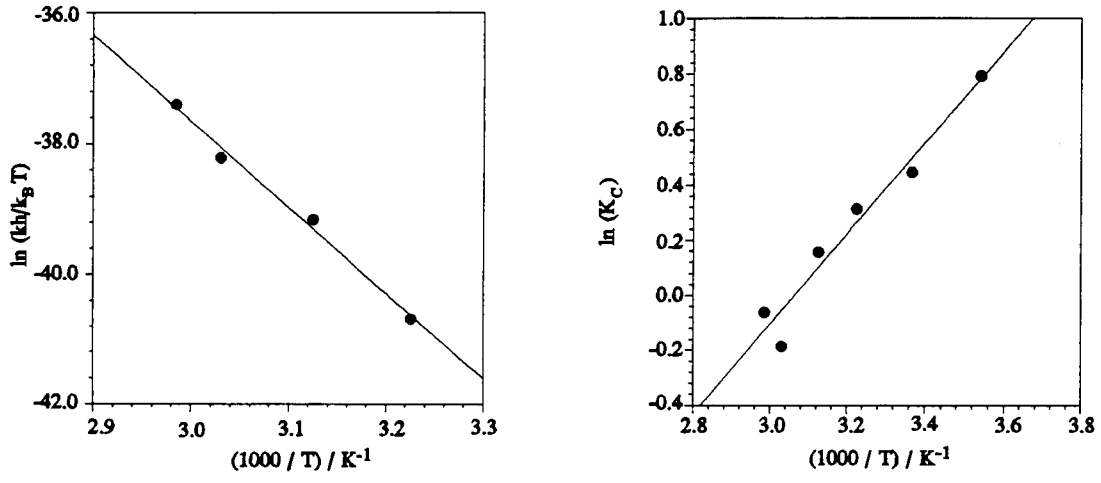

Figure 2.15: Semilogarithmic plots of the rate constant (left) and the equilibrium constants (right) versus 1/T for **7a** → **7b**.

equilibrate the temperature within the sample. On the other hand, at temperatures required to study the interconversion by magnetization transfer techniques (≈400 K), decomposition of the compound occurs rapidly.

In addition to kinetic information, integration of the equilibrated signals also allows for the determination of the temperature dependence of the equilibrium constant K_c(ab). This behavior is described by the equation

$$K_c = e^{-\frac{\Delta G^0}{R_G T}} \quad or \quad \Delta G^0 = -R_G T \ln(K_c) \tag{2.3}$$

The right side of Figure 2.15 shows a plot of ln(K_c) versus inverse temperature. From a linear fit to these data, the thermodynamic parameters were determined to be ΔH^0 = -14(2) kJ mol^{-1}, ΔS^0 = -42(5) J mol^{-1} K^{-1} and ΔG^0(298K) = -1.2 kJ

mol^{-1}. In the case of the Ir analogue **8** on the other hand no second isomer is observed up to 120°C.

2.5.2. Carbene Exchange Between Rh-Co Edges

In addition to the cross peaks of methylene protons with the Cp and Cp^* signals discussed above, the phase sensitive NOESY spectrum of a mixture of **7a** and **7b** at 300 K exhibits a strong negative cross peak between the two methylene protons due to their spatial proximity. If NOESY spectra are taken at higher temperatures, the *negative* cross peak between the two methylene proton resonances of isomer **7a** becomes weaker and eventually turns positive above 360 K. Furthermore, positive cross peaks were observed connecting both methylene protons in isomer **7a** with a very weak signal at 8.45 ppm. The corresponding crosspeaks for the methylene hydrogens of isomer **7b** on the other hand remain negative at these temperatures. Figure 2.16 shows a NOESY spectrum of the methylene region of a mixture of **7a** and **7b** taken in toluene-d_8 at 365 K.

In the extreme narrowing limit, a positive cross peak in a NOESY spectrum indicates the presence of chemical exchange between the two sites connected by the cross peak. In this case, interchange between the protons of the methylene ligand across the Rh-Co edge (**7a**) takes place on a timescale detectable by NOESY, but not for the ones of the methylene ligand across the Co-Co edge in **7b**. In addition, a NOESY spectrum optimized to observe cross

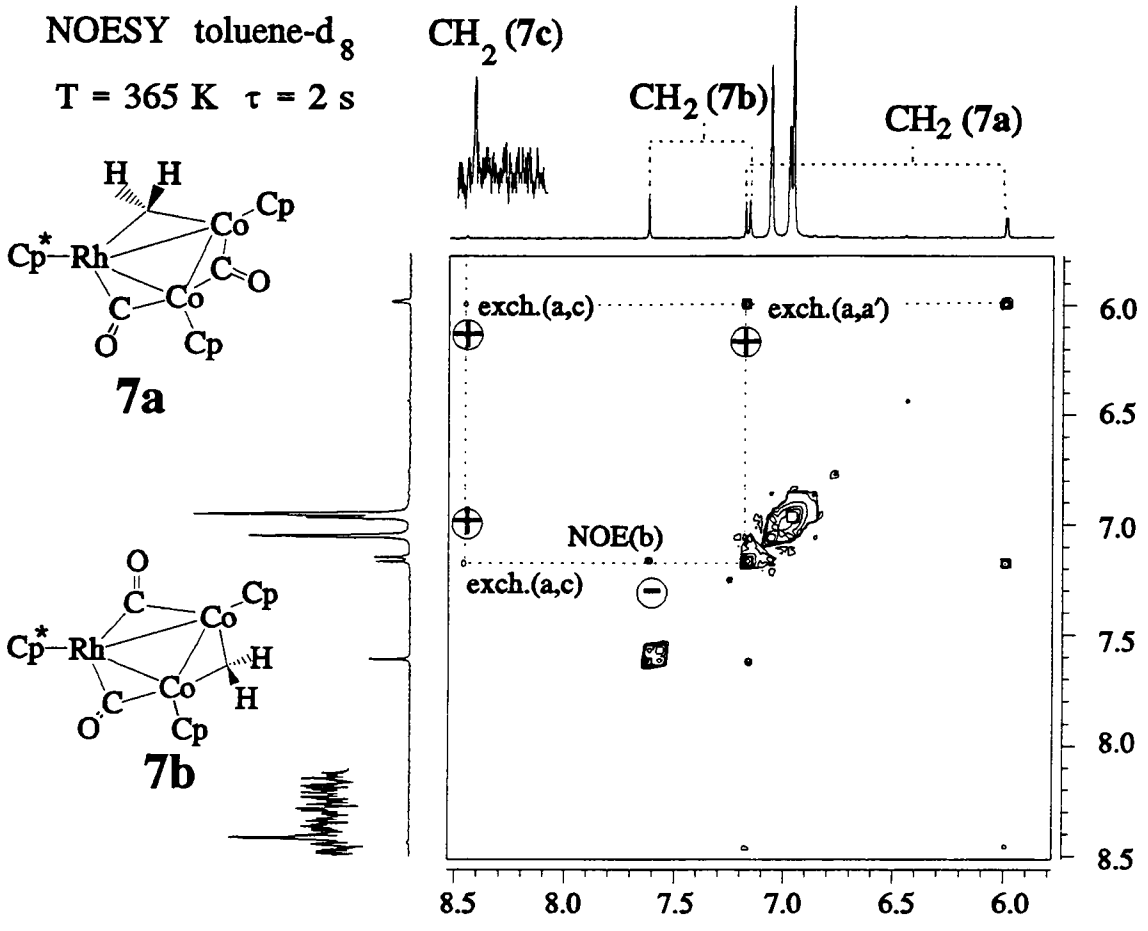

Figure 2.16: Carbene region of the NOESY spectrum of a mixture of isomers **a**, **b** and **c** at 365 K. "+" and "-" signs indicate positive and negative peaks.

peaks near the diagonal in the Cp region with maximum resolution showed a positive cross peak between the two Cp signals of **7a** at 355 K (Figure 2..17). This indicates the presence of a dynamic process interchanging the identities of the two CpCo vertices.

It should also be noted that the rate of the carbene migration **7a** → **7b** discussed in the paragraph above is too slow at this temperature to have an observable effect in a NOESY spectrum. Therefore a different process has to be

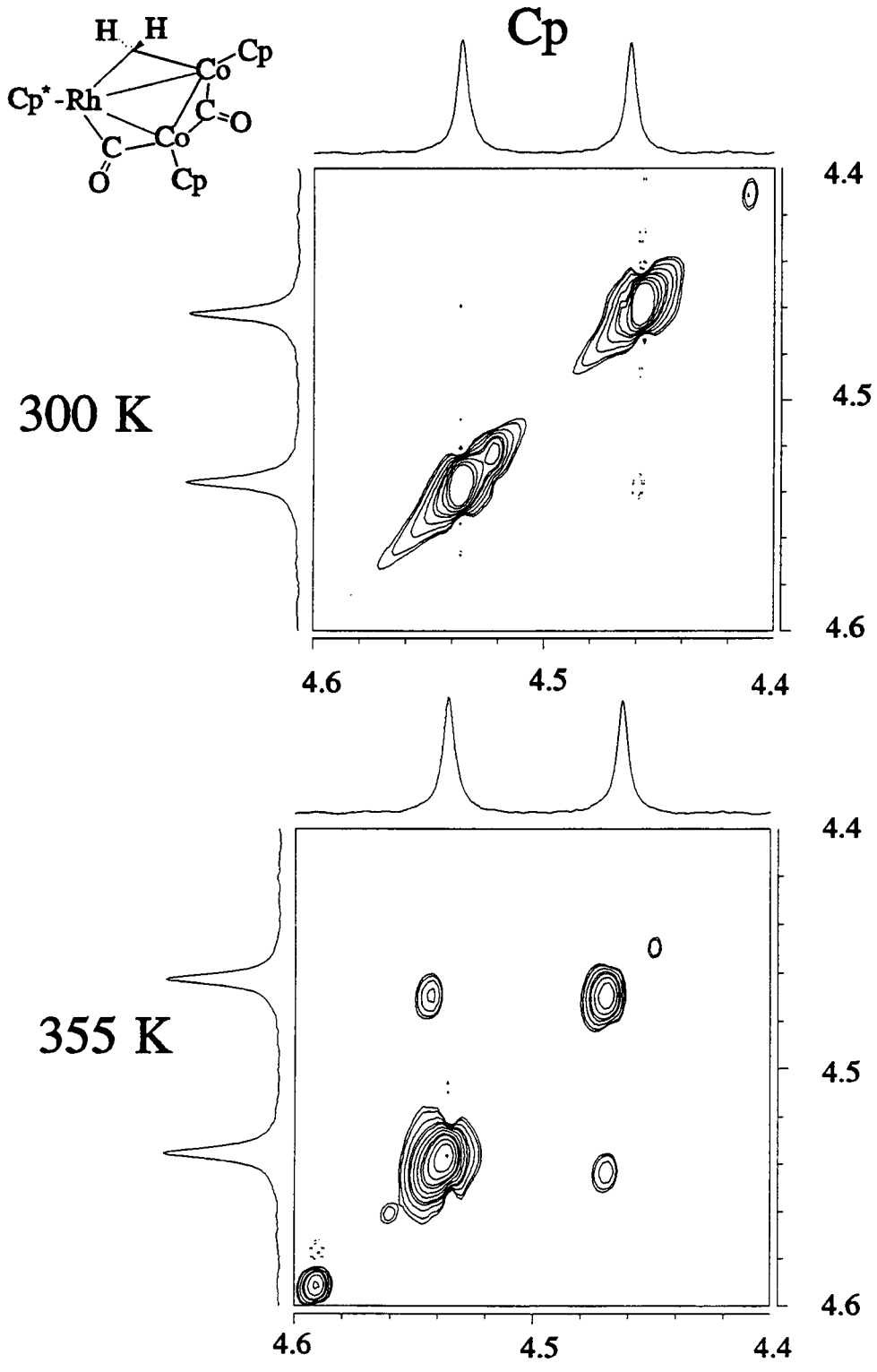

Figure 2.17: NOESY spectrum of the Cp region of **7** at 300 K (top) and 355 K (bottom) indicating exchange between the CpCo edges at high temperature.

present which interconverts the two methylene protons on a faster timescale. Furthermore, the cross peaks to the small signal at 8.45 ppm indicate the presence of an intermediate **7c** in that process. Interchange of the two methylene protons could be accomplished by simple rotation of the carbene ligand while in place on the Rh-Co edge. This process would involve an intermediate in which the H-C-H plane of the carbene ligand is parallel to the Rh-Co edge:

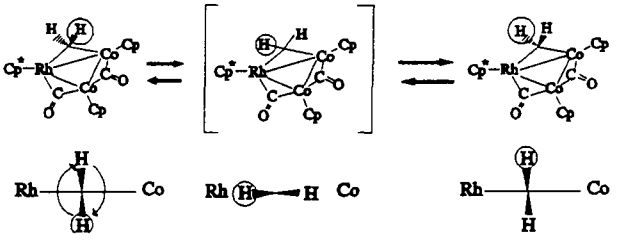

However, such a process would not explain the observed interchange of the two CpCo vertices. In addition, several other arguments make a stationary carbene rotation highly unlikely. Theoretical calculations performed by Hoffmann and coworkers for carbene ligands on metal surfaces indicate that a carbene coordinated with the CH_2 group parallel to a metal-metal bond is energetically very unfavored.[2] Furthermore, for such a species two distinct methylene proton signals are expected, whereas only one signal is observed in the NOESY spectra for both protons in **7c**.

A different process which can achieve interchange of the two methylene hydrogens and at the same time accounts for the interchange of the CpCo vertices involves migration of the methylene group from one Rh-Co edge to the other,

similar to the migration from the Rh-Co to the Co-Co edge. For such processes the existence of an intermediate with the carbene ligand in a *terminal* binding mode has been proposed.[5e] In the case of the complex **7** discussed here, the terminal carbene ligand would be located on the Rh atom as shown in Figure 2.18. If the migration occurs without rotation of the methylene group, the two carbene hydrogens in the terminal ligand in the intermediate are equivalent. Further migration to the opposite Rh-Co edge exchanges their identities.

Another possible mechanism of carbene migration involves a triply bridging carbene ligand (Figure 2.18). Calculations suggest an energy considerably higher for a face bridging carbene ligand than for a terminal one,[2] but such a mechanism is also consistent with our experimental observations acquired so far.

A quantitative analysis of the exchange process was performed by taking NOESY spectra with different mixing times τ and plotting the cross peak intensity versus mixing time. Using relative intensities normalized to the intensity of the corresponding diagonal peak, the effects of T_1 relaxation and decomposition of the complex can be taken into account. Decomposition becomes especially significant at the temperatures required for the exchange process to be monitored. Figure 2.19 shows the intensities of the crosspeaks between the two methylene protons for isomers **7a** and **7b**. At 300 K the cross peaks are negative in both isomers and grow in with similar rates. At 365 K the cross peak for the Rh-Co bridging methylene group becomes positive, whereas the corresponding signal for the Co-Co bridging isomer remains negative, even so the rate of magnetization

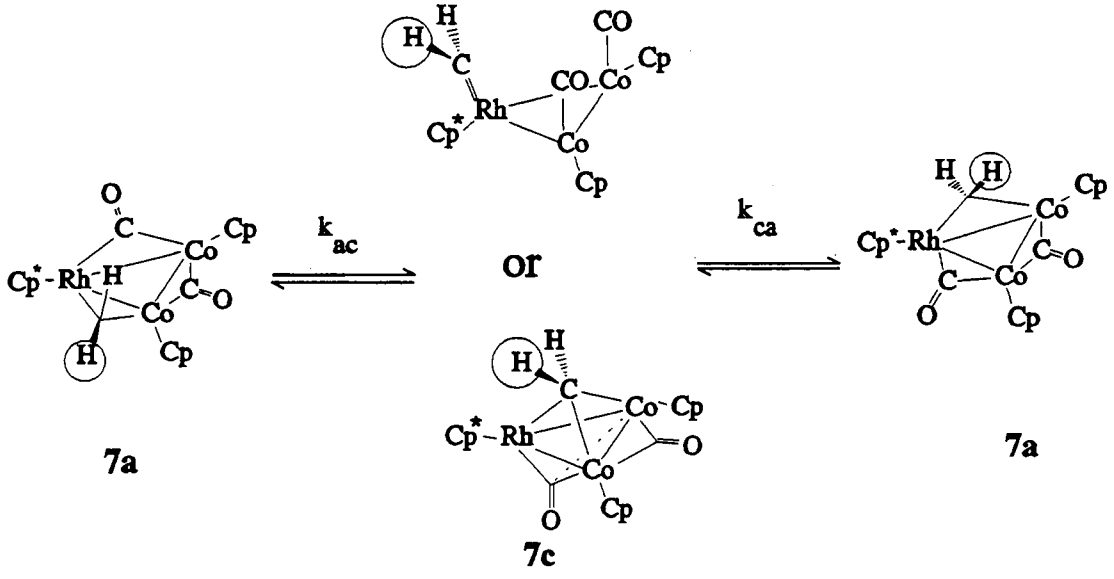

Figure 2.18: Carbene migration between RhCo edges showing two possible coordination modes for the carbene ligand in the intermediate **7c**.

transfer is decreased. In the extreme narrowing limit, the dependence of the intensity of NOESY cross peaks (A_{ij}) between two signals i and j on the mixing time is

$$\frac{A_{ij}}{A_{ii}} = \frac{1 - e^{-(R_D - k)\tau}}{1 + e^{-(R_D - k)\tau}} \qquad (2.4)$$

if the two signals are of equal intensity.[34a] In this equation, R_D is the dipolar cross relaxation rate, k the rate of exchange between the two sites and A_{ii} the intensity of the diagonal peak i. One can see that for slow exchange ($k < R_D$) equation (2.4) yields negative cross peak intensities, whereas for $k > R_D$ positive

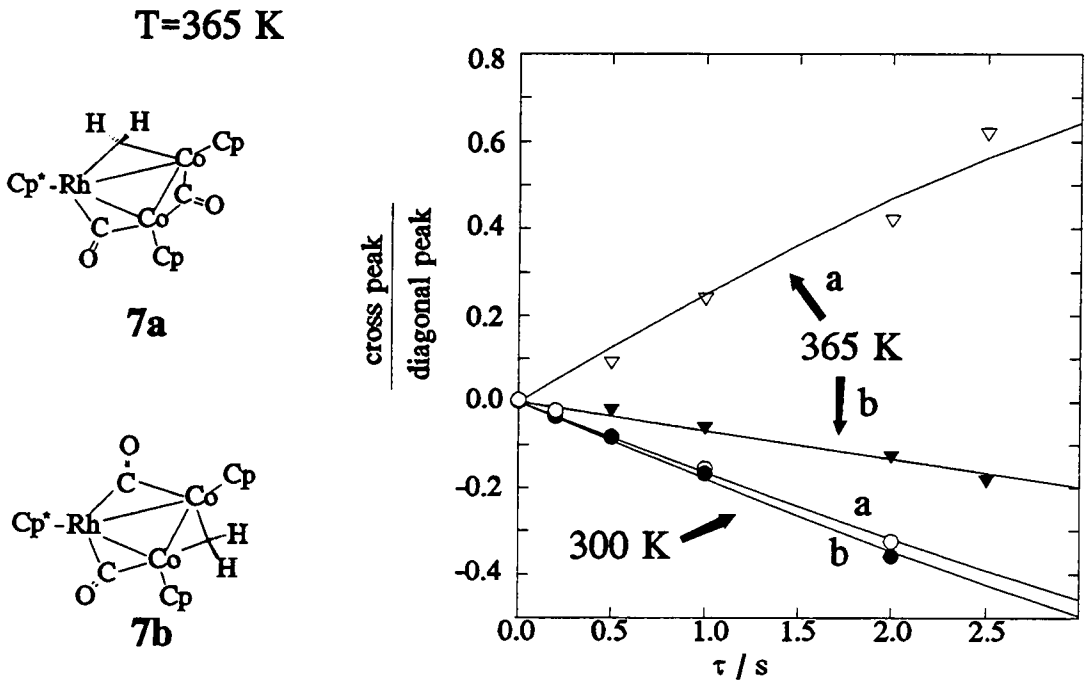

Figure 2.19: Cross peak intensities of methylene protons in **7** versus mixing time for isomers **a** and **b**. circles: 300 K; triangles: 365 K.

intensities are obtained. The intermediate condition $k = R_D$ results in cancellation of the two contributions and no cross peak is observed.

The lines in Figure 2.19 show the fit of the experimental data to equation (2.4). From that fit the effective cross relaxation rate $R_{eff} = R_D - k$ is obtained. Two approaches have been made in order to separate the two components. One approach involves the fact that the rate of methylene proton exchange in isomer **7b** is too slow to have an effect on the NOESY spectrum and $R_{eff}(\mathbf{b}) = R_D$. If one assumes that the cross relaxation rates are the same in both methylene groups one can use the cross peak in isomer **7b** as measure of the cross relaxation rate

R_D in isomer **7a**. Alternatively, the longitudinal relaxation times T_1 of the methylene protons and the NOE's upon irradiation of one of the two were measured at temperatures below the onset of exchange (270 - 310 K). The dipolar cross relaxation rate for that temperature is then obtained by

$$R_D = \frac{\eta}{\eta_{max}} \frac{1}{T_1} \qquad (2.5)$$

where the maximum NOE for a pair of protons $\eta_{max} = 0.5$. Measuring the temperature dependence of T_1 allows one to extrapolate to temperatures above the onset of exchange. These calculations are summarized in Table 2.7. Both methods yield comparable results, but the first approach appears to be the more accurate one. At 365 K, the value of the rate constant describing the exchange between the two enantiomers of **7a** was found to be $k_{aa} = 0.64(4)\ s^{-1}$. Measurements at 360 and 350 K yielded values of $k_{aa} = 0.29\ s^{-1}$ and $0.13\ s^{-1}$, respectively. Equation (2.2) relates this value with an activation energy $\Delta G^{\ddagger}(365\ K) = 91.8\ kJ\ mol^{-1}$.

Mixing time dependent measurements were also performed for the cross peaks between the two Cp signals in **7a**. In this case, the analysis is somewhat simpler since the NOE between the two Cp groups is negligible. A value of $k_{aa} = 0.14\ s^{-1}$ was obtained for the experiment performed at 355 K. This result falls right in line with the values obtained from the methylene signals. From a linear fit of a plot of $\ln(k_{aa}\, h / k_B T)$ versus inverse temperature according to (2.2) values

Table 2.7: T_1 and NOE values of the carbene protons of **7a** and rate constants calculated for carbene migration.

	downfield CH_2 of **7a** (i)			upfield CH_2 of **7a** (j)						k_{aa}
T / K	$1/T_1$(i)	η(ij)[a]	R_D(ij)	$1/T_1$(j)	η(ji)[b]	R_D(ij)	R_{eff}(a)	R_{eff}(b)	d	e
270	1.01	0.31	0.61	1.31	0.23	0.62				
280	0.81	0.28	0.49	1.03	0.26	0.49				
300	0.58	0.33	0.35	0.72	0.31	0.35	0.33	0.36	0.03	0.02
310	0.51	0.29	0.31	0.63	0.22	0.30				
350			0.20[c]			0.20[c]	0.096	0.23	0.13	0.10
360			0.19[c]			0.18[c]	-0.15	0.14	0.29	0.34
365			0.18[c]			0.18[c]	-0.51	0.13	0.64	0.69

a) NOE observed on downfield CH_2 proton i upon irradiation of the upfield CH_2 proton j.
b) NOE observed on upfield CH_2 proton j upon irradiation of the downfield CH_2 proton i.
c) extrapolated from data between 270-310K.
d) calculated according to $k_{aa} = R_{eff}(b) - R_{eff}(a)$
e) calculated according to $k_{aa} = R_D(ij) - R_{eff}(a)$

of $\Delta H^{\ddagger}$ = 115(30), $\Delta S^{\ddagger}$ = 63(79) and $\Delta G^{\ddagger}$(298K) = 96.0 kJ mol^{-1} were obtained for the activation enthalphy, -entropy and free energy.

Similar experiments were performed on the all-Cp and Cp^*Ir containing carbene complexes **6** and **8**. Even though these complexes were not as thoroughly studied as the Rh complex **7**, the results indicate that carbene migration between the M-Co edges takes place in both isomers at a rate comparable to the one found in **7a**. Table 2.8 summarizes the activation barriers found for the carbene mobility of all of these complexes.

2.5.3. The Nature of the Intermediate 7c

In the previous section, the intermediate involved in the migration of the carbene ligand between the Rh-Co edges was proposed to be most likely a species containing a terminal carbene ligand. This coordination geometry of carbene ligands is well known for mononuclear complexes, but in polynuclear complexes

Table 2.8: Free energies of activation $\Delta G^{\ddagger}$ for carbene migration in **6** - **8**. Values are given in kJ mol^{-1}.

process	Cp^*Rh (**7**)	Cp^*Ir (**8**)	CpCo (**6**)
MCo → MCo	96.0[a], 92.1[b]	99.9[b]	86.5[c]
MCo → CoCo	104.7[a], 104.0[b]	-	-

a) 298 K b) 360 K c) 350 K

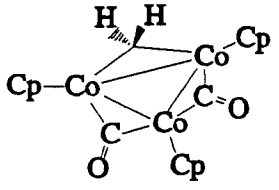

6

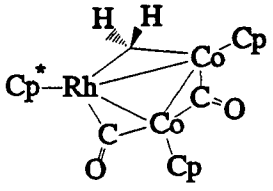

7

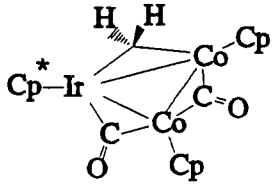

8

the μ_2-bridging coordination dominates. Only a few examples of dinuclear[44] and trinuclear[45] complexes containing terminal carbene ligands have been reported, and all contain Fischer type carbene ligands. To our knowledge, no unsubstituted "Schrock type" carbene ligands with a terminal coordination have been described in cluster complexes. However, such ligands have been proposed as intermediates in carbene rotation[46] and migration[5e] processes. A theoretical study by Hoffmann and coworkers suggests that on metal surfaces bridging and terminal carbene ligands have comparable energies.[2] A triply bridging carbene, on the other hand, has never been observed and is less favored by the calculations. The complex $Cp^*Rh(CpCo)_2(\mu_2\text{-}CO)_2(\mu_2\text{-}CH_2)$ (**7**) appears to be the first example in which an intermediate in carbene migration between different edges is observed

experimentally. In this section, experiments are described which were performed in order to more accurately determine the nature of the species **7c**.

As mentioned above, the NOESY spectrum connects both methylene hydrogens in the bridging isomer **7a** with the signal of **7c** at 8.45 ppm, indicating that this signal belongs to a methylene group in which both hydrogens are equivalent. In order to identify the Cp and Cp^* signals belonging to isomer **7c**, a single crystal consisting only of bridging isomer was placed in an NMR tube and dissolved in CD_2Cl_2 at low temperature. A spectrum taken immediately at 270 K did not show any signal in the region around 8.3 ppm. The Cp and Cp^* regions of this spectrum were used as background (bottom of Figure 2.20) and compared with the spectrum obtained after the sample was allowed to warm to room temperature. At room temperature the carbene migration becomes fast enough to observe intermediate **7c** appear within seconds. As shown in top of Figure 2.20 one new signal for each of the Cp and Cp^* ligands appears simultaneously with the methylene signal at 8.3 ppm. The observation of only one Cp ligand is also consistent with a terminal carbene ligand coordinated to the rhodium rendering the two CpCo vertices equivalent. However, the low concentration of isomer **7c** made accurate integration of its proton signals difficult. For the new Cp signal a value between 5 and 10 protons relative to two methylene protons was obtained, so that the possibility of a second Cp signal overlapping with one of signals of the major isomers can not be ruled out.

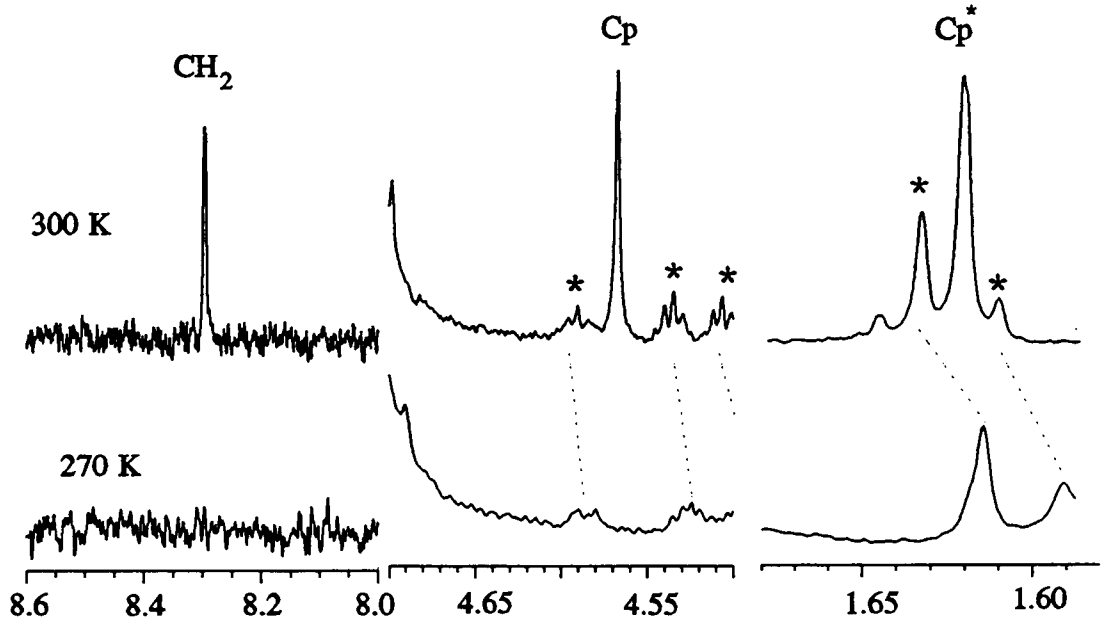

Figure 2.20: Identification of Cp and Cp^* signal of **7c** against the background of ^{13}C satellite peaks (marked with asterixes).

Close inspection of the room temperature NOESY spectrum revealed a cross peak connecting the methylene signal of **7c** with its Cp^* signal confirming that the CH_2 group has to be located in the proximity of the Cp^*Rh fragment (Figure 2.21). Furthermore coupling between the carbene protons to the Rh of 1.4 Hz also indicates proximity to the Rh atom. Both terminal and μ_3-bridging binding modes of the carbene ligand might give rise to these observations as indicated in Figure 2.19.

One very decisive method to distinguish a terminal carbene ligand from one in a bridging position is ^{13}C NMR spectroscopy. The ^{13}C chemical shift which is normally observed for a terminal carbene ligand ranges from 240 to 370 ppm, whereas bridging carbene ligands give rise to signals between 100 and 210 ppm.[23]

Furthermore, a terminal carbene ligand located at the Cp^*Rh vertex is expected to exhibit a characteristic one bond carbon-rhodium coupling constant $^1J_{RhC}$ about twice in magnitude than a bridging carbene ligand. However, due to the low concentration of **7c** in solution, observing the carbon signal for the carbene carbon of that isomer is extremely difficult. At natural abundance, a proton detected heteronuclear correlation experiment using heteronuclear multiple quantum coherence ($^1H\{^{13}C\}$ HMQC)[47] failed to yield a signal for isomer **7c**. Therefore, a sample with the carbene ligand enriched in the ^{13}C isotope was prepared using

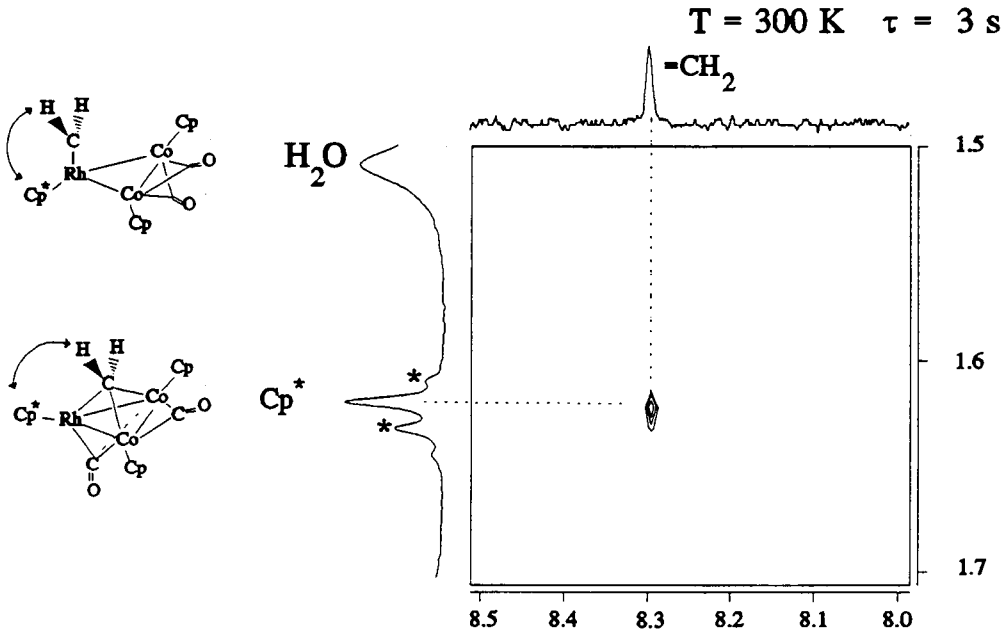

Figure 2.21: Portion of the NOESY spectrum of **7** showing the cross peak between carbene and Cp^* protons of isomer **c**.

labeled diazomethane. Much to our surprise, the proton signal at 8.3 ppm exhibited a cross peak with a signal at a ^{13}C chemical shift of 145.3 ppm as shown in Figure 2.22. Such a shift almost certainly rules out a terminal carbene ligand in complex **7c**. The carbon resonance at 145.3 ppm exhibited coupling constants of J_{CH} = 145 Hz and J_{CRh} = 30 Hz for the coupling to the proton and rhodium, respectively. These values also resemble the ones found for a bridging carbene ligand (see Table 2.6). No spectroscopic data are available for triply bridging carbene ligands, however it appears to be reasonable to expect such a ligand to be similar to edge bridging ones. A one dimensional "attached proton test" confirms the presence of two protons connected to the carbon at 145 ppm. This verifies that in the intermediate **7c** the methylene unit remains intact and rules out any structure involving dissociation of the C-H bond. Furthermore, by using a sample ^{13}C enriched in both the carbene and carbonyl carbons, the formation of a ketene type ligand resulting from coupling of the carbene ligand with a carbonyl ligand could be ruled out. In such a species one expects to observe ^{13}C-^{13}C coupling between the neighbored carbon atoms in this ligand which is not observed. This leaves us with a triply bridging carbene ligand as the most plausible, though as yet unknown, structure in **7c**.

Another aspect concerning the role of **7c** as intermediate in the mobility of the bridging carbene ligand between the two Rh-Co edges is the position of the carbonyl ligands. As the carbene moves from one Rh-Co edge to the other, the carbonyl ligand on this edge also has to change its position. Based on how the

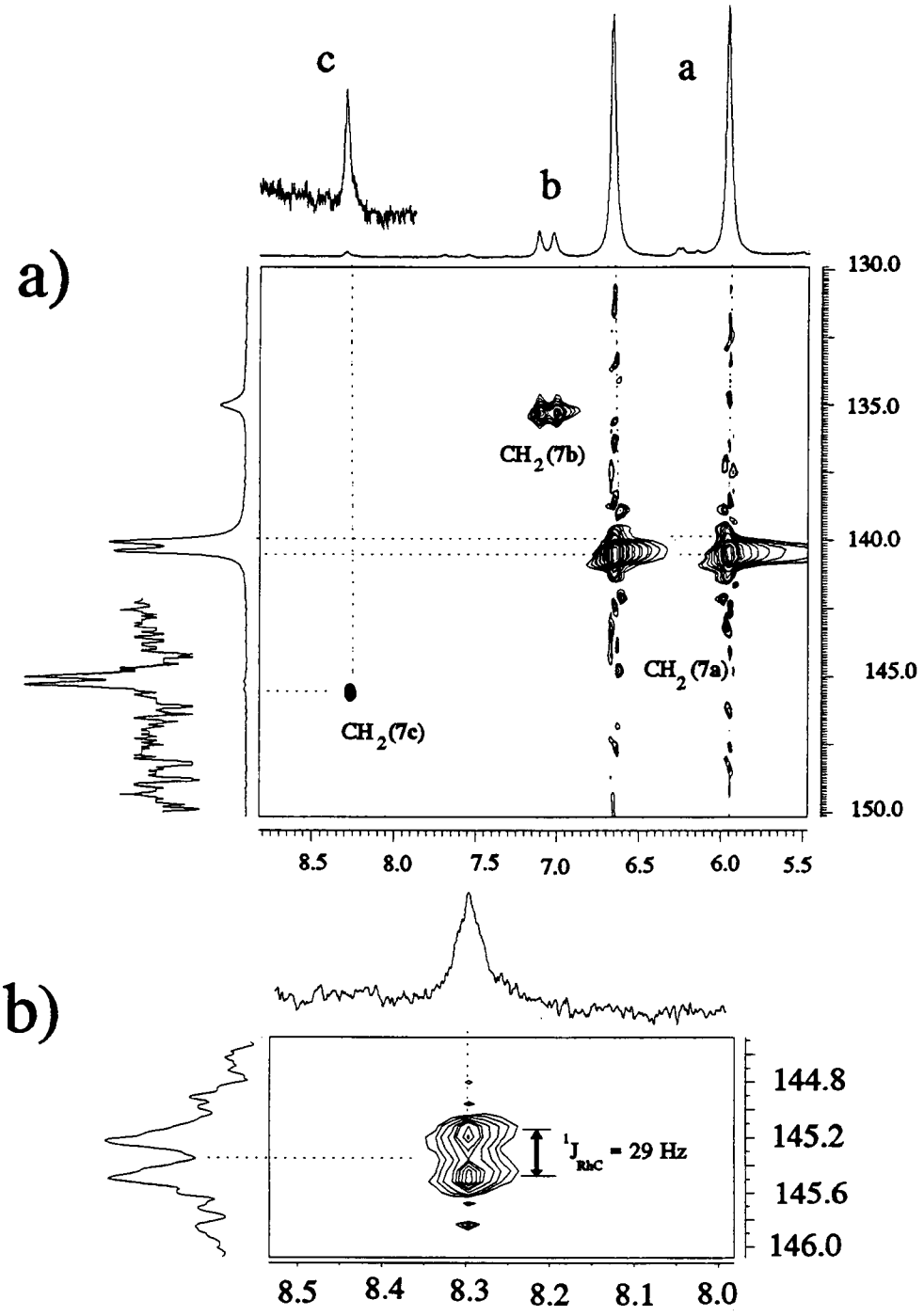

Figure 2.22: Carbene region of a HMQC spectrum of **7** using a sample with the carbene enriched in ^{13}C (a) and expanded cross peak of isomer **7c** (b).

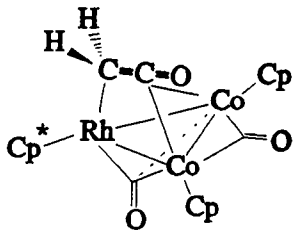

μ-ketene

CO ligands are exchanged, three different pathways (I - III) with three different structures for **7c** are possible as shown in Figure 2.23.

One possible intermediate (pathway I) has both carbonyl ligands in a terminal coordination mode on the cobalt atoms resulting in an all-terminal arrangement of the carbene and the two carbonyl ligands. In this case carbene mobility between the Rh-Co edges involves analogous rearrangement of *both* carbonyl ligands. The carbonyl ligand originating on the Rh-Co edge (marked by a circle in Figure 2.23) will end up on the Co-Co edge, whereas the original carbonyl ligand from the Co-Co edge moves to the coordination site vacated by the carbene ligand on the other Rh-Co edge. Thus, in this process interchange of the identities of the carbonyl ligands will go hand-in-hand with the migration of the carbene ligand.

A second possibility is shown in pathway II in which the carbonyl ligand on the Rh-Co edge moves into a triply bridging position on the opposite side of the metal triangle as the carbene ligand. The second carbonyl ligand remains on the Co-Co edge and is largely unaffected by the exchange. In this case no exchange of the carbonyl carbons would be observed.

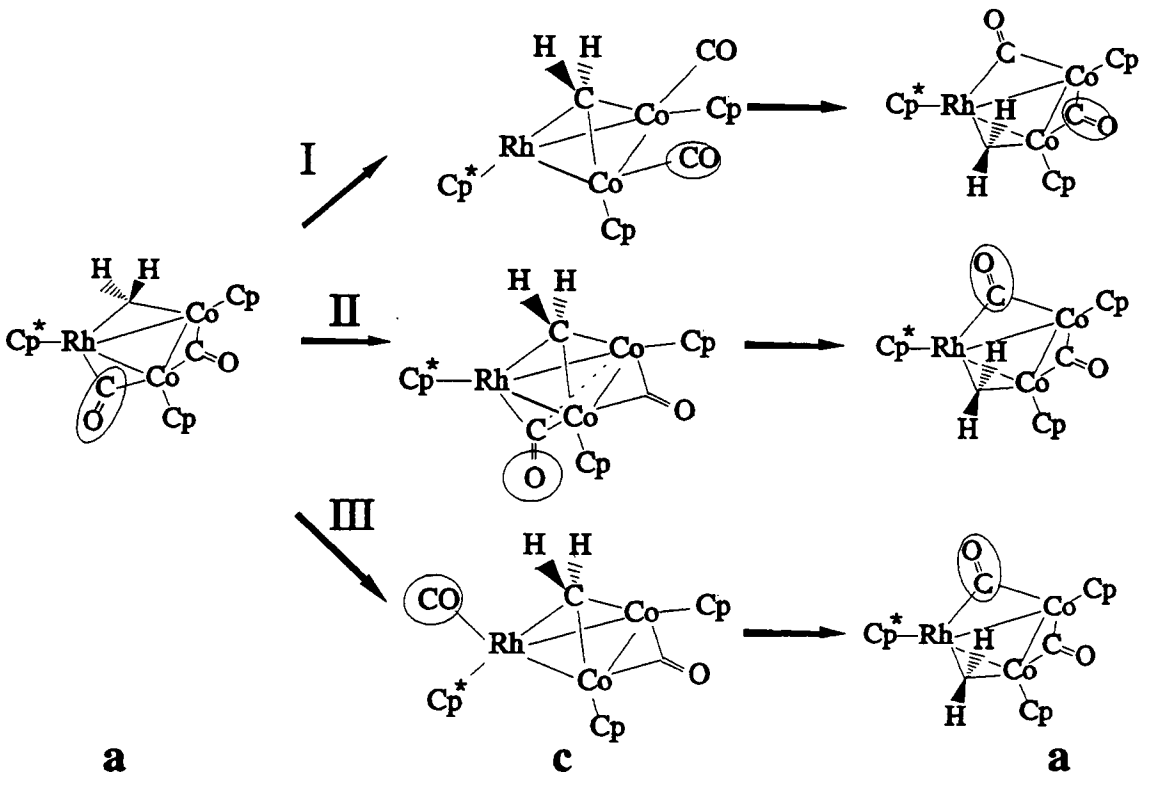

Figure 2.23: Possible pathways for carbonyl migration in the case of a triply bridging carbene ligand.

Finally, a third possible structure for **7c** involves a terminal binding mode on the rhodium atom for the carbonyl ligand originating from the Rh-Co edge (pathway III). In such a pathway the carbonyl ligand on the Co-Co edge again remains unaffected whereas the other carbonyl ligand switches between Rh-Co edges.

One should be able to distinguish between the different pathways I - III by examining the carbonyl stretching frequencies in the IR spectrum of isomer **7c**. Terminal or face bridging carbonyl ligands are expected to give rise to absorption

bands clearly separated from strong signal due to the edge bridging carbonyl ligands of the major isomers **7a** and **7b**. Several spectra with concentrated samples containing a mixture of isomers **7a** and **7b** were taken. In one run a small band at 1651 cm^{-1} was observed. Further experiments are necessary to reproduce this signal and link it to the presence of isomer **c**. However, these preliminary findings favor pathway II and a structure for **7c** which contains one of the two carbonyl ligands in a face bridging bonding mode.

Another attempt to eludicate the position of the CO ligand in **7c** used ^{13}C NMR spectroscopy. For that purpose, a sample of the carbene complex enriched in ^{13}CO was prepared. However, no additional signal was observed in the spectrum. This is probabely due to insufficient signal-to-noise ratio obtained during the experiment. The different exchange pathways discussed above are also expected to exhibit different exchange patterns for the carbene ligands. In the case of pathway I the identities of the carbonyl ligands bridging the Rh-Co and Co-Co edge are interchanged. If either pathway occurs, one should be able to detect a cross peak in a two dimensional ^{13}C-exchange spectrum at high temperature. However, scalar coupling of the carbonyl carbons nuclei to the quadrupolar Co nuclei causes the carbonyl resonances to be significantly broadened above 250 K and the experiment could not be performed.

In light of the variety of binding modes discussed for the carbonyl and carbene ligands it is worth mentioning that for the analogous tricarbonyl complexes a large variety of structures are known. Very often several isomers of

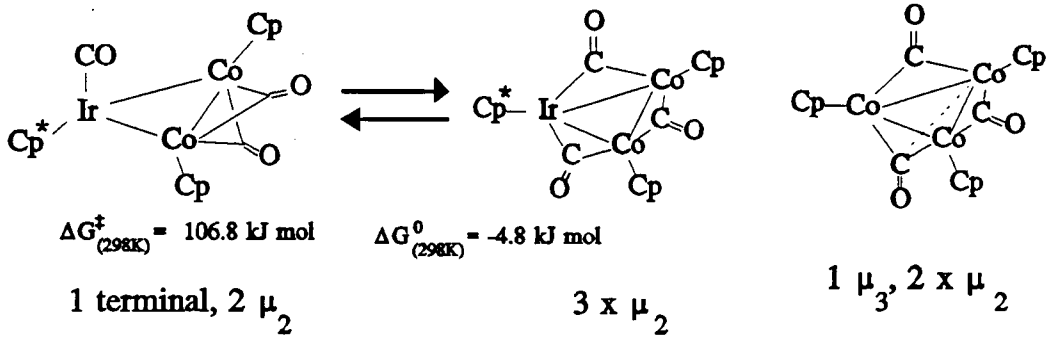

Figure 2.24: Terminal/bridging to all bridging isomerization in the tricarbonyl $Cp^*Ir(CpCo)_2(CO)_3$ (left) and one structure of $(CpCo)_3(CO)_3$.

similar energy are known to exist. For example, two arrangements of the carbonyl ligands are known for the complex $Cp^*Ir(CpCo)_2(CO)_3$ (**17**).[11, 48] Addition of carbon monoxide to the unsaturated dicarbonyl cluster complex **1** yields the isomer of **17** that contains a terminal CO ligand on the iridium and two bridging carbonyl ligands across the Co-Co edge. We found that this isomer of **17** is in equilibrium with the isomer containing three bridging carbonyl ligands as shown in Figure 2.24. This all-bridging structure is analogous to the structures of the major carbene isomers **7a** and **7b**. Furthermore, the structure of the analogous all CpCo tricarbonyl complex is known to be solvent dependent.[49] One isomer of this complex is also shown on the right side of Figure 2.24.

The variety of structures observed for tricarbonyl complexes illustrates that it is not possible to make an a simple energetic argument in favor of any structure in the case of the carbene complex **7c**. The data discussed in this section,

especially the ^{13}C NMR chemical shift of the carbene carbon, indicate that isomer **7c** does not involve a terminal carbene ligand, but more likely a triply bridging one. The mechanism of the carbonyl migration could not be clearly established, but preliminary IR data indicate that **7c** might contain a triply bridging carbonyl ligand.

2.6. Formation of a Carbyne Hydride Complex[50]

2.6.1. General Scheme :

The carbene complexes $(CpCo)_3(\mu_2\text{-}CO)_2(\mu_2\text{-}CH_2)$ (**6**) and $Cp^*Rh(CpCo)_2(\mu_2\text{-}CO)_2(\mu_2\text{-}CH_2)$ (**7**) decompose very easily at temperatures above 380 K. The Cp and Cp^* regions of the ^1H NMR spectra of the decomposition products indicate that several compounds are formed, and no clean single product was isolated in either case. The mass spectra of all carbene adducts show a strong fragment ion peak due to loss of one CO ligand suggesting that one decomposition pathway involves initial loss of one CO ligand (see Table 2.4). The Cp^*Ir complex $Cp^*Ir(CpCo)_2(\mu_2\text{-}CO)_2(\mu_2\text{-}CH_2)$ (**8**) is somewhat more stable towards heating than the Co and Rh analogues, but upon refluxing in toluene, CO is lost and the carbyne-hydride complex $Cp^*Ir(CpCo)_2(\mu_3\text{-}CO)(\mu_3\text{-}CH)(\mu_2\text{-}H)$ (**18**) is formed in a relatively clean reaction (Figure 2.25). A formal electron count shows that this new compound is also saturated, containing 48 cluster valence electrons if the carbyne ligand is regarded as a three, and the hydride ligand as a one electron donor. The open coordination site caused by loss of the CO ligand

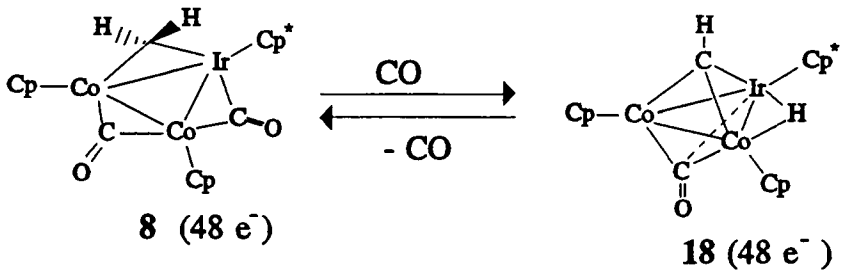

8 (48 e⁻) **18** (48 e⁻)

Figure 2.25: Formation of carbyne-hydride complex **18** from the carbene complex **8**.

is filled by the two electrons of one of the two C-H bonds in the carbene ligand which are incorporated into the cluster electron count. This example demonstrates the importance of vacant coordination sites on a metal surface for C-H activation.

2.6.2. Crystal Structure of $Cp^*Ir(CpCo)_2(\mu_3\text{-}CH)(\mu\text{-}H)$ (18)

Recrystallization by slow solvent evaporation at room temperature in a glove box yielded single crystals of **18** suitable for x-ray diffraction. The structure was solved by direct methods. Refinement was then performed including all atoms except the hydride hydrogen. Anisotropic displacement parameters were used to model all non-hydrogen atoms. The position of the carbyne hydrogen was refined using an isotropic sphere as a model but allowing the C-H bond distance to vary. Constant bond C-H distances were used for the Cp and Cp^* hydrogen atoms. A possible position for the hydride atom was then located in the final fourier difference map. Figure 2.26 shows two views of the crystal structure and Table 2.9 summarizes the most important bond distances and angles.

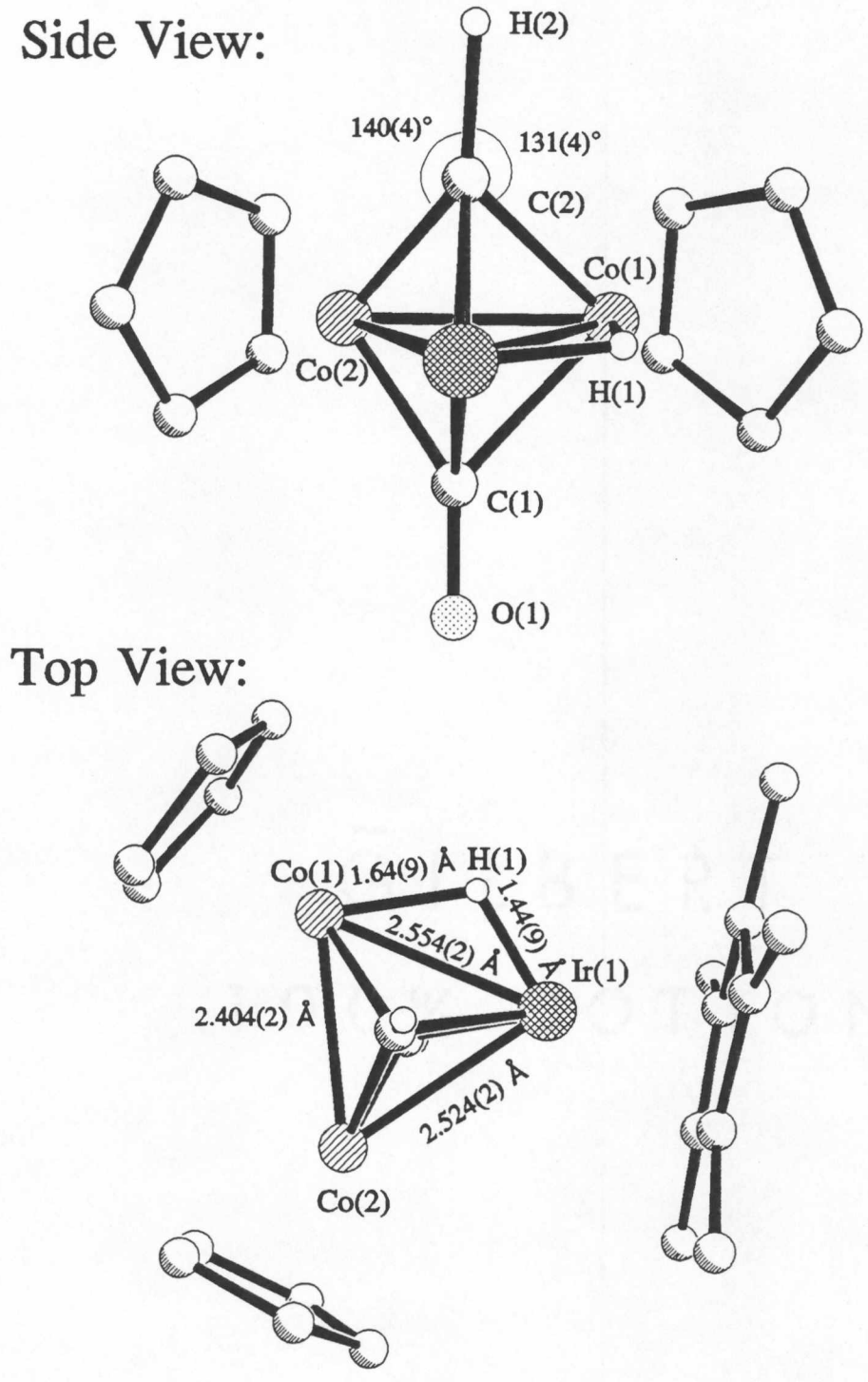

Figure 2.26: Crystal structure of carbyne hydride complex **18**. The Cp^* ligand is omitted for clarity. The hydride position was determined from the fourier difference map.

Table 2.9: Selected bond distances and -angles in **18**

Bond distances / Å			
Ir(1)-Co(2)	2.523(2)	Ir(1)-Co(1)	2.553(2)
Co(2)-Co(1)	2.405(2)	Ir(1)-C(1)	2.034(10)
Ir(1)-C(2)	2.055(12)	Co(2)-C(1)	1.844(12)
Co(2)-C(2)	1.912(13)	Co(1)-C(1)	2.035(13)
Co(1)-C(2)	1.990(13)	C(2)-H(2)	1.204(21)
Ir(1)-H(1)	1.44(9)	Co(1)-H(1)	1.64(9)
Bond angles / °			
Ir(1)-C(2)-H(2)	125.(4)	Co(2)-C(2)-H(2)	140.(4)
Co(1)-C(2)-H(2)	131.(4)	Co(2)-Ir(1)-Co(1)	56.6(1)
Co(2)-Ir(1)-C(1)	46.2(3)	Ir(1)-Co(1)-Co(2)	61.1(1)
Co(1)-Ir(1)-C(1)	51.2(4)	Ir(1)-Co(2)-Co(1)	62.3(1)
C(1)-Ir(1)-C(2)	83.0(5)	Co(2)-Ir(1)-C(2)	48.0(4)
C(1)-Co(2)-C(2)	92.3(5)	Co(1)-Ir(1)-C(2)	49.7(4)
C(1)-Co(1)-C(2)	84.6(5)	Ir(1)-C(1)-O(1)	129.1(10)
Co(2)-C(1)-O(1)	138.2(11)	Co(1)-C(1)-O(1)	131.7(11)

The Ir and two Co atoms are arranged in a triangular manner with the Co-Ir-Co angle slightly smaller than the two Ir-Co-Co angles. The carbonyl and carbyne ligands bridge the two opposite faces of the metal triangle. The Cp and Cp^* ligands cap the three vertices in orientations perpendicular to the plane defined by the metal atoms. One of the two Ir-Co edges is slightly longer (2.553(2) versus 2.523(2) Å). Even thought this difference is rather small it might indicate that the hydride ligand is bridging that edge.[51] Consistent with this observation, the final fourier map showed residual electron density at a location near this Ir-Co edge which is attributed to the hydride ligand (see Figure 2.27). The hydride ligand is located in the plane of the three metal atoms, and the bond distances to the metals (Ir-H = 1.44(9) Å; Co-H = 1.64(9) Å) are within the range found for hydrides bridging Co or Ir atoms.[51] The C-H bond of the carbyne ligand is not perpendicular to the plane of the metals but leans slightly towards the Ir-Co edge containing the hydride ligand, resulting in different M-C-H angles for Co(1) (131(4)°) and Co(2) (140(4)°). However, this tilt appears to be too small to be caused by an agostic C-H-M interaction of this hydrogen.

The accuracy of hydrogen positions determined by x-ray diffraction is not very high[51] and therefore other means of determining the position of the hydride and carbyne hydrogens might be explored in the future. Neutron diffraction is normally a better way to obtain exact bond distances involving hydrogen atoms. However, this method is limited by both the limited sources of neutron beams suitable for diffraction studies and the large size single crystals required. Neutron

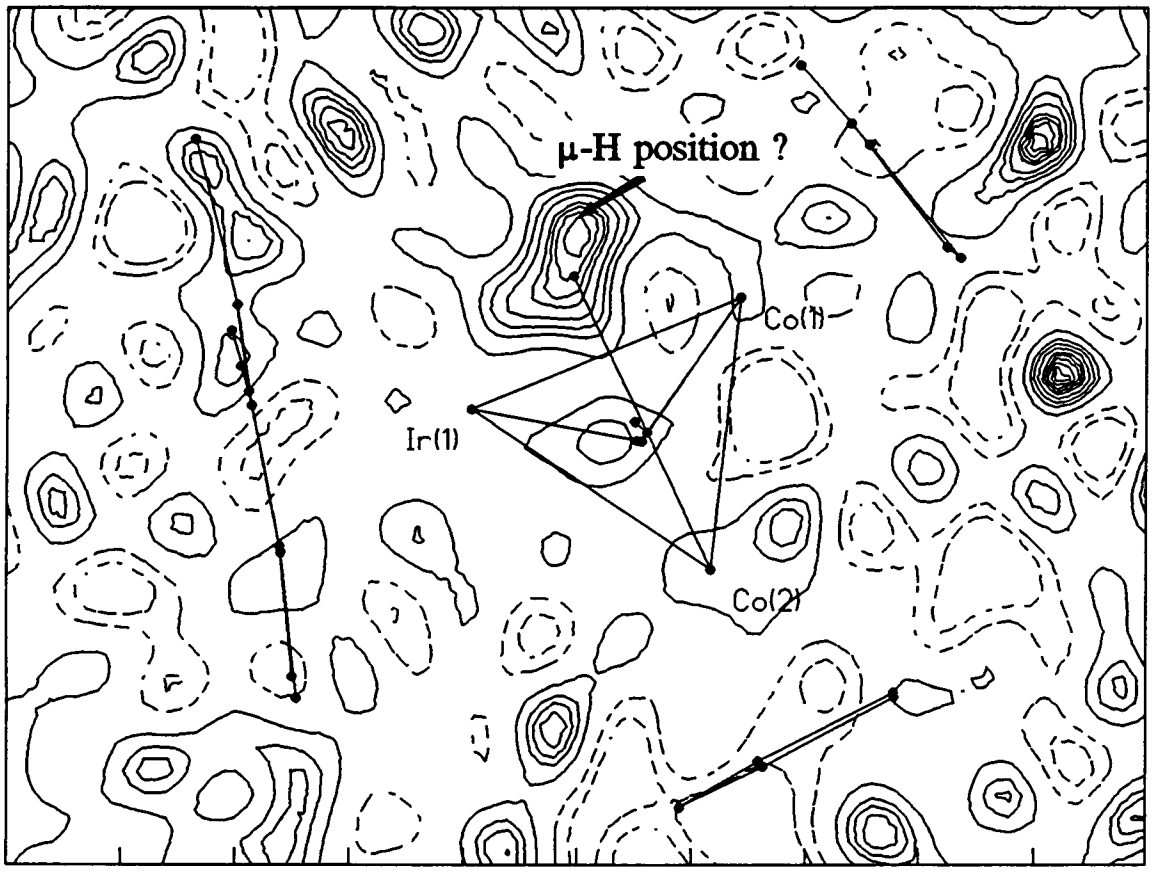

Figure 2.27: Electron density difference map of the carbyne-hydride complex **18** indicating the possible position of the hydride ligand.

diffraction on powders can be used to refine hydrogen positions in a structure obtained from x-ray diffraction, but this approach is made extremely difficult in the case of **18** because deuteration of the remaining hydrogen atoms is required. A different method which might allow for an independent determination of the carbyne-C-H bond length are ^{13}C NMR relaxation time measurements. One attempt of this experiment was unsuccessful due to an insufficient signal-to-noise-ratio. However, ^{13}C labeling of the carbyne position might improve the sensitivity

of this experiment. Such labeling could be achieved relatively easily by using diazomethane-^{13}C in the synthesis of the carbene precursor **8**.

2.6.3. Spectroscopic Properties of $Cp^*Ir(CpCo)_2(\mu_3\text{-}CH)(\mu\text{-}H)$

Table 2.10 lists the spectroscopic data for **18**. The IR spectrum exhibits a carbonyl stretch consistent with a triply bridging carbonyl ligand, and the mass spectrum shows in addition to the molecular ion peak at m/q = 618 fragment peaks indicative of loss of a H atom and a CH fragment.

The ^1H NMR (Figure 2.28)spectrum at 180 K (toluene-d_8) shows the signal due to the carbyne hydrogen as singlet at 14.85 ppm and the hydride hydrogen at

Table 2.10: Spectroscopic data for the carbyne-hydride complex **18**.

	T = 300 K	T = 190 K
^1H NMR	C_6D_6	Toluene-d_8
	15.1 (s, 1H, μ_3-CH)	14.85 (s,1H, μ_3-CH)
	4.68 (s, 10H, Cp)	4.84 (s, 5H, Cp), 4.72 (s, 5H, Cp)
	1.77 (s, 15H, Cp^*)	1.73 (s, 15H, Cp^*)
	-25.3 (s, 1H, μ-H)	-25.68 (s, 1H, μ_2-H)
^{13}C NMR	264 (d, $^1J_{CH}$=162 Hz, CH)	265 (d, $^1J_{CH}$=162 Hz, μ_3-CH)
	232.9 (s, CO)	241.3 (s, CO)
	97.8 (s, Cp^*-C)	102.7 (s, Cp^*-C)
	82.3 (d, Cp)	89.5 (d, Cp), 86.7 (d, Cp)
	9.86 (q, Cp^*-CH_3)	15.3 (q, Cp^*)
IR	ν_{CO}= 1690 cm^{-1}	
MS	618 (25%, M^+ based on ^{193}Ir)	
	617 (30%, -H); 605 (100%, -CH);	
	590 (18%, -CO); 393 (55%, Cp^*IrCp^+);	
	189 (65%, Cp_2Co^+)	

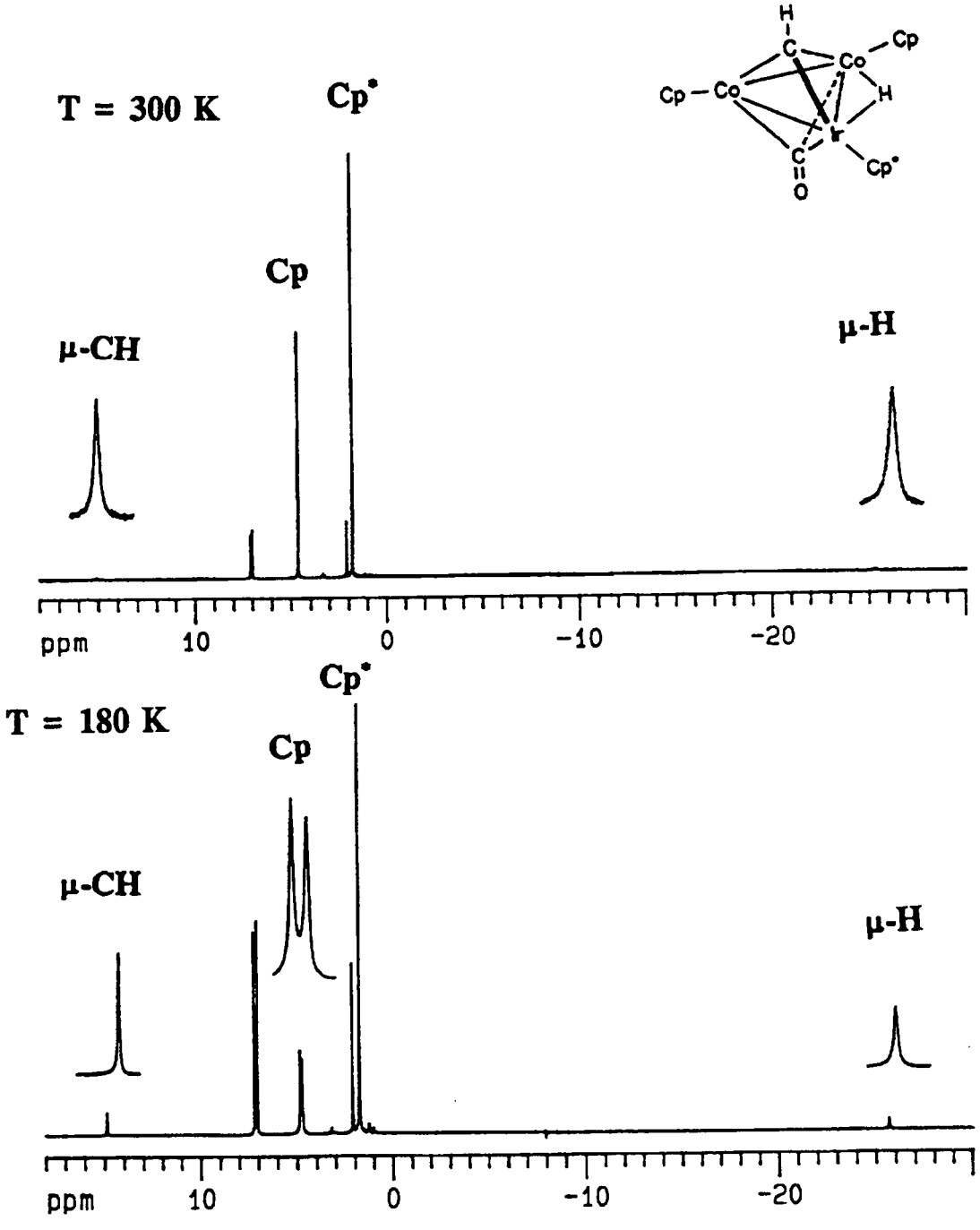

Figure 2.28: ^{1}H NMR spectra of **18**. Top: room temperature Bottom: 180 K

-25.68 ppm. Two signals are observed for the hydrogens of the Cp ligands indicating that at low temperature the hydride ligand bridges an Ir-Co edge. In the ^{13}C NMR the carbyne carbon is observed at 265 ppm. The carbon-proton coupling constant $^{1}J_{CH}$ of 162 Hz is consistent with a terminal carbyne without agostic M-H-C interactions, which reduce $^{1}J_{CH}$ to a range of 60-80 Hz.[6,52] Furthermore, no coupling is observed between the carbyne carbon and the hydride, consistent with the structure of this compound to contain separate carbyne and hydride groups. The carbonyl carbon exhibits a shift of 241.3 ppm consistent with a bridging carbonyl ligand.

2.6.4. Hydride Mobility About Metal Triangle

Upon warming to room temperature, the two Cp resonances observed at low temperature broaden and coalesce (T_c = 194 K) to form a single peak at 300 K. The reason for this behavior is fluxionality of the hydride about the metal triangle interchanging the identities of the two CpCo vertices. A quantitative analysis using full line shape analysis[53] of the proton NMR signals of the Cp ligands was performed using the program DNMR5[54] assuming a two site exchange. Figure 2.29 shows the simulated and calculated spectra with the rate constants obtained for each temperature. It appears that there is a slight asymmetry in the broadening of the signals with the upfield signal to broaden first. Such behavior could arise from the presence of small amounts of an intermediate involving a Co-Co bridging or agostic Ir-C bridging hydride. A good example how

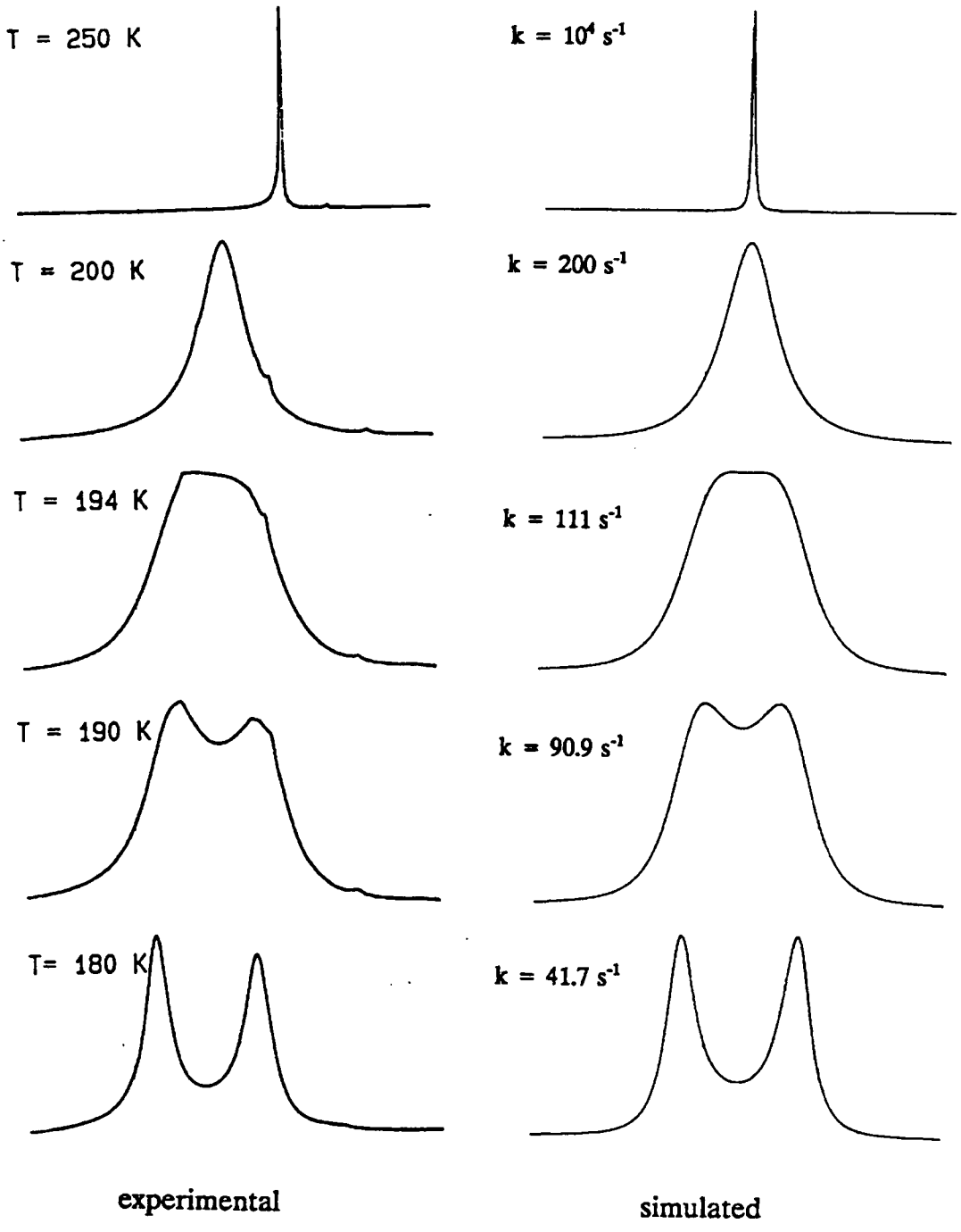

Figure 2.29: Experimental and calculated lineshapes of the Cp proton signals of **18** at variable temperatures.

small amounts of an intermediate can have a visible impact on an apparent two site exchange is discussed in the next chapter. In this case the deviation from ideal two site exchange is small implying that if there is any intermediate in the process it can only occur in very small amounts. No additional signal could be found in any region of the spectrum. From an Eyring plot, an enthalphy of activation $\Delta H^{\ddagger}$ = 28.1(9) kJ mol^{-1} and an activation entropy $\Delta S^{\ddagger}$ = -57(5) J K^{-1} mol^{-1} were obtained. From these values, free energies of activation $\Delta G^{\ddagger}$(194 K) = 39.1 kJ mol^{-1} and $\Delta G^{\ddagger}$(298 K) = 45.0 kJ mol^{-1} were obtained.

An analysis of the coalescence of the corresponding carbon-13 signals yielded somewhat different values of $\Delta H^{\ddagger}$ and $\Delta S^{\ddagger}$ (36.1 kJ mol^{-1} and -15.3 J K^{-1} mol^{-1}, but the values of $\Delta G^{\ddagger}$ are very similar (39.1 kJ mol^{-1} at 194 K and 40.7 kJ mol^{-1} at 298 K. The discrepancy in the values for $\Delta H^{\ddagger}$ and especially $\Delta S^{\ddagger}$ indicates that the temperature interval in which rate constants were obtained is too small to yield reliable values for these parameters.[55] The free activation energies are less dependent on the temperature range since they directly depend on the rate constant according to the Eyring equation.

2.6.5. Carbyne-Hydride Exchange

At room temperature, the carbyne and hydride signals in the ^{1}H NMR spectrum appear to be slightly broadened, indicating exchange between the two sites. A NOESY spectrum does indeed show a strong cross peak connecting the carbyne signal at 15.1 ppm with the hydride signal at -25.3 ppm. Exchange

between a CH proton and a metal hydride is an example of C-H activation. Several examples of such processes have been reported in the literature. Most cluster systems studied were carbonyl based cluster complexes,[16] however, to our knowledge there is no example for carbyne hydride exchange in Cp based cluster complexes.

An exchange process which is slow on the NMR chemical shift time scale can be examined by magnetization transfer techniques.[56] One variant of this experiment involves applying a selective 180° pulse to one of the exchanging nuclei. During a waiting time τ, transfer of the magnetization created by this pulse occurs to the other nuclei involved in the exchange process. At the end of the waiting time τ a nonselective 90° pulse is applied and the resulting spectrum acquired. In our case the two resonances are well separated (16 kHz) and a rectangular, low power pulse (p1 = 5 ms) applied through the decoupler channel achieved sufficient selectivity. Varying the time period τ allows one to monitor the exchange of magnetization. Figure 2.30 illustrates the effect of magnetization transfer in the case that the hydride resonance is inverted. For small values of τ, the hydride resonance appears inverted, whereas the carbyne signal is unchanged. With increasing waiting time τ the hydride signal evolves towards equilibrium. At the same time, inverted magnetization is transferred to the carbyne proton, causing a decrease in that signal. Eventually, both signals relax back to their equilibrium values.

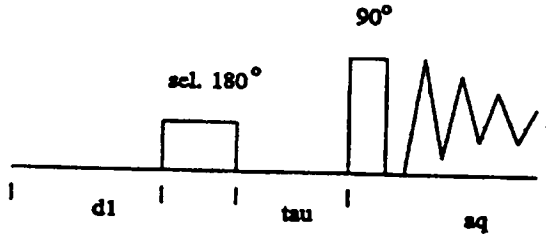

Pulse sequence for selective inversion transfer

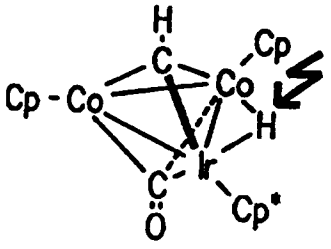

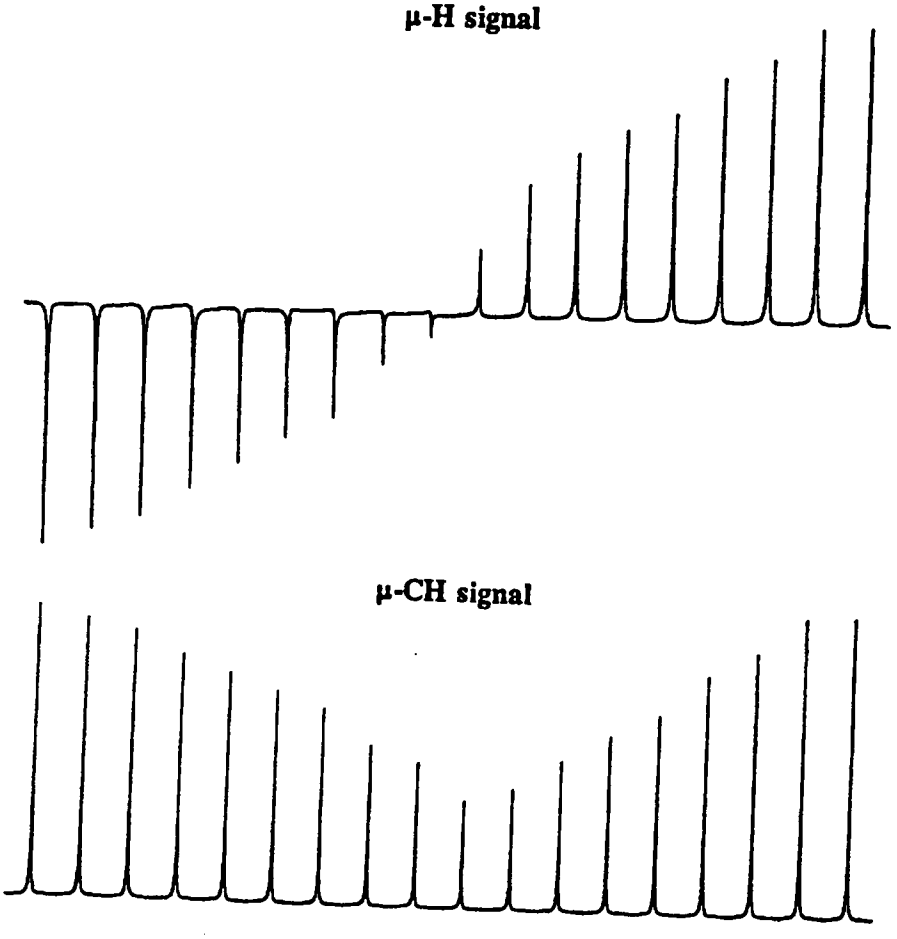

Figure 2.30: Pulse sequence for selective inversion transfer (top), hydride (middle) and carbyne signal (bottom) with increasing τ.

In order to describe this behavior in a quantitative way one has to consider the Bloch equations for chemical exchange:

$$\frac{dM_{\mu\text{-}H}(t)}{dt} = -\frac{M_{\mu\text{-}H}(t) - M^{eq}_{\mu\text{-}H}}{T_{1,\mu\text{-}H}} - kM_{\mu\text{-}H} + kM_{CH} \qquad (2.6)$$

$$\frac{dM_{CH}(t)}{dt} = -\frac{M_{CH} - M^{eq}_{CH}}{T_{1,CH}} + kM_{\mu\text{-}H} - kM_{CH} \qquad (2.7)$$

$M_{\mu\text{-}H}(t)$ and $M_{CH}(t)$ are the time dependent magnetizations of the hydride and carbyne protons, M^{eq} are the respective equilibrium magnetizations, $T_{1,\mu\text{-}H}$ and $T_{1,CH}$ are the longitudinal relaxation times of the carbyne and hydride sites and k is the rate of exchange between the two sites. In the case that the μ-CH resonance is inverted, one obtains[56b]

$$M_{\mu\text{-}H}(t) = C_1 e^{\lambda_+ t} + C_2 e^{\lambda_- t} + M^{eq}_{\mu\text{-}H} \qquad (2.8)$$

$$M_{CH}(t) = \frac{C_1}{k}(\lambda_+ + r_{\mu\text{-}H} + k)e^{\lambda_+ t} + \frac{C_2}{k}(\lambda_- + r_{\mu\text{-}H} + k)e^{\lambda_- t} + M^{eq}_{CH} \qquad (2.9)$$

with

$$\lambda_\pm = \frac{1}{2}\left(-(r_{\mu\text{-}H} + r_{CH} + 2k) \pm \sqrt{(r_{\mu\text{-}H} + r_{CH} + 2k)^2}\right) \qquad (2.10)$$

$$C_2 = \frac{k}{\lambda_+ - \lambda_-}\left(\frac{\lambda_+ + r_{\mu\text{-}H} + k}{k}(M^0_{\mu\text{-}H} - M^{eq}_{\mu\text{-}H}) + (M^0_{CH} - M^{eq}_{CH}) \right) \qquad (2.11)$$

$$C_1 = M^0_{\mu\text{-}H} - M^{eq}_{\mu\text{-}H} - C_1$$

where $r_{\mu\text{-}H}$ and r_{CH} are the relaxation rates $1/T_{1,\mu\text{-}H}$ and $1/T_{1,CH}$, whereas $M_{\mu\text{-}H}{}^0$ and $M_{CH}{}^0$ are the initial magnetizations immediately after the 180° pulse. With these equations, nonlinear fits of the data were obtained using the rate constants, relaxation times and initial magnetizations as free variables. Under ideal conditions, one expects $M_{\mu\text{-}H}{}^0 = - M_{\mu\text{-}CH}{}^{eq}$, however for experimental reasons this is not exactly the case and therefore this parameter was included as free variable.

A plot of experimental and calculated data is shown in Figure 2.31 for a temperature of 275 K. One can see that the calculated curves fit the data very well. As expected, rate constants obtained from fitting either the carbyne and the hydride resonance agree within 10%. By conducting the experiment over a temperature range of 250 - 300 K the activation parameters were obtained as $\Delta H^{\ddagger} = 73.3$ kJ mol^{-1}, $\Delta S^{\ddagger} = 36$ J K^{-1} mol^{-1} and $\Delta G^{\ddagger}(300\text{ K}) = 62.7$ kJ mol^{-1}. These values are significantly smaller than the ones found for the carbonyl based cluster complexes $M_3(CO)_9(\mu\text{-H})_3(\mu_3\text{-CH})$ (M = Ru, Os)[16] (See Table 2.11). If the sample is heated above 300 K, the carbyne and hydride signals broaden significantly and eventually are lost in the noise. Due to the large difference in chemical shift it was not possible to measure the coalescence region or the high temperature region of the exchange. However, lineshape analysis of the spectra

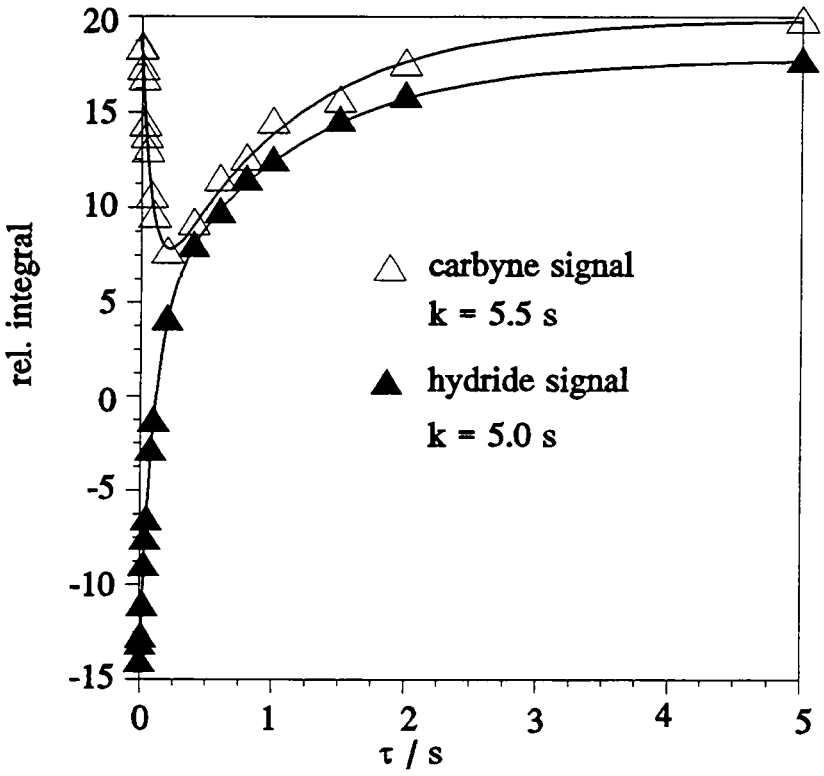

Figure 2.31: Experimental data from selective inversion experiment at 275K (triangles) and fit through the data according to (2.8) and (2.9).

Table 2.11: Activation barriers for carbyne hydride exchange and hydride scrambling in **18**.

18	$\Delta H^{\ddagger}$ / kJ mol^{-1}	$\Delta S^{\ddagger}$ / J mol^{-1} K^{-1}	$\Delta G^{\ddagger}$(300 K) / kJ mol^{-1}
carbyne-hydride exchange	73.3[a], 61(2)[b]	35.5[a], -28(6)[b]	73.3[a], 69[b]
hydride edge exchange	28.1[b], 36.1[c]	-57[b], -15[c]	45.0[b], 40.7[c]
Carbyne - hydride exchange in $M_3(CO)_9(\mu_3\text{-}CH)(\mu_2\text{-}H)_3$[d]			
M = Ru	-	-	86.1
M = Os	100.3	8.4	97.8

a) from inversion transfer b) from ^{1}H NMR lineshape c) from ^{13}C NMR lineshape d) Ref. 16

up to 340 K yielded activation parameters similar to the ones obtained from the inversion transfer study.

2.6.6. Mechanism of Carbyne Hydride Fluxionality

The barriers activation $\Delta G^{\ddagger}$(300 K) obtained for the carbyne-hydride exchange and for the hydride fluxionality about the metal triangle differ by about 20 kJ mol^{-1} (Table 2.11), indicating that the two processes are independent from one another. A mechanism for carbyne-hydride exchange involving agostic hydrogens has been proposed by Shapley and coworkers for $M_3(CO)_9(\mu\text{-}H)_3(\mu_3\text{-}CH)$ (M = Ru, Os).[16] We believe that a similar process causes the carbyne-hydride exchange in **18** as shown in Figure 2.32. The initial step of this process involves the hydride ligand moving from a metal-metal edge in **a** to an "agostic" geometry on a metal-$C_{methylidyne}$ edge (**b**). Qualitative analysis of the energetics of agostic interactions in homo- and heteronuclear clusters of iron, ruthenium and osmium[6e] suggest that C-H-M bridging bridged hydrogens will prefer binding to the metal with the lower electronegativity on the Mullay scale,[57] which, in the case of **18**, is the Ir-C edge. A transition state **c** in which the M-H interaction is released simultaneously with the methylidyne hydrogen moving towards an "agostic" position on the opposite C-H-M edge then exchanges the identities of these protons. This transition state can be regarded as a complex with a triply bridging carbene ligand with weak agostic C-H-M interactions. The final step is simply the reverse of the initial step with the former terminal carbyne hydrogen

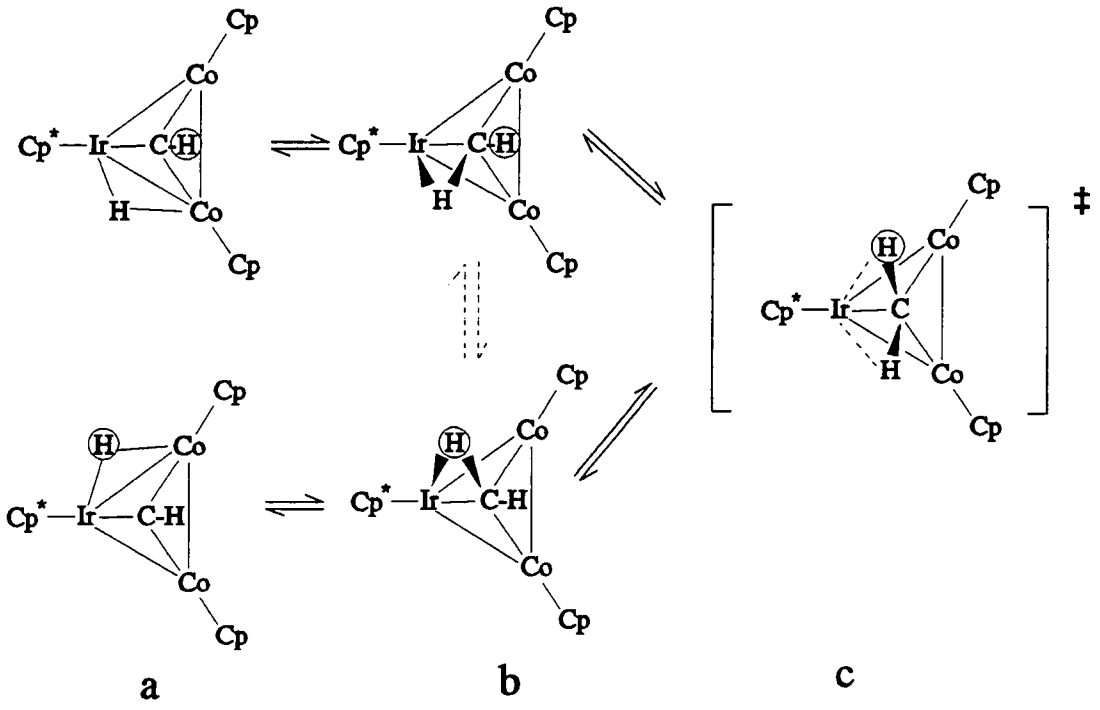

Figure 2.32: Proposed mechanism for exchange of the carbyne and hydride hydrogens involving agostic hydrogens. The dotted arrows indicate a pathway for hydride migration.

now ending up on the opposite Ir-Co edge.

Although the mechanism described above equilibrates the two CpCo vertices in **18**, our kinetic analyses indicate that a second, lower energy process must also be available to accomplish this task without exchanging the hydride and methylidyne hydrogen identities (see above). Migration of hydride ligands in several tri- and tetranuclear cluster systems has been observed with similar activation energies[8, 9,58] and may simply involve movement of the hydride ligand from the ground state bridging geometry to a terminal coordination mode and

finally back to a bridging mode on a different metal edge in the complex. However, in some of the systems mentioned above, alkylidyne ligands are also present and may be involved in these processes. A possible mechanism which would include the carbyne ligand in hydride migration involves reversible movement of the bridging hydride ligand to an agostic position on the Ir-C edge in **18** without moving the carbyne hydrogen. This interchanges the two structures **b** as indicated by the dotted arrow in Figure 2.32. Since the terminal carbon-hydrogen bond is not broken in this case, a lower activation barrier compared with the carbyne-hydride exchange can be expected for this process. This is only possible if the formation of agostic hydrogens is a low energy process; in that case the rate determining step for exchange of carbyne and hydride hydrogen has to be the interchange with the terminal carbyne hydrogen through transition state **c**. Our data do not allow us to distinguish between different mechanisms for the hydride edge exchange. However, a mechanism involving agostic hydrogens could explain why $Cp^*Rh(Cp^*M)_2(CO)_2(\mu\text{-}H)_2$ (M=Co, Ir)[59] and $Os_3Pt(\mu\text{-}H)_2(CO)_{10}P(C_6H_{11})_3$[60], which do not exhibit carbyne ligands, exhibit much higher activation energies for hydride migration around their metal skeletons.

2.6.7. Reactivity Towards Donor Ligands

The facile exchange of hydrogen atoms between the methylidyne and hydride sites suggests that it may be possible to transform the carbyne-hydride

complex **18** into a carbene complex if a ligand is present to supply the two valence electrons which are lost when the hydride migrates back to the methylidyne carbon. Consistent with this prediction, we find that **18** reforms the carbene complex **8** when exposed to CO at room temperature. Quantitative conversion is observed within 2 hrs at 270 K as monitored by ^{1}H NMR spectroscopy in toluene-d_8. Longer exposure to CO then leads to cluster fragmentation.

The isoelectronic osmium carbonyl cluster $Os_3(CO)_{10}(\mu\text{-CH})(\mu\text{-H})$ **4** does not exhibit hydrogen atom exchange between the carbyne and hydride site and also does not add carbon monoxide. Instead nucleophiles attack directly at the carbyne carbon.[5c] The trihydride clusters $M_3(CO)_9(\mu_3\text{-CH})(\mu\text{-H})_3$ (M = Ru, Os)[16] do exhibit hydrogen atom transfer between the methylidyne and hydride ligands but the barriers of activation are much higher than in **18** ($\Delta G^{\ddagger}$ = 86 kJ mol^{-1} for M = Ru and 100 kJ mol^{-1} for M = Os). None of these systems are observed to add CO, even at higher temperatures.[16] It is interesting to note that only the isomer with the carbene ligand bridging an Ir-Co edge is formed in the reaction of the carbyne-hydride complex with CO. None of the isomer bearing the carbene ligand on the Co-Co edge is observed.

With these results in mind, we attempted to add other two electron donor ligands like dihydrogen, triphenylphosphine, ethylene and alkynes to the carbyne-hydride complex **18**. Our intent was to use **18** as starting point to make a new series of adducts as indicated in Figure 2.33. Such complexes would be of particular interest since coupling of the carbene ligand and the new ligand might

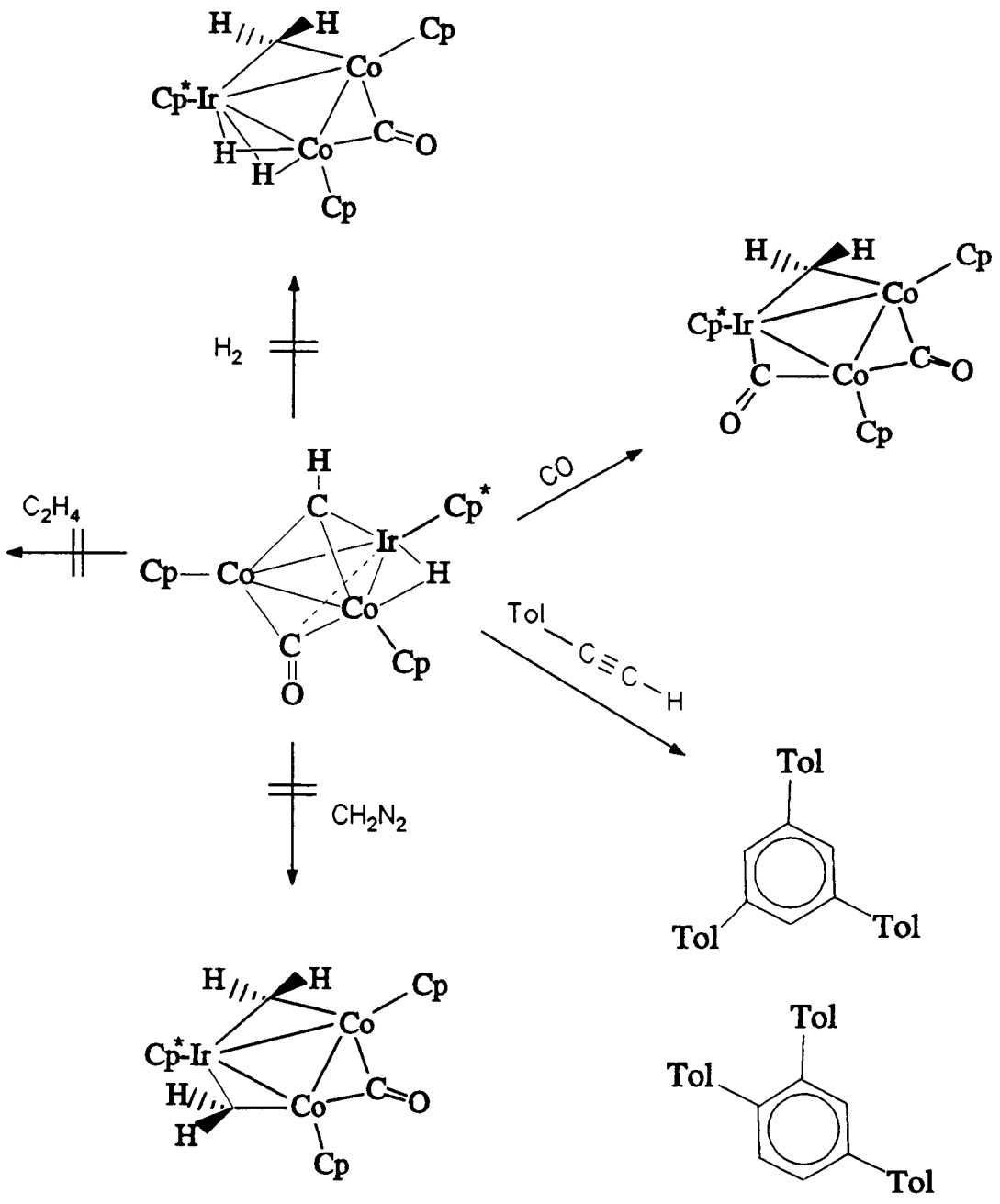

Figure 2.33: Reactions attempted with the carbyne hydride complex **18**; only addition of CO lead to clean addition.

be observed, illustrating examples of C-C bond formation in a metal cluster. Our results indicate, however, that **18** is not reactive towards ligands other than CO. For example, reaction with CH_2N_2 and PPh_3 resulted in the recovery of starting material. Furthermore, a sample of carbyne hydride complex under ethylene atmosphere in a sealed NMR tube remained unchanged when left at room temperature for several days. Alkynes, on the other hand, appear to fragment the cluster. These fragments then catalyze trimerization of the alkyne and eventually form aggregates of high nuclearity. In a sample of **18** in a NMR tube under 1 atm acetylene in toluene-d_8 a signal at 7.133 ppm was observed to grow in over the period of several days, consistent with the formation of benzene. At the same time, the concentration of **18** in solution was decreasing and eventually a precipitate of metal aggregates formed. In another reaction, a mixture of carbyne hydride complex **18** and an excess of tolylacetylene was refluxed in toluene for one minute. After that, no Cp or Cp^* containing species soluble in any common NMR solvent was present in the reaction mixture. However, NMR and MS analysis showed that the alkyne was completely converted to its cyclic trimer, tritolylbenzene. The NMR data are consistent with a 1:1 mixture of the 1,3,5 and 1,2,4 substituted isomers indicating that there is no preference for head-to-head or head-to-tail coupling in the trimerization process. Cyclic trimerization of alkynes is known to be catalyzed by mononuclear metal complexes.[61] We therefore assume that the catalytic species in this process are CpCo or Cp^*Ir fragments formed from cluster fragmentation. Since no intermediate was observed in the

trimerization of acetylene fragmentation of the cluster complex appears to occur with a rate faster than the addition of the alkyne to the cluster.

Even though this survey on the reactivity of the carbyne-hydride complex **18** was not exhaustive, the results described above are not encouraging. Further research might be needed, but so far it appears to that the carbyne hydride complex can not be used as starting point for a new series of compounds.

2.6.8 CpCo and Cp*Rh Analogues

As mentioned above, the Co and Rh analogous carbene complexes **6** and **7** decompose in solution at temperatures considerably lower than found for the Ir containing carbene complex **8**. However, more than one product appear to be formed and so far no clean product could be isolated in either case. In particular, the very characteristic set of signals contributed from a carbyne-hydride complex was not observed. At this point, one can only speculate about the nature of these products. A low temperature spectrum taken of the decomposition product of the Rh containing carbene complex **7** revealed what appeared to be decoalescence of one signal at 15 ppm and several signals in the hydride region between -20 and -25 ppm. One therefore has to consider the possibility that the CpCo and Cp*Rh containing carbene complexes form carbyne hydride complexes in which the exchange between the carbyne and hydride protons is fast enough to cause a coalescence broadening which renders the signals unobservable at room temperature. However, the pattern of signals decoalescing at low temperature is

too complex to be caused just by a carbyne hydride complex. Further research is needed to establish the nature of these products.

2.7. Summarizing Discussion about Carbene Chemistry

The reaction of a series of homo and heteronuclear cluster complexes with diazoalkanes has been investigated. Addition of diazomethane leads to both carbene and hydrazone adducts. In the case of the heteronuclear complexes $Cp^*M(CpCo)_2(CO)_2$, the tendency of carbene formation depends on the nature of the metal and increases in the order M = Co < Rh < Ir. The Ir complex forms

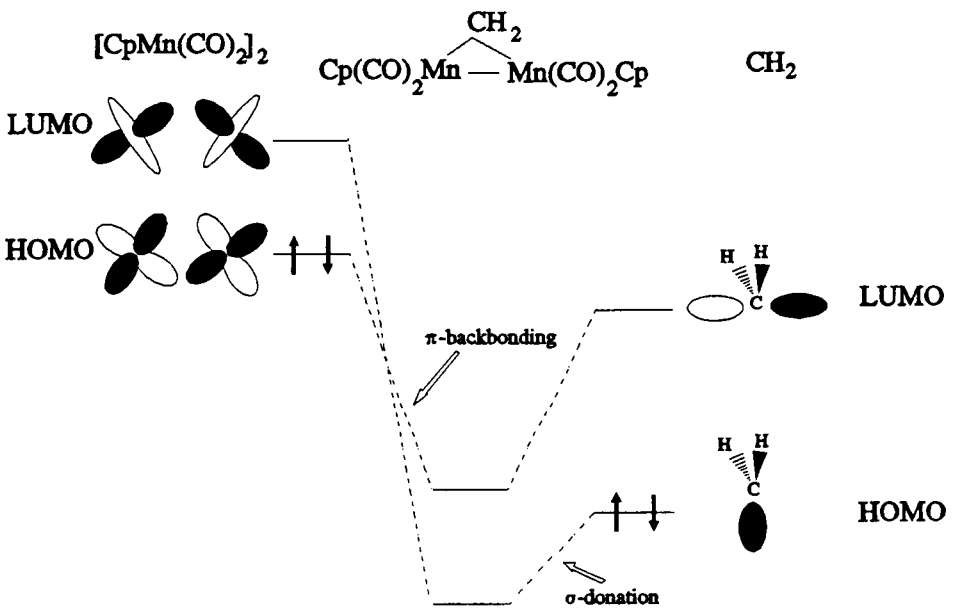

Figure 2.34: Frontier orbitals of $[CpMn(CO)_2]_2$. Source: Reference 62.

only the carbene adduct, whereas the Co complex forms only hydrazone adduct. The Rh complex takes an intermediate position between these two extremes, forming both carbene and hydrazone adducts. This trend might be correlated with the increase in π-backbonding capability from Co to Ir. It is believed that an important contribution to the bonding of a bridging methylene ligand involves backbonding from the metal-metal σ-bond into the empty p_π-orbital of the carbene ligand.[23] Photoelectron spectroscopy and molecular orbital calculations performed for the dinuclear complex $[CpMn(CO_2)]_2$ indicate that the HOMO of the dinuclear framework has the type π^*_{xy} and is only slightly higher in energy than the empty p_π orbital of the carbene ligand (Figure 2.34),[62] leading to a strong backbonding interactions. Similar arguments hold true for the frontier orbitals of the corresponding trinuclear framework M_3L_9.[63] The hydrazone ligand, on the other hand, is not a π-acceptor. It is therefore conceivable that increased backbonding will thermodynamically stabilize a carbene ligand over a hydrazone ligand. In addition, increased π-backbonding of the metal also makes loss of CO more difficult, thus introducing a higher kinetic barrier to the formation of hydrazones. Consistent with this theory, the complex $Cp^{\ddagger}Co(CpCo)(\mu_3\text{-}CO)_2$, in which the Cp^*Co fragment is substituted by the less electron rich $Cp^{\ddagger}Co$ fragment, also forms the hydrazone adduct only. On the other hand, the all-CpCo containing cluster complex **6** is more electron deficient than the Cp^*Co analogue, but in this case both carbene and hydrazone adducts

are formed in comparable amounts. This fact indicates that in addition steric factors might influence the course of the reaction.

In the case of the heteronuclear carbene complexes $Cp^*M(CpCo)_2(\mu_2\text{-}CO)_2(\mu_2\text{-}CH_2)$ only one of two positional isomers is formed upon addition of diazomethane. This preferred isomer is the one in which the carbene ligand bridges a Cp^*M-CpCo edge. In the case M = Rh this effect is clearly not due to a thermodynamic preference of the Rh-Co over the Co-Co since at equilibrium, both isomers are present in comparable amounts. The reasons for the initial preference of the carbene to be on the Rh-Co edge has therefore to be a kinetic one. A possible explanation for this behavior is found when the mechanism of diazomethane addition is examined more closely. As shown in Figure 2.35, it is believed that in a first step the diazoalkane adds to one of the metal atoms to form a terminal diazoalkane adduct. The most likely point of attack is hereby the Cp^*M fragment despite the sterically demanding Cp^* ligand because in the original 46 electron cluster complex the two CO ligands are bound in a semi triply bridging fashion closer to the CpCo-Cpco edge.[29] From that point the reaction can take one of two possible pathways. The nitrogen can move into a triply bridging position, causing loss of one CO ligand to form the final diazoalkane adduct. Or the carbon end of the diazomethane can bend over one of the neighboring edges, causing abstraction of dinitrogen and formation of a carbene ligand. In this case the carbene ligand will end up on a metal-metal edge adjacent to the Cp^*M vertex bearing the terminal diazoalkane ligand, i. e. the

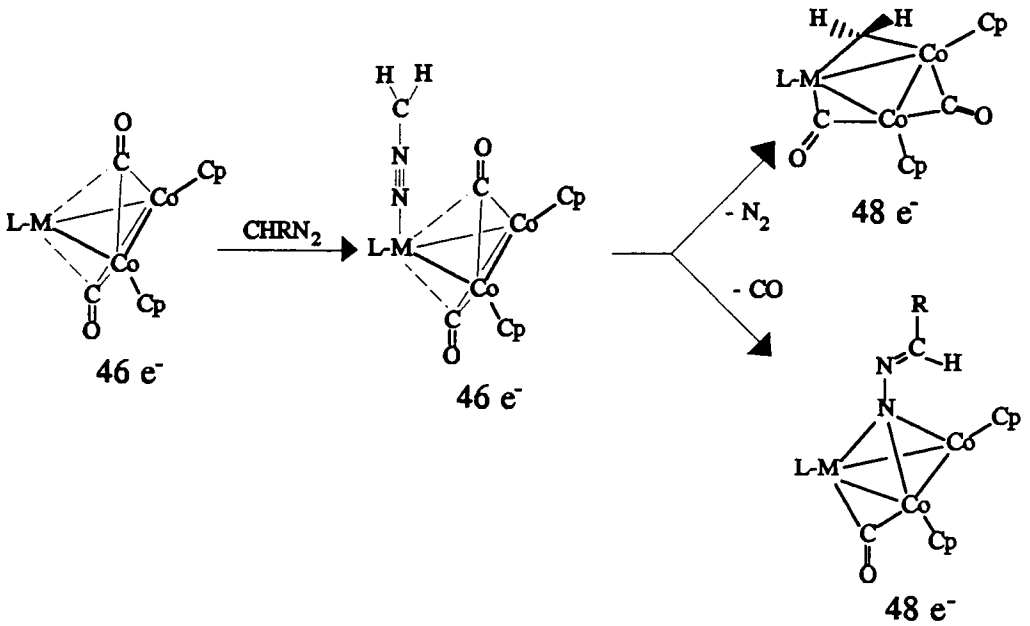

Figure 2.35: Possible intermediate in the formation of hydrazone and carbene adducts.

Cp^*M-CoCp edge. Such an intermediate involving a terminal diazomethane ligand has not yet been observed, but in the case of addition of carbon monoxide to the Ir substituted 46 electron complex **1** the tricarbonyl $Cp^*Ir(CO)(CpCo)_2(\mu_2\text{-}CO)_2$ is formed which contains one carbonyl in a terminal position on the iridium.[11]

In both the Rh and Ir containing carbene complexes the carbene ligand migrates between the two Cp^*M-CpCo edges interconverting two enantiomers of this positional isomer. Above 350 K this migration is fast enough to be monitored by magnetization transfer techniques such as NOESY spectroscopy. A similar process is observed in the all CpCo containing complex **6** where the carbene

ligand moves about the different Co-Co edges. In the case of the Rh complex **7** an intermediate in that process is observed with an abundance of around 1%. This intermediate is most likely due to a species containing a triply bridging carbene ligand. So far, carbene migration processes were assumed to proceed through intermediates containing a terminal carbene ligand. This is the first example where such an intermediate has been directly observed, and the first evidence for the presence of a triply bridging carbene ligand.

Upon refluxing in toluene the Ir carbene complex **8** loses one carbonyl ligand and forms the carbyne hydride complex **18** containing a μ_3-bridging carbyne ligand and a hydride ligand bridging an Ir-Co edge. Two fluxional processes are observed in this complex: A low energy process moves the hydride between the two Ir-Co edges, whereas a slower process interchanges the identities of the carbyne and hydride hydrogens. Addition of CO leads again to the initial carbene complex **8**.

2.8 References

1. a) Sheppard, N.; *Ann. Rev. Phys. Chem.* **1988**, *39*, 589. b) Collman, J. P.; Hegedus, L. S.; Norton, J. R.; Finke, R. G.; *Principles and Application of Organotransition Metal Chemistry*, University Science Books; Mill Valley, CA **1987**, Ch. 12.

2. Zheng, C.; Apeloig, Y.; Hoffmann, R.; *J. Am. Chem. Soc.* **1988**, *110*, 749-774.

3. a) Kaminsky, M. P.; Winograd, N.; Geoffroy, G. L.; Vannice, M. A. *J. Am. Chem. Soc.* **1986**, *108*, 1315 and references therein. b) Lee, M. B.; Yang, Q. Y.; Tang, S. L.; Ceyer, S. T.; *J. Chem. Phys.* **1986**, *85*, 1693. c) Loggenberg, P. M.; Carlton, L.; Copperwaite, R. G.; Hutchings, G.; *J. Chem. Soc. Chem.Commun.* **1987**, 541.

4. a) Muetterties, E. L.; Rhodin, T. N.; Band, E.; Brucker, C. F.; Pretzer, W. R.; *Chem. Rev.* **1979**, *79*, 91-135. b) Muetterties, E. L.; *Pure Appl. Chem.* **1982**, *54*, 83-96.

5. a) Calvert, R. B.; Shapley, J. R.; *J. Am. Chem. Soc.*, **1977**, *99*, 5225-5226. b) Calvert, R. B.; Shapley, J. R.; *J. Am. Chem. Soc.*, **1978**, *100*, 7726-7727. c) Shapley, J. R.; Cree-Uchiyama, M. E.; St. George, G. M.; *J. Am. Chem. Soc.* **1983**, *105*, 140-142. d) Holmgren, J. S.; Shapley, J. R.; *Organometallics* **1984**, *3*, 1322-1323. e) Holmgren, J. S.; Shapley, J. R.; *Organometallics* **1985**, *4*, 793-794. f) Yeh, W. Y.; Wilson, S. R.; Shapley, J. R.; *J. Organomet. Chem.* **1989**, *371*, 257-265.

6. a) Wong, K. S.; Fehlner, T. P.; *J. Am. Chem. Soc.* **1981**, *103*, 966-967. b) Vites, J. C.; Jacobson, G.; Dutta, T. K.; Fehlner, T. P.; *J. Am. Chem. Soc.* **1985**, *107*, 5563-5565. c) Dutta, T. K.; Vites, J. C.; Jacobsen, G. B.; Fehlner, T. P.; *Organometallics* **1987**, *6*, 842-847. d) Barreto, R. D.; Fehlner, T. P.; *J. Am. Chem. Soc.* **1988**, *110*, 4471-4472. e) Fehlner, T. P.; *Polyhedron* **1990**, *15/16*, 1955-1963.

7. Steinmetz, G. R.; Geoffroy, G. L.; *J. Am. Chem. Soc.* **1981**, *103* 1278-1279.

8. Vollhard, K.P.; Fritch, J.R.; *Angew. Chem, Int. Ed. Engl.* **1980**, *19*, 559-561.

9. Wadepohl, H.; Pritzkow, H.; *J. Organomet. Chem.*, **1993**, *450*, 9-19.

10. a) Kersten, J. L.; Rheingold, A. L.; Theopold, K. H.; Casey, C. P.; Widenhoefer, R. A.; Hop, C. E.; *Angew. Chem.* **1992**, *104*, 1346; *Angew.*

Chem, Int. Ed. Engl. **1992**, *32*, 1341. b) Casey, C. P.; Widenhoefer, R. A.; Hallenbeck, S. L.; *Organometallics*, **1993**, *12*, 3788-3789.

11. Herrmann, W. A.; Barnes, C. E.; Zahn, T.; Ziegler, M. L.; *Organometallics* **1985**, *4*, 172-179.

12. Pruett, R. L.; Schoenig, R. C.; Vidal, J. L.; Fiato, R. A.; *J. Organomet. Chem.* **1979**, *182*, C57-C60.

13. Shriver, D. F.; Sailor, M. J.; *Acc. Chem. Res.* **1988**, *21*, 374-379.

14. Barreto, R. D.; Puga, J.; Fehlner, T. P.; *Organometalics* **1990**, *9*, 662-668.

15. Skinner, D. M.; Rosenberg, E.; Bracker-Novak, J.; Aime, S.; Osella, D.; Gobetto, R.; Milone, L.; *Organometalics* **1988**, *7*, 856-858.

16. VanderVelde, D. G.; Holmgren, J. S.; Shapley, J. R.; *Inorg. Chem.* **1987**, *26*, 3077-3078.

17. Fischer, E. O.; A. Maasbol, A.; *Angew. Chem.* **1964**, *76*, 64.

18.

19. a) Schrock, R. R.; *J. Am. Chem. Soc.* **1975**, *97*, 6577. b) Guggenberger, L. J.; Schrock, R. R.; *J. Am. Chem. Soc.* **1975**, *97*, 6578.

20. a) Sternberg, H. W.; Shukys, J. G.; Donne, C. D.; Markby, R.; Friedel, R. A.; Wender, J.; *J. Am. Chem. Soc.* **1959**, *81*, 2339.

21. a) Albanesi, G.; Tovagliere, M.; *Chim. Ind. (Milan)* **1959**, *41*, 189. b) Albanesi, G.; *Chim. Ind. (Milan)* **1964**, *46*, 1169. c) Albanesi, G.; Gavezotti, E.; *Chim. Ind. (Milan)* **1965**, *47*, 1322.

22. Herrmann, W. A.; Reiter, B.; Biersack, H.; *J. Organomet. Chem.* **1975**, *97*, 245.

23. Herrmann, W. A.; *Advan. Organometal. Chem.* **1982**, *20*, 159-263.

24. Wittig, G.; Schöllkopf, U.; Chem. Ber. **1954**, *87*, 1318.

25. Korswagen, R. Alt, R.; Speth, D; Ziegler, M. L.; *Angew. Chem.* **1981**, *93*, 1073; *Angew. Chem., Int. Ed. Engl.* **1981**, *20*, 1049.

26. Sumner Jr, P. E.; Riley, P. R.; Davis, R. E.; Pettit, R.; *J. Am. Chem. Soc.* **1980**, *102*, 1752.

27. Leopold, K. H.; Bergmann, R. G.; *J. Am. Chem. Soc.* **1980**, *102*, 5694.

28. Several review articles concerning diazoalkane complexes: a) Herrmann, W. A.; *Angew. Chem.* **1978**, *17*, 800-812. b) Sutton, D.; *Chem. Rev.* **1993**, *93*, 995-1022. c) Mazobe, Y.; Ishii, Y.; Hidai, M.; *Coord. Chem. Rev.* **1995**, *139*, 281-311.

29. Barnes, C. E.; Dial, M. R.; *Organometallics*, **1988**, *7*, 782-784. Barnes, C. E.; Dial, M. R.; Orvis, J. A.; Staley, D. L.; Rheingold, A.L. *Organometallics* **1990**, *9*, 1021-1035.

30. Finniss, G. M.; Master Thesis, Knoxville **1992.**

31. Dial, M.; *Master Thesis*, University of Tennessee, Knoxville.

32. Barnes, C. E.; Orvis, J.; *Organometallics* **1993**, *12*, 1016-1017.

33. a) Hörlein, R.; Herrmann, W. A.; Barnes, C. E.; Weber, C.; Krüger, C.; Ziegler, M. L.; Zahn, T.; *J. Organomet. Chem.* **1987**, *321*, 257-272. b) Farone, F.; Schiavo, S. L.; Bruno, G.; Piraino, P.; Bombieri, G.; *J. Chem. Soc., Dalton Trans.* **1983**, 1813.

34. a) Jeener, J.; Meier, B. H.; Bachmann, P.; Ernst, R. R.; *J. Chem. Phys.* **1979**, *71*, 4546-4553. b) Macura, S.; Ernst, R. R.; *Molecular Physics* **1980**, *41*, 95-117.

35. Pople, J. A.; *Mol. Phys.* **1958**, *1*, 168.

36. Cox, A. P.; Thomas, L. F.; Sheridan, J.; *Nature* **1958**, *181*, 1157.

37. Levine; *J. Chem. Phys.* **1963**, *38*, 2326.

38. A list of C-C and C-X bond distances can be found in: March, J.; *Advanced Organic Chemistry: Reactions, Mechanisms, and Structure*, John Wiley & Sons, Third Edition, **1985**; p. 19.

39. Greenwood, N. N.; Earnshaw, A.; *Chemistry of the Elements*, First Edition, Pergamon Press, **1984**; p. 505, 528.

40. a) W. B. Jennings, D. M. Jerina; J. Am. Chem. Soc. **94** (1972) 8501 b) T. Yonezawa, I. Morishima; J. Mol. Spectr. **31** (1969) 341

41. Gassman, P. G.; Mickelson, J. W.; Sowa, J. R.; *J. Am. Chem. Soc.* **1992**, *114*, 6942.

42. Drenth, W.; *Kinetics applied to organic reactions*, M. Dekker, New York 1980.

43. a) Eyring, H.; *Chem. Revs.* **1935**, *17*, 65. b) Glasstone, S.; Laidler, K. J.; Eyring, H.; *The Theory of Rate Processes*, McGraw-Hill, New York, **1941**.

44. a) Fischer, E. O.; Offhaus, E.; *Chem. Ber.* **1969**, *102*, 2549-2455. b) Fischer, E. O.; Offhaus, E.; Müller, J.; Nöthe, D.; *Chem. Ber.* **1972**, *105*, 3027-3035. c) Casey, C. P.; Anderson, R. L.; *J. Am. Chem. Soc.* **1971**, *93*, 3554-3555.

45. a) Shapley, J. R.; Yeh, W. Y.; Churchill, M. R.; Li, Y.; *Organometallics* **1985**, *4*, 1898-1900. b) Yeh, W. Y.; Shapley, J. R.; Ziller, J. W.; Churchill, M. R.; *Organometallics* **1987**, *6*, 1-7. c) Yeh, W. Y.; Wilson, S. R.; Shapley, J. R.; *J. Organomet. Chem.* **1989**, *371*, 257-265.

46. a) Theopold, K. H.; Bergmann, R. G.; *J. Am. Chem. Soc.* **1983**, *105*, 464-475. b) Dyke, A. F.; Knox, S. A. R.; Mead, K. A.; Woodward, P.; *J. Chem. Soc., Chem. Comm.* **1981**, 861-862.

47. a) Müller, L.; *J. Am. Chem. Soc.* **1979**, *101*, 4481-4484. b) Bax, A.; Griffey, R. H.; Hawkins, B. L.; *J. Magn. Res.* **1983**, *55*, 301-315. c) Bendal, M. R.; Pegg, D. T.; Doddrell, D. M.; *J. Magn. Res.* **1990**, *86*, 346-357.

48. Hörlein, R.; Herrmann, W. A.; Barnes, C. E.; Weber, C.; Krüger, C.; Ziegler, M. L.; Zahn, T.; *J. Organomet. Chem.* **1987**, *321*, 257-272.

49. Tulyathan, B.; Geiger, W. E.; *J. Am. Chem. Soc.* **1985**, *107*, 5960.

50. Part of this section has been published as communication: Försterling, F. H.; Barnes, C. E.; *Organometallics* **1994**, *13*, 3770-3772.

51. Teller, R. G.; Bau, R.; *Structure and Bonding* **1981**, *44*, 1-82.

52. Brookhart, M.; Green, M. L. H.; *J. Organomet. Chem.* **1983**, *250*, 395-408.

53. For a review about dynamic NMR see: Binch, G.; Kessler, H.; *Angew. Chem.* **1980**, *92*, 445-463.

54. a) Stephenson, D. S.; Binch, G.; *Quantum. Chem. Progr. Exch.* **1978**, *10*, 365. b) Stephenson, D. S.; Binch, G.; *J. Magn. Res.* **1978**, *32*, 145.

55. Sandström, J.; *Dynamic NMR Spectroscopy*, Academic Press, London, **1982**.

56. a) Forsen, S.; Hoffman, R. A.; *J. Chem. Phys.* **1963**, *39*, 2892-2901.
b) Alger, J. R.; Prestegard, J. H.; *J. Magn. Res.* **1977**, *27*, 137-141.
c) Mariappan, S. V.; Rabenstein, D. L.; *J. Magn. Res.* **1992**, *100*, 183-188.

57. Mullay, J.; *J. Am. Chem. Soc.* **1984**, *106*, 5842.

58. Van Horn, D. E.; Vollhard, K. P. C.; *J. Chem. Soc., Chem. Comm.* **1982**, 203-204.

59. Bray, A. C.; Green, M.; Hankey, D. R.; Howard, J. A.; Johnson, H.; Stone, F. G.; *J. Organomet. Chem.* **1985**, *285*, C12-C16.

60. Ewing, P.; Farrugia, L. J.; Rycroft, D. S.; *Organometallics* **1988**, *7*, 859-870.

61. a) Reppe, W.; von Kutepow, N.; Magin, A.; Angew. Chem., Int. Ed. Engl. **1969**, *8*, 727. b) Vollhardt, K. P. C.; *Angew. Chem., Int. Ed. Engl.* **1984**, *23*, 539. Bönnemann, H.; *Angew. Chem., Int. Ed. Engl.* 1985, *24*, 248.

62. Calabro, D. C.; Lichtenberger, D. L.; Herrmann, W. A.; *J. Am. Chem. Soc.* **1981**, *103*, 6852.

63. Schilling, E. R.; Hoffmann, R.; *J. Am. Chem. Soc.* **1979**, *101*, 3456-3467.

CHAPTER 3

Alkyne Adducts of Mixed Metal Trinuclear Clusters of the Cobalt Group: Synthesis and Fluxional Behavior

3.1. Introduction

In the previous chapter we discussed the chemistry of carbene and carbyne ligands coordinated to trinuclear cluster complexes. In this chapter the properties of some complexes containing the alkyne ligand will be discussed. Coordinated alkynes occur as ligands in a variety of mono- and polynuclear complexes. The reason for this diversity is the fact that alkynes can act like two orthogonal alkene units, donating either two or four electrons to the metal complex.[1] In their different bonding modes alkynes also can formally occupy one, two, three or four coordination sites as shown below making it a versatile ligand.

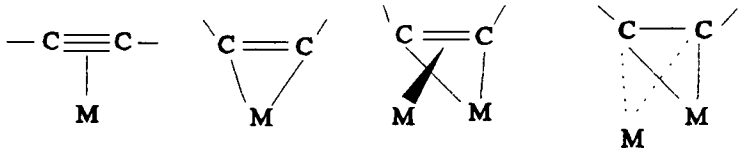

In trinuclear metal complexes, alkyne ligands always occur in a bridging binding mode acting as four electron donors. In a homonuclear cluster complex there are two possible orientations of the alkyne ligand with respect to the metal triangle. It can be aligned either perpendicular or parallel to one edge of the metal triangle. These geometries are commonly referred to by the abbreviations μ_3-$\parallel$ and μ_3-$\perp$:

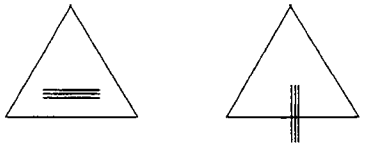

μ_3-$\parallel$ μ_3-$\perp$

The orientation of the alkyne ligand can be related to the formal electron count of the cluster complex. In 46 valence electron cluster complexes like $Fe_3(CO)_9(PhC{\equiv}CPh)$[2] the alkyne is found to be perpendicular to the Fe-Fe edge whereas in clusters containing 48 valence electrons like $FeCo_2(CO)_9(EtC{\equiv}CEt)$[3] or $(CpRh)_3(CO)(PhC{\equiv}CPh)$[4] the alkyne ligand is parallel to a metal-metal edge. The question of relative alkyne orientation has been addressed in a molecular orbital study by R. Hoffmann and Schilling.[5] Their study explains the different orientations of the alkyne ligand with the different relative symmetries of the alkyne and metal cluster frontier orbitals in the parallel and perpendicular orientation. The trinuclear cluster complexes containing alkyne ligands parallel to a metal-metal edge are by far the most common. This is not all that surprising

since trinuclear transition metal complexes containing 48 electrons are saturated and therefore generally more stable than unsaturated trinuclear complexes containing only 46 valence electrons. Actually several complexes initially thought to be unsaturated 46 electron alkyne adducts have later been identified as saturated bis-carbyne complexes with 48 valence electrons.[6] All alkyne adducts discussed in this work belong to the class of saturated clusters containing 48 valence electrons and have the alkyne ligand oriented parallel to a metal-metal edge.

In heteronuclear cluster complexes containing different metal fragments the possibility of isomers with different orientations of the alkyne ligand has to be considered. A review summarizing a variety of heteronuclear cluster complexes containing alkyne ligands has been published.[7] Based on various crystal structures and low temperature solution structures the authors suggest that the least electron rich metal is not included in the metal-metal edge parallel to the alkyne. MO calculations reported by McGlinchey indicate that the alkyne is most strongly bound to the two metals which define the edge parallel to the alkyne.[8] Since the alkyne-metal bond is predominantly electron donation from the ligand to the metal, the alkyne will bind preferably to fragments which will accept electrons most readily. The preferred orientation of the alkyne moiety is therefore correlated with the electronegativity of the metal and the electron donating properties of the ligands bound to the fragment. One example which

illustrates this line of reasoning is the series of cluster complexes $CpNiCoM(CO)_6(PhC{\equiv}CPh)$[9], M = Fe, Ru, Os shown below:

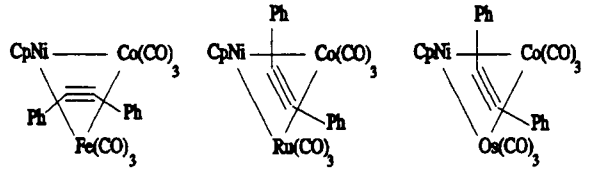

One can see that for M = Fe the alkyne is parallel to the Ni-Co edge, whereas for M = Ru and Os the alkyne is parallel to the Ni-M edge. This change in alkyne geometry can be correlated with an increase in the Pauling electronegativity[10] of Ru and Os compared with Fe (Fe = 1.8, Ru = Os = 2.2).

In our group we have synthesized a large variety of alkyne adducts of the mixed Cp^*/Cp complex $Cp^*Co(CpCo)_2(CO)_2$ (**3**)[11] (Cp^* ≡ pentamethylcyclopentadienyl, C_5Me_5) and of the all-Cp cobalt cluster complex $(CpCo)_3(CO)_2$ [12] (**5**). In this thesis, the alkyne adducts of the entire series of heteronuclear cluster complexes $Cp^*M(CpCo)_2(CO)_2$ with M = Ir, Rh or Co (**1** - **3**) were synthesized. These complexes are made from the unsaturated 46 electron complexes $Cp^*M(CpCo)_2(CO)_2$ by the addition of alkynes and subsequent loss of one carbon monoxide ligand as shown in Figure 3.1. A formal electron count reveals that these complexes contain 48 valence electrons if the alkyne ligand is considered a 4 electron donor: 27 (3 x d^9 metal) +15 (3 x Cp or Cp^*) + 2 (CO) + 4 (1 alkyne) = 48.

The heteronuclear clusters based on the $Cp^*M(CpCo)_2$ triangle have two different types of edges, a Cp^*M-CpCo and a CpCo-CpCo edge. As one varies

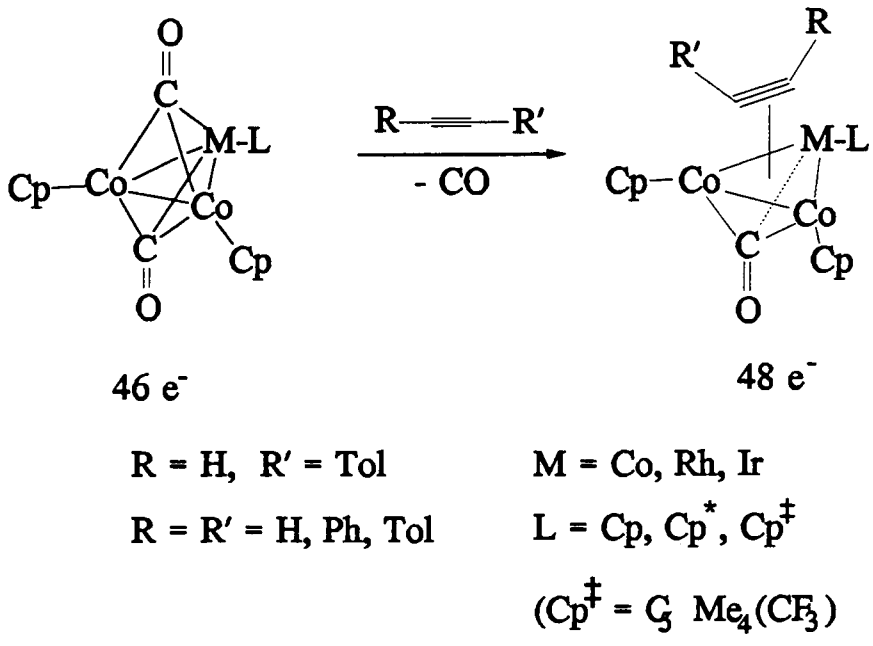

Figure 3.1: Formation of the alkyne adducts from 46 e^- complexes.

the metal from cobalt to iridium one can investigate the influence of the electronegativity of the metal on the orientation of the alkyne ligand. Also described is the use of the metal fragment $Cp^{‡}Co$ (Cp ≡ trifluoromethyl-tetramethylcyclopentadienyl, $C_5Me_4(CF_3)$). The $Cp^{‡}$ ligand resembles sterically a Cp^* ligand, but its electronic properties are more like those of the Cp ligand since the electron donating effect of the methyl groups is compensated by the electron withdrawing CF_3 group.[13]

3.2. Acetylene Adducts

The unsaturated cluster complexes $Cp^*M(CpCo)_2(\mu_3\text{-}CO)_2$ **1 - 3** react readily with acetylene gas to form the adducts $Cp^*Ir(CpCo)_2(\mu_3\text{-}CO)(\mu_3,\eta_2\text{-}HC{\equiv}CH)$ (**19**), $Cp^*Rh(CpCo)_2(\mu_3\text{-}CO)(\mu_3,\eta_2\text{-}HC{\equiv}CH)$ (**20**) and $Cp^*Co(CpCo)_2(\mu_3\text{-}CO)(\mu_3,\eta_2\text{-}HC{\equiv}CH)$ (**21**) in good yields. During the synthesis of the Ir containing complex **19** minor amounts of a dinuclear sideproduct are obtained which will be briefly described at the end of this subchapter. Table 3.1 summarizes the NMR, IR and MS data of the Ir and Rh containing complexes **19** and **20**. The synthesis and characterization of complex **21** have already been described elsewhere.[11]

3.2.1. Crystal Structure

The crystal structure of the rhodium acetylene complex **20** was determined by single crystal x-ray diffraction. Refinement all non hydrogen atoms was performed by modeling them as ellipsoids using anisotropic displacement parameters. The two alkyne hydrogens were refined as isotropic spheres, whereas all other hydrogen atoms were kept in idealized positions with constant bond distances. Figure 3.2 shows two different views of the crystal structure and Table 3.2 summarizes the most important bond lengths, bond angles and interplanar angles. A complete listing of atomic positions, bond lengths and angles and thermal displacement parameters can be found in Appendix 8. The complex as a whole may be described as triangular array of metal atoms supporting a triply bridging carbonyl ligand on one side and an alkyne ligand on the other. Each

Table 3.1: Spectroscopic data for acetylene adducts $Cp^*M(CpCo)_2(CO)(HC{\equiv}CH)$ at 300K.

	^{1}H NMR (toluene-d_8)	^{13}C NMR	ν_{CO} /cm^{-1}	MS
M=Ir	300 K:	300 K[b]:	1665.6	630 (91%, M^+) 602 (100%, M^+-CO)
19	10.21 (br. s, 2H, ≡C-H) 4.45 (10H, Cp) 1.79 (s, 15H, Cp^*)	262.2 (CO); 100.9 (Cp^*-C); 89.3 (Cp); 14.6 (Cp^*-CH_3)		393 (24%, $[Cp^*IrCp]^+$) 189 (18%, Cp_2Co^+)
	170 K: **a** (97%) **b** (3%)			
	11.61; 9.16 9.3 4.62 (10H, Cp) -[a] 1.75 (15H, Cp^*) -[a]			
M=Rh	300 K	300 K	1684.0	540 (100%, M^+) 512 (44%, M^+-CO)
20	9.64 (d, J_{Rh-H} = 3 Hz) 4.46 (s, 10H) 1.67 (s, 15H)	283.2 (CO) 137.3 (d, J_{Rh-H}= 12 Hz) 100.2 (Cp^*-C) 84.1 (Cp) 10.1 (Cp^*-CH_3)		303 (93%, $[Cp^*RhCp]^+$)
	170K: **a** **b**			
	9.41 10.9, 8.75 4.54 -[a] 1.61 -[a]			

a) These signals probably overlap with the ones of isomer **a**. b) The alkyne carbon-13 resonance was not observed either due to broadening or overlap with a solvent signal.

Side View :

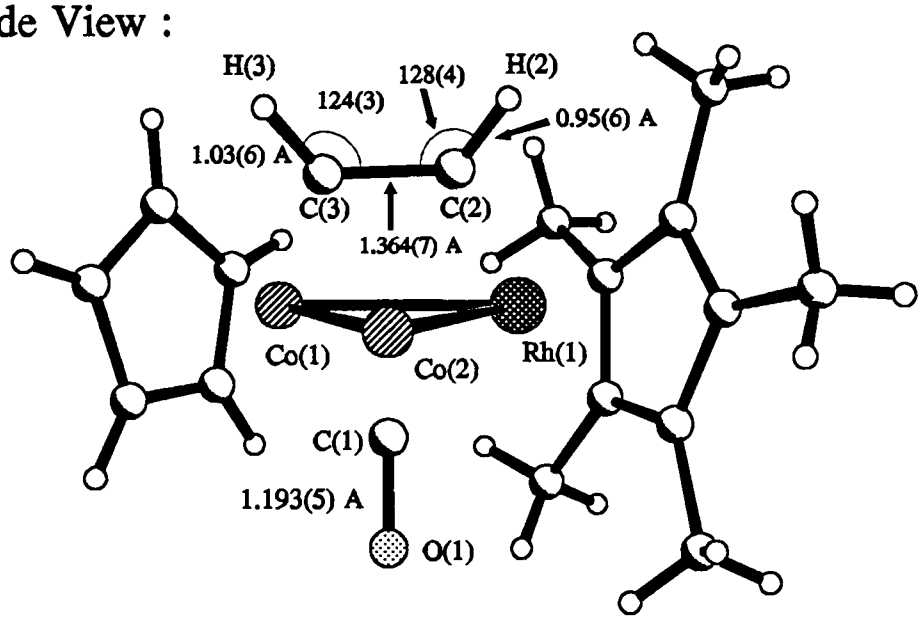

Top View :

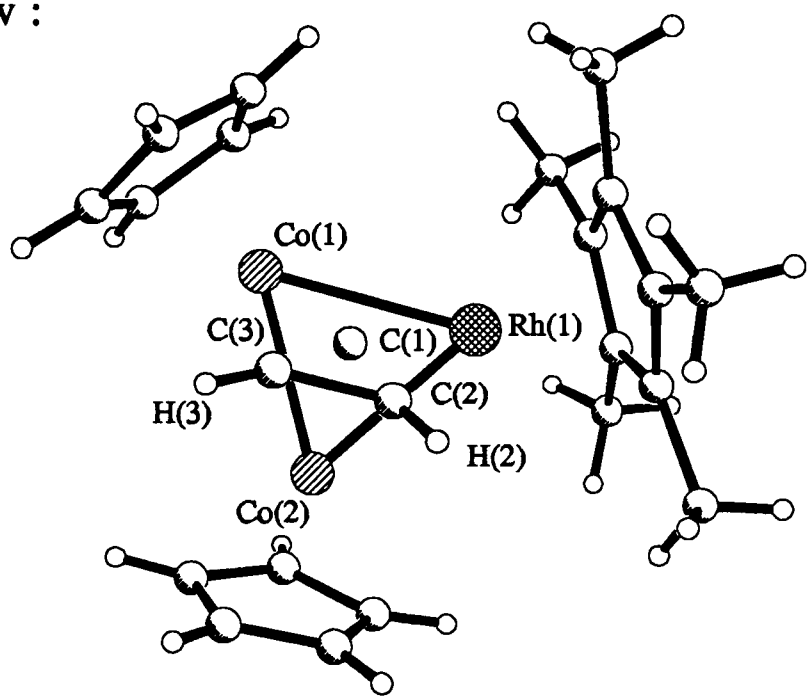

Figure 3.2: Crystal Structure of **20**. In the side view, a Cp ligand has been omitted for clarity.

Table 3.2: Selected bond distances, bond angles and interplanar angles in **20**

Bond distances / Å			
Rh(1)-C(2)	1.983(5)	Rh(1)-C(1)	2.015(5)
Rh(1)-Co(2)	2.5288(8)	Rh(1)-Co(1)	2.5954(8)
Co(2)-C(3)	1.969(5)	Co(2)-C(2)	2.016(5)
Co(2)-C(1)	2.088(5)	Co(2)-Co(1)	2.4475(9)
Co(1)-C(1)	1.888(5)	Co(1)-C(3)	1.892(5)
O(1)-C(1)	1.193(5)	C(3)-C(2)	1.364(7)
Bond angles / °			
Co(2)-Rh(1)-Co(1)	57.04(2)	Co(2)-Co(1)-Rh(1)	60.11(2)
Co(1)-Co(2)-Rh(1)	62.85(2)	C(2)-C(3)-H(3A)	125.(3)
Rh(1)-C(2)-H(2A)	121.(4)	Co(1)-C(3)-H(3A)	126.(3)
C(3)-C(2)-Rh(1)	109.1(4)	C(3)-C(2)-H(2A)	129.(4)
Interplanar angles / °			
[Rh(1)-Co(1)-Co(2)],[H(2A)-C(2)-C(3)]			67
[Rh(1)-Co(1)-Co(2)],[H(3A)-C(3)-C(2)]			68.5
[H(2A)-C(2)-C(3)],[H(3A)-C(3)-C(2)]			1.5
[Rh(1)-Co(1)-Co(2)],[Rh(1)-Co(1)-C(2)-C(3)]			56.0
[Rh(1)-Co(1)-C(2)-C(3)],[H(3A)-C(3)-C(2)-H(2A)]			11.9

metal vertex is capped with a Cp or Cp* ligand that is approximately perpendicular to the plane of the metals. The carbonyl ligand is displaced from the center of the metal triangle towards one Rh-Co edge (C(1)-Co(1) = 1.888(5) Å, C(1)-Co(2) = 2.088(5) Å). The acetylene is parallel to one Rh-Co edge and interacts with the metal atoms in a η^2,μ_3- fashion. The hydrogen atoms of the alkyne ligand are bent up away from the metal triangle forming an HCC angle close to 120°. They are also tilted away from the Rh-Co edge towards the opposite CpCo fragment such that the HCCH plane has an angle of 68° with respect to the plane defined by the metal atoms. The alkyne carbon-carbon bond length of 1.364(7) Å is much closer to the value of the double bond in ethylene (1.33 Å) than to the triple bond in acetylene (1.20 Å).[14] Furthermore, the geometry around the alkyne carbons is close to trigonal planar, with the carbon-hydrogens bonds slightly above the plane defined the two alkyne carbons and either Co(1) or Rh(1), yielding an out of plane angle of 11.9° as illustrated in Figure 3.3. These structural features indicate that upon coordination to the trinuclear metal cluster the hybridization of the alkyne carbons changes from sp to sp^2.[15] A bonding scheme consistent with these observations describes the coordinated alkyne as a dimetal substituted olefin with σ-bonds to the Rh and one Co atom, while the remaining π-bond undergoes a σ-donating-π-backbonding interaction with the second cobalt atom (Figure 3.4).

The crystal structure obtained for the Ir analogue acetylene complex **19**, even though of less accuracy due to poor quality of the crystals, is analogous to

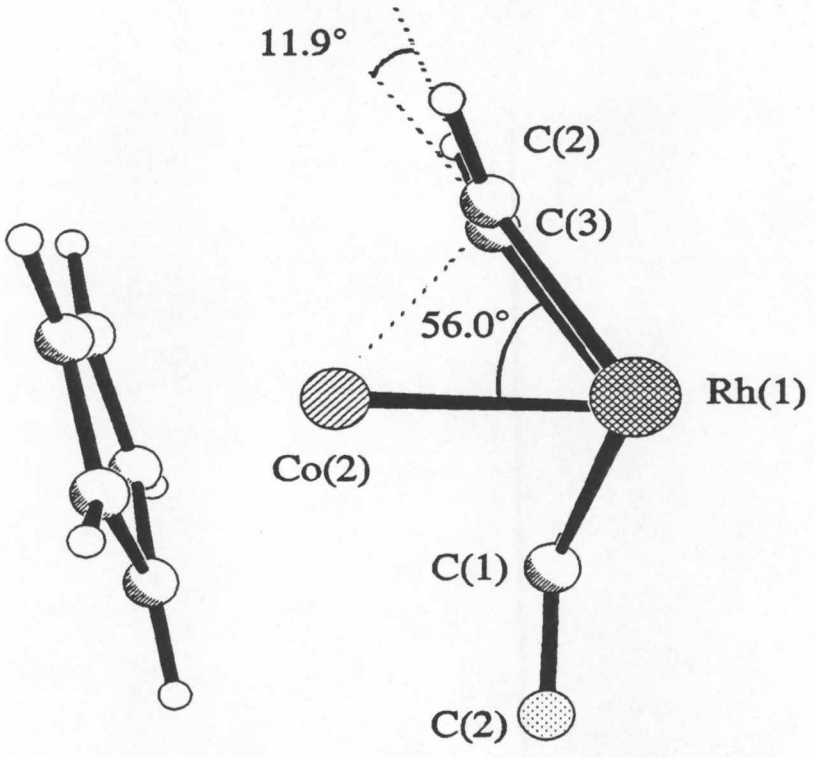

Figure 3.3: Side view visualizing the almost planer geometry around the alkyne carbons.

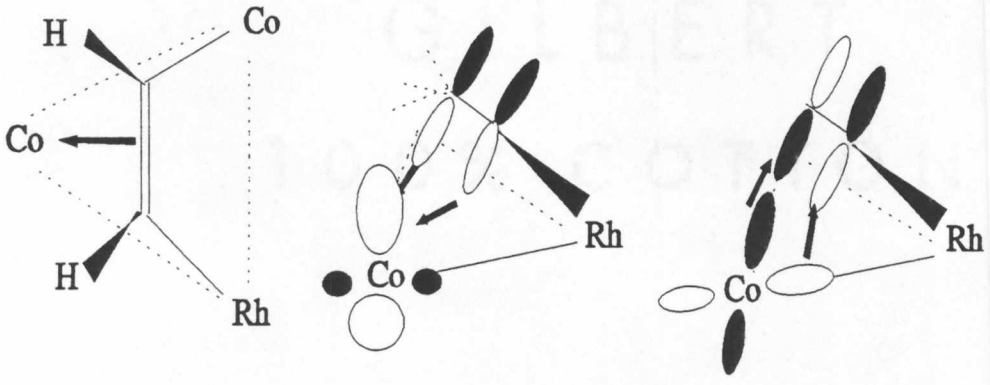

Figure 3.4: Bonding of the alkyne in **20**. Left: Structure showing electron pairs involved; middle: σ-donation from alkyne HOMO; right: π-backbonding into alkyne LUMO.

the one of the rhodium complex. The acetylene ligand is again observed to be oriented parallel to one of the Co-Ir edges.

3.2.2. IR and MS Data

The infrared spectra of the acetylene adducts have been measured in hexane solution for compounds **19 - 21**. Values of 1656 cm^{-1}, 1684 cm^{-1} and 1665.6 cm^{-1} were found for the carbonyl stretching frequencies in the respective Cp^*Co[11], Cp^*Rh and Cp^*Ir containing complexes. These values are consistent with a triply bridging carbonyl ligand in solution as found in the crystal structures of **20** and **19**, suggesting that the solution structures of these compounds are similar to the ones in the solid state. In the mass spectra of **19** and **20** strong parent ion peaks are found at m/z = 630 and 540, respectively. In addition a fragment peak due to of loss of CO is observed with comparable intensity. The only other fragment peak of significance is due to sandwich complex $[Cp^*MCp]^+$. The intensity ratios of M^+ / $[M - CO]^+$ found for the acetylene adducts resemble those of the hydrazone adducts **10 - 13** described in the previous chapter. In contrast the corresponding carbene complexes **8, 7** and **6** exhibit a very weak parent ion peak with respect to the $[M - CO]^+$ fragment ion peak. Such a difference is consistent with the stronger binding of a triply bridging carbonyl ligand in the case of the alkyne and hydrazone adducts, compared with an edge bridging carbonyl ligand in the case of the carbene adduct.

3.2.3. Variable Temperature NMR Spectroscopy and Fluxional Behavior of $Cp^*Ir(CpCo)_2(CO)(HC{\equiv}CH)$ (19)

3.2.3.1. General

At the top of Figure 3.5 the room temperature proton NMR spectrum of the iridium acetylene complex **19** is shown. The signal at 10.21 ppm is assigned to the acetylene proton which experiences a large deshielding effect upon coordination to the metal cluster (the chemical shift for free acetylene is 1.80 ppm).[16] The crystal structure shown in Figure 3.2 indicates that the two alkyne protons should be chemically inequivalent and should give rise to two signals in the proton NMR spectrum. Similarly, based on the crystal structure one would also expect two signals for the protons of the Cp rings on the two unique CpCo vertices. The room temperature NMR spectrum, however, shows only one signal each for the alkyne and Cp protons.

The alkyne resonance is broadened at room temperature ($\Delta\nu 1_{/2}$ = 34 Hz) indicating that the acetylene ligand is fluxional in solution at room temperature. A spectrum taken at 170 K shows two signals for the acetylene ligand at 11.61 and 9.16 ppm as expected for a rigid structure with the alkyne coordinated parallel to an Ir-Co edge. On the other hand, one still observes only one signal for the protons of the two Cp ligands, indicating that not all of the fluxional processes have been frozen out. A NOESY[17] spectrum taken at low temperature (T = 170 K, τ = 200 ms) shows crosspeaks connecting both alkyne signals with the Cp signal (Figure 3.6). However, only the upfield alkyne signal at 9.16 ppm shows a

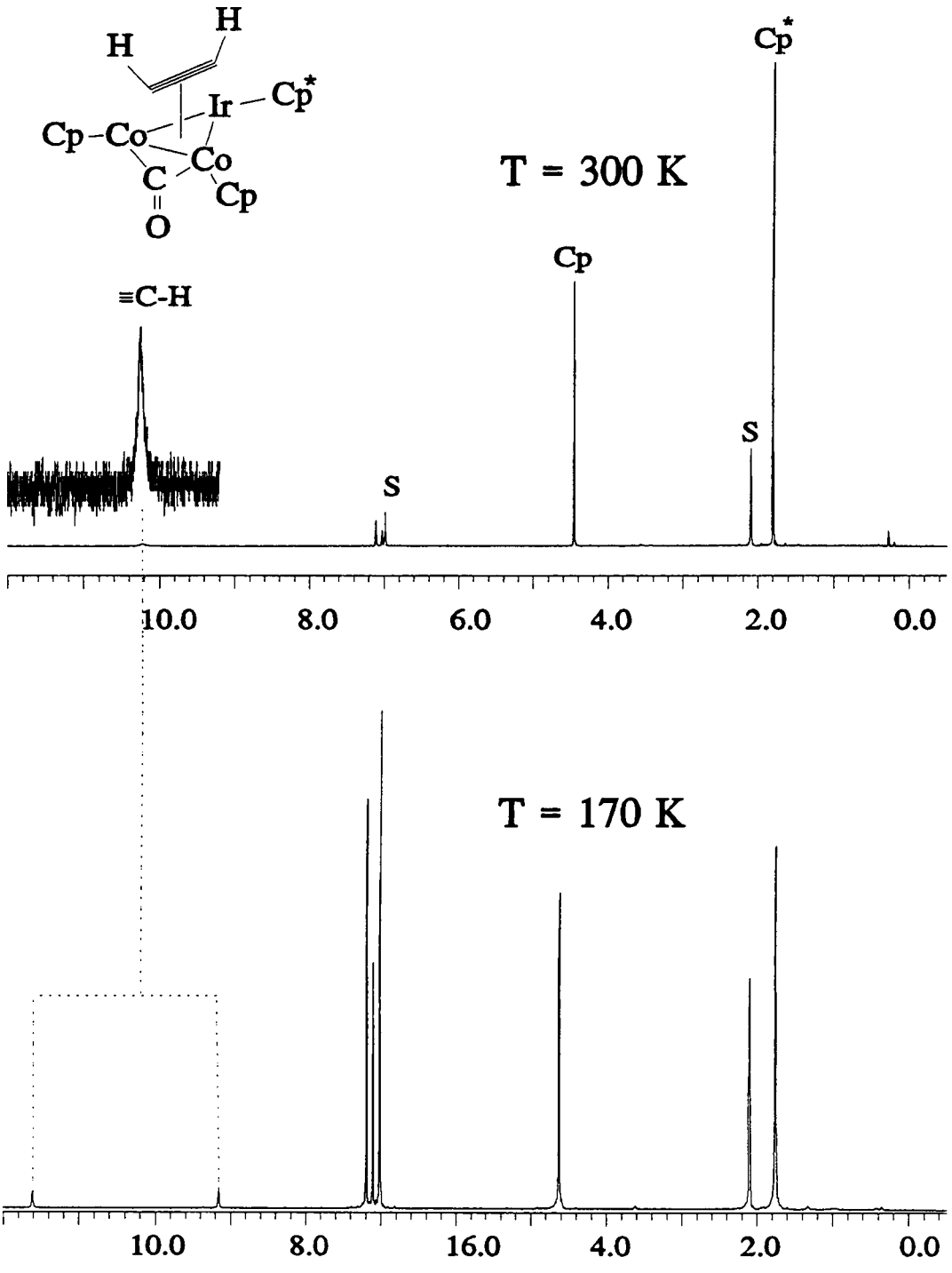

Figure 3.5: ^{1}H NMR spectra of **19** in toluene-d_8 at 300 K (top) and 170 K (bottom). Solvent peaks are marked with S.

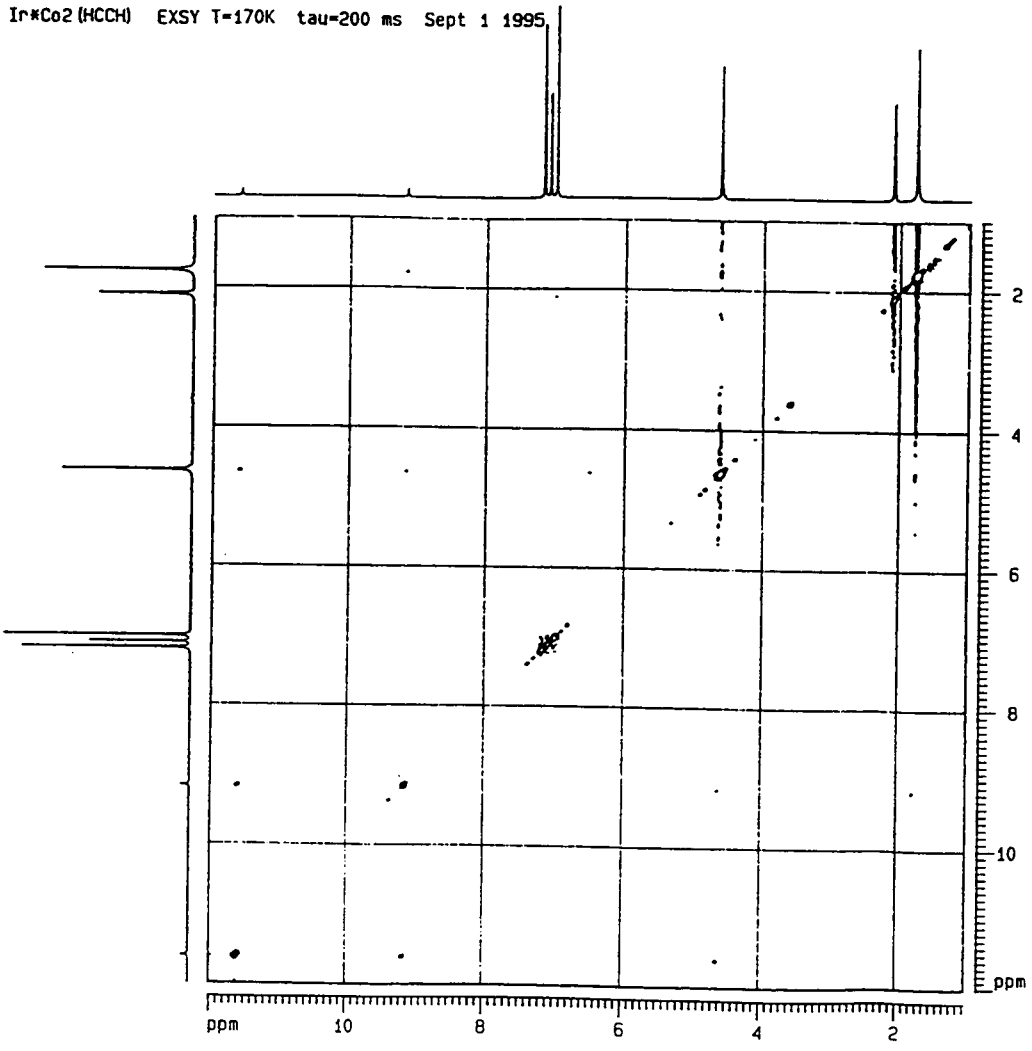

Figure 3.6: Full NOESY spectrum of **19**. T = 170 K τ = 200ms

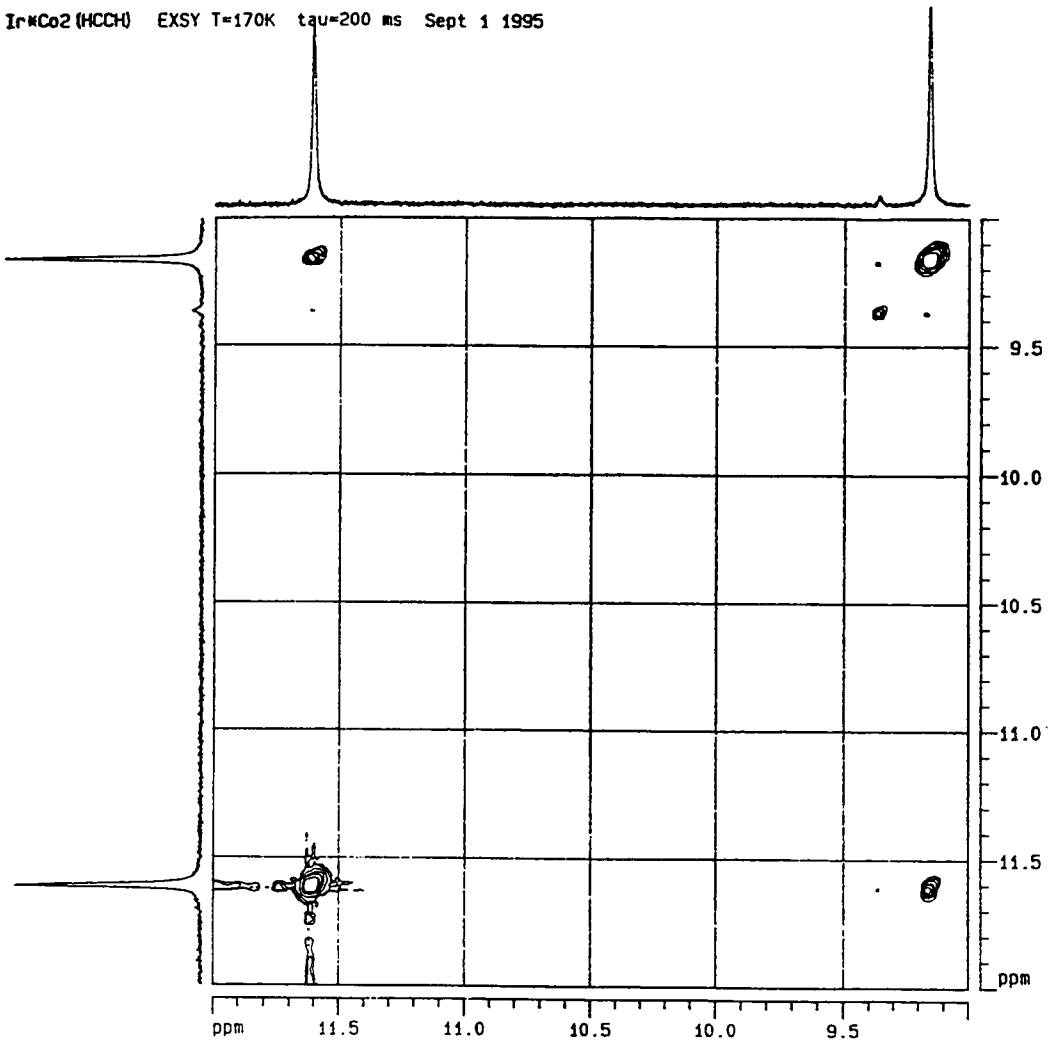

Figure 3.7: Alkyne region of NOESY spectrum of **19.**

crosspeak with the signal of the Cp^* methyl group. These results suggest the assignment of the upfield alkyne resonance to the alkyne proton above the Ir-Co edge whereas the downfield signal belongs to the alkyne proton above the Co-Co edge.

A scheme consistent with freezing out exchange of the two alkyne protons but maintaining equivalency between the two CpCo vertices is shown in Figure 3.8. The preferred isomer, which contains the acetylene coordinated parallel to a Cp^*Ir-CpCo edge, is labeled isomer **A**. One can see that direct interchange between the two enantiomers **A** and **A′** interchanges the identities of the two CpCo vertices but retains the identities of the two alkyne protons. A process which interchanges the two alkyne protons must involve isomer **B** with the alkyne parallel to the Co-Co edge. If **B** is a transition state, the exchange of the two alkyne protons could be described as a one step process, but if **B** is an actual intermediate, exchange of the alkyne proton identities has to occur in two steps via **A** → **B** and **B** → **A′**. Under the condition that $k_{A,A'}$ is significantly faster than k_{AB} it is possible to freeze out the exchange of the alkyne protons without freezing out the exchange of the CpCo vertices. Close inspection of the low temperature spectrum reveals a small peak at 9.3 ppm consistent with the presence of small amounts of another species in solution at low temperature. The NOESY spectrum shows cross peaks due to exchange connecting the two major alkyne peaks with each other as well as with the small peak at 9.3 ppm (Figure 3.7). This suggests that this signal belongs to a compound which is in equilibrium with

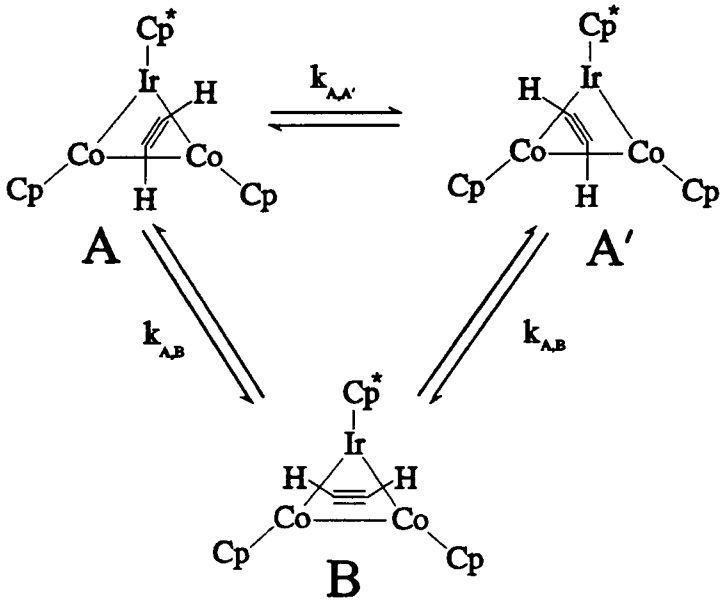

Figure 3.8: Mobility of the alkyne ligands between the two possible positions parallel to the Ir-Co and Co-Co edge.

the major species and can be assigned to isomer **B** as an intermediate in the exchange of the two enantiomers A and A′. No clearly separated signals could be found for the Cp and Cp* signals of isomer **B** but the Cp signal exhibited a small shoulder on its base. In general all adducts containing symmetric alkyne ligand parallel to a Cp*M-CpCo edge will be identified as isomer **A** and the ones with the alkyne parallel to the CpCo-CpCo edge will be referred to as isomer **B**.

3.2.3.2. Lineshape analysis

A quantitative analysis of the alkyne fluxionality was obtained by a full line shape analysis[18,19] of the alkyne ^{1}H NMR signals at different temperatures using the program DNMR5.[20] In Figure 3.9 the experimental spectra at various temperatures are shown on the left side and the simulated spectra with

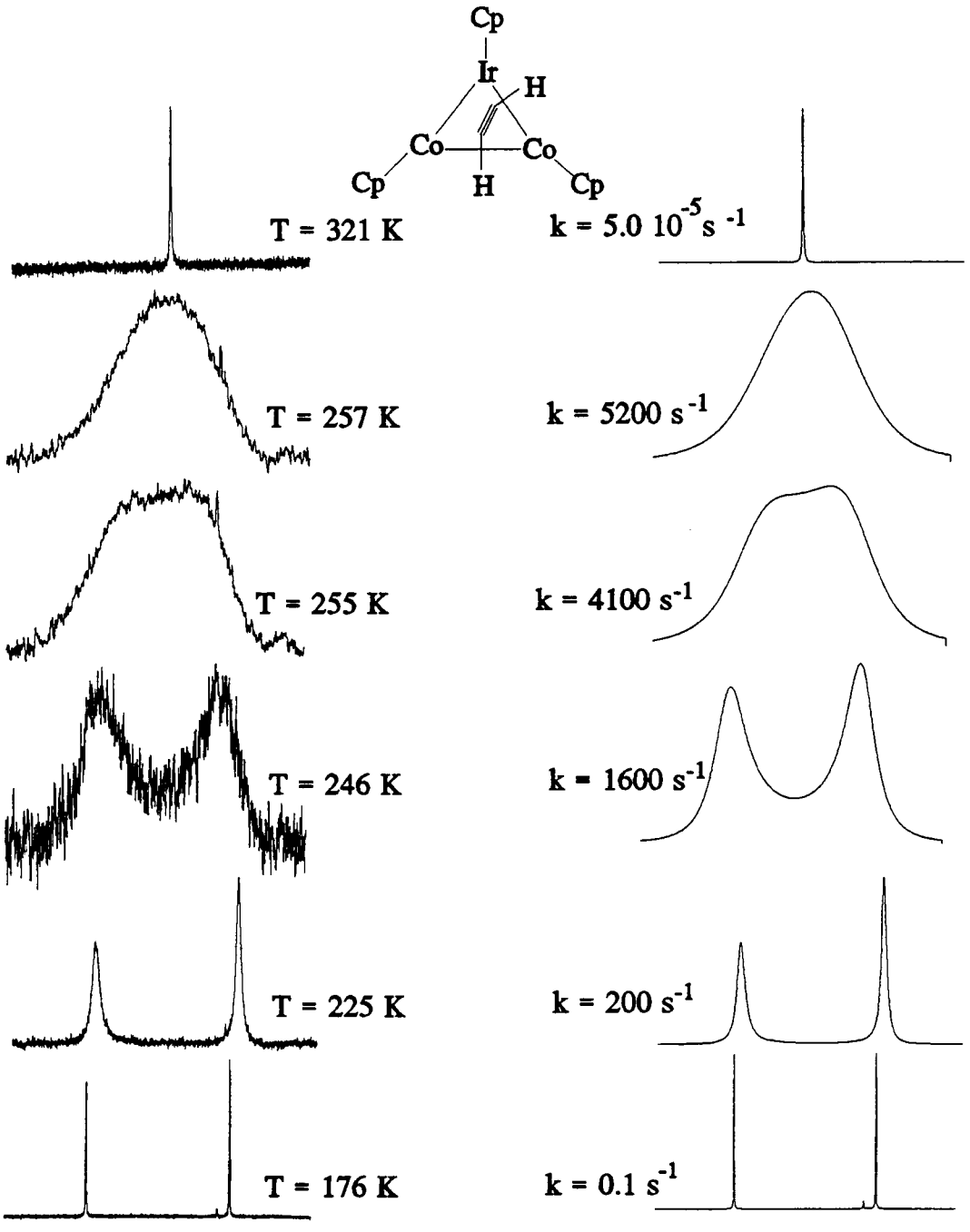

Figure 3.9: Variable temperature ^1H spectra of the alkyne region of **19**. Left: experimental data; right: simulated spectra using DNMR5.

corresponding rate constants are shown on the right side. As one can see from the figure, the broadening of the two alkyne signals occurs in an unsymmetrical manner where the downfield signal broadens at a lower temperature than the upfield signal. Such behavior can only be modeled satisfactorily by including structure B in the exchange process. Both alkyne signals of the major species A are transformed into the one signal at 9.3 ppm belonging to **B**. Compared with the upfield alkyne signal of **A**, the downfield signal has a much larger chemical shift separation $\Delta\nu$ from the alkyne signal of **B**. In the slow exchange region the observed broadening is proportional to $\Delta\nu$ and the downfield alkyne signal will broaden first. Indeed a match between experimental and simulated spectra could only be obtained by assuming a two step exchange (**A** → **B**, **B** → **A′**) including both positional isomers.

By integrating the alkyne proton NMR signals in the spectrum at 176 K the relative abundance of both isomers was determined to be 40:1 (**19A/19B**). The populations used as input parameters for DNMR5 express the abundance of one isomer as fraction of the total amount of compound present. Furthermore, values for the chemical shifts of the alkyne signals of isomer **A** and **B** were obtained from the low temperature spectra. An estimate of the temperature dependence of the chemical shifts of the two signals of isomer **A** was obtained from a plot of chemical shifts of the two alkyne protons versus temperature using the range of 176 - 225 K where separated signals are observed. From that plot, chemical shift values for higher temperatures could be obtained by extrapolation. Such

extrapolation could not be done for the chemical shift of the alkyne signal of isomer **B** since only one data point is available for the lowest temperature. That chemical shift was therefore kept fixed throughout the analysis. However, a slight temperature dependance of the relative ratio of the two isomers had to be assumed in order to match the experimental spectra in the simulation.

The rate constants k are related to the free energy of activation $\Delta G^{\ddagger}$ by the Eyring equation

$$k = \frac{k_B T}{h} e^{-\frac{\Delta G^{\ddagger}}{R_G T}} \qquad (1)$$

where h is Planks constant, k_B is Boltzmann's constant and R_G equals the ideal gas constant. Plotting $\ln(kh/k_B T)$ versus inverse temperature then yields a linear dependence of these two parameters as shown in Figure 3.10. Using the relationship $\Delta G^{\ddagger} = \Delta H^{\ddagger} - T\Delta S^{\ddagger}$ allows one to obtain the energy and entropy of activation for the process from the slope and intercept of a linear fit through the data in Figure 3.10 according to

$$\ln\left(\frac{kh}{k_B T}\right) = -\frac{\Delta G^{\ddagger}}{R_G T} = -\frac{\Delta H^{\ddagger}}{R}\frac{1}{T} + \frac{\Delta S^{\ddagger}}{R} \qquad (2)$$

For (**19**) values of $\Delta H^{\ddagger}$ = 46.5(5) kJ mol^{-1}, $\Delta S^{\ddagger}$ = 7(2) J mol^{-1} K^{-1} and a room temperature value for $\Delta G^{\ddagger}$(298 K) of 44.3 kJ mol^{-1} are found.

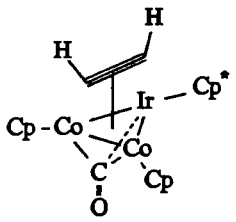

$\Delta G^{\ddagger}(298K) = 44.3\ kJ\ mol^{-1}$

$\Delta H^{\ddagger} = 46.5\ kJ\ mol^{-1}$

$\Delta S^{\ddagger} = 7.4\ J\ mol^{-1}\ K^{-1}$

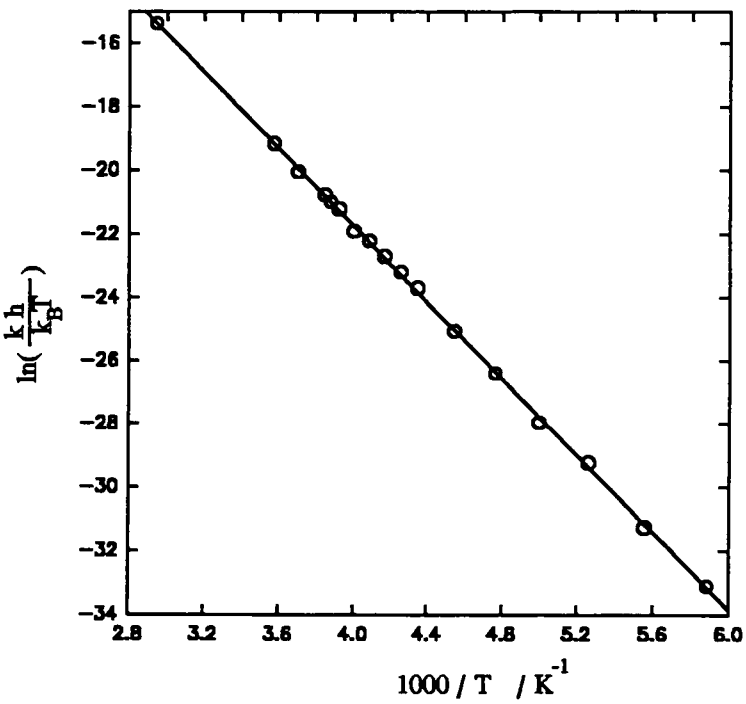

Figure 3.10: Eyring plot for exchange between positional isomers **19A** and **19B**.

3.2.4. NMR spectra of $Cp^*Rh(CpCo)_2(\mu_3\text{-}CO)(HC{\equiv}CH)$ (20)

As for the iridium substituted acetylene complex, the room temperature ^1H NMR spectrum of the analogous rhodium acetylene complex **20** also exhibits only one signal each for the acetylene and the Cp protons. The alkyne signal at 9.64 ppm (toluene-d_8) is split into a doublet due to coupling with the rhodium (J_{RhH} = 3 Hz). At low temperature, however, the alkyne region of the spectrum indicates the presence of both orientational isomers as shown at the bottom of Figure 3.12. The major signal at 9.41 ppm indicates that the preferred isomer is the one in which the triple bond is parallel to the Co-Co with both alkyne protons equivalent corresponding to isomer **B** in Figure 3.8. The other set of two signals (8.8 and 10.9 ppm) belongs to the isomer of type **A** with the acetylene parallel to a Rh-Co edge. Integration yields a ratio of 1.8:1 for **B** versus **A**. Even at the lowest temperature (163 K) the spectrum obtained yields signals which are still somewhat exchange broadened and no proton-rhodium coupling could be resolved for any of the signals. A NOESY spectrum taken at that temperature (τ = 200 ms) exhibits strong exchange cross peaks connecting the alkyne signal of isomer **B** with both alkyne signals of isomer **A** as well as connecting the alkyne signals of isomer **A** with each other (Figure 3.11). No splitting of the signals was observed for either the Cp or Cp^* ligands but both exhibited significant broadening at the lower temperatures presumably due to the onset of decoalescence. Upon raising the temperature both sets of alkyne signals coalesce to give one sharp alkyne signal at room temperature (Figure 3.12). A full

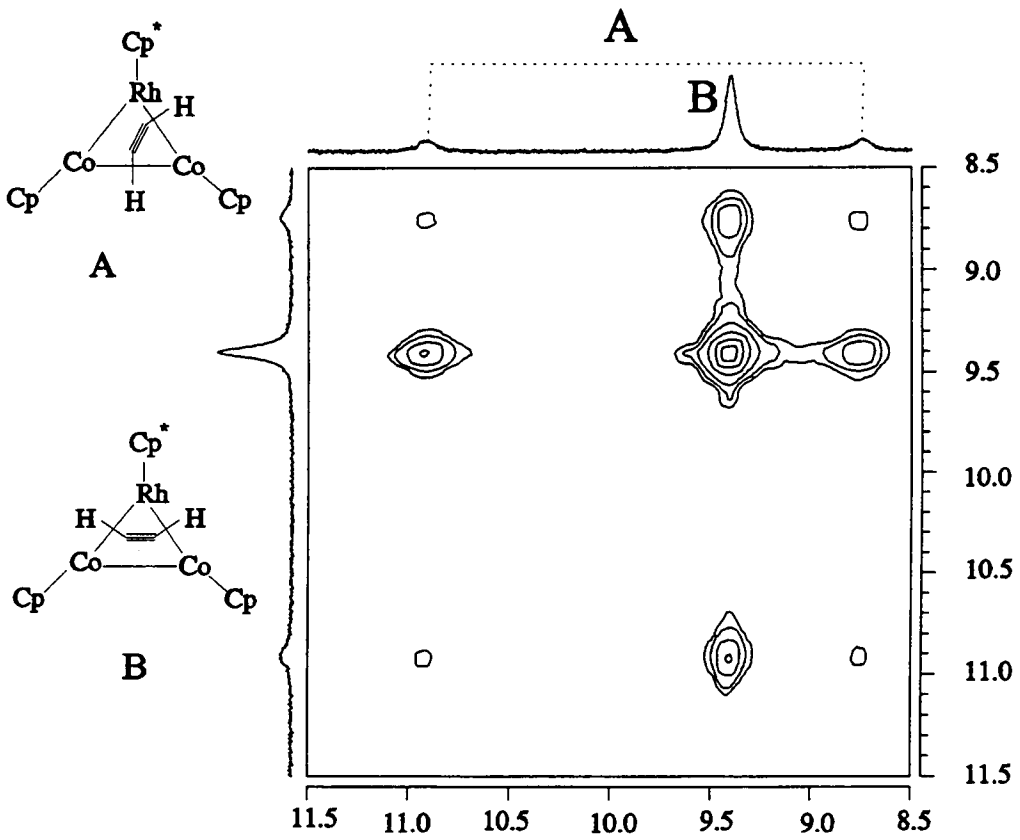

Figure 3.11: Alkyne region of the NOESY spectrum of **20** at 170 K. τ = 200 ms

lineshape analysis analogous to the one described for complex **19** yielded the activation parameters $\Delta H^{\ddagger}$ = 38 kJ mol^{-1}, $\Delta S^{\ddagger}$ = 26 J mol^{-1} K^{-1} and $\Delta G^{\ddagger}$(298K) = 30.3 kJ mol^{-1}. That is a significantly lower barrier than that found for the analogous Cp*Ir cluster complex.

It should be noted that the preferred orientation of the alkyne found in solution for **20** is different from the one found in the solid state. One explanation for that observation might be a temperature dependence of the equilibrium constant which favors isomer **A** close to room temperature. When performing the lineshape analysis it turned out that the relative abundance of isomer **A** used as

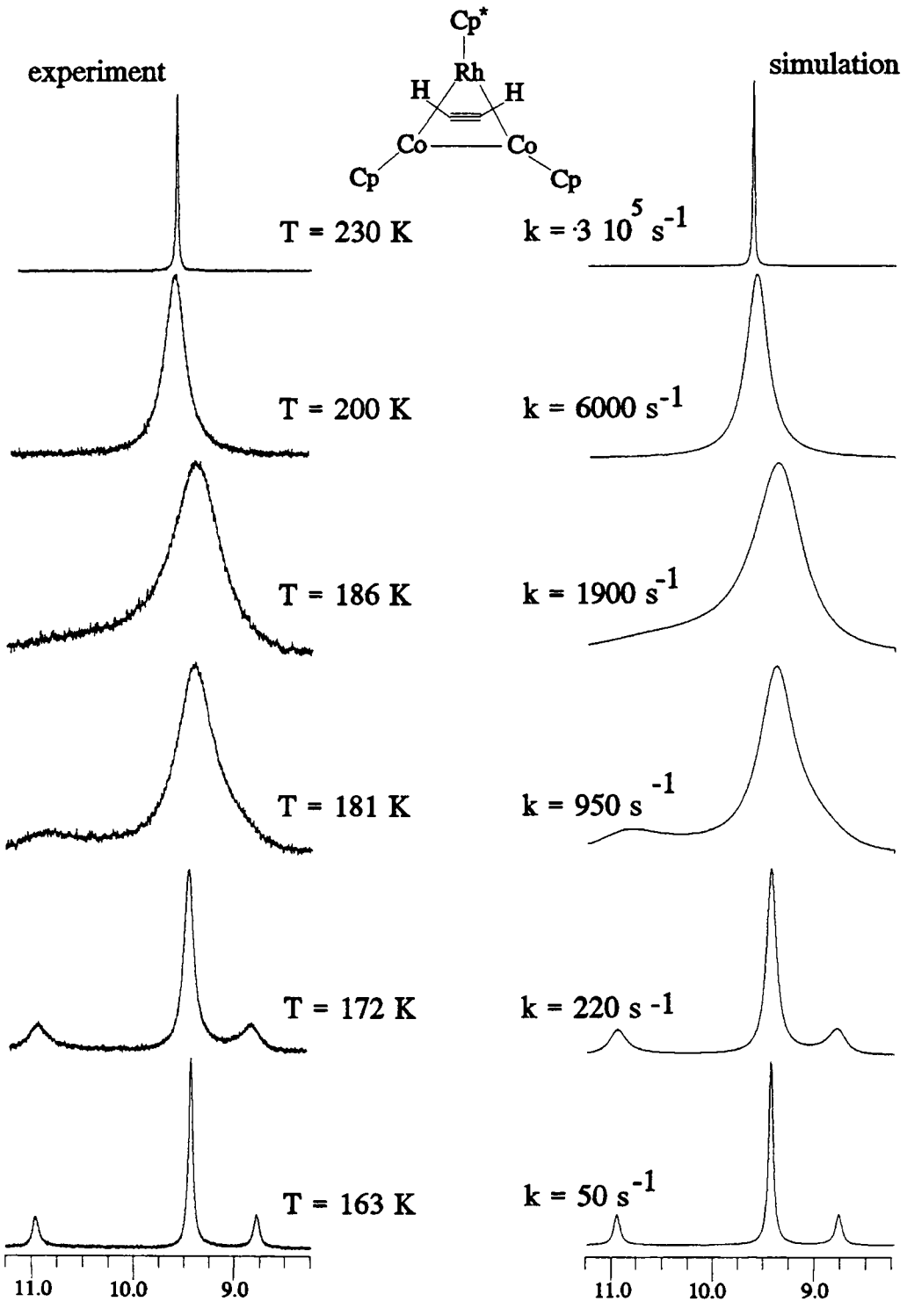

Figure 3.12: Variable temperature spectra of the alkyne region of **20**.

ΔH^0 = -3.0 kJ mol^{-1}

ΔS^0 = -12 J mol^{-1} K^{-1}

ΔG^0(170K) = -1.1 kJ mol^{-1}

ΔG^0(298K) = +0.5 kJ mol^{-1}

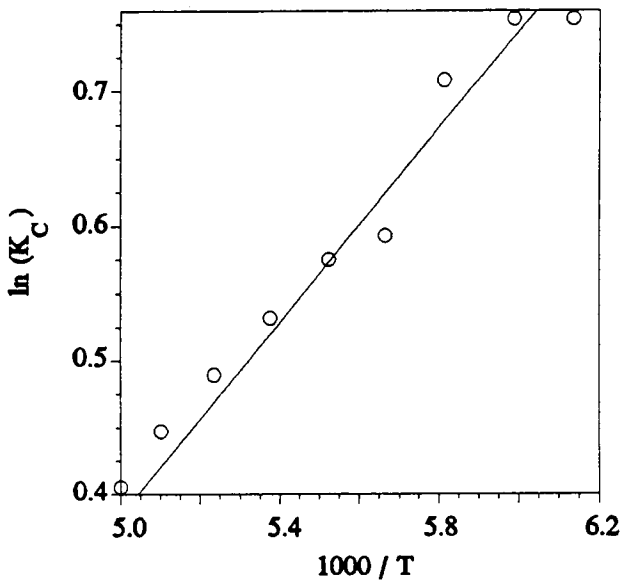

Figure 3.13: Temperature dependence of the equilibrium constant for **A** → **B** in the rhodium complex **20**.

parameter in the simulation had to be increased as the temperature was raised in order for the simulation to match the experimental spectra. Lineshape analysis therefore allowed one to obtain values for the equilibrium constant K_c even at temperatures where the signals were no longer separated. It was therefore possible to obtain equilibrium constants K_c over a larger temperature range. Figure 3.13 shows that a logarithmic plot of K_c versus inverse temperature is close to linear. One can see that extrapolation to room temperature yields a positive value for ΔG^0(298K) corresponding to a preference of isomer **A** at room temperature. That is consistent with the fact that isomer **A** was the one to crystallize since the crystals were obtained by slow solvent evaporation in the glove box at room temperature.

3.2.5. $Cp^*Co(CpCo)_2(CO)(HC{\equiv}CH)$ (21) and Trends

The proton NMR spectrum of the Co analogue **21**[21] also is indicative of a fluxional structure at room temperature. However, the spectrum remains unchanged upon cooling down to 170 K exhibiting no broadening of any of the signals. Two explanations are consistent with this observation. First, one can consider the possibility that the motion of the acetylene ligand is much faster in **21** than in the two previous acetylene complexes resulting in a fluxional structure even at the lowest accessible temperature. Second, the low temperature spectrum can be explained by assuming a static structure containing exclusively isomer **B** in which both alkyne protons are equivalent. In this case the symmetry of the molecule prevents any broadening of splitting of signals to be observed. Observation of only isomer **B** would continue the trend observed for the other two acetylene adducts where the preference in orientation changed from parallel to the Ir-Co edge in **19** changed to an almost equal distribution of both isomers in the Rh analogue **20**. Figure 3.14 illustrates this trend. However, there is a decrease in barrier to alkyne rotation when going from the Ir containing complex (**19**) to the Rh containing complex (**20**). Later studies described in this chapter will show that it is possible to expect a static structure for **21**.

3.2.6. Dinuclear Side Product Obtained from $Cp^*Ir(CpCo)_2(CO)_2$ + $HC{\equiv}CH$

In addition to the alkyne adduct described above, minor amounts of a second product were obtained from the reaction of Ir containing cluster complex **1**

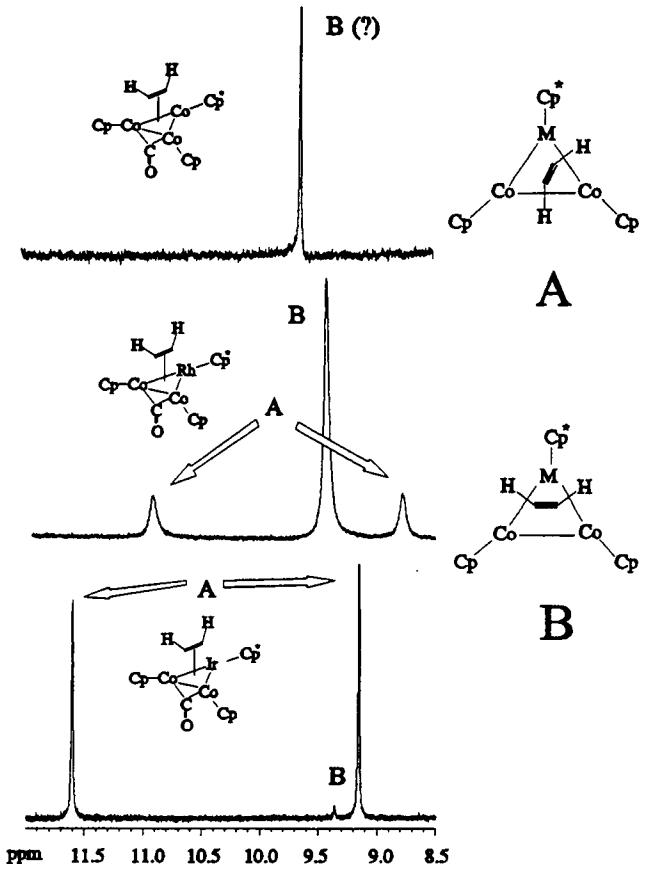

Figure 3.14: Comparism of the low temperature spectra of **19 - 21** showing the change in the preferred orientational isomer.

with acetylene as reddish brown fraction eluting with hexane/ether. The spectroscopic data of this compound are listed in Table 3.3. The mass spectrum suggests a molecular ion of mass 534 consistent with the molecular formula $Cp^*IrCpCo(CO)_2(HC{\equiv}CH)$. Furthermore the presence of the fragment $[Cp^*IrCp]^+$ is strong evidence for the presence of both a Cp^*Ir and a CpCo fragment in the molecule. The relative intensities of Cp^* versus Cp protons in the ^1H NMR spectrum suggest a dinuclear species containing one Co and one Ir atom. An interesting feature in the spectrum are the two doublets at 9.28 and

Table 3.3: Spectroscopic data for the byproduct **33**.

^{1}H NMR[a)]	9.28 (d, J_{HH} = 6.4 Hz, 1H); 4.84 (s, 5H); 3.65 (d, J_{HH} = 6.4 Hz, 1H); 1.73 (s, 15H).
^{13}C NMR[a)]	232.8 (CO); 172.9 (CO); 128.8 (CH); 98.3 (Cp^*-C); 83.1 (Cp); 33.1 (CH); 9.8 (Cp^*).
IR: ν_{CO}[b)]	1963; 1757
MS	MS(EI): 534.8 (8%, M^+); 506 (35%, M^+- CO); 478 (27%, M^+- 2CO); 393 (100%, $[Cp^*IrCp]^{\cdot+}$)

a) C_6D_6 b) hexane

3.65 ppm which are coupled to each other (J_{HH}= 6.4 Hz). The chemical shift of 9.28 ppm is expected for the proton of a coordinated acetylene. However, the signal at 3.65 ppm is upfield from the region of the spectrum where one would expect a coordinated alkyne to be. The ^{13}C NMR spectrum shows two quartenary signals at 232.8 and 172.9 ppm. The downfield signal has a chemical shift consistent with an edge bridging carbonyl, but the other one at higher field is not found in a range one would normally expect for a terminal carbonyl ligand. Besides the Cp^* and Cp carbon signals two more CH or CH_3 signals are observed at 128.8 and 33.1 ppm. Similar to the ^{1}H NMR spectrum one of the shifts matches the one expected for a coordinated alkyne, whereas the other one is upfield from this expectation. The IR spectrum is also consistent with the presence of one bridging carbonyl ligand and a terminal carbonyl. A possible

structure consistent with the spectroscopic data is the alkyne-carbonyl coupling product containing a η^2,μ_2-1-propene-3-one ligand shown below:

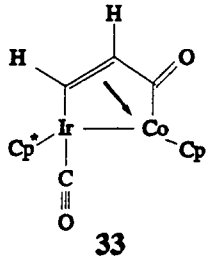

33

A trinuclear complex containing such a ligand type is formed in the reaction of $(CpCo)_3(\mu_3\text{-}CO)_2$ with t-Bu-C≡CH and was recently characterized by x-ray diffraction.[22] Further work is still required to unambiguously determine the structure of compound **33**.

3.3. Phenyl- and Tolylacetylene Adducts

The tolylacetylene adducts **23**, **24**, **25** and **27** were synthesized in good yields by adding a solution of the alkyne in ether to an ether solution of the unsaturated cluster complex and stirring the mixture for several minutes:

M	Ir	Rh	Co	Co
L	Cp^*	Cp^*	Cp^*	$Cp^‡$
	23	**24**	**25**	**27**

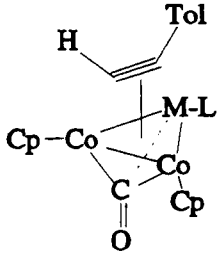

Only small amounts of tricarbonyl are found in the reaction mixture indicating that addition of the alkyne proceeds faster than the reaction of the released carbon monoxide with remaining starting complex. Table 3.4 summarizes the NMR, IR and mass spectra data for these complexes.

3.3.1. Crystal Structure

Figure 3.15 shows the crystal structures of the rhodium and iridium substituted tolylacetylene adducts **24** (top) and **23** (bottom) as viewed from above each molecule. Selected bond distances, bond angles and interplanar angles are shown in Table 3.5 and 3.6. The general features of both structures are similar to the structures of the acetylene adducts described above. The alkyne ligand bridges one face of the metal triangle parallel to a metal-metal edge and a μ_3-triply bridging carbonyl ligand is found capping the opposite face. In both cases the coordination about the alkyne carbons is close to trigonal planar with the HC≡C-Tol moiety bent up and towards the third metal vertex.

The relative orientations of the alkyne ligands with respect to the metal triangle differ for the rhodium and iridium containing cluster complexes. In the iridium containing complex **23** the alkyne ligand is parallel to one of the two Ir-Co edges with the tolyl group crossing over the Co-Co edge avoiding the sterically more demanding Cp^* ligand. In the rhodium containing complex **24** on the other hand the alkyne ligand is parallel to the Co-Co edge and the phenyl ring is oriented above a Rh-Co edge placing it near the Cp^*ligand. In both compounds

Table 3.4: Spectroscopic data for tolylacetylene adducts $LM(CpCo)_2(\mu_3\text{-}CO)$(Tol-C≡CH) **23** - **27** at 300 K.

	ML = Cp*Ir **23**	ML = Cp*Rh **24**	ML = Cp*Co **25**	ML= Cp‡Co **27**
^{1}H NMR:	CD_2Cl_2	C_6D_6	C_6D_6	
≡C-H	9.7 br. s	9.70 s	9.83 s	
Tol-H	7.46 d, $^3J_{HH}$=7.6 Hz	7.50 d, J_{HH}=10.9 Hz	7.65 d, J_{HH}= 8 Hz	9.95 s
	7.19 d, $^3J_{HH}$=7.6 Hz	7.11 d	7.16 d	7.49 d, J_{HH} = 8 Hz
				7.21 d J_{HH} =
Cp	4.31 s	4.51 s	4.46 s	8 Hz
Tol-CH_3	2.37 s	2.22 s	2.24 s	4.40 s
Cp*-CH_3	1.912 s	1.54 s	1.47 s	2.37 s
				1.94 d; J_{HF} = 0.8 Hz, 1.67 s (Cp‡-CH_3)
^{13}C NMR:				
CO	260	281 d	288.9	-
≡C-Tol	151	151.5	153.9	150.6;
Tol-C	135.7, n.o.	148.4; 137.8	147.1; 136.4	138.4
Tol-CH	128.7; 128.3	130.5; 130.0	128.8; 128.6	130.8; 129.9
≡C-H	117	135.7;	141.7	-
Cp'-C	96.7[a)]	102.4[a)]	95.0[a)]	99.1; 96.9[b)]
Cp	85.3	86.8	85.5	87.9
Tol-CH_3	21.4	23.1	21.4	23.2
Cp'-CH_3	9.3[a)]	11.5[a)]	9.6[a)]	11.6; 11.3[b)]
IR: ν_{CO}/cm^{-1}	1649 (KBr)	1681 (hexane)	1663.0 (KBr)	1688.3 (hexane)
MS:	720 (33%, M^+)	630 (65%, M^+)	586 (90%, M^+)	640 (98%,M^+)
	692 (56%, M^+-CO)	602 (76%, -CO)	558 (100%, - CO)	612 (25%, -CO)
	393 (62%, $[Cp^*IrCp]^{+\cdot}$)	303 (100%, $[Cp^*RhCp]^+$)	259 (44%, $[Cp^*CoCp]^+$);	442 (100%,?)
	189 (100%, $[Cp_2Co]^{+\cdot}$)		189 (17%, Cp_2Co^+)	313 (23%, $[Cp^‡CoCp]^+$)

a) Cp' = Cp* b) Cp' = Cp‡ The CF_3 carbon was not observed

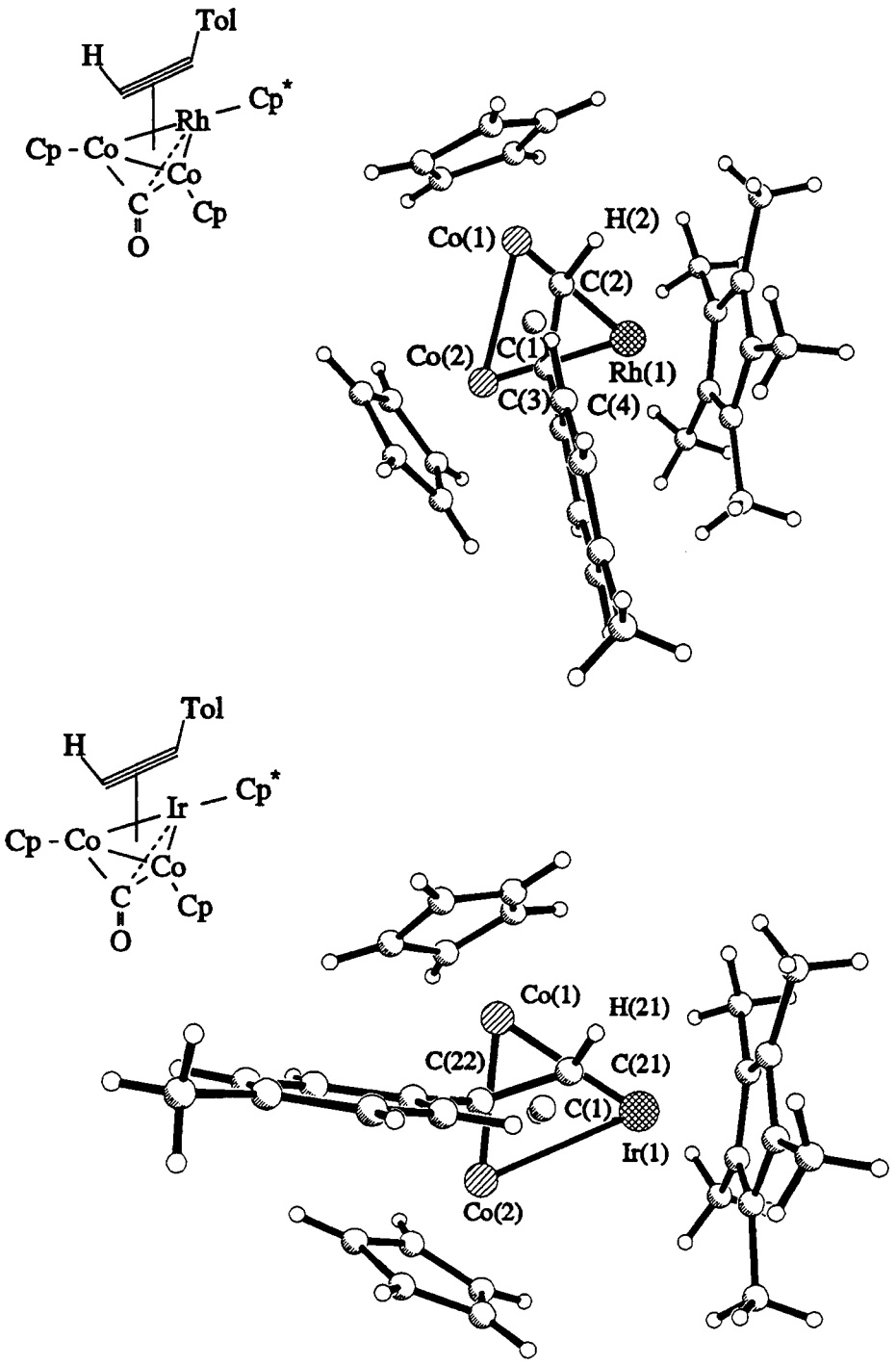

Figure 3.15: Crystal structure of the tolylacetylene adducts $Cp^*Rh(CpCo)_2(CO)(TolC{\equiv}CH)$ (top) and $Cp^*Ir(CpCo)_2(CO)(TolC{\equiv}CH)$ (bottom).

Table 3.5: Selected bond distances and -angles for $Cp^*Ir(CpCo)_2(CO)(Tol\text{-}C{\equiv}CH)$ **(23).**

Bond length / Å			
Ir(1)-C(30)	1.96(2)	Ir(1)-C(21)	1.98(2)
Ir(1)-Co(1)	2.561(3)	Ir(1)-Co(2)	2.586(3)
Co(1)-C(22)	1.99(2)	Co(1)-C(30)	2.07(2)
Co(1)-C(21)	2.05(2)	Co(1)-Co(2)	2.441(4)
Co(2)-C(22)	1.93(2)	Co(2)-C(30)	1.98(2)
C(21)-C(22)	1.38(3)	C(22)-C(23)	1.45(2)
C(30)-O(1)	1.21(2)	C(21)-H(21A)	0.96
Bond Angels / °			
Co(1)-Ir(1)-Co(2)	56.62(8)	C(22)-Co(1)-Ir(1)	76.1(5)
Co(2)-Co(1)-Ir(1)	62.20(9)	Co(1)-Co(2)-Ir(1)	61.18(10)
O(1)-C(30)-Co(2)	131.(2)	O(1)-C(30)-Ir(1)	136.(2)
O(1)-C(30)-Co(1)	131.3(14)	C(21)-C(22)-C(23)	126.(2)
C(22)-C(21)-H(21A)	121.8(13)	Ir(1)-C(21)-H(21A)	123.4(10)
Dihedral and interplanar angels / °			
[H(21A),C(21),C(22)]-[Phenyl]			41.42
[C(21),C(22),C(23)]-[Phenyl]			32.76
H(21A)-C(21)-C(22)-C(23)			12.67
[Ir(1),Co(1),Co(2)]-[H(21A),C(21),C(22)]			61.35
[Ir(1),Co(1),Co(2)]-[C(21),C(22),C(23)]			74.02
[Ir(1),Co(1),Co(2)]-[Phenyl]			94.83

Table 3.6: Selected bond distances and -angles in $Cp^*Rh(CpCo)_2(CO)(Tol\text{-}C{\equiv}CH)$ **(24).**

Bond Length / Å			
Rh(1)-C(2)	2.097(4)	Rh(1)-C(3)	2.114(4)
Rh(1)-C(1)	2.136(4)	Rh(1)-Co(1)	2.5191(7)
Rh(1)-Co(2)	2.5644(7)	Co(2)-C(1)	1.908(4)
Co(2)-C(3)	1.928(4)	Co(2)-Co(1)	2.4775(9)
Co(1)-C(2)	1.897(4)	Co(1)-C(1)	1.922(4)
O(1)-C(1)	1.191(5)	C(4)-C(3)	1.478(5)
C(3)-C(2)	1.379(5)	C(2)-H(2)	1.194(8)
Bond Angel / °			
C(2)-Rh(1)-C(1)	89.7(2)	C(3)-Rh(1)-C(1)	90.9(2)
Co(1)-Rh(1)-Co(2)	58.33(2)	Co(1)-Co(2)-Rh(1)	59.92(2)
Co(2)-Co(1)-Rh(1)	61.75(2)	C(2)-C(3)-C(4)	127.3(3)
O(1)-C(1)-Co(2)	134.9(3)	O(1)-C(1)-Rh(1)	128.4(3)
C(3)-C(2)-H(2)	128.4(5)	Co(1)-C(2)-H(2)	120.7(5)
Dihedral and interplanar angles / °			
[Rh(1),Co(1),Co(2)]-[C(2),C(3),C(4)]			69.3
H(2)-C(2)-C(3)-C(4)			6.7
[Rh(1),Co(1),Co(2)]-[Phenyl]			84.8
[C(2),C(3),C4)]-[Phenyl]			26.3
[Rh(1),Co(1),Co(2)]-[Cp]			99.0; 98.7
[Rh(1),Co(1),Co(2)]-[Cp^*]			75.8
[Rh(1),Co(1),Co(2)]-[C(2),Co(1),Co(2),C(3)]			57.8
[H(2),C(2),C(3)]-[C(2),Co(1),Co(2),C(3)]			5.4
[C(2),C(3),C(4)]-[C(2),Co(1),Co(2),C(3)]			11.8

the phenyl ring is twisted out of the plane described by the alkyne ligand and is aligned almost perpendicular to the metal triangle. In this orientation the tolyl group fits into the space between two Cp ligands or a Cp and Cp^* ligand respectively. The centroids of Cp and Cp^* ligands in **23** and **24** are slightly tilted out of the plane defined by the metal atoms towards the bottom side of the cluster (capped by the CO) by an angle θ of around 10° as indicated in Figure 3.16. In the Rh complex **24** this tilt is largest for the Cp^* ligand (θ = 15°) which might be attributed to larger steric interactions of that ligand with the tolyl group. This *vertical* tilt causes the angles between the planes of the Cp and Cp^* rings and the one defined by the metal triangle to be between 98° and 115° compared with 90° expected for a structure with symmetric faces. In addition, the Cp and Cp^* ligands are tilted *horizontally* away from the edge bridged by the tolyl substituent (Figure 3.16), giving further evidence for steric interactions between these groups. This issue will be discussed further in section 3.4 under the aspect of hindered rotation of the tolyl substituent in solution.

3.3.2. Variable Temperature NMR Spectra of $Cp^*Ir(CpCo)_2(CO)(Tol\text{-}C{\equiv}C\text{-}H)$ (23)

At room temperature the proton NMR spectra of the tolylacetylene complexes exhibit one signal each for the alkyne, Cp and the Cp^* protons indicative of a fluxional structure at room temperature. In addition the tolyl group gives rise to two doublets in the aromatic region and a singlet around 2 ppm. In the carbon-13 NMR spectrum the carbonyl carbon exhibits a chemical shift of

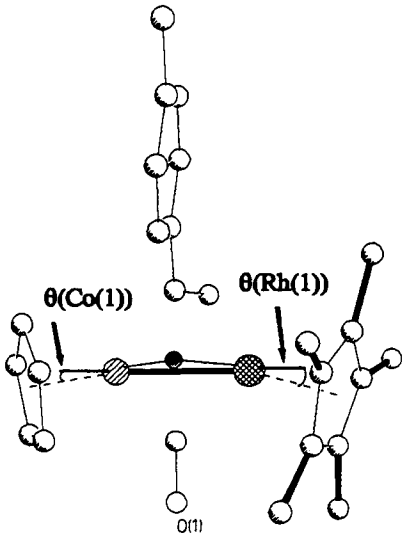

23

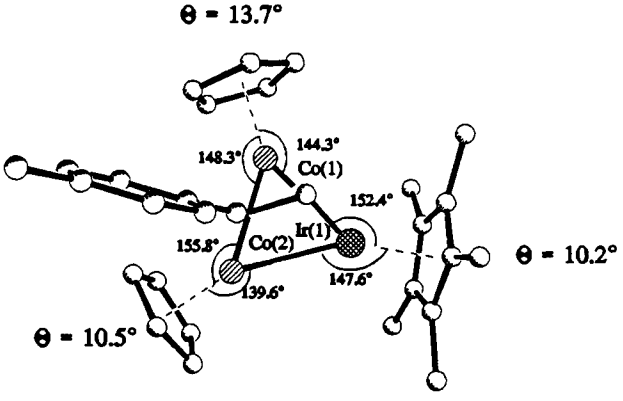

24

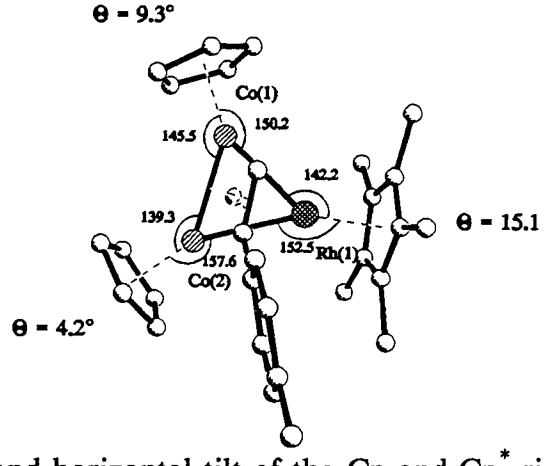

Figure 3.16: Vertical and horizontal tilt of the Cp and Cp^* rings in the crystal structures of **23** and **24**.

260 ppm consistent with a triply bridging carbonyl, whereas the alkyne carbons appear at 151 (≡C-Tol) and 117 ppm (≡C-H). A complete listing of the room temperature NMR data can be found in Table 3.4.

The alkyne proton resonance is very broad at room temperature ($\Delta\nu_{1/2}$ = 25 Hz) indicative of a fluxional process influencing this signal. Indeed the spectrum becomes more complex upon lowering the temperature and at 181 K three sets of signals due to different isomers can be distinguished as shown in Figure 3.17. In the alkyne region, one can distinguish one major and two minor isomers. In order to understand the spectrum one has to consider that the introduction of an non-symmetric alkyne doubles the number of possible isomers arising from different orientations of the alkyne ligand with respect to the metal-metal edges. Considering only complexes containing the alkyne parallel to a metal-metal edge there are three different diastereomers **A**, **B** and **C** which differ in the relative orientation of the alkyne ligand. Each of these diastereomers occurs as a pair of enantiomers resulting in 6 different structures as shown in Figure 3.18. Isomers **A** and **C** both have the alkyne ligand parallel to the Ir-Co edge with the tolyl group across the Co-Co edge in **A** and across the other Ir-Co edge in **C**. As in the case of the acetylene adducts, isomer **B** has the alkyne parallel to the Co-Co edge. Figure 3.18 illustrates these isomers and the fluxional processes relating them with each other for the Ir containing complex **23**, but this general principle applies to all $M^{\bullet}M_2$ cluster complexes with asymmetric alkyne ligands.

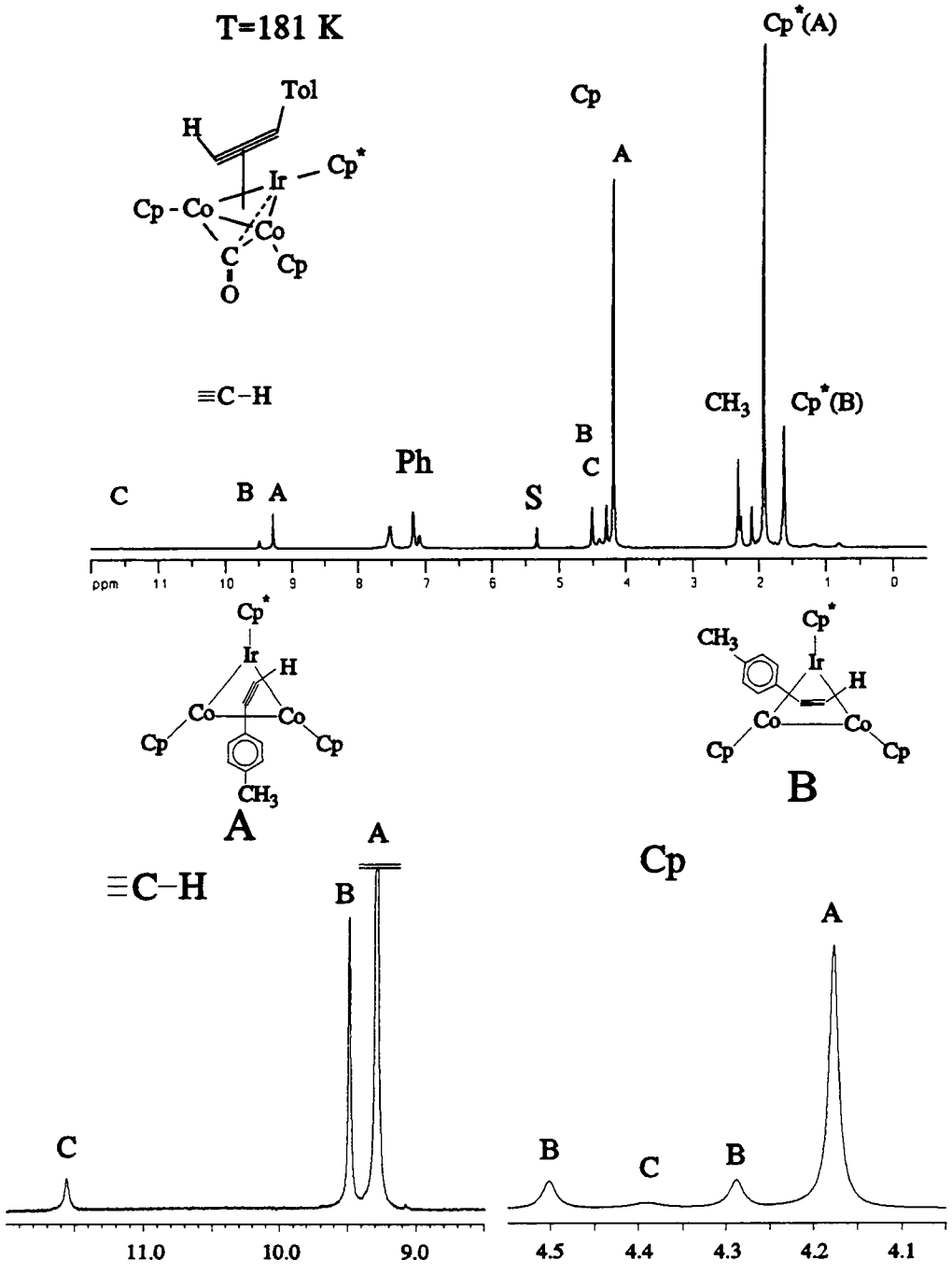

Figure 3.17: Proton NMR spectrum of **23** at 181 K showing three different isomers. Full spectrum (top); expansions on alkyne and Cp region (bottom).

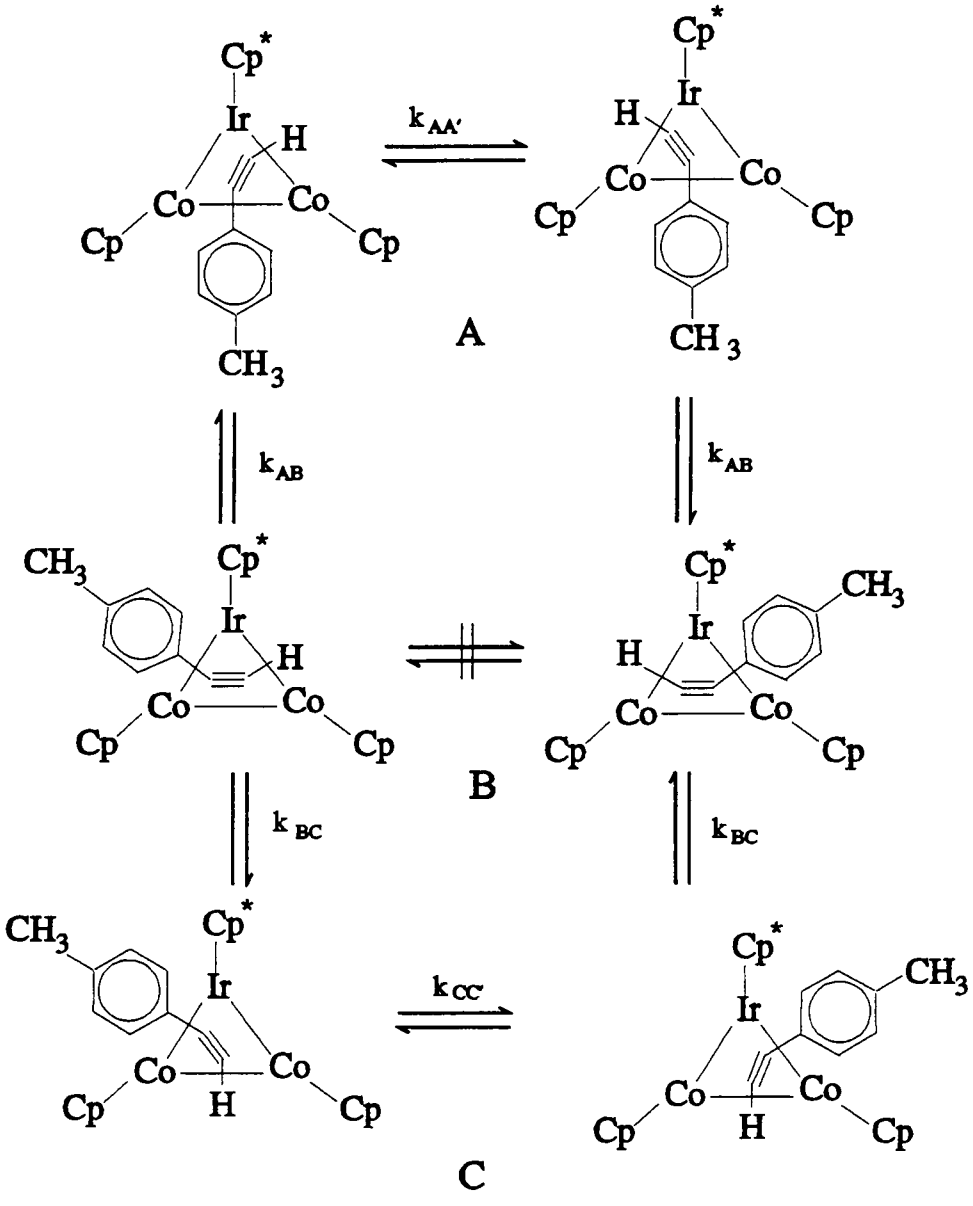

Figure 3.18: Possible structures for the tolylacetylene adducts showing the three pairs of enantiomers.

From Figure 3.17 we can see that at low temperature the preferred isomer

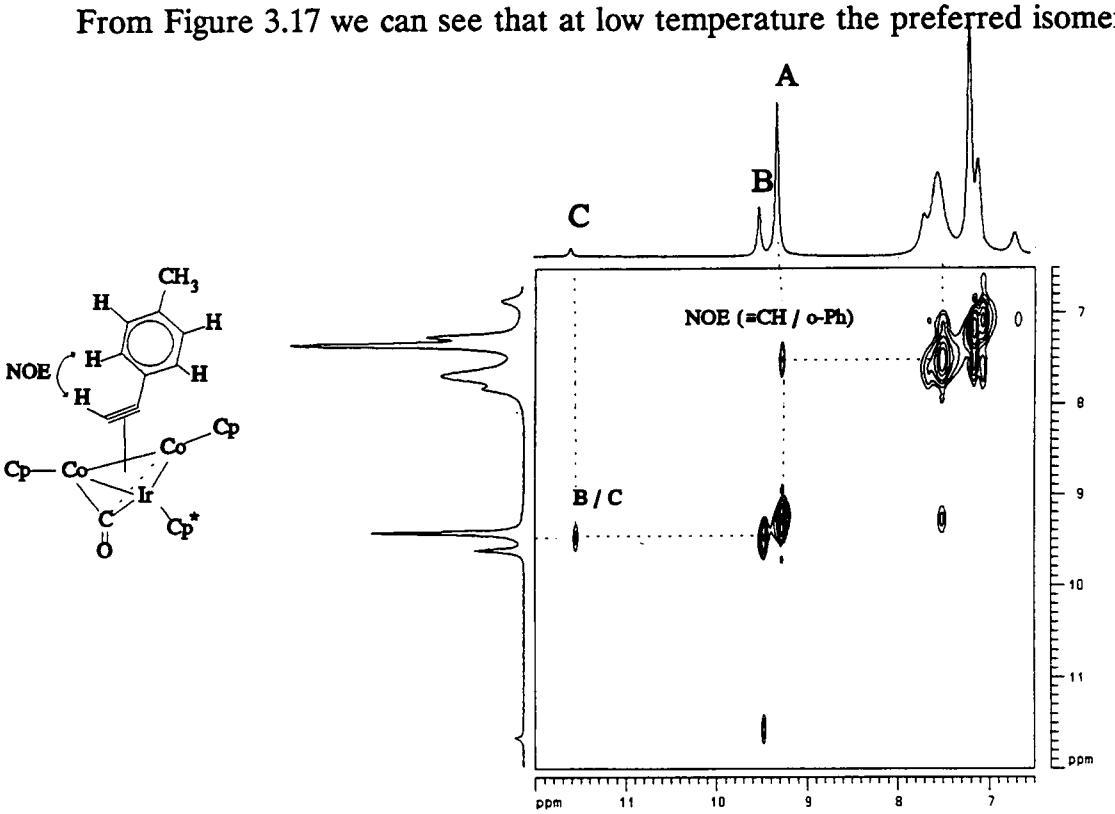

Figure 3.19: Downfield part of the NOESY spectrum of **23** at 175 K.

exhibits one signal in the Cp region of the proton NMR spectrum. At first glance, none of the three isomers has two equivalent CpCo edges. On the other hand, from the earlier discussion of the acetylene adducts **19** and **20** we know that the alkyne is still moving rapidly between its two orientations parallel to the Ir-Co edge interchanging the two enantiomers. If no new steric interactions are present, one can expect this to be the case for isomers **A** and **C** of the tolylacetylene adducts. A NOESY spectrum at 175 K shows only an exchange peak between the two alkyne signals of the minor isomers but none connecting major and minor isomer (Figure 3.19). This confirms that the major isomer has to be either **A** or **C**

but cannot be **B** since in that case the minor isomers would have to be **A** and **C** and any exchange between them would have to involve isomer **B**.

When comparing the chemical shift of the alkyne proton of the major isomer (9.3 ppm) to the ones of the corresponding acetylene adduct **19** (11.61 and 9.16 ppm) one can see that it matches the shift of a proton pointing towards an Ir-Co edge. The major isomer is therefore most likely diastereomer **A** which is also the one found in the solid state from the x-ray analysis. With the same argument we can assign the more abundant of the two minor isomers to be isomer **B** since the chemical shift of the alkyne proton (9.55 ppm) also indicates that the alkyne C-H bond is pointing towards the Ir-Co edge. The alkyne proton in the least abundant isomer, on the other hand, has a chemical shift of 11.6 ppm which suggests that isomer in **C** the alkyne C-H bond is pointing towards the Co-Co edge. Consistent with these assignments two Cp signals are observed for isomer **B** at low temperature since once the interconversion **B** → **C** (k_{BC}) is slow enough to observe separate sets of signals, the interconversion between the two enantiomers of **B** is also frozen out. As mentioned earlier, the interchange **B** → **C** is still fast enough to give rise to cross peaks in the NOESY spectrum whereas the interchange **A** → **B** at that temperature is too slow to be detected. Furthermore, isomer **C** appears to have only one type of Cp proton. Due to the high viscosity of the solution at the lowest temperature, integration of the Cp signal is not very accurate thus prohibiting an exact determination of the number of Cp rings contributing to that signal. However, if we assume that there is no overlap of a

second Cp signal of **C** with signal of the more abundant isomers, then there is rapid exchange between the two enantiomers **C** and **C′**. These observations reveal, without further quantitative treatment, the order of rate constants for the exchange processes to be $k_{AA'} \approx k_{CC'} > k_{BC} > k_{AB}$. By integrating the well separated alkyne proton signals of the different isomers we can determine the ratio **A** : **B** : **C** to be 18 : 5.5 : 1 at 181 K.

The spectrum of the phenyl region at 181 K shows two sets of signals arising from isomers **A** and **B**. Upon further cooling to 170 K, however, additional splitting is observed. This behavior involves freezing out the rotation of the phenyl ring about the Tol-C≡ bond in the case of isomer **B** and will be discussed in more detail at a later point together with other complexes where this phenomenon is more pronounced.

When the sample is warmed from 170 K one first observes coalescence of the alkyne signals due to **B** and **C** whereas isomer **A** remains unchanged up to 250 K. At the same time, the two Cp signals of **B** and the Cp signal due to **C** coalesce while the signal due to isomer **A** remains unchanged (Figure 3.20). No change is observed in the Cp^* region in that temperature range probably because the two signals of **B** and **C** overlap.[23] At 250 K one combined set of signals is observed for **B** and **C** which is still distinct from the signal due to isomer **A**. Furthermore, at this temperature exchange between the two enantiomers of **B** is fast on the NMR time scale resulting in only one Cp signal for isomer **B**. The correlation of the coalescence of signals due to isomers **B** and **C** with the

interconversion of the two CpCo vertices in **B** can be understood from the exchange scheme shown in Figure 3.18. Since at 250 K k_{AB} is still slow, exchange between the enantiomers **B** and **B′** involves the pathway **B** → **C**. Finally, above 250 K the signals of **A** and (**B**,**C**) coalesce to yield one set of signals at room temperature.

A quantitative treatment of the exchange rates was achieved by performing full lineshape analyses of the exchange broadened spectra. All aspects of the spectra, except of the low temperature behavior in the phenyl region, could be simulated by adjusting only the two rate constants k_{AB} and k_{BC} and assuming that k_{AA} and k_{CC} are still too fast on the NMR time scale down to the lowest measured temperature to have a measurable effect on the spectra. Since k_{AB} and k_{BC} are quite different in magnitude, at most temperatures the lineshape depends only on *one* of the two rate constants: Above 240 K only k_{BC} is too fast and below 225 K k_{AB} is too slow to have any measurable effect on the lineshape. These observations simplify the lineshape analysis considerably since only one rate constant has to be used as fitting parameter at a time. Figure 3.20 shows experimental and simulated spectra for the Cp signals. Similar simulations were obtained for the alkyne and Cp^* signals. From these data values for the activation enthalphy $\Delta H^{\ddagger}$, -entropy $\Delta S^{\ddagger}$ and free energy of activation $\Delta G^{\ddagger}$ listed in Table 3.7 were obtained. One can see that two distinct barriers of activation are observed for processes **A** → **B** and **B** → **C**. Even so values of $\Delta H^{\ddagger}$ and $\Delta S^{\ddagger}$ for each of these processes vary somewhat depending on which set of signals is evaluated, the

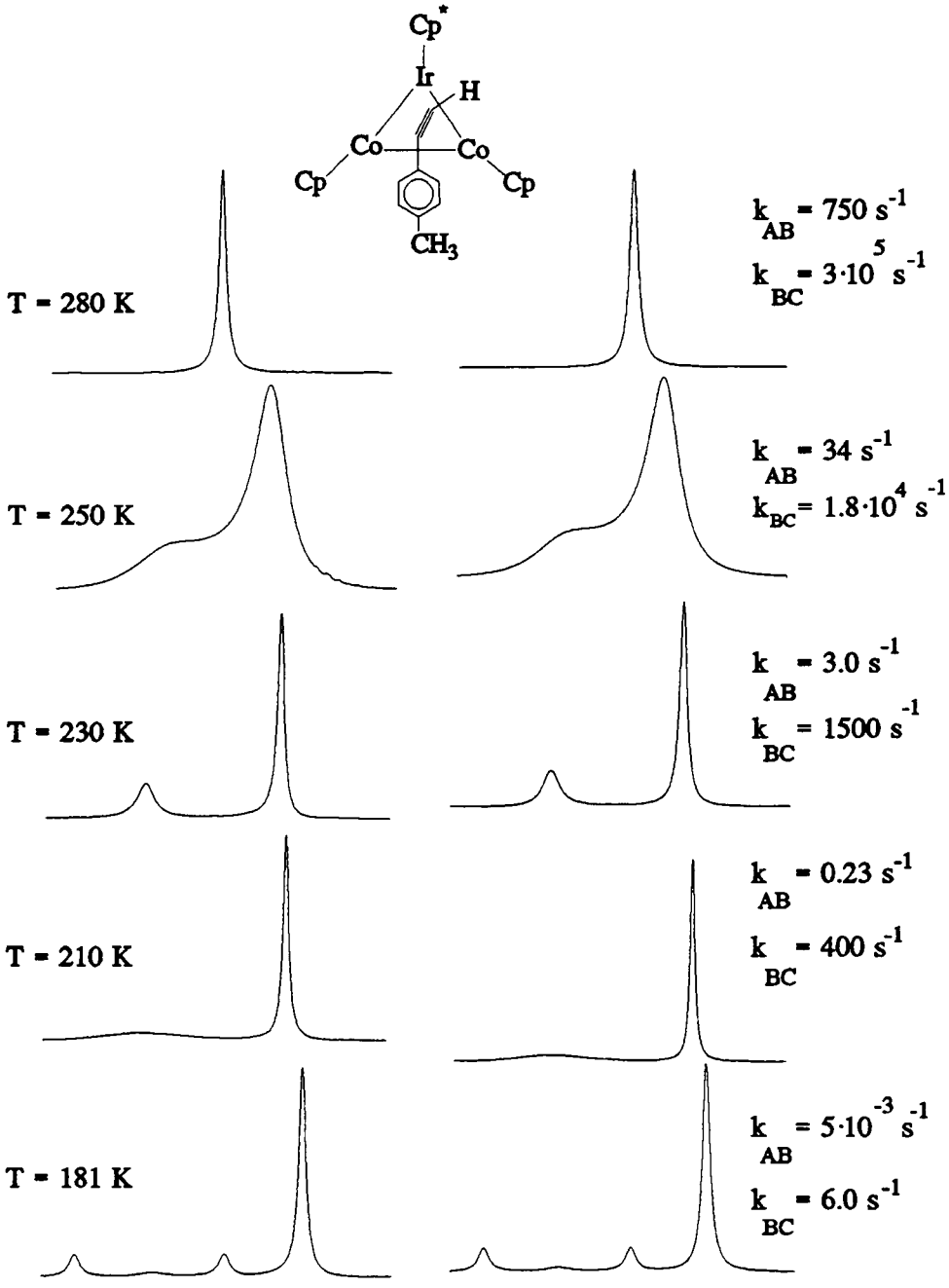

Figure 3.20: Cp region of the experimental (left) and simulated (right) ^{1}H NMR spectra of **23** at variable temperatures.

values obtained for the free energy of activation $\Delta G^{\ddagger}$ agree very well with each other for each process.

The low temperature carbon NMR spectrum reveals two sets of signals for isomers **A** and **B**. Two different types of Cp carbons are found for isomer **B** whereas isomer **A** exhibits only one type of Cp as expected. The carbonyl signals of **A** and **B** are observed at 262.8 and 271 ppm, respectively, whereas the protonated alkyne carbons are found at 113.1 and 118 ppm. Carbon signals due to isomer **C** can only be seen in the Cp and Cp^* region of the spectrum and have been confirmed to belong to isomer **C** by $^{13}C\{^1H\}$ heteronuclear correlation spectroscopy (δ_{Cp} = 84 ppm, δ_{Cp^*} = 8.6 ppm).

3.3.3. Cp^*Rh- and Cp^*Co Containing Complexes 24, 25 and 26

The low temperature ^1H NMR spectra of $Cp^*Rh(CpCo)_2(CO)(Tol\text{-}C{\equiv}CH)$ (**24**) (Figure 3.21) and $Cp^*Co(CpCo)_2(CO)(Tol\text{-}C{\equiv}CH)$ (**25**) each show the presence of two isomers, one of which dominates the spectrum. The alkyne protons of the dominating isomers exhibit a chemical shift of 9.66 and 10.32 ppm, respectively. These shifts are indicative of the alkyne hydrogen pointing towards a Cp^*M-CpCo edge as discussed earlier. Furthermore, two signals are observed for the Cp hydrogens of the major isomer in either case indicating that the major isomer has structure **B** with the alkyne ligand parallel to the Co-Co edge. The alkyne protons of the minor isomers are observed at 8.9 and 9.78 ppm indicative of alkyne hydrogens pointing towards a Cp^*M-CpCo edge, and only one Cp signal

Table 3.7: Activation parameters for the interconversion of isomers **A**, **B** and **C** of the alkyne complex **23**.

process	$\Delta H^{\ddagger}$/ kJ mol^{-1}	$\Delta S^{\ddagger}$/ J mol^{-1} K^{-1}	$\Delta G^{\ddagger}$(298K)/ kJ mol^{-1}	$\Delta G^{\ddagger}$(170K)/ kJ mol^{-1}	ΔG^{0}(170K)/k J mol^{-1}
A→B	48.4[a)]	-17.5	53.6	51.4	+ 1.8
	45.4[b)]	-29	54.0	50.3	
	54.8[c)]	8.1	52.4	53.4	
B→C	40.3[b)]	1.9	39.8	40.6	+ 2.4
	43.5[c)]	19.2	37.8	40.2	
	44.5[d)]	25.1	37.0	40.2	

a) Cp* signal b) Cp signals c) alkyne signals, full analysis involving isomers **A**, **B** and **C**. d) alkyne signals, low temperature region, considering only isomer **B** and **C**.

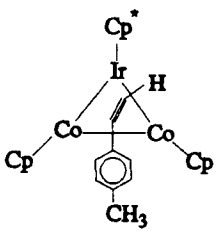

23 A

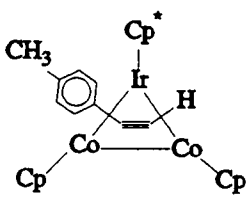

23 B

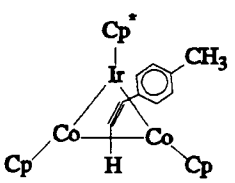

23 C

is observed in each case. These observations are consistent with isomer **B** where the alkyne ligand is parallel to a Cp*M-CpCo edge with the Tolyl group across the Co-Co edge and the hydrogen pointing towards the Cp*M-CpCo edge. No evidence for isomer **C** could be found in any of the spectra. The low temperature ^{13}C NMR spectra are also consistent with these assignments containing two signals for the Cp carbons. The dominance of isomer **B** is larger for these complexes when compared with isomer **A** in the Ir analogue; from integrations one obtains a

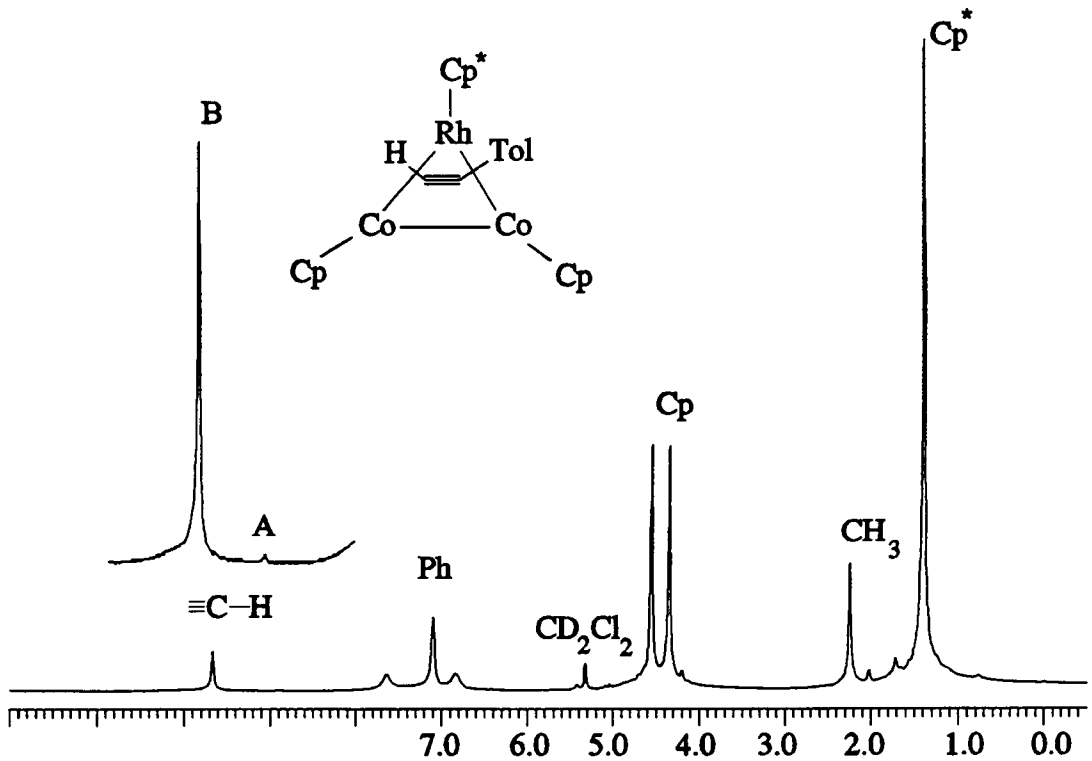

Figure 3.21: Low temperature ^1H NMR spectrum of **24**. T = 170K

ratio **B** : **A** of 46 : 1 for $Cp^*Rh(CpCo)_2(CO)(Tol\text{-}C{\equiv}CH)$ and 18 : 1 for $Cp^*Co(CpCo)_2(Tol\text{-}C{\equiv}CH)$. Upon warming of the sample the signals due to isomers **A** and **B** coalescence to give one set of signals above 210 K. At the same time the two Cp signals of isomer **A** coalesce as expected due to the fast interchange of the two enantiomers of **A**. The coalescence temperature of 210 K is significantly lower than the one observed for the exchange **A** → **B** in the Ir analogue **23**. The fact that the exchange of the two enantiomers of **B** is linked to the interconversion **B** → **A** indicates that the pathway **B** → **C** → **B** involving a possible isomer **C** has to be higher in energy than **B** → **A** → **B** and appears not to

play a significant role in these complexes. Otherwise one would expect to observe exchange between the enantiomers of **B** even while the interchange **A** → **B** is frozen out, similar to what is observed for the Ir analogue. One is therefore able to model the exchange processes by considering only one rate constant k_{AB}.

Figure 3.22 shows that simulated spectra obtained with this model for the Cp region of $Cp^*Co(CpCo)_2(CO)(Tol\text{-}C{\equiv}CH)$ agree very well with the experimental data. From the rate constants k_{AB} the activation parameters $\Delta H^{\ddagger}$ = 35.6 kJ mol^{-1}, $\Delta S^{\ddagger}$ = -8 J mol^{-1} K^{-1} and $\Delta G^{\ddagger}(298K)$ = 37.9 kJ mol^{-1} are obtained. Similar values are obtained from an analysis of the coalescence behavior of the alkyne signal. One can see that this barrier is considerably lower than the one found for the Ir analogue. For reasons that are yet unknown, the ^1H spectra obtained of the Rh analogue were of poor quality and not suitable for lineshape analysis; however, a coalescence temperature for the interchange of the Cp signals of T_C = 210 K was observed. Using a chemical shift separation of $\Delta\nu$ = 82 Hz for the Cp protons one can use the relationship

$$k(T_c) = \frac{\pi\Delta\nu}{\sqrt{2}} \qquad (3)$$

to calculate a rate constant of 182 s^{-1} at T_C for the interchange of the CpCo edges in **24**. From that one obtains a barrier $\Delta G^{\ddagger}(210K)$ = 41.7 kJ mole^{-1} using equation (1). That indicates that alkyne mobility in the Rh substituted cluster complex is also more facile than in the Ir analogue with a barrier to rotation

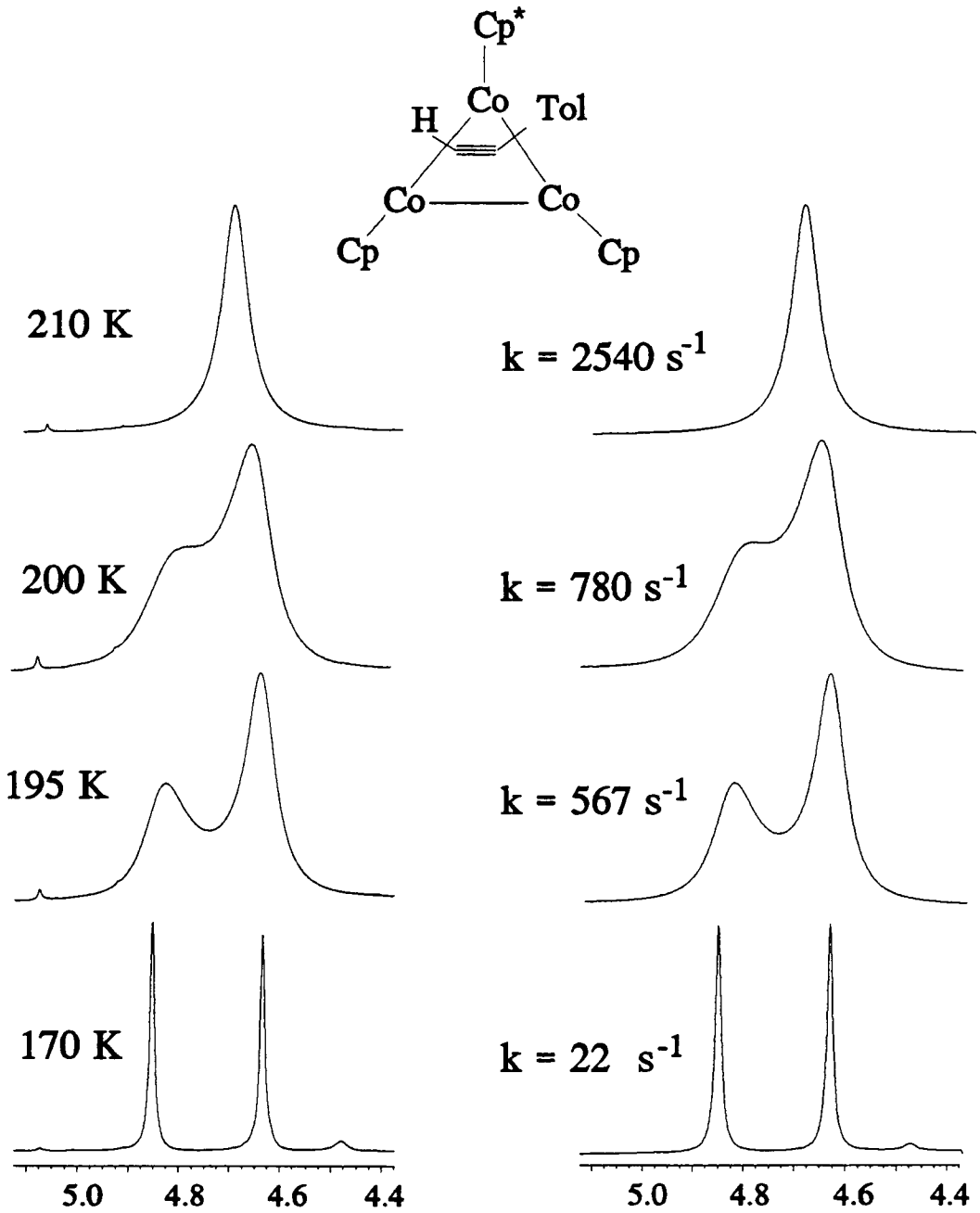

Figure 3.22: Experimental (left) and simulated (right) spectra for the Cp region of **25**.

similar to the one observed in $Cp^*Co(CpCo)_2(CO)(Tol\text{-}C{\equiv}CH)$.

3.3.4. $Cp^{\ddagger}Co(CpCo)_2(CO)(Tol\text{-}C{\equiv}CH)$ (27) and $(CpCo)_3(CO)(Ph\text{-}C{\equiv}CH)$ (28)

The $C_5(CH_3)_4(CF_3)$ ligand, here abbreviated as $Cp^{\ddagger}$, is sterically equivalent to the Cp^* ligand, but is a weaker electron donor and therefore electronically closely related to the Cp ligand.[13] The room temperature ^1H NMR spectrum (see Table 3.4) is analogous to the one of the other tolylacetylene adducts with the exception that two signals of intensity 6 each are observed for the $Cp^{\ddagger}$ ligand. The same applies to the ^{13}C NMR spectrum, however we were not able to detect the signals due to the CO ligand and the CF_3 group.

At low temperature, the predominant isomer exhibits only one signal for the Cp protons and a shift of 9.82 ppm for the alkyne proton (see Figure 44). This is consistent with a species with the alkyne ligand parallel to a $Cp^{\ddagger}Co$-CpCo edge resembling isomer **A**. This observation is exactly the opposite of what is observed for the Cp^*Co analogue. Furthermore, one of the two protons of the tolyl group shows significant broadening indicating a slowing down of the rotation of the tolyl group as described in paragraph 3.4 below. A minor isomer containing two different signals for the Cp protons and a chemical shift of 10.45 ppm for the alkyne hydrogen is also observed. These signals are assigned to isomer **B** with the alkyne parallel to a CpCo-CpCo edge. From integrations, a ratio **A** : **B** of 14 : 1 is observed. Even though the preferred orientation of the alkyne in this complex appears to resemble the Cp^*Ir complex **23** there are several

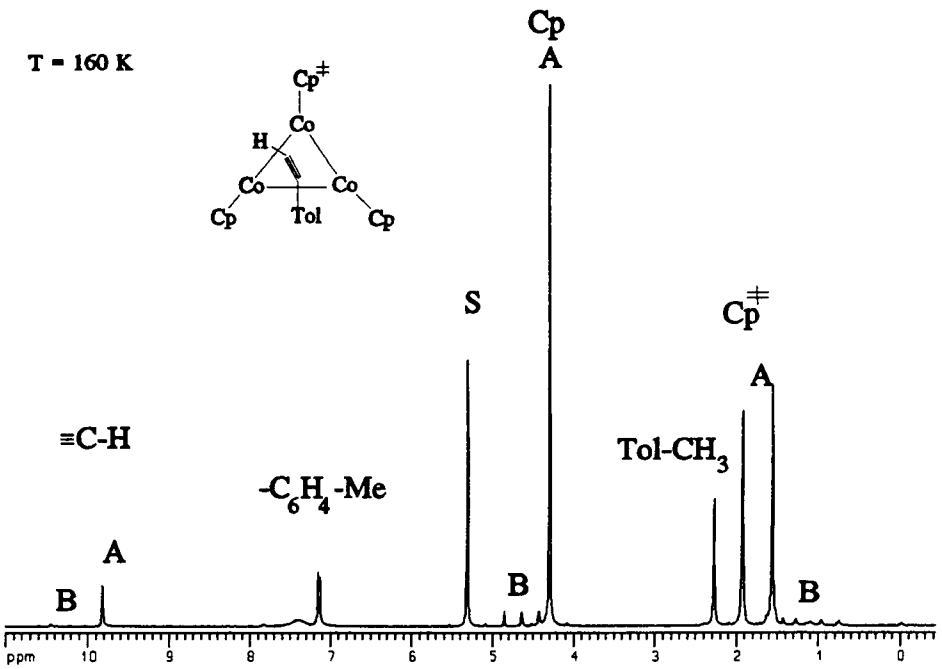

Figure 3.23: Low temperature ^1H NMR spectrum of tolylacetylene complex **27**.

differences between the two. No third isomer of type **C** is observed and consequently no exchange of the CpCo edges in isomer **B** takes place once the interconversion of isomer **A** and **B** is frozen out. Furthermore, the barrier of activation for the interchange of isomer **A** and **B** appears to be considerably lower than in the Cp^*Ir complex **23**. No lineshape analysis was obtained for **27**, but above 195 K only one set of signals is observed whereas in **23** coalescence between isomer **A** and **B** takes place well above 250 K.

Finally, the all CpCo complex $(CpCo)_3(CO)(Ph\text{-}C{\equiv}CH)$[24] (**28**) was investigated at low temperature. In this complex all three edges of the metal triangle are identical resulting in only one possible orientation of the alkyne with

respect to the metal triangle. Accordingly, no change is observed for the alkyne signal over the entire temperature range from 300 K to 170 K. The signal observed for the Cp protons, on the other hand, decoalesces from one sharp signal above 220 K into two signals of the relative ratio 5 : 10 at 170 K. For a completely static structure, one would expect all three CpCo edges to be inequivalent. One could think of a coincidental equivalency of two of the CpCo edges, but that is rather unlikely since in the static structure of $(CpCo)_3(CO)(t\text{-}Bu\text{-}/C{=}CH\text{-}CO\backslash)$ three different C signals are observed. It appears to be more likely that, similar to the interconversion of the two enantiomers of **A** in the Cp^*Ir containing complex **23**, the phenyl end of the alkyne is locked on one Co-Co edge, but the hydrogen end is still moving fast between two positions equilibrating the identities of two of the three CpCo edges. Since all three vertices are equivalent, such a difference in the rates of reorientation is most likely due to steric interactions. In addition to splitting of the Cp signal into two, the signal due to the ortho-phenyl hydrogen shows significant broadening whereas the meta and para resonances appear to remain unchanged at low temperature. This observation is similar to the $Cp^‡Co$ analogue and is caused by slowing of phenyl ring rotation and is consistent with the presence of steric interactions between the phenyl ring and the Cp ligands. Upon raising the temperature, the phenyl end of the alkyne moves between the metal edges and coalescence of the two Cp signals is observed at around 200 K. A full line shape analysis was performed and the

activation parameters were determined as $\Delta H^{\ddagger}$ = 37.9 kJ mol^{-1}, $\Delta S^{\ddagger}$ = -9.7 J K^{-1} mol^{-1}, $\Delta G^{\ddagger}$(170K) = 39.5 kJ mol^{-1} and $\Delta G^{\ddagger}$(298K) = 40.7 kJ mol^{-1}.

3.3.5. Hindered Phenyl Ring Rotation: Evidence for Correlated Motion:

In all three tolylacetylene adducts, two doublets are observed for the aromatic protons of the tolyl group at room temperature. Upon lowering the temperature this pattern becomes more complex. In the case of the dominating isomer of the Cp*Rh and Cp*Co containing complexes **24** and **25**, one of the two doublets broadens and is split into two well separated signals of equal intensity at

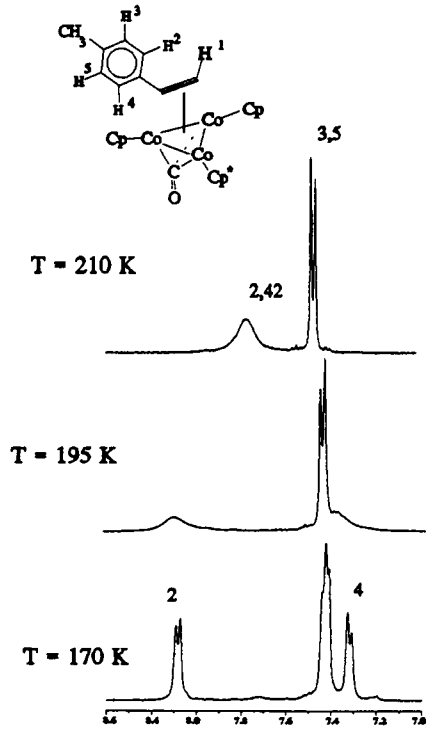

Figure 3.24: Temperature dependent ^{1}H NMR spectra showing the phenyl region of **25**.

170 K (Figure 3.24). The other signal does not split into two, but its fine structure at low temperature indicates that the two protons giving rise to that signal have slightly different chemical shifts. These shifts are so close to each other that they partially overlap. This interpretation is confirmed by the ^{13}CNMR spectrum in which the four corresponding carbon atoms all have different chemical shifts at 170 K. In the case of the Rh containing complex **24** the lines are still very broad whereas four sharp lines are observed for the Co analogue **25**. The quaternary phenyl carbons on the other hand do not show any splitting.[25] As mentioned before, this additional splitting of signals cannot be explained by freezing out different orientations of the alkyne ligand alone, since the dominance of one isomer leads to splitting in signals of very different intensities. The observed splitting therefore most likely arise from slowing down the rotation of the tolyl ring about the ≡C-Tol bond. Restricted rotation of the phenyl ring makes the two sides of the phenyl ring inequivalent, resulting in different signals for the protons and carbons on opposite sides of the ring. The quaternary carbons on the other hand are located on the rotational axis and therefore remain unaffected by slowing the rotation of the tolyl group.

From Figure 3.24 one can see that the chemical shift separation observed for the two pairs of exchanging protons (or carbons) is very different. An explanation for this observation can be found in the anisotropic shielding introduced by the metal cluster core. In a static structure, the protons next to the alkyne (numbered 2 and 4 in Figure 3.24) are located in two chemically very

different environments. Proton 2 is pointing up and bent above the metal triangle whereas proton 4 is pointing downwards towards the Cp ligands. These two protons are therefore expected to split into two well separated signals at low temperature. The geometry is somewhat similar to the one found for the two carbene hydrogens mentioned in the previous chapter for which also a chemical shift difference of around 1 ppm was observed. Protons 3 and 5 on the other hand are further away from the metal triangle and their environments are very similar, hence causing only a small separation between the two corresponding proton signals. Similar results are found in the phenyl analogue $Cp^*Co(CpCo)_2(CO)(Ph\text{-}C{\equiv}CH)$ (**26**). In this complex the ortho hydrogen signal decoalesces into two signals which are separated by 1 ppm. The two meta hydrogens on the other hand show only a marginal splitting whereas the para hydrogen signals remain unaffected through the entire temperature range.

Further evidence for hindered phenyl ring rotation is found in a NOESY spectrum of **25** shown in Figure 3.25 which was taken at 170 K. The spectrum shows a NOE crosspeak connecting the alkyne resonance (labeled 1 in Figure 3.25) with the downfield tolyl signal. No cross peak is observed to the corresponding upfield signal. This is consistent with the phenyl ring locked in an orientation perpendicular to the metal triangle as found in the solid state structure. The downfield signal is assigned to the proton on the tolyl ring which is adjacent to the alkyne and points up away from the metal triangle (hydrogen 2 in figure 3.25), which puts it closest to the alkyne hydrogen. The upfield signal at

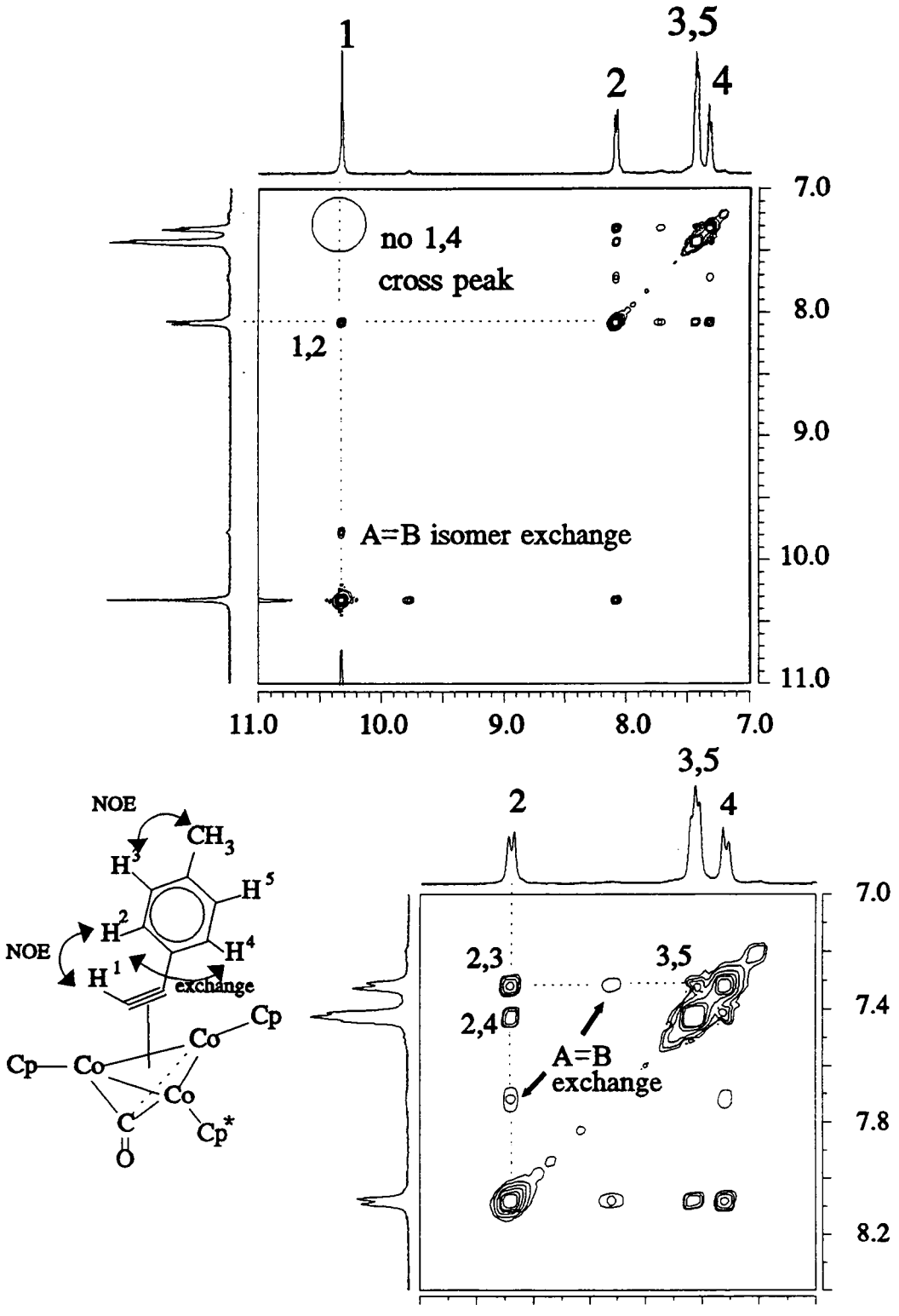

Figure 3.25: NOESY spectrum of **25** at 170 K (τ = 200 ms).

7.5 ppm on the other hand, belongs to the corresponding hydrogen pointing downwards towards (hydrogen 4 in Figure 3.25) and away from the alkyne proton. The two overlapping signals at 7.4 ppm with the relative total intensity of two hydrogens shows a NOE derived cross peak to the methyl group of the tolyl ring consistent with the assignment of these signals to hydrogens 3 and 5.

A strong crosspeak connecting the phenyl protons 2 and 4 with each other indicates that slow rotation of the tolyl group takes place at this temperature. Other crosspeaks observed in the phenyl region are due to NOE's between neighbored phenyl hydrogens and due to exchange between the dominating isomer **B** with minor amounts of isomer **A** as indicated in Figure 3.25. At this point it must be noted that at a temperature as low as 170 K the solution is so viscous that the molecular tumbling is slowed down to the point where the diffusion coefficients are smaller than the NMR resonance frequency (spin diffusion limit). Under these conditions cross peaks due to exchange and NOE have the same sign and can not be distinguished.[26] One way to resolve this problem is using the ROESY experiment[27] which yields cross peaks which are negative in sign for NOE and positive in sign for exchange under these conditions. A ROESY spectrum obtained for $Cp^*Co(CpCo)_2(CO)(Ph\text{-}C{\equiv}CH)$ (**26**) confirmed the assignments made in Figure 3.25. Cross peaks assigned to exchange peaks showed positive phases whereas the peaks labeled as NOE peaks showed either a negative phase or were not seen at all since in the spin diffusion limit NOE cross

peak intensities are normally weaker in the ROESY than in the NOESY experiment.

As already indicated by the crystal structures of the tolylacetylene adducts **23** and **24** (section 3.3.1), one explanation for the hindered rotation of the phenyl group may be found in steric interactions between the phenyl hydrogens and the methyl groups of the Cp^* ring. This theory gets further support if one examines the phenyl region of the ^1H NMR spectrum in the Ir complex $Cp^*Ir(CpCo)_2(CO)(Tol\text{-}C{\equiv}CH)$ (**23**) at low temperature. In this complex both isomers **A** and **B** occur in appreciable amounts allowing one to directly compare the motion of a tolyl group next to a Cp^* ligand (isomer **B**) with the motion of a tolyl ring only neighbored by sterically less demanding Cp ligands (isomer **A**). The low temperature proton spectrum of **23** is shown in Figure 3.26. Two sets of signals in the phenyl region corresponding to isomers **A** and **B** are observed. Though all signals are considerably broadened due to the high viscosity of the solution, one can see that for isomer **B** protons 2 and 4 give rise to two different signals. For isomer **A** only one signal is observed for these protons. Assuming a similar chemical shift difference between protons 2 and 4 for isomer **A** and **B** with a frozen tolyl group these observations suggest that in isomer **A** the tolyl group is rotating at a significantly faster rate than in isomer **B**. This is consistent with the fact that in isomer **B** the tolyl substituent is located above one Cp^*M-CpCo edge next to a sterically demanding Cp^* ligand as in complexes **24** and **25**, whereas in **A** the tolyl group is above a CpCo-CpCo edge. The above assignment is confirmed

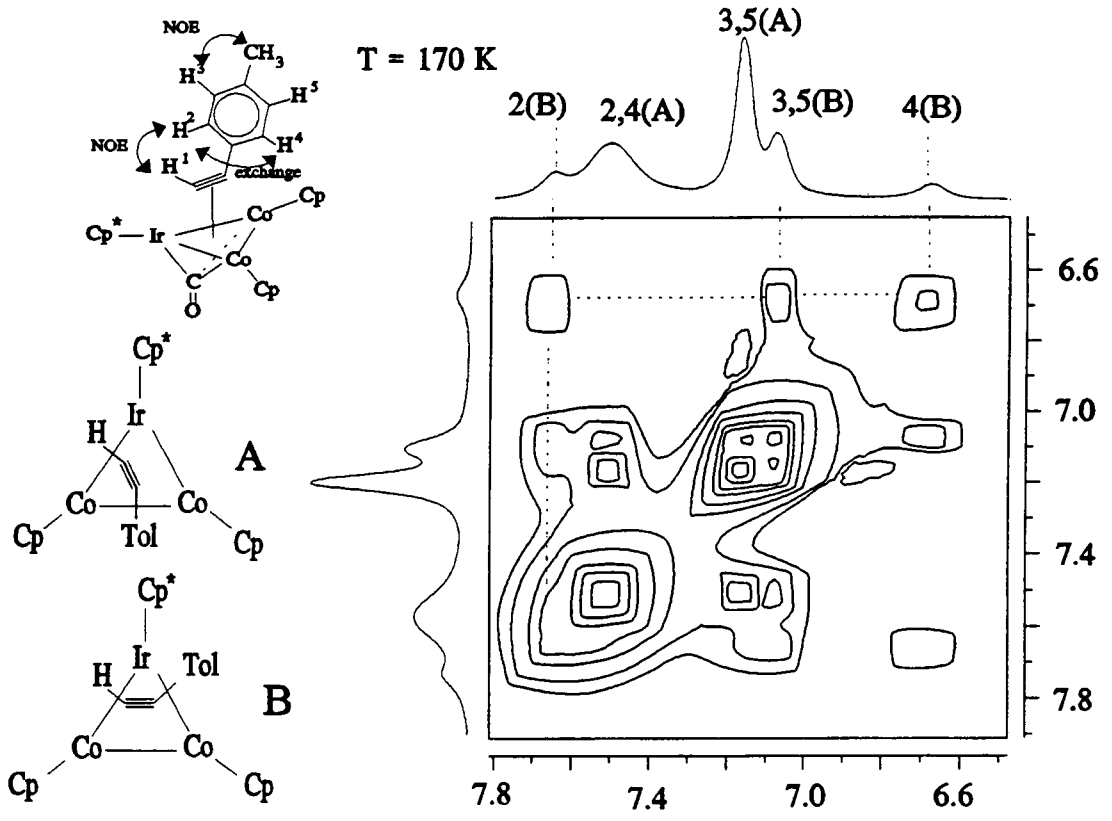

Figure 3.26: Phenyl region of the NOESY spectrum of **23** at 170 K.

by the NOESY spectrum which shows a strong exchange cross peak between protons 2 and 4 in isomer **B** and NOE peaks connecting the neighbored aromatic hydrogens. Furthermore a NOE cross peak is observed for the combined signal of protons 3 and 5 with the methyl group of the tolyl substituent confirming that these hydrogens are the ones next to the methyl group. No signals were observed for isomer **C** probably due to overlap, but the environment of the phenyl ring in that isomer is expected to resemble the one found in isomer **B**. In the case of $Cp^{\ddagger}Co(CpCo)_2(CO)(Tol\text{-}C{\equiv}CH)$ and $(CpCo)_3(CO)(Ph\text{-}C{\equiv}CH)$ the tolyl or phenyl group are also in contact with Cp ligands only and thus broadening, but not

decoalescence is observed for protons 2 and 4. The data and analysis above provide convincing evidence that steric interactions between the Cp and Cp^* ligands on one side and the tolyl substituents of the alkyne on the other play a major role in the barrier to rotation of the phenyl rings.

Within the context of this discussion the question arises as to whether the rotation of the tolyl group is independent of the reorientation of the alkyne ligand or whether the two motions are correlated. If the later is true, then the rate constants for the two processes should be comparable. Because of the complexity of the spin system line shape analysis of the phenyl region of the proton NMR spectrum was not possible. The ^{13}C NMR spectra for the corresponding carbon atoms in these complexes are simpler, but only poor signal-to-noise ratios were obtained for the exchange broadened signals. Therefore, NOESY spectra with different mixing times were obtained for $Cp^*Co(CpCo)_2(CO)(Tol\text{-}C{\equiv}CH)$ (**25**) at 170 K. The volume integrals of the cross peaks are a measure of the magnetization transferred between resonances connected by the cross peak. The change in cross peak intensity as a function of the mixing time τ is dependent on the rate constant for the exchange process as described in Chapter 2 of this thesis. Such an analysis was performed for the cross peak between the two Cp signals and for the one connecting the two phenyl hydrogens next to the alkyne (2 and 4). One obtains very similar rate constants for the interchange of the two phenyl protons ($k_{2,4}$ = 3.9 s^{-1}) and the interchange of the Cp signals ($k_{B,B}$ = 4.7 s^{-1}). This result indicates that rotation of the tolyl group located across a $CpCo\text{-}Cp^*M$ edge

is correlated with the mobility of the alkyne ligand. On the other hand, the rotation of the tolyl group in isomer **A**, which is oriented across a CpCo-CpCo edge, appears to rotate at a faster rate and therefore is independent of alkyne reorientation. Once the interconversion **B** → **A** is frozen out, the phenyl ring rotation in **24B** and **25B** also ceases. In the Ir complex **23** on the other hand, phenyl ring rotation in isomer **B** appears to be linked to the interconversion **B** → **C**. It has to be noted that no evidence for a slowed rotation of the Cp^* ligand has been observed in these studies indicating that the Cp^* ligand and the phenyl substituent do not undergo a geared motion with respect to each other. Instead, the Cp^* ligand acts in an umbrella fashion without being affected in its own rotation. These steric interactions are illustrated in Figure 3.27 which shows a view of crystal structure of the Rh analogue **24** along the tolyl ring axis. When looking along the C_2 axis of the tolyl group one can see that the substituent is located in a "groove" between the Cp^* and a Cp ligand with the major steric interactions on the side of the Cp^*ligand.

3.4. Diphenyl- and Bistolylacetylene Adducts

3.4.1 General

The addition of alkynes substituted with *two* phenyl or tolyl groups to unsaturated Cp^* containing cluster complexes **1**, **2** and **3** takes place at a rate much lower than for acetylene or phenylacetylene. Normally, a solution of the 46 electron complex was stirred for several hours at room temperature to obtain

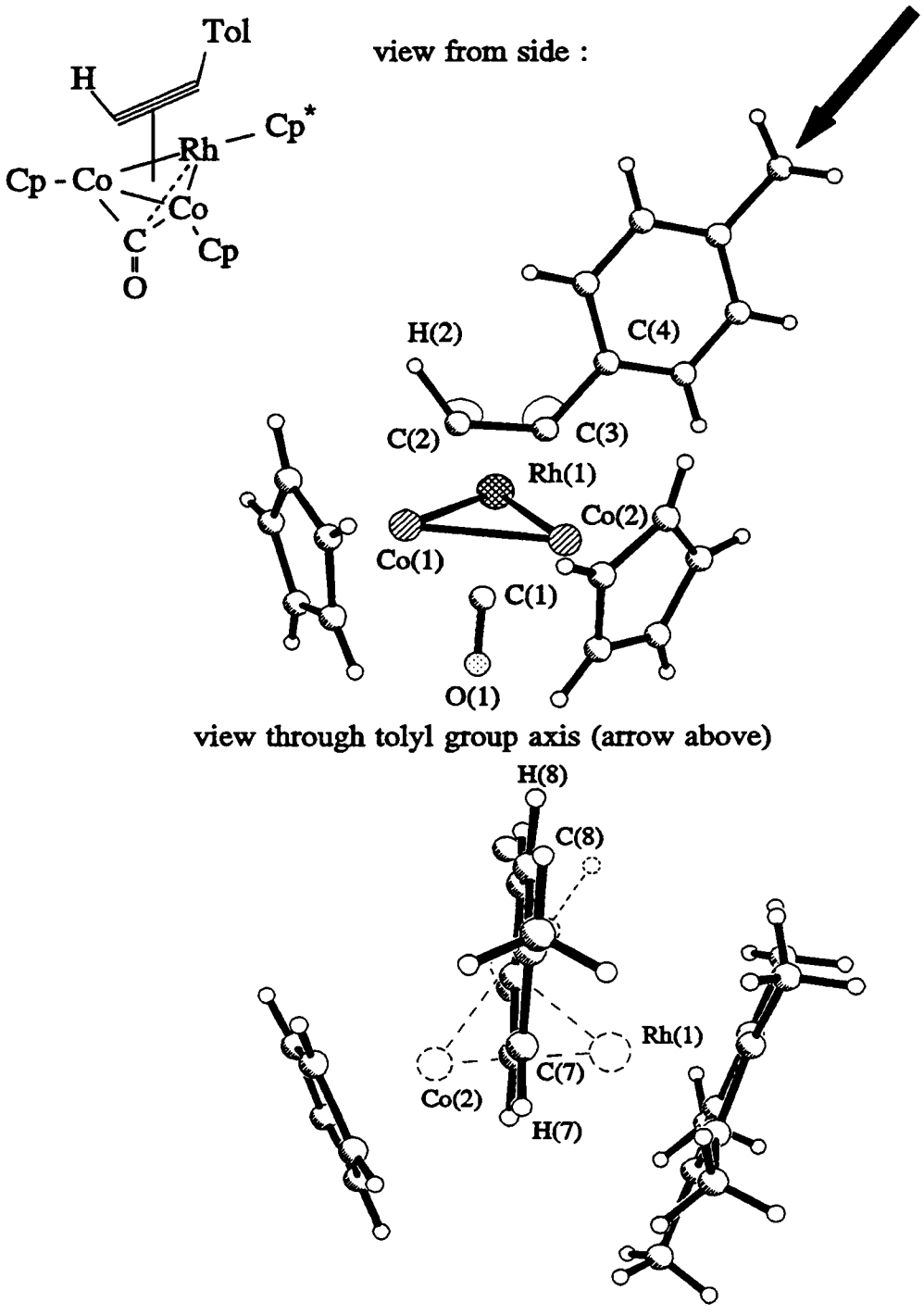

Figure 3.27: View along the rotation axis of the tolyl substituent in **24**. One can see how the tolyl group fills the gap between Cp^* and Cp ligand.

Table 3.8: Spectroscopic data of diphenylacetylene adducts $Cp^*M(CpCo)_2(\mu_3$-CO)(RC≡CR).

	M = Ir,R = Ph	M = Ir R = Tol	M = Rh, R = Ph	M = Rh, R = Tol
^{1}H NMR:	C_6D_6:	C_6D_6:	C_6D_6:	C_6D_6:
ortho-Ph	7.44 d J_{HH}= 7.4 Hz	7.41 d, J_{HH} = 8 Hz	7.45 d J_{HH}= 8.3 Hz	7.41 d
meta-Ph:	7.17 t J_{HH}= 7.6 Hz	7.00 d, J_{HH} = 8 Hz	7.18 t J_{HH}= 7.4 Hz	7.01 d
para-Ph:	6.99 t J_{HH}= 7.3 Hz	-	7.02 d J_{HH}= 7.2 Hz	-
Cp	4.49 s, 10H	4.53 s	4.49 s	4.53
Tol-CH_3	-	2.18 s	-	2.17
Cp^*	1.57 s	1.62 s	1.48 s	1.54
^{13}C NMR[a)]	C_6D_6	C_6D_6:		
CO	254.9	260		
Ph-C	152.4	149.7 142.7;		
≡C-Ph	142.5	134.1		
Ph-CH(o)	129.1	130.9		
Ph-CH(m)	127.2	129.1		
Ph-CH(p)	125.0	-		
Cp^*-C	97.5	97.4		
Cp	86.8	86.8	-	
Tol-CH_3		21.1		
Cp^*-CH_3	9.0	9.1		
IR: ν_{CO}/cm^{-1}	hexane 1663.		(hexane): 1682	-
MS	782 (12%, M^+) 754 (100%, M^+-CO)	810 (58%, M^+) 782 (100%, M^+-CO) 393 (24%, $[Cp^*IrCp]^{\cdot+}$	692 (57%, M^+) 664 88% (M^+-CO) 303 (100%, $[Cp^*RhCp]^{\cdot+}$	720 (75%, M^+) 692 (100%, M^+-CO) 303 (97%, $[Cp^*RhCp]^{\cdot+}$

a) C_6D_6, 300 K

complete reaction. The reaction is also not as clean as observed for acetylene and phenylacetylene. Formation of tricarbonyl complexes $Cp^*M(CpCo)_2(CO)_3$ and cluster fragmentation are the most important undesired processes. Yields of the desired adducts normally were only between 10 and 20%. The room temperature spectroscopic data are summarized in Table 3.8.

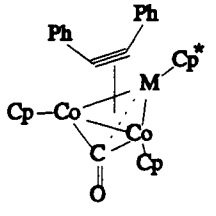

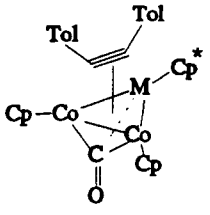

M = Ir: **29** **30**
M = Rh: **31** **32**

From preparation of the Rh containing diphenyl- and ditolylacetylene adducts a reddish side product was isolated with a yield comparable to the one of the alkyne adducts. We were not able to establish the exact nature of these compounds, but NMR and mass spectrometric evidence indicate a dimeric species containing two Cp^*Rh fragments (see experimental part, section 6).

3.4.2. Low Temperature Structure

The low temperature spectrum of the Ir containing ditolylacetylene adduct **30** is shown in Figure 3.28. No change assigned tho the signals of the Cp and Cp^* groups is observed upon lowering the temperature to 170 K and only one signal is observed for each type of proton. In the phenyl region of the spectrum, however,

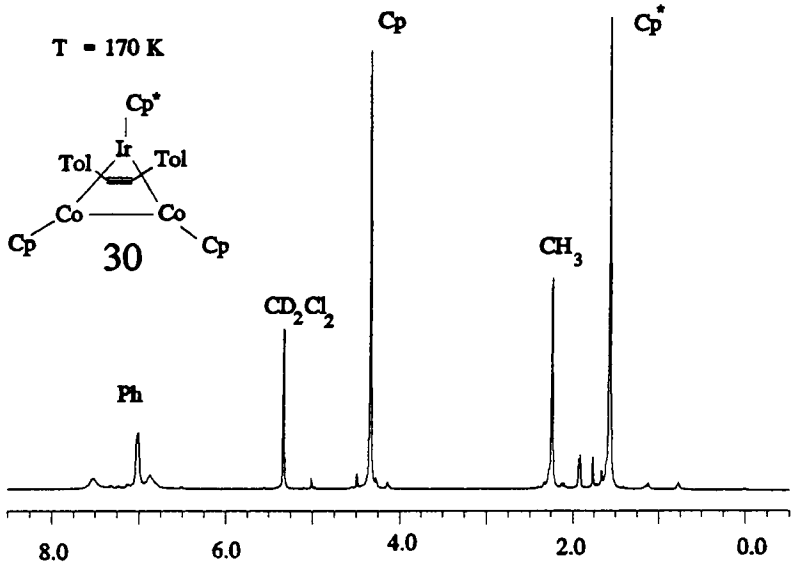

Figure 3.28: Low Temperature spectrum of the ditolylacetylene adduct **30**.

one of the two doublets observed at room temperature has decoalesced into two signals separated by almost one ppm. The splitting pattern suggests that at low temperature the rotation of both phenyl rings is locked. Based on the discussion above (section 3.4) this is only possible if also the reorientation of the alkyne ligand is also frozen out. It appears that only one of the two possible isomers due to different orientations of the alkyne ligand is present.

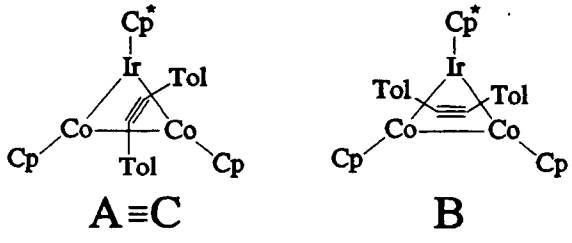

If isomer **A** was present at low temperature, one could explain the observation of only one Cp signal by assuming fast equilibration between the two enantiomers

as discussed for isomer **C** of $Cp^*Ir(CpCo)_2(CO)(Tol\text{-}C{\equiv}CH)$ (**23**). However, one would also expect to observe two types of tolyl rings, one above the CpCo-CpCo edge and one above a Cp^*Ir-CoCp edge. In this case, only the rotation of one of the two types of phenyl rings is expected to be locked at the lowest temperature measured (the one above the Cp^*Ir-CpCo edge). This would yield a pattern signals in the phenyl region similar to the one observed for the mixture of isomers **A** and **B** in $Cp^*Ir(CpCo)_2(\mu\text{-}CO)(Tol\text{-}C{\equiv}CH)$ (**23**) with the only difference that the two sets of signals would be of equal intensity. However, the observed splitting pattern rather resembles the one observed in the Cp^*Rh containing tolylacetylene complex **24** in which the alkyne is parallel to the CpCo-CpCo edge. It therefore appears that in the case of the tolylacetylene adduct the preferred orientational isomer is **B** with the alkyne ligand parallel to a Co-Co edge.

Similar results are obtained for the analogous diphenylacetylene adduct. The corresponding Cp^*Rh containing adducts were not measured at low temperature, but our previous results on the acetylene and tolyl acetylene suggest that the orientation of the alkyne parallel to the Co-Co edge becomes more favored when going from Ir to Rh. If this trend continues for the diphenylacetylene adducts, one would expect to find the alkyne ligand in **31** and **32** to be also parallel to the Co-Co edge.

3.5. Discussion of Thermodynamics and Kinetics of Alkyne Rotation

Table 3.9 summarizes the activation barriers and free energies of reaction for the isomerization of isomer **A** → **B** which corresponds to the reorientation of the alkyne ligand from a position parallel to a LM-CpCo edge to a orientation parallel to the CpCo-CpCo edge. The different preferences in the orientation of the alkyne ligand can be explained in terms of electron density on the metal.

In the case of the Cp^*Co containing cluster **25** the methyl groups of the Cp^* ligand have an electron donating effect thus increasing the electron density on the Co atom carrying the Cp^* ligand as compared to the metal in CpCo groups. As was mentioned earlier, the alkyne ligand is bound most strongly to the two metals which define the edge parallel to the alkyne carbon-carbon triple bond in a σ-donating manner. Preferred binding will therefore occur to the metal fragments which will accept additional electron density most easily, i.e., a CpCo fragment will be preferred over a Cp^*Co fragment. This results in an orientation of the alkyne parallel to the CpCo-CpCo edge and $\Delta G^0_{A \rightarrow B}$ is negative. In the case of the $Cp^‡$ ligand, the electron withdrawing effect of the CF_3 group balances to some degree the electron donating effect of the remaining four methyl groups resulting in electronic properties for the $Cp^‡$ ligand similar to the Cp ligand.[13] In the $Cp^‡Co$ containing complex **27** one would therefore expect both isomers to be present in comparable amounts. The fact that isomer **A** is preferred can be explained in at least two ways. The $Cp^‡Co$ fragment ligand might be even more electronegative than the CpCo fragment. Based on a comparism of the carbonyl

Table 3.9: Kinetic and thermodynamic parameters determined for interconversion **A** → **B** in acetylene and tolyl acetylene adducts.

#	L-M	R	$\Delta H^{\ddagger}$/ kJ mol^{-1}	$\Delta S^{\ddagger}$/ J mol^{-1} K^{-1}	$\Delta G^{\ddagger}$(170K)/ kJ mol^{-1}	ΔG^{0}(170K)/ kJ mol^{-1}
21	Cp*Co	H	-	-	-	< - 7
20	Cp*Rh	H	38.0(4)	-26(2)	33.6	- 0.9
19	Cp*Ir	H	46.5(5)	7(2)	45.5	+ 5.5
26	Cp*Co	Ph	-	-	38.4(195K)[a]	- 3.8
25	Cp*Co	Tol	35.6	-8	37.0	- 4.1
24	Cp*Rh	Tol	-	-	41.7(210K)[a]	- 5.4
23	Cp*Ir	Tol	48.4(8) 40.3(8)[b]	-18(3) -2(4)[b]	51.4 40.0[b]	+ 1.8 + 2.4[b]
27	Cp‡Co	Tol				+ 3.0
28	CpCo	Ph	37(2)	-9(7)	39.5	-

a) obtained from T_C of the Cp resonance according to equation ((3))
b) for isomerization **B**→**C**

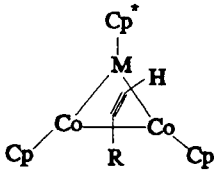

A

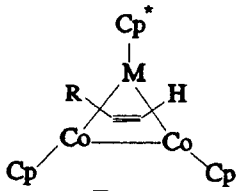

B

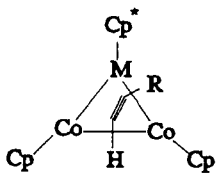

C

stretching frequencies of the mononuclear complexes $CpCo(CO)_2$, $Cp^*Co(CO)_2$ and $Cp^‡Co(CO)_2$, however, the electron donating capability of the $Cp^‡$ ligand is believed to be between thoses of the Cp and Cp^* ligands.[28] On the other hand, if one assumes that all edges in **27** are electronically "equivalent", steric interactions between the $Cp^‡$ ligand and the tolyl substituent might be the cause of the observed preference for isomer **A**. That steric interactions play a role is also suggested by the fact that no evidence for the presence of isomer **C** is found in which the alkyne is also parallel to the $Cp^‡$ edge as in isomer **A**, but with the tolyl substituent above a CpCo-$Cp^‡$Co edge.

When changing the metal from Co to Rh and Ir one observes an increased preference for the alkyne to lie across a Cp^*M-CoCp edge (isomer **A**) indicating an increase in the group electronegativity of the metal-Cp^* group when moving down the family. These observations can be correlated with the Pauling electro-negativities which increase from Co to Rh and Ir (Co: 1.8; Rh: 2.2; Ir: 2.2). That such correlations have to be regarded with caution, however, is illustrated by the fact that the electronegativity scale of Allred and Rochow exhibits a different trend (Co: 1.7; Rh: 1.5; Ir: 1.6). Since both the acetylene and tolylacetylene complexes show the same trend, it is reasonable to assume that electronic reasons are the main cause of the change in the preferred orientation of the alkyne ligand. In the case of the Ir containing complex **23** steric interactions between the tolyl group and the Cp^* ligand might be the reason for the low abundance of isomer **C** versus isomer **A**. The fact that isomer **C** is even less abundant than isomer **B**

suggests that steric interactions between the two groups is larger in **C** than in **B**. Since no crystal structure is available for an isomer of type **C** it is hard to verify such speculations.

However, this line of reasoning might also explain why in the case of the ditolylacetylene adduct **30** only isomer **B** appears to be present. From both electronic and simple steric arguments one would expect the alkyne to be oriented parallel to a Ir-Co edge resulting in the close approach of only one of the two tolyl substituents to a Cp^* ligand. However, it appears that the steric interactions of one tolyl group in such a conformation (**C**) are worse than the one of two tolyl groups in the orientation parallel to a Co-Co edge (**B**).

Alkyne rotation around the metal triangle appears to involve discrete jumps between μ_3-$\parallel$ intermediates. Transition states for these steps would appear to involve μ_3-$\perp$ alkyne geometries over the trimetal skeleton as illustrated in Figure 3.29. From extended Hückel calculations, Schilling and Hoffmann have calculated an activation barrier of 38 kJ mol^{-1} for alkyne rotation in the cluster complex $H_2Os_3(CO)_9(HC{\equiv}CH)$ involving a transition state in which the alkyne is oriented perpendicular to a metal-metal edge.[29] For the triosmium clusters $H_2Os_3(CO)_3$(alkyne) values of $\Delta G^{\ddagger}$ of 60 kJ mol^{-1} (alkyne = μ_3-indyne), 71 kJ mol^{-1} (μ_3-cyclooctyne) and 58 kJ mol^{-1} (cyclopentyne)[30] were found experimentally. The values obtained for the complexes described in this chapter are summarized in Table 3.9. These values are somewhat smaller, but of similar magnitude than the ones cited in the literature. They are also one order of

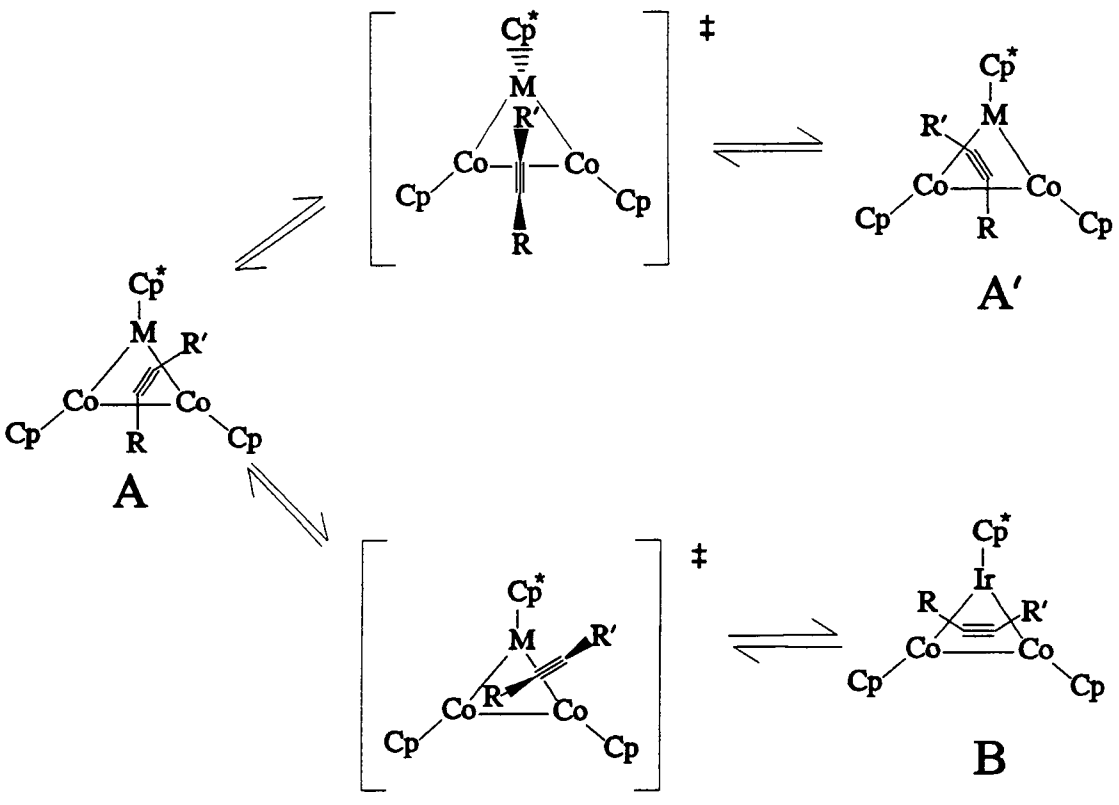

Figure 3.29: Proposed mechanism of alkyne rotation between different μ-$\parallel$ orientations through a μ-$\perp$ transition state.

magnitude larger than the difference in energy between the different isomers.

The acetylene adduct $Cp^*Ir(CpCo)_2(\mu_3\text{-}CO)(HC{\equiv}CH)$ (**19**) exhibits a free energy of activation $\Delta G^{\ddagger}$(170K) for the interconversion **A** → **B** that is significantly larger than the corresponding Rh compound **20** (45.5 versus 33.6 kJ mol^{-1}) (See Figure 3.30. In both cases, the alkyne rotation involves movement of a ≡C-H group across a CpCo vertex. In the case of the Cp^*Ir complex containing *tolyl*acetylene (**23**) the interconversion **A** → **B** involves the movement of the sterically more demanding tolyl group across a CpCo vertex. The barrier is therefore higher (6 kJ mol^{-1}) but still similar to the one found in the acetylene

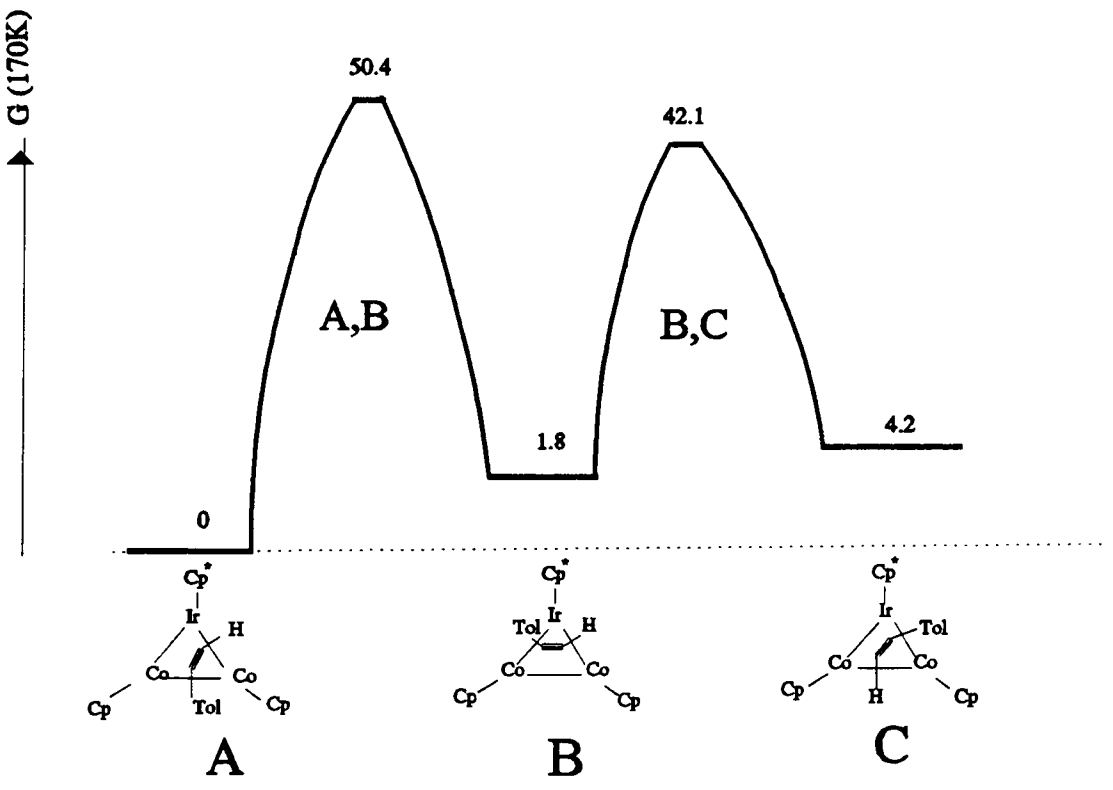

Figure 3.30: Energy profile for alkyne rotation in **23**. The differences in energy between the ground states are exaggerated. Energies are in kJ mol^{-1}.

adduct. The movement of a ≡C-H group across a CpCo edge is described in **23** by process **B** → **C** with a barrier of 40.0 kJ mol^{-1}. This value equals the corresponding barrier in the acetylene adduct **19** if one considers the analogous process **B** → **A** ($\Delta G^{\ddagger}_{BA} = \Delta G^{\ddagger}_{AB} - \Delta G^{0}_{AB}$ = 40.0 kJ mol^{-1}). These findings imply that electronic factors are dominant in defining the barrier of activation whereas steric interactions have only a secondary effect.

In all complexes, the interconversion between the two enantiomers of isomer **A** occurs fast on the NMR timescale. In this interconversion, the hydrogen end of the alkyne ligand sweeps across a $Cp^{*}M$ (or $Cp^{\ddagger}Co$) vertex interchanging

the identities of the two Cp^*M-CpCo edges. Furthermore, in the complex $Cp^*Ir(CpCo)_2(\mu_3\text{-}CO)$(Tol-C≡CH) (**23**) the interchange between the two enantiomers of isomer **C** which requires the tolyl end of the alkyne to move across the Cp^*Ir vertex, appears to be fast on the NMR time scale (or at least as fast as the interchange **B** → **C**). This observation also supports the hypothesis that steric interactions contribute only little to the barrier of alkyne rotation. On the other hand, in none of the Cp^*Rh or Cp^*Co containing complexes an interconversion involving interchange of isomers of type **C** is observed.

In the case of the all CpCo containing cluster complex $CpCo_3(\mu_3\text{-}CO)$(Ph-C≡CH) (**28**) two different rates of alkyne reorientation are observed. Mobility of the ≡CH end of the ligand is fast on the NMR time scale even at the lowest temperature accessible, whereas the ≡C-Ph end moves at a rate comparable to that found in $Cp^*Co(CpCo)_2(\mu_3\text{-}CO)$(Tol-C≡CH). Since all three edges are equivalent in this compound, this difference has to arise from either a steric or electronic effect of the phenyl substituent. The alkyne adducts of $(CpCo)_3(\mu_3\text{-}CO)_2$ (**5**) containing symmetrically substituted alkynes do not show any slowing of the alkyne rotation even at the lowest temperature measured. Since that observation applies to both acetylene and diphenylacetylene, the slowed rotation observed in **28** might be linked to the asymmetry of the alkyne.

Although the barrier to alkyne rotation is controlled mainly by electronic rather than steric interactions, the fact that slowed phenyl ring rotation is observed in these complexes shows that steric interactions have to be considered

in the overall picture of alkyne reorientation. Alkyne reorientation rates are completely independent of steric interactions if there are no or only small steric interactions in the transition state. In the alkyne movement leading to the interconversion of isomers **A** and **B**, the phenyl substituent moves across a CpCo vertex and the alkyne - Cp^* interaction doesn't play a major role in this transition state. Steric interactions between the phenyl substituent and the Cp ligand are small, however, since phenyl ring rotation is still fast for the isomers of type **A** with the phenyl substituent of the alkyne above the CpCo-CpCo edge. In order to understand the interconversion of the enantiomers **C** in the Ir complex **23**, on the other hand, one has to find a way to move the tolyl end of the alkyne across the Cp^*Ir edge with minimal steric interaction. One plausible pathway involves displacement of the alkyne moiety towards the Co-Co edge while turning into a position perpendicular to that edge as represented by the arrows in Figure 3.31. The phenyl ring is then "unlocked" from Cp^* steric interactions in the transition state and allowed to move in front of the Cp^*Ir vertex towards the other Cp^*Ir-CpCo edge. Alternatively, steric interactions can be minimized by tilting the phenyl substituent of the alkyne ligand up away from the metal plane.

3.6. Scission Reactions

One important reaction of coordinated alkyne complexes is the metal induced cleavage of the carbon-carbon triple bond. In trinuclear cyclopentadienyl complexes of the cobalt group of the general type $(CpM)_3(CO)(R\text{-}C{\equiv}C\text{-}R')$ (M =

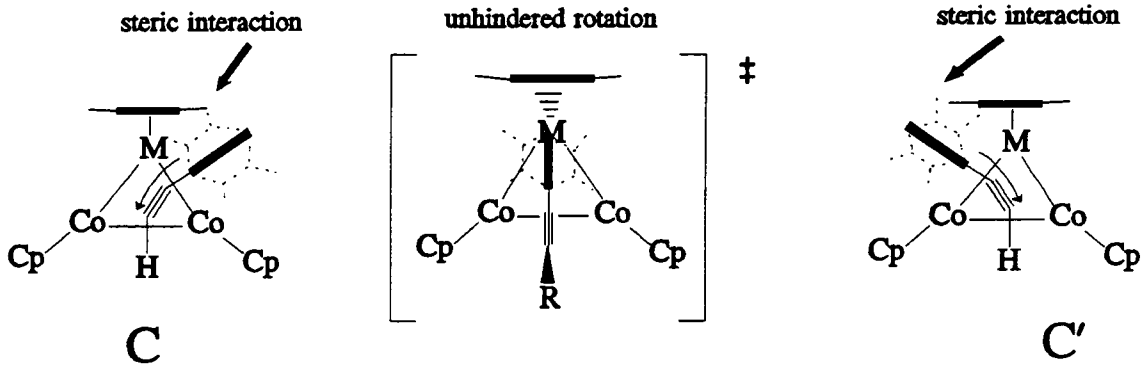

Figure 3.31: Illustration of unhindered rotation of the phenyl ring in the transition state. The dotted ring represents a rotation of the phenyl ring by 90°.

Co, Rh, Ir) scission of the C≡C bond is thermally induced upon refluxing in m-xylene[31], decahydronaphthalin ("decalin")[32] or by flash vacuum pyrolysis[33]. In all cases the CO ligand is lost and the bis-carbyne complexes $(CpM)_3(C\text{-}R)(C\text{-}R')$ are formed. In our group we recently investigated this reaction with a variety of alkyne adducts. For example, bisalkynes such as bistolan (Ph-C≡C-C_6H_4-C≡C-Ph) were used to synthesize linked bis-carbyne cluster complexes. An investigation of the internal mobility of phenyl substituents in some of such bis-carbyne clusters will be described in the next chapter.

At this point the influence of replacing a Cp ligand by a Cp^* ligand on the rate of the scission reaction will be discussed. For that purpose the three alkyne adducts $Cp^*Ir(CpCo)_2(\mu_3\text{-}CO)$(Tol-C≡CH) (**23**), $Cp^*Co(CpCo)_2(\mu_3\text{-}CO)$(Tol-C≡CH) (**25**) and $(CpCo)_3(\mu_3\text{-}CO)$(Ph-C≡CH) (**28**) were heated in refluxing decalin. The all Cp containing complex **28** yielded the bis-carbyne complex

$(CpCo)_3(\mu_3\text{-}CH)(\mu_3\text{-}CPh)$ (**35**) in 60 % yield after 30 h. In addition, starting material and small amounts of tetranuclear alkyne adduct $(CpCo)_4(Ph\text{-}C{\equiv}CH)$[34] were isolated from the reaction mixture. In the case of the Cp^* containing complexes **23** and **25**, on the other hand, no scission of the C≡C bond is observed. After heating in refluxing decalin for 48 h only starting material was recovered.

According to a theoretical study by Shapley and Hoffmann[33] on $(CpCo)_3(\mu_3\text{-}CO)(HC{\equiv}CH)$ this reaction involves rotation of the alkyne into a position perpendicular to a metal-metal edge followed by movement over that edge resulting in a μ_2-coordinated alkyne (Figure 3.32). The carbonyl ligand then moves from a μ_3-coordination to a terminal position followed by alkyne scission

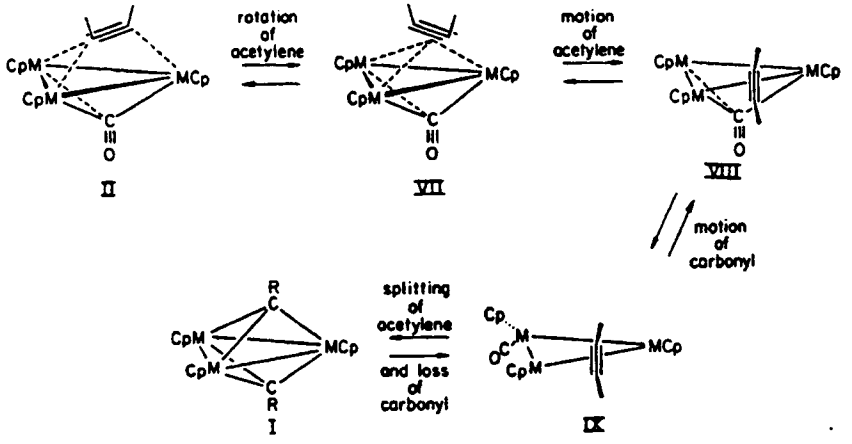

Figure 3.32: Mechanism of alkyne scission in a trinuclear cluster complex. Reproduced from Ref. 33.

and loss of CO. The highest energy step in this process was the movement of the carbonyl ligand from its face bridging to the terminal position (145 kJ mol^{-1}). Our study on alkyne fluxionality shows that the barriers to alkyne rotation are similar for $Cp^*Co(CpCo)_2(\mu_3\text{-}CO)(Tol\text{-}C{\equiv}CH)$ (**25**) and $(CpCo)_3(\mu_3\text{-}CO)(Ph\text{-}C{\equiv}CH)$ (**28**) suggesting that the reason for absence of alkyne scission in the Cp^* containing complexes is a higher barrier to movement of the triply bridging carbonyl ligand. A more strongly bound CO ligand is consistent with the increase in electron density on the metals caused be the electron donating effect of the methyl groups in the Cp^* ligand compared with a Cp ligand. An increased electron density on the metal causes stronger π-backbonding from a metal d-orbital to the π^* orbital of the CO ligand. In such a case one would expect the intermediate or transition state to contain the terminal CO on the Cp^*M vertex and the alkyne to be coordinated across the CpCo-CpCo edge.

3.7. Summary

A series of heteronuclear metal cluster complexes containing alkyne ligands of the general type $L\text{-}M(CpCo)_2(\mu_3\text{-}CO)(RC{\equiv}CR')$ (L-M = Cp^*Co, Cp^*Rh, Cp^*Ir, CpCo, $Cp^{\ddagger}Co$) have been synthesized. Using x-ray crystallography and variable temperature NMR spectroscopy the alkynes have been shown to be coordinated parallel to a metal-metal edge. For the acetylene and phenylacetylene adducts the preferred orientations depends on the electronic properties of the L-M fragment. In the case of L-M = Cp^*Ir and $Cp^{\ddagger}Co$ the alkyne prefers to be

parallel to a LM-CpCo edge, whereas for the other complexes orientation parallel to the CpCo-CpCo edge is preferred. In the case of the diphenylacetylene adducts only the orientation of the alkyne parallel to the CpCo-CpCo edge is observed. The barrier of interconversion between these two orientations appears to depend on the nature of the metal and increases in the order Co < Rh < Ir. On the other hand, even at the 170 K equilibration of the two LM-CpCo edges appears to be fast on the NMR time scale for all compounds. Furthermore, the phenyl ring rotation is locked at low temperature for all isomers containing the phenyl group next to a Cp^* ligand.

3.8. References:

1. Elchenbroich, Ch.; Salzer, A.; *Organometallchemie*, Teubner Verlag, 2. Auflage, Stuttgart **1988**, pp. 325ff.

2. Blount, J. F.; Dahl, L. F.; Hoogzand, C.; Hübel, W.; *J. Am. Chem. Soc.* **1966**, *88*, 292.

3. Aime, S.; Milone, L.; Osella, D.; Tirripicchio, A.; Lanfredi, A. M. M.; *Inorg. Chem.* **1982**, *21*, 501.

4. Trinh-Toan; Broach, R. W.; Gardner, S. A.; Rausch, M. D.; Dahl, L. F.; *Inorg. Chem.* **1977**, *16*, 279.

5. Schilling, B. E. R.; Hoffmann, R.; *J. Am. Chem. Soc.* **1979**, *101*, 3456-3467.

6. a) Gardner, S. A.; Andrews, P. S.; Rausch, M. D.; *Inorg. Chem.* **1973**, *12*, 2396-2402. b) Todd, L. J.; Wilkinson, J. R.; Rausch, M. D.; Gardner, S. A.; Dickson, R. S.; *J. Organomet. Chem.* **1975**, *101*, 133-138.

7. Sappa, E.; Tiripicchio, A.; Braunstein, P.; *Coord. Chem. Rev.* **1985**, *65*, 219-284.

8. Halet, J. F.; Saillard, J. Y.; Lissillour, R.; McGlinchey, M. J.; Jaouen, G.; *Inorg. Chem.* **1985**, *24*, 218-224.

9. Einstein, F. W. B.; Tyers, K. G.; Tacey, A. S.; Sutton, D.; *Inorg. Chem.* **1986**, *25*, 1631-1640.

10. Pauling, L.; *The Nature of the Chemical Bond*, Third Edition, Cornell University Press, Ithaca, New York **1960**.

11. Mc. Kenzie, J.; Master Thesis; University of Tennessee, Knoxville **1994**.

12. Barnes, C. E.; Orvis, J. A.; Finniss, G. M.; *Organometallics* **1990**, *9*, 1695-1697.

13. Gassmann, P. G.; Mickelson, J. W.; Sowa, J. R.; *J. Am. Chem. Soc.* **1992**, *114*, 6942.

14. Streitwieser, A.; Heathcock, C. H.; *Organische Chemie*, 1. Auflage, Verlag Chemie, Weinheim 1980.

15. a) Dodge, R. P.; Shoemaker, V. J.; *J. Organomet. Chem.* **1965**, *3*, 274-284. b) Ferraris, G. Gervasio, G.; *J. Chem. Soc., Dalton Trans.* **1973**, 1933-1936. c) Tachikawa, J. R.; Shapley, J. R.; Pierpont, C. G.; *J. Am. Chem. Soc.* **1975**, *97*, 7172-7174.

16. Hesse, M.; Meier, H.; Zeeh, B.; *Spektroscopische Methoden in der organischen Chemie*; 3. Auflage; Thieme Verlag, Stuttgart/New York **1987**.

17. a) Jeener, J.; Meier, B. H.; Bachmann, P.; Ernst, R. R.; *J. Chem. Phys.* **1979**, *71*, 4546-4553. b) Meier, B. H.; Ernst, R. R.; *J. Am. Chem. Soc.* **1979**, *101*, 6441. c) Macura, S.; Ernst, R. R.; *Molecular Physics* **1980**, *41*, 95-117.

18. Binsch, G.; Kessler, H.; *Angew. Chem.* **1980**, *92*, 445-463.

19. J. Sandström; *Dynamic NMR Spectroscopy*; Academic Press, London **1982**.

20. a) Stephenson, D. S.; Binsch, G.; *Quantum Chem. Progr. Exch.* **1978**, *10*, 365. b) Stephenson, D. S.; Binsch, G.; J. Magn. Res. **1978**, *32*, 145.

21. For a full characterization of this compound, see reference 11.

22. Barnes, C. E.; King, W. D.; Player, M. J.; unpublished results.

23. In the lowest temperature spectrum, the Cp^* signal of **B** shows a small shoulder which might be caused by isomer **C**.

24. For synthesis and spectroscopic data see: King, W. D.; *Ph. D. Thesis*, Knoxville, **1996**.

25. Some broadening is observed for these carbons due to exchange between **B** and **A**.

26. Van de Ven, F. J. M.; *Multidimensional NMR in Liquids*, Verlag Chemie, **1995**, 181-187.

27. a) Bothner-By, Aksel A.; Stephens, R. L.; Lee, Ju-mee; *J. Am. Chem. Soc.* **1984**, *106*, 811-813. b) Bax, A.; Davis, D. G.; *J. Magn. Res.* **1985**, *63*, 207-213.

28. Vierkötter, S. A.; Ph. D. Thesis, University of Tennessee, Knoxville, **1994**.

29. Schilling, B. E.; Hoffmann, R.; *Acta Chem. Scand.* **1979**, *B 33*, 231-232.

30. Deeming, A. J.; *J. Organomet. Chem.* **1978**, *150*, 123-128.

31. Eaton, B.; O'Connor, J. M.; Vollhardt, K. P. C.; *Organometalics* **1986**, *5*, 394-397.

32. a) King, W. D.; *Ph. D. Thesis*; University of Tennessee, Knoxville **1996**. b) King, W. D.; Barnes, C. E.; manuscript in preparation.

33. Clauss, A. D.; Shapley, J. R.; Wilker, C. N.; Hoffmann, R.; *Organometallics* **1984**, *3*, 619-623.

34. The formation of teranuclear alkyne complexes under these conditions has also been observed for analogous alkyne adducts containing a *furyne* ligand: Barnes, C. E.; King, W. D.; Orvis, J. A.; *J. Am. Chem. Soc.* **1995**, *117*, 1855-1856.

CHAPTER 4

Diffusional and Internal Rotation in Single and Linked Trinuclear Bis-Carbyne Cluster Complexes Determined by Carbon-13 NMR Relaxation Time Measurements

4.1. Introduction

The first two chapters of this thesis described dynamic processes of several simple organic fragments and olecules such as carbenes, carbynes and alkynes coordinated to a trinuclear metal framework. In both chapters the objective was to better understand the electronic and steric factors influencing such processes on a metal surface with the long term goal of developing new catalysts in a controlled manner. In this chapter, cluster complexes will be viewed from a different perspective, namely as building blocks for new polymeric materials.

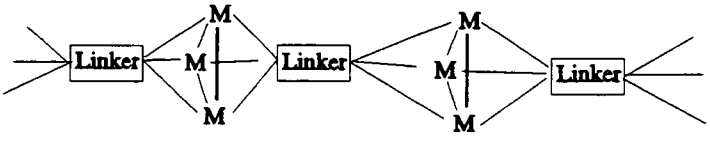

At the end of the previous chapter (section 3.6) the formation of bis-carbyne complexes from alkyne adducts was discussed. It was also mentioned that

this reaction has been utilized to synthesize linked bis-carbyne cluster complexes. Here a study of the rotation of phenyl substituents in these complexes will be presented. This chapter is based on a manuscript which has been submitted to *Inorganic Chemistry* for publication.

The use of organometallic complexes as precursors to new materials has begun to play an important role in current research in the area of organometallic chemistry.[1] The reasons for this are several fold. The ability of metal centers to exhibit multiple, stable valence states[2,3a], including ones involving partially filled molecular orbitals can lead to materials with partially filled electronic bands which are conductive. More recently, new inorganic materials have been investigated which have both novel and useful magnetic properties such as high magnetic saturation characteristics and shielding properties. Although much work remains to be done in the development of such materials, a common thread in their design is the molecular level engineering of specific linking groups which facilitate the desired interactions between metal centers or units. Properties which are known to be important in the interactions between metal units are: the distance separating units, the nature of intervening or linking groups between units and the orientation of one unit relative to another. The distance separating two units determines the magnitude of so-called "through space" interactions which include electrostatic charge interactions and dipolar interactions between unpaired spins. The nature of the linking group encompasses many factors such as the electronic structure of the group and its flexibility and dynamics. The relative orientation of

the MO's of the metal units is of critical importance in determining the magnetic behavior of a material. Understanding the role of each of these factors and developing methodologies to control and tailor each is one of the current goals in molecular materials engineering.

Recently, molecular metal cluster complexes have been used as building blocks for such materials and dimers and oligomers have been formed as the result of linking of several clusters. The linking groups have involved metal ions[4] or a number of organic functional groups including alkynes[3b], alkanes[5] and cyclopentadienone.[3c] We have begun to explore the properties of a family of linked bis-carbyne cluster complexes of the form R-C<$(CpCo)_3$>C-X-C<$(CpCo)_3$>C-R as possible models for conducting organometallic polymers and new liquid crystalline materials. These complexes, which can be prepared from the corresponding alkyne complexes by scission of the C≡C bond,[6,8] are both thermally and chemically quite robust. At the same time, they undergo a number of reversible oxidation reduction reactions which produce a wide range of mixed valence states. In the studies described here, the linking group will be a 1,4 disubstituted phenyl group. Several properties make this group ideal for consideration as a connecting group between metal centers. It is chemically stable, has a well defined and rigid structure which determines the distance and orientation of the metal groups bound to it and has a π-MO system which can be utilized in mediating electronic interactions between metal units. The trinuclear cluster complexes used as monomers are composed of three CpCo fragments in a

triangular array capped on both sides by face bridging carbyne ligands. In this particular study the monomeric complexes **1** and **3** and the linked complex **2** are investigated as shown in Figure 4.1. In conjunction with our investigations of the electronic properties of these complexes we became interested in the dynamics of the phenyl group and whether motions of this group affect its ability to mediate electronic interactions between the metal units they link together. A study of the crystal structures and electrochemical properties of these complexes will be published elsewhere.[7] Herein we describe the results of a detailed analysis of both the molecular motions and internal rotational dynamics of phenyl linked bis-carbyne complexes. Such information is of interest in the design of polymer systems based on these and other organometallic units and linking entities.

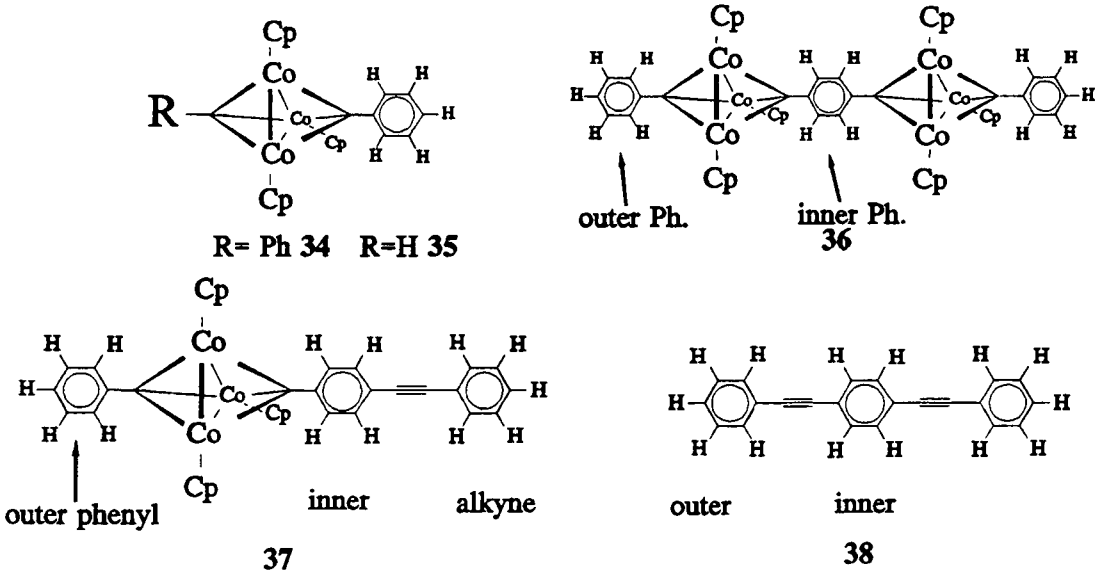

Figure 4.1: Complexes investigated in this study. Phenyl groups are labled according to their relative positions in the molecule and the substituuents carried by them.

4.2. Experimental

The cluster complexes **34 - 37** were prepared from the corresponding diphenylacetylene and bistolan alkyne adducts via thermally induced alkyne scission reactions by refluxing in decahydronaphthalene as described by Vollhardt and coworkers.[8] Bistolan **38** was synthesized following the procedure of Nguyen et. al.[9] CD_2Cl_2 was dried over CaH_2 and degassed by several freeze-pump-thaw cycles before use. NMR samples were prepared in flame sealed tubes after vacuum transfer of the solvent. Concentrations were 76 mM for **34**, 10.4 mM for **36**, 30 mM for **37** and 93 mM for **38**. Due to its low solubility, samples of **36** were made up in 10 mm tubes whereas 5 mm tubes where used for all other samples.

Spectra were acquired at 9.4 T using a Bruker AMX400-WB NMR spectrometer operating at a carbon-13 frequency of 100.62 MHz. Assignment of the carbon resonances was made using heteronuclear $^{13}C\{^1H\}$ correlation spectroscopy[10] as shown in Figure 4.2 for the case of the linked cluster system **36**. The proton resonances were normally readily assigned using relative intensities and multiplicities of the signals.

^{13}C spin-lattice relaxation times were measured with the fast inversion recovery pulse sequence[11] (180°-τ-90°-acq) using relaxation delays of 2-3 T_1 and 12 τ values ranging from 3μs to 5$\cdot T_1$. A three parameter fit was used to obtain the relaxation times from the data. Nuclear Overhauser enhancements (NOE) were measured by comparing the intensities of the carbon-13 signals in regular

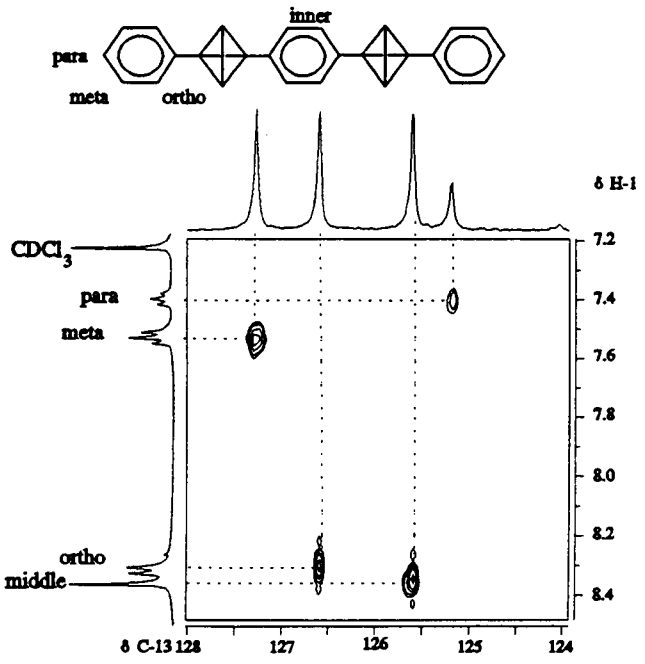

Figure 4.2: ^{13}C-{^{1}H} correlation spectrum of the linked cluster complex **36** illustrating the assignment of the ^{13}C resonances.

decoupled and inverse gated decoupled[12] spectra. Probe temperatures were calibrated using methanol or ethylene glycol according to the procedure described by Van Geet[13] and are believed to be accurate within 1°C.

4.3. Determination of Diffusion Coefficients

The general shape of the compounds investigated in this study can be approximated by a prolate symmetric top with one long semiaxis (*a*) and two shorter semiaxes of equal length (*b*) as illustrated in Figure 4.3 for the linked cluster system **36**. Values for *a* and *b* were obtained from crystal structures of complex **34** and the linked cluster complex **36**.[7] As indicated in Figure 4.3, *b* is defined as the distance from the center of the Co_3 triangle to an average

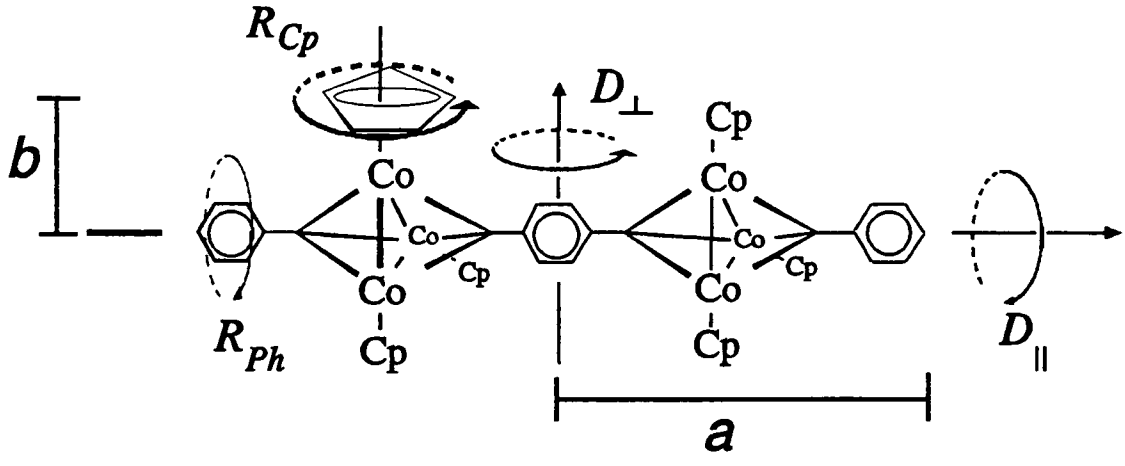

Figure 4.3: $D_\perp$: motion of molecule perpendicular to main axis, $D_|$: motion of entire molecule about main axis, R : internal rotation of phenyl substituents

cyclopentadienyl hydrogen position. Bond distances obtained from these crystal structures were also used to estimate the axes lengths for the alkyne substituted cluster **37** and for bistolan (**38**).

The diffusional motion of the rigid molecules can then be described by two diffusion coefficients: Tumbling of the molecule perpendicular to the unique axis described by the diffusion coefficient $D_\perp$ and spinning about the long axis as described by $D_|$.

In the cases of **36** and **37**, the large difference in axis lengths (*a* much larger than *b*) leads to the expectation that molecular tumbling ($D_\perp$) will be significantly slower than rotation about the long axis ($D_|$). Furthermore, internal rotation of the phenyl and cyclopentadienyl rings must also be considered as

contributing factors to the dynamics of molecular reorientation of these molecules. These motions are described by the internal rotation rates R_{Ph} and R_{Cp}.

4.3.1. Phenyl Ring Rotation

If both the overall spinning of the entire molecule and the internal rotation of the phenyl groups take place about the same axis,[14] then the total effective spinning rate experienced by the phenyl groups about the long axis is the sum $D_{s,Ph} = D_{\parallel} + R_{Ph}$. Equations relating the dipolar relaxation times of ellipsoidal molecules undergoing internal rotation to the rotational diffusion coefficients have been developed by Woessner and coworkers.[15] Application of this theory to phenyl ring rotation in carbyne ligands of metal cluster complexes has been described by Richmond and Schwartz.[16] If internal rotation occurs about an axis parallel to the main symmetry axis of the ellipsoid then, in the extreme narrowing limit ($\tau_c\omega \ll 1$), the relationship between diffusion coefficients and relaxation time is given by

$$\frac{1}{T_1} = \frac{\gamma_C^2 \gamma_H^2 \hbar^2}{r_{CH}^6} \left(\frac{A}{6D_{\perp}} + \frac{B}{5D_{\perp} + D_{\parallel} + R} + \frac{C}{2D_{\perp} + 4(D_{\parallel} + R)} \right) \quad \textbf{(4.1)}$$

where $A = (3\cos^2\theta - 1)/4$, $B = 3\sin^2\theta\cos^2\theta$ and $C = (3\sin^4\theta)/4$ and θ is the angle between the C-H bond and the rotational axis.

For the carbons in the para position the angle Θ is equal to zero. In this case the factor A in equation (4.1) equals 1 and B = C = 0. Equation (4.1) then simplifies to

$$\frac{1}{T_{1,para-C}} = \frac{\gamma_C^2 \gamma_H^2 \hbar^2}{r_{CH}^6} \frac{1}{6D_\perp} = \frac{3.781 \cdot 10^9}{D_\perp} \qquad (4.2)$$

where standard values for γ_H, γ_C and $\hbar$ and a value of 1.08 Å for the C-H bond length[17] have been used. From equation (4.2) one can see that the relaxation of the para carbon gives directly the tumbling rate, $D_\perp$, for the entire molecule independent of all other motions.

For the ortho and meta carbons Θ equals 60° and 120°, respectively. In either case the coefficients in equation (4.1) are $A = {}^1/_{64}$, $B = {}^9/_{16}$ and $C = {}^{27}/_{64}$. The relaxation time therefore depends on R_{Ph}, $D_\parallel$ and $D_\perp$. Using equations (4.1) and (4.2) and the definition $D_s = D_\parallel + R_{Ph}$, the ratio $T_{1,ortho}/T_{1,para}$ is given by

$$\frac{T_{1,ortho}}{T_{1,para}} = \frac{T_{1,meta}}{T_{1,para}} = \frac{64}{1 + \dfrac{216}{5 + \dfrac{D_S}{D_\perp}} + \dfrac{162}{2 + 4\dfrac{D_S}{D_\perp}}} \qquad (4.3)$$

The ratio $D_s / D_\perp$ may then be determined by fitting the ratio $T_{1,ortho}/T_{1,para}$ to equation (4.3) using $D_s / D_\perp$ as an adjustable parameter. D_s can then be obtained using $D_\perp$ calculated from equation (4.2). It should be noted that this analysis yields only independent values for $D_\perp$ and D_s which is the sum $D_\parallel + R_{Ph}$.

Separation of D_s into $D_\parallel$ and R_{Ph} is not possible from measuring dipolar relaxation times of the phenyl carbons alone.

Finally, the above equations are valid only if the motion of the molecule is in the fast narrowing limit ($\tau_c\omega \ll 1$). As discussed below, this assumption may not be valid for complex **36**.

4.3.2. Cp Ring Rotation

The NOE for the cyclopentadienyl carbon atoms in **34** is 1.61 at 300 K and is independent of temperature. This suggests that coupling with the quadrupole moment of the cobalt atoms contributes significantly to their overall relaxation. In such cases, dipolar contributions to the carbon relaxation times T_1^{DD}(Cp) may be obtained from the relation[18]

$$T_1^{DD}(Cp) = \frac{1.994}{NOE(\text{exp})}\, T_1(\text{exp}) \qquad (4.4)$$

In compounds **34**, **36** and **37** the rotational axes of the Cp rings are perpendicular to the main axis of the molecule. Equations relating the relaxation times of the Cp carbons to diffusion coefficients can be obtained from Woessner's general equations describing relaxation in ellipsoidal molecules with internal rotation[15b] and have been presented by Schwartz and Richmond.[19] The correlation time of a carbon on the Cp ring depends on three parameters, the internal rotation rate R_{Cp}, the diffusion coefficient $D_\perp$ and the spinning rate $D_{s,Co3} = D_\parallel + R_{Co3}$ describing the rotation of the Cp_3Co_3 triangle about the main axis. For the

bis-carbyne systems **34** and **35** one can approximate $D_{s,Co3}$ by D_I since the Cp_3Co_3 moiety accounts for the bulk of the molecule. In the linked cluster system **36,** however, the spinning rate of two Cp_3Co_3 units will be equal to D_I only if there is a high barrier to internal rotation of these units about the main axis. If this barrier is low, the two Cp_3Co_3 units will rotate independently of one another at a rate faster than that for the molecule as a whole and D_{s,Co_3} can not be approximated by D_I.

4.4. Results and Discussion

As discussed above, carbon-13 NMR relaxation times are sensitive to the diffusional and internal motions a molecule exhibits in solution. Recently Richmond, Schwartz and coworkers utilized ^{13}C NMR relaxation data to describe the rotational diffusion coefficients for phenyl ring rotation in several trinuclear metal clusters containing capping carbyne ligands[16] such as **39** and **40.**

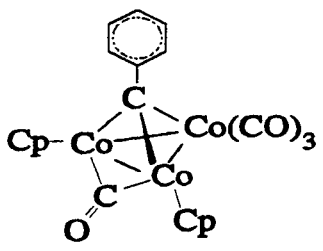

5

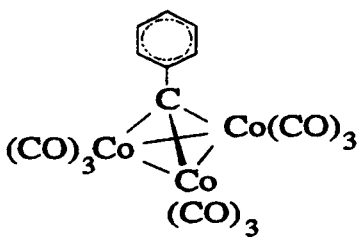

6

The studies described here extend these measurements to include a series of linked cluster systems based on the $(CpCo)_3$ fragment. These compounds contain up to three different types of phenyl rings within **one** molecule allowing us to

directly compare the rates of rotation of phenyl rings bound to different numbers of carbyne and/or alkyne carbons.

4.4.1. Direct Evaluation of T_1 Values

Carbon-13 T_1 relaxation times were measured over a range of temperatures from 310 K to 250 K. Table 4.1 shows the experimental relaxation times for the bis-carbyne cluster **1**. The relaxation times for the ortho and meta carbons of the phenyl ring are the same within the experimental uncertainty of our measurements whereas the relaxation times for the para carbons are significantly shorter. This difference is a strong indication that the reorientation of the phenyl group is anisotropic. All relaxation times increase with increasing temperature as expected for rotational motions faster than the carbon-13 Lamor frequency. The relaxation

Table 4.1 : T_1 carbon-13 relaxation times obtained for **34**.

T/K	$T_{1,para}$/s	$T_{1,ortho}$/s	$T_{1,meta}$/s	$T_{1,Cp}$/s	$T_{1,Cp}^{DD}$/s
300.0	1.3(1)	4.0(2)	4.1(2)	4.3(2)	5.4(2)
290.4	1.1(1)	3.4(2)	3.5(2)	3.7(2)	4.2(2)
280.2	1.0(1)	3.0(2)	3.1(2)	3.2(2)	3.7(2)
269.8	0.83(8)	2.5(2)	2.6(2)	2.7(2)	3.1(2)
259.4	0.69(7)	2.1(1)	2.2(1)	2.3(1)	2.4(1)
248.9	0.56(6)	1.7(1)	1.8(1)	1.9(1)	2.1(1)
238.4	0.46(5)	1.3(1)	1.3(1)	1.5(1)	1.7(1)

times obtained for the other complexes show similar behavior. A complete compilation of the corresponding data for complexes **35** - **38** is listed in Appendix 3. Nuclear Overhauser enhancements of 200% were found for the phenyl carbons in compounds **34,35**, **37** and **38** as expected for molecules whose correlation times are in the extreme narrowing limit ($\tau_c \cdot \omega \ll 1$) when relaxation is dominated by dipolar coupling with the protons.

In the case of the linked cluster **36** however, NOE's smaller than 200% were observed for the phenyl carbons, especially at lower temperatures (para carbon: 140%, ortho/meta 170%). Due to the chemical and structural similarities between **36** and the other molecules it is unlikely that other relaxation mechanisms such as chemical shift anisotropy play a significant role in the relaxation of **36**. Furthermore, spin rotation mechanisms can be ruled out since it is most efficient in small molecules with high rotation rates and its influence is expected to decrease with molecular weight. It is therefore most plausible to assume that we also have exclusively dipolar relaxation in the linked cluster **36** but that the tumbling of a molecule of this size is slow such that the condition for extreme narrowing is no longer satisfied. In Figure 4.4a values for the NOE are calculated for the para hydrogen in dependence of the diffusion coefficient $D_\perp$. One can see that if the molecular rotation drops below 0.8 ns^{-1} (slow tumbling) the NOE value decreases rapidly from the value found in the extreme narrowing limit. The more general frequency dependent equations for dipolar relaxation have therefore been used to extract the diffusion coefficients for **36** from the T_1 values:[20]

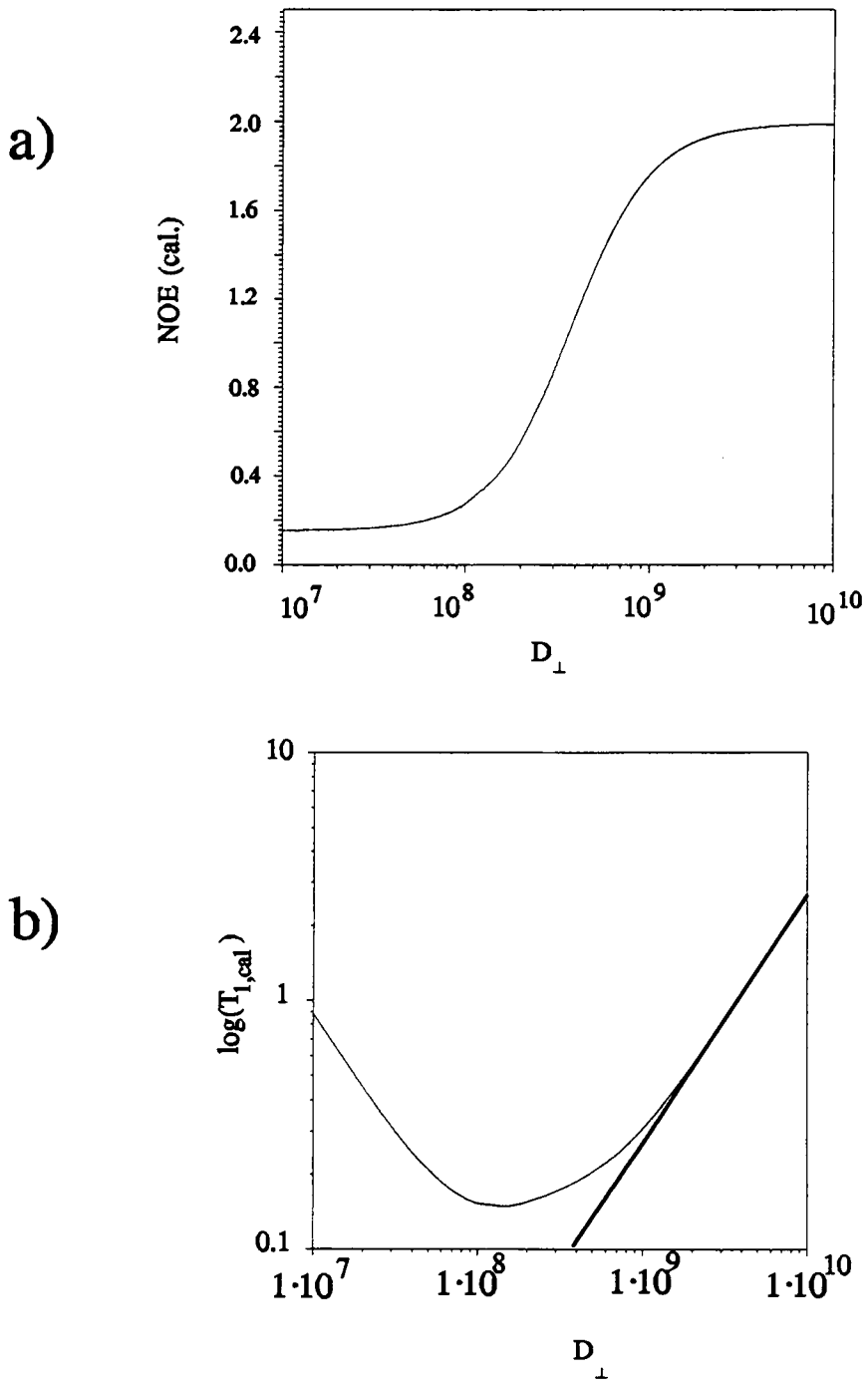

Figure 4.1: (a) Calculated NOE values (b) T_1 values calculated with general equations (solid) and for extreme narrowing limit (dotted).

$$\frac{1}{T_1} = \frac{\gamma_C^2 \gamma_H^2 \hbar^2}{r^6} \frac{1}{10}[\, J(\omega_C-\omega_H) + 3 \cdot J(\omega_C) + 6 \cdot J(\omega_C+\omega_H) \,] \qquad (4.5)$$

$J(\omega)$ is the spectral density with $\omega_C = 2\pi\nu_C$ and $\omega_H = 2\pi\nu_H$ where ν_H and ν_C are the proton and carbon Lamor frequencies.

The spectral density can be related to the correlation time and the diffusion coefficients following the same procedures as above. For the tumbling motion described by $D_\perp$ one obtains

$$J_\perp(\omega) = \frac{1}{1 + \frac{\omega^2}{6} D_\perp} \qquad ; \omega = (\omega_C+\omega_H),\ \omega_C,\ (\omega_H-\omega_C) \qquad (4.6)$$

where ω takes the values $(\omega_C + \omega_H)$, ω_C and $(\omega_H - \omega_C)$ to give the three terms in (4.5). Similarly one obtains for the spinning motion D_s

$$J_s(\omega) = \frac{1}{384 D_\perp \left(1+\left(\frac{\omega}{6D_\perp}\right)^2\right)} + \frac{9}{16(5D_\perp+D_s)\left(1+\left(\frac{\omega}{5D_\perp+D_s}\right)^2\right)} + \frac{27}{64\,(2D_\perp+4D_s)\left(1+\left(\frac{\omega}{2D_\perp+4D_s}\right)^2\right)} \qquad (4.7)$$

In the fast narrowing limit where $D_\perp \gg \omega$, equations (4.6) and (4.7) simplify to (4.2) and (4.3). Figure 4.4b compares values of T_1 calculated with both models for the para hydrogens of phenyl rings. One can see that for relaxation times

below 0.4 s^{-1} (or for tumbling slower than 1 ns^{-1}) there is a significant difference between the values obtained from the general equations and the ones used in the extreme narrowing limit.

Using equations (4.2) and (4.3), diffusion coefficients were obtained from the relaxation times for **34** through **38**. Semilogarithmic plots of the diffusion coefficients versus inverse temperature are shown in Figure 4.5. Dotted lines represent values of $D_\perp$ and $D_\parallel$ obtained from hydrodynamic models discussed below. Regression analyses through the experimental data are shown as solid lines. Tables 4.2 and 4.3 compare the room temperature diffusion coefficients derived from the data over all measured temperatures for all four compounds.

As can be seen in Figure 4.5, the overall spinning rates of the phenyl substituents D_s are about an order of magnitude larger than the rate of tumbling $D_\perp$ for all of the complexes described here. This highly anisotropic motion of the phenyl groups can be explained by noting that the tumbling of a phenyl group involves tumbling of the entire molecule about its long axis while the spinning motion of a phenyl group involves not only the overall rotation of the molecule but also internal rotation about the single bond connecting the phenyl substituent to the carbyne carbon. Our experimental data yield only the total rotation rate D_s. However, comparing the values of D_s for nonequivalent phenyl groups within one molecule allows one to distinguish between the contributions of internal rotation and molecular shape to the anisotropy in the motions in these molecules. For example complexes **36**, **37** and **38** each contain two different types of phenyl

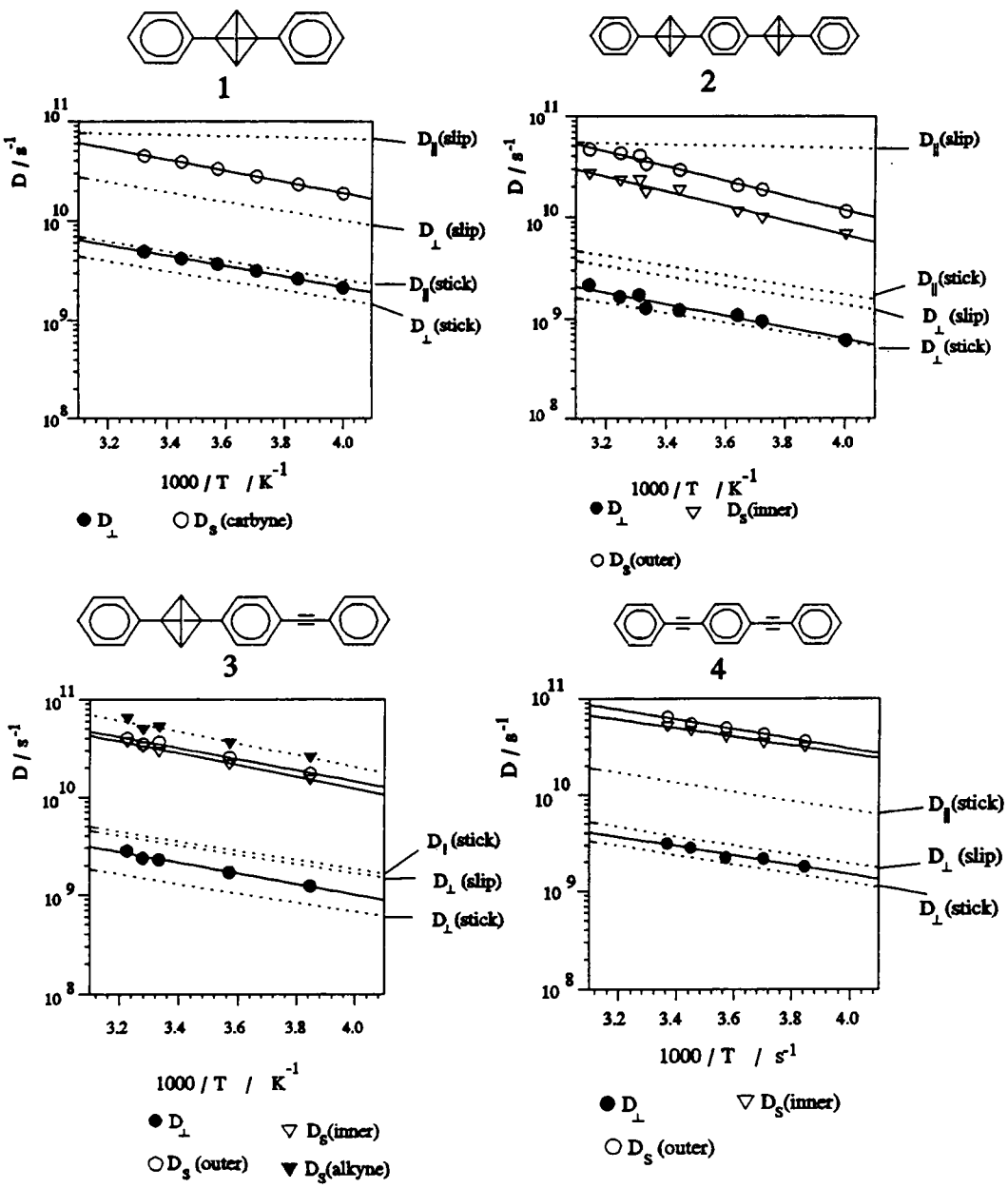

Figure 4.5: Experimental and calculated diffusion coefficients versus inverse temperature. Symbols: experimental data; solid lines: regression; dotted lines: hydrodynamic models

groups which rotate at different rates about the main axis of each molecule. Such behavior can only arise if the different phenyl groups show different *internal* rotation rates since the contribution of the overall molecular rotation (D_I) to D_s is equal for all phenyl groups within one molecule. Therefore any difference in D_s within a molecule must arise from different values of R_{Ph} and can be taken as a qualitative proof of the presence of internal motion.

The observed differences in the spinning rates allow further conclusions to be drawn. In the linked cluster system **36** the total rotation rate for the inner phenyl group ($D_{s,inner}$(**36**)) is considerably slower than that for the outer phenyl groups ($D_{s,outer}$(**36**)) (Table 4.2). On the other hand rotation rates for the linking phenyl group ($D_{s,inner}$(**37**)) and the terminal phenyl substituent on the carbyne ($D_{s,outer}$(**37**)) in **37** are quite similar while the terminal phenyl substituent on the alkyne shows a significantly faster rotation rate. These observations support the assertion that the presence of a $(CpCo)_3$(carbyne-) substituent introduces a significantly larger barrier to the rotation of the phenyl group than does an alkyne substituent. Binding to a second carbyne reduces the rate of rotation even further resulting in the order for phenyl group rotation rates with regard to number and type of substituents: 1 alkyne > 1 carbyne ≈ 1 carbyne + 1 alkyne > 2 carbyne substituents.

From Raman studies the rate of rotation of a benzene molecule in CD_2Cl_2 about its C_2 axis has been previously found to be 100(±20) ns^{-1} at room temperature.[21] This rate can be regarded as the maximum rotation rate for any phenyl

Table 4.2 : Diffusion parameters at 298 K: Overall motion D_s, estimated internal rotation R, barriers to rotation V_i.

Complex	34	35	36		37			38	
Phenyl group type	carbyne	carbyne	outer (carbyne)	inner (2x carbyne	alkyne	outer (carbyne)	inner (carbyne, alkyne)	outer (alkyne)	inner (2x alkyne
$D_\perp$ / ns^{-1}	4.92(4)	7.7(4)	1.5(1)			2.3(1)		3.0(1)	
$(D_s$ / $(ns)^{-1}$	45.3(7)	54(1)	36(2)	20(2)	50(4)	34(2)	30(1)	63(1)	50(1)
R / $(ns)^{-1}$ [a]	37.5(7)	44	31(2)	16(2)	45(4)	28(2)	24(1)	46(1)	33(1)
$D_\parallel$ / ns^{-1} [a]	7.8	9.8	4.4			6.3		17.1	
$(D_s/D_\perp)_{exp}$	9.2	7.0	23.3	13.1	21.9	14.9	13.2	20.7	16.7
$(D_\parallel/D_\perp)_{stick}$	1.58	1.26	2.93			2.72		5.69	
E_a/kJ mol^{-1}	10.7		11.1	10.8	11.4	10.9	11.4	9.34	9.71
V_i / kJ mol^{-1}	2.4		2.9	4.6	2.0	3.1	3.5	1.9	2.7

a) based on hydrodynamic "stick" model approximation.

substituent with no barrier to rotation other than interactions with a CD_2Cl_2 solvent cage. None of the phenyl substituents in this series of molecules exhibits this rotation rate.

As can be seen from Table 4.2, the values of $D_{s,outer}$(**37**) and $D_{s,outer}$(**36**) are identical within their uncertainties whereas both are significantly different from D_s for **34** and **35** though all of these rates describe the spinning of a phenyl group carrying a single $(CpCo)_3$(carbyne) substituent. $D_{s,alkyne}$ in **37** and $D_{s,outer}$ in **38** are also significantly different even though both characterize the rotation of a phenyl ring with one alkyne substituent. These differences are due to the contribution which overall molecular diffusion ($D_\parallel$) makes to the total rotation of the phenyl

rings. That contribution differs from molecule to molecule. In order to compare molecular diffusion between different molecules an independent determination of $D_{\parallel}$ is needed. In other studies, carbon-13 relaxation times of carbonyl ligands rigidly bound to the metal skeleton have been used for this purpose;[16] in the molecules under discussion, however, such a ligand is not available.[22]

4.4.2. Hydrodynamic Models

An alternative to the direct measurement of $D_{\parallel}$ is the use of hydrodynamic models to calculate theoretical values of $D_{\perp}$ and $D_{\parallel}$. The simplest theories of anisotropic reorientation of molecules in fluid solution are modifications of the Stokes-Einstein-Debye theory of reorientation of spheres in a viscous medium.[23] In these models, the reorientation of an symmetric top molecule in a solvent with viscosity η is given by :

$$D_i = \frac{1}{f_i} \frac{kT}{8\pi\eta\, ab^2} \qquad (4.8)$$

where a and b are the radii along the long and the short main axes of the solute molecule, D_i stands for either $D_{\parallel}$ or $D_{\perp}$ and f_i are the friction coefficients for the rotation about either axis relative to a sphere of equal volume.

In the so-called "stick" limit the solute is assumed to be large in size compared with the solvent molecules. The solvent molecules are thought to stick to the solute and cause a viscous drag opposing its rotation. Equations relating the ratio of the length of the two axes of the ellipsoid with $f_{\perp}$ and $f_{\parallel}$ have been

developed by Perrin.[24] Using literature values for solvent viscosity,[25] diffusion coefficients for this model have been calculated and are shown in Figure 4.5. For the molecules under discussion, the stick model gives the correct order of magnitude for $D_\perp$, but slightly underestimates its value. The temperature dependencies of the experimental data are also quite similar to those derived from equation (4.8). Fitting the data to the Arrhenius equation gives a range of 9 to 11 kJ mol^{-1} for the activation energy associated with molecular tumbling. These values, when compared to the with the calculated temperature dependence of T/η for CH_2Cl_2 according to equation (4.8) (9.13 kJ mol^{-1}),[26] indicate that the temperature dependence of the tumbling is determined mainly by the viscosity of the solvent.

The stick model is valid for large molecules where $r_{solute} \gg r_{solvent}$. When this condition is not met, the frictional drag on the solute is overestimated, resulting in diffusion coefficients which are smaller than observed. Hu and Zwanzig have described a different model for small solute molecules[27] which assumes that the solute slips through the solvent molecules without the solvent sticking to the molecule. The friction experienced by the molecules is then described exclusively by the displacement of solvent molecules during rotation. The expression one obtains for $D_\perp$ in the slip limit is analogous to (4.8) except that the friction coefficients $f_\perp$(slip) are different. For $D_\parallel$ in symmetric top molecules, however, the rotation in the slip limit depends only on the moment of inertia of the molecule:

$$D_\parallel(slip) = \frac{3}{4\pi}\sqrt{\frac{kT}{I_\parallel}} \qquad (4.9)$$

From Figure 4.5 one can see that for complexes **34** - **38** the slip model overestimates the values of $D_\perp$ to an even larger degree than the "stick" model underestimates them. Furthermore the predicted temperature dependence of $D_\parallel$(slip) is significantly different than experimentally observed demonstrating that the motions of these molecules are in the diffusional region governed by solvent viscosity rather than the inertial region.[28] Table 4.3 summarizes the experimental values for $D_\perp$ at 298 K and compares them to the values calculated from the two models. The observed rate of tumbling decreases in the order **34** > **38** > **37** > **36** following increasing size of the molecule as measured by the long axis length ($2a$). The "stick" model describes the diffusional behavior of our molecules better and is therefore the one used to estimate internal rotation rates.

Having calculated values of $D_\parallel$, one is now able to separate D_s into its components and obtain approximate values for the rate of internal rotation. In the lower part of Table 4.2 the experimental ratio D_s / $D_\perp$ ($D_s = D_\parallel + R_{Ph}$) is

Table 4.3 : Diffusion coefficients $D_\perp$ at T = 298 K and comparison with calculated values using hydrodynamic stick and slip models.

Complex	**34**	**36**	**37**	**38**
$2a$ / Å	13.0	21.2	20.0	18.3
$D_\perp$(exp) / $(ns)^{-1}$	4.92(4)	1.5(1)	2.3(1)	3.0(1)
$D_\perp$(stick) / $D_\perp$(exp)	0.68	0.80	0.61	0.82
$D_\perp$(slip) / $D_\perp$(exp)	4.23	1.85	1.60	1.30

compared with the ratio $D_{\parallel} / D_{\perp}$ expected for a rigid molecule, obtained from the "stick" model. One can see that for all investigated molecules D_s is significant larger than the value of $D_{\parallel}$, consistent with a significant contribution from internal phenyl rotation R_{Ph} to the total spinning rate D_s. Using the theoretical ratio $(D_{\parallel}/D_{\perp})_{stick}$ together with the experimental value for $D_{\perp}$, gives an approximate value for $D_{\parallel}$ from which internal rotation rates R_{Ph} for individual phenyl groups may be obtained. These values are summarized in the middle of Table 4.2.

Phenyl groups bearing similar substituents in different molecules in this series exhibit identical rotation rates: 45(4) versus 46(1) ns^{-1} for R_{outer}(**38**) and R_{alkyne}(**37**) respectively and 28(2) versus 31(2) ns^{-1} for R_{outer}(**37**) and R_{outer}(**36**). One would also expect the phenyl groups in **34** to have the same internal rotation rate as the terminal phenyl groups next to a carbyne in **36** and **37**. That this is not observed (R_{Ph}(**34**): 37.5(7) ns^{-1} and R_{Ph}(**35**): 44 ns^{-1} opposed to R_{outer}(**36**) $\approx R_{outer}$(**37**) $\approx$ 30 ns^{-1}) might reflect the fact that the "stick" model does not describe the anisotropy of the diffusional motion consistently for molecules with widely varying shapes. Self consistent rotation rates are obtained for the more anisotropic, rod-like molecules **36**, **37** and **38** as opposed to **34** and **35** which are more spherical in shape than the others. There is also experimental evidence that the "stick" model tends to underestimate the ratio $D_{\parallel}/D_{\perp}$ in molecules which are more spherically shaped.[29]

We can obtain approximate values for the internal barrier to phenyl group rotation from different substituents V_i using the relationship[30]

$$V_i = - R_G T \ln(\frac{R_{Ph}}{R_{C_6H_6}}) \qquad \textbf{(4.10)}$$

where R_G is the gas constant and $R_{C_6H_6}$ is the rotation rate of free benzene in methylene chloride. The results (Table 4.2, line 8) indicate that the presence of one Cp_3Co_3-carbyne substituent raises the barrier by 3 kJ mol^{-1}; while second cluster fragment adds another 1.7 kJ to the barrier. These substituent effects on the barriers to rotation of phenyl groups originate from a combination of effects which may be broadly divided into those involving steric and those involving electronic interactions between the substituent and the phenyl group. The discussion that follows describes the relative contributions of these interactions.

Previous studies of phenyl rotation rates for the tricobalt carbyne systems $Cp_2Co_3(CO)_3(\mu\text{-}CO)(CPh)$ (**39**) and $Co_3(CO)_9(CPh)$ (**40**)[16] have revealed interesting differences. For complex **39** phenyl ring rotation was found to be effectively locked on a nanosecond time scale, whereas for complex **40**, phenyl ring rotation rate was found to be comparable to the rate of rotation for free benzene. Consistent with these observations, frontier orbital theory suggests that in **39** the presence of the bridging CO ligand leads to a preferred orientation of the phenyl substituent with respect to that ligand[31, 32] resulting in a higher barrier to phenyl rotation in **5** than in complex **40**. Even considering the uncertainty of our

values of R_{Ph}, the carbyne bound phenyl substituents in **34**, **36** and **37** appear to be somewhere between these two extremes.

4.4.3. Steric versus Electronic Interactions

In trinuclear clusters with three equivalent vertices such as **40** and the complexes investigated in our study, electronic interactions between the metal fragments and the phenyl groups do not depend on the orientations of the phenyl group and lead to a low barrier of activation for phenyl ring rotation. There are at least two possible causes for the remaining difference in rotation rates of **40** on one hand and **34**, **36** and **37** on the other. The first is that the two phenyl rings interact electronically through the Cp_3Co_3 ring resulting in a preferred orientation of the π-systems relative to each other. The second is that the barrier might be related to steric interactions between Cp ligands and the phenyl ring.

Using the crystal structure of **34**[7] we qualitatively examined the steric interactions of the phenyl and cyclopentadienyl groups. Figure 4.6 illustrates the rotational cones defined by the rotation of the hydrogens atoms in the phenyl and Cp rings derived from the crystal structure. Vectors *c* and *d* describe the distance from these cones to the center of the metal triangle and the angles γ and δ the angles between these vectors with the respective rotational axis. With $\gamma \approx \delta \approx$ 34.5°, a = 3.6 Å and b = 3.8 Å one can calculate the smallest possible distance between the hydrogen atoms of the two rings in the course of mutual free rotation to be x_{min} = 1.22 Å. This is less than twice the Van der Vaal radius of a hydrogen

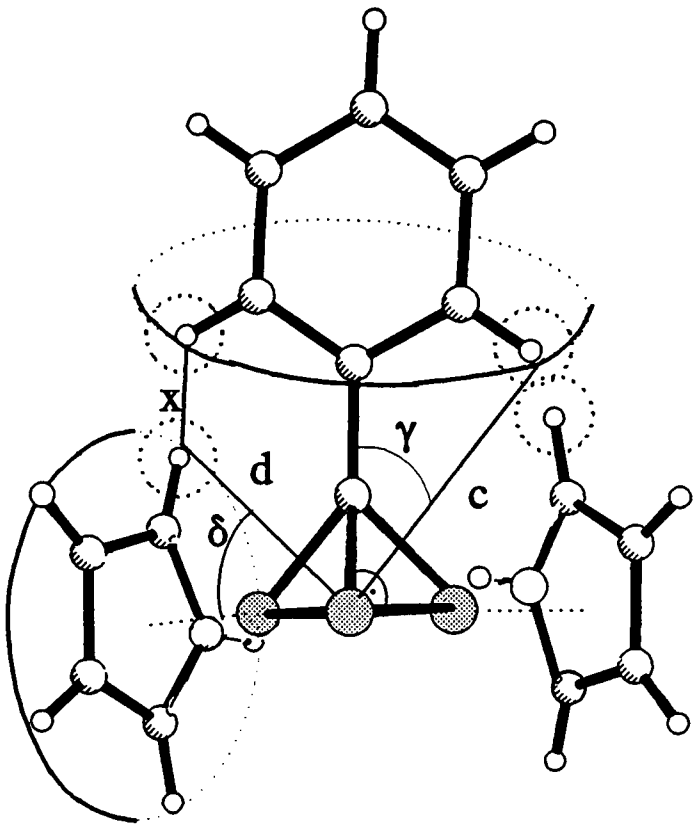

Figure 4.6: Rotational cones of the hydrogens in the phenyl and Cp rings. $\gamma \approx \delta \approx$ 34.5°; a = 3.6 Å; b = 3.8 Å, x_{min} = 1.22 Å.

atom in benzene (1.0 Å)[33] represented by the dottet circles indicating possible steric interactions. With the cyclopentadienyl rings kept rigid in the positions obtained from the crystal structure, force field calculations using SYBYL[34] yield a barrier to rotation on the order of 1000 kJ mol^{-1}, i. e., orders of magnitude higher than observed. If one correlates the rotation of the Cp and phenyl groups to minimize steric interactions the calculated barrier to rotation for the phenyl group drops to 13.8 kJ mol^{-1}. Although this barrier is still higher than what is observed, the previous calculation do not allow for librational motions of the

phenyl rings which are expected to result in an even lower barrier of rotation. It therefore appears that steric interactions between the phenyl and Cp rings could explain the magnitude of the barrier to rotation of the phenyl groups with $(CpCo)_3(\mu_3\text{-}C)$-substituents.

Such steric interactions raise the question of whether the motions of the two phenyl and Cp rings are completely correlated resulting in equal rotation rates for both groups. If we assume $D_{s,Co3} \approx D_I$ in **34** and use the approximate value of D_I from the hydrodynamic stick model as described above, one obtains a value of R_{Cp} = 95 ns^{-1} for **34** at 298 K. This value is considerably larger than the internal rotation rate of the phenyl rings and is not consistent with the presence of correlated motion. The value obtained for R_{Cp} depends strongly on the estimate made for D_I, however the above conclusion holds still true even if D_I was twice as large as the one obtained from the "stick" model.[35] At first glance this argument appears to rule out steric interactions as an explanation for the observed barrier of rotation. However, when evaluating the crystal structure and molecular modelling results one finds that in its most favored configuration, a phenyl ring bound to a $(CpCo)_3$(carbyne-) fragment is oriented parallel to one of the three Cp ligands. It therefore sterically interacts with only two of the three Cp rings at a time (Figure 4.7) whereas the third Cp ring is able to spin freely with a very low barrier (0.8 kJ mol^{-1}). This condition allows the cyclopentadienyl rings to rotate, on average, faster than the phenyl ring even in the presence of steric interaction between the two groups.

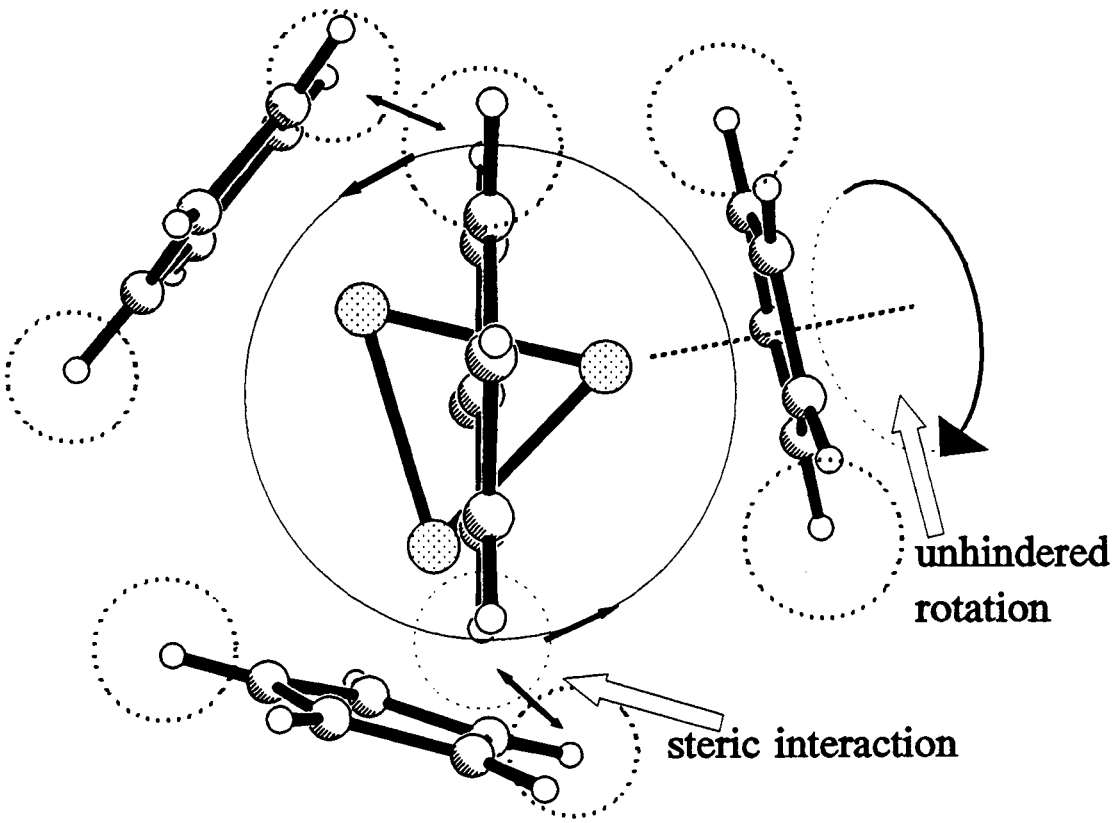

Figure 4.7: Top view of crystal structure of **34** showing interaction of the phenyl ring with only two of the three Cp rings.

It should also be noted that in the case of a full gear type motion between the phenyl groups and Cp rings, one would also expect the rates of rotation of the two phenyl rings in **36** (R_{outer} and R_{inner}) to be equal. The experimental observation of two distinct rotation rates indicates that steric interactions are large enough to slow down the motion of the phenyl groups but too small to engage a full gear type motion of the entire system.

Although steric interactions appear to be a significant factor in explaining the rotational behavior exhibited by the phenyl rings with Cp_3Co_3 substituents electronic interactions between the phenyl rings cannot be ruled out. The fact

that R_{Ph} is somewhat larger in **35** than **34** may be explained by either type of interaction. The absence of a second phenyl ring in **35** excludes any mutual phenyl ring interactions, but one can also expect the Cp ring centroids in **35** to move towards the sterically less demanding μ_3-CH group, thus reducing steric interactions between the Cp and phenyl rings.

In the case of the rotation of the alkyne substituted phenyl rings in the cluster complex **37** and bistolan **38** steric interactions can be ruled out and consistently much lower barriers to rotation are observed. In these cases the barrier is therefore believed to be caused by electronic interaction between the π-systems of the phenyl rings through the C≡C triple bond.

4.5. Conclusions

Analysis of the carbon-13 NMR relaxation times of the protonated carbons in the phenyl rings of the bis-carbyne cluster systems **34** - **37** and in bistolan **38** reveal anisotropic reorientation of the phenyl rings. Tumbling rates perpendicular to the main axis decrease with increasing size within this family of complexes. Internal rotation of the phenyl rings is the main contributor to the observed molecular spinning rate and accounts for the motional anisotropy observed for these complexes. The rate of internal rotation depends on the type of substituent attached to the phenyl ring. Steric interaction between the phenyl group and the Cp ligands of the Cp_3Co_3 fragment appear to be the major factor influencing the barrier to phenyl group rotation.

4.6. References

1. a) Hoskins, B. F.; Robson, R.; *J. Am. Chem. Soc.* **1992**, *114*, 1546. b) Stein, A.; Keller, S. W.; Mallouk, T. E.; *Science* **1993**, *259*, 1558.

2. Brown, G. M.; Meyer, T. J.; Cowan, D. O.; LeVanda, C.; Kaufman, F.; Roling, P. V.; Rausch, M. D.; *Inorganic Chemistry*, **1975**, *14*, 506-511.

3. a) Colbran, S. B.; Robinson, B. H.; Simpson, J.; *Organometallics* **1984**, *3*, 1344-1353. b) Elder, S. M.; Robinson, B. H.; Simpson, J.; *J. Organomet. Chem.* **1990**, *398*, 165-176. c) Worth, G. H.; Robinson, B. H.; Simpson, J.; *J. Organomet. Chem.* **1990**, *387*, 337-355.

4. Bautista, M. T.; White, P. S.; Schauer, C. K.; *J. Am. Chem. Soc.* **1994**, *116*, 2143-2144.

5. Barnes, C. E.; Orvis, J. A.; Finniss, G. M.; *Organometallics*, **1990**, *9*, 1695-1697.

6. Clauss, A. D.; Shapley, J. R.; Wilker, C. N.; Hoffmann, R.; *Organometallics* **1984**, *3*, 619-623.

7. King, W.D.; Barnes, C.E.; manuscript in preparation

8. Eaton, B.; O'Connor, J. M.; Vollhardt, K. P. C.; *Organometallics* **1986**, *5*, 394-397.

9. Nguyen, P.; Yuan, Z.; Agocs, L.; Lesley, G.; Marder, T. B.; *Inorg. Chim. Acta* **1994**, *220*, 289.

10. Freeman, R.; Morris, G. A.; *J. Chem. Soc. Chem. Comm.* **1978**, 684-686.

11. Canet, D.; Levy, G. C.; Paet, I. R.; *J. Magn. Res.* **1975**, *18*, 205-208.

12. Derome, A.; *Modern NMR Techniques for Chemistry Research*; Pergamon Press : Oxford 1987; Chapter 7.6.

13. a) Van Geet, A. L.; *Anal. Chem.* **1968**, *40*, 2227-2229. b) Van Geet, A. L.; *Anal. Chem.* **1970**, *42*, 679-680.

14. The crystal structures of **1** and **2** show that the phenyl groups in these complexes are bent slightly away from the main axis in the solid state. This bending is most likely due to packing effects since in solution, time averaged axial symmetry is observed for all complexes at all temperatures.

15. a) Woessner, D. E.; *J. Chem. Phys.* **1962**, *37*, 647-654. b) Woessner, D. E.; Snowden, B. S.; Meyer, G. H.; *J. Chem. Phys.* **1969**, *50*, 719-721.

16. a) Schwartz, M.; Richmond, M. G.; Chen, A. F. T.; Martin, G. E.; Kochi, J. K.; *Inorg. Chem.* **1988**, *27*, 4603-4703. b) Wang, S. P.; Chen, A. F. T.; Richmond, M. G.; Schwartz, M.; *J. Organomet. Chem.* **1989**, *371*, 81-86. c) Yuan, P.; Richmond, M. G.; Schwartz, M.; *Inorg. Chem.* **1991**, *30*, 679-683. d) Yuan, P.; Don, M. J.; Richmond, M. G.; Schwartz, M.; *Inorg. Chem.* **1991**, *30*, 3704-3707.

17. Churchill, M. R.; *Inorg. Chem.* **1973**, *12* 1213. 1.08 Å is the spectroscopically determined value reflecting the inter*nuclear* distance rather than the distance of electron density obtained by x-ray diffraction.

18. Lyerla, J. R.; Levy, G. C.; *Topics in Carbon-13 NMR Spectroscopy*, **1974**, *1*, 79-148.

19. See equation 5 of reference 16c. For the complexes in this study, a value of 90° was used for the angle α between the rotational axis of the Cp ligand and the main axis of the molecule.

20. Spiess, H. W.; *NMR : Basic Principles and Progress*, Volume 15, Springer Verlag **1978**, pp. 55-214.

21. Tanabe, K; Hiraishi, J.; *Mol. Phys.* **1980**, *39*, 493.

22. The possibility of measuring ^{59}Co relaxation times was considered. However in order to extract motional information from one would need a reasonable estimate of the value and orientation of ^{59}Co quadrupolar coupling tensors. The values reported in the literature for similar compounds cover too large a range to obtain such an estimate. It should also be noted that in the linked cluster system **2** the cobalt rings can be expected to rotate with their own internal rotation rate rather than $D_{\parallel}$.

23. Debye, P.; *Polar Molecules*; Dover : New York, 1929.

24. Perrin, F.; *J. Phys. Radium* **1934**, *5*, 497.

25. Viswanath, D. S.; Natrajan, G.; *Data Book on the Viscosity of Liquids* : Hemisphere Publ. 1989., pp.

26. Note that the activation energies E_a are used solely to compare the temperature dependence of experimental and calculated data; it should not be taken to represent the kinetic barrier related to a certain transition state.

27. Hu, C.-M.; Zwanzig, R.; *J. Chem. Phys.* **1974**, *60*, 4354.

28. Boeré, R. T.; Kidd, R. G.; *Ann. Rep. NMR Spectroscopy* **1982**, *13*, 319-384.

29. Gillen, K. T.; Schwartz, M.; Noggle, J. H.; *Mol. Phys.* **1971**, *20*, 899. b) Gillen, K. T.; Noggle, J. H.; *J. Chem. Phys.* **1970**, *53*, 801. c) Wilson, N. K.; *J. Am. Chem. Soc.* **1975**, *97*, 3573. d) Levy, G. C.; Holak, T.; Steigel, A.; *J. Am. Chem. Soc.* **1976**, *98*, 495.

30. a) Alger, T. D.; Grant, D. M.; Harris, R. K.; *Chem. Phys.* **1972**, *76*, 281. b) Lyerla, J. R.; Grant, D. M.; *J. Phys. Chem.* **1972**, *76*, 3213.

31. Evans, D. G.; Howard, J. A.; Jeffery, J. C.; Lewis, D. B.; Lewis, G. E.; Grosse-Ophoff, M. J.; Parrot, M. J.; Stone, G. A.; *J. Chem. Soc., Dalton Trans.* **1986**, 1723.

32. Schilling, B; Hoffmann, R.; *J. Am. Chem. Soc* **1979**, *101*, 3456-3467.

33. Bondi, A.; *J. Phys. Chem.* **1964**, *68*, 441-451.

34. Clark, M.; Cramer III, R. D.; Van Openbosch, N. V.; *J. Comp. Chem.* **1989**, *10*, 982-1012.

35. Using a larger value of D_l in the analysis results in a decreased value obtained for R_{Cp}. However, one has to keep in mind that $R_{Ph} = D_s - D_l$ will change in the same direction, even though the dependence is normally smaller. For example, if D_l was twice the value calculated from the "stick" model, one obtains $R_{Cp} \approx 48$ ns^{-1} and $R_{Phenyl} \approx 30$ ns^{-1}.

CHAPTER 5

Addition of Oxygen to Mixed Metal Trinuclear Cluster Complexes: Formation of Oxo Adducts

5.1 Introduction

In addition to the formation of carbene and alkyne adducts of unsaturated trinuclear cluster complexes described in the previous chapters, we have also observed a rather unique μ_3-oxo containing cluster complex. We believe that this compound arises from the slow reaction of several of the 46e$^-$ complexes with dioxygen. There have been a number reports of trinuclear cluster complexes containing oxygen in a triply bridged bonding mode. Incorporation of the oxygen was accomplished by different means including oxygen abstraction from tetrahydrofuran[1] or methylaminoxide.[2] One very common pathway, however, is the often unintended addition of dioxygen to carbonyl based cluster complexes.[3] This reaction is normally thermally induced and a carbonyl ligand is displaced by a μ_3-O ligand which therefore acts as an four electron donor. A side product is carbon dioxide which is believed to result from oxidation of the displaced carbonyl ligand with the other oxygen atom of the dioxygen molecule. However, the

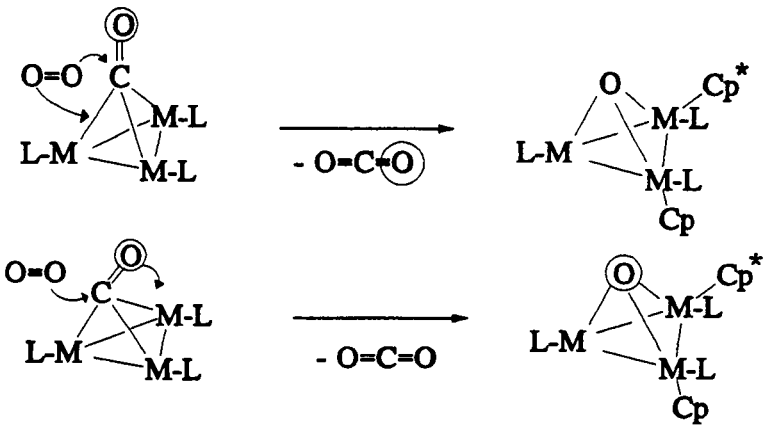

Figure 5.1: Different possible pathways for addition of dioxygen to trinuclear cluster complexes.

possibility of CO dissociation has also been discussed, in which case the bridging oxygen arises from the carbonyl ligand and the dioxygen takes up the remaining carbon atom to form carbon dioxide as shown in Figure 5.1. In the following, the formation of the heteronuclear μ_3-oxo complexes $Cp^*Co(CpCo)_2(\mu_3\text{-}CO)(\mu_3\text{-}O)$ (**41**), $Cp^*Rh(CpCo)_2(\mu_3\text{-}CO)(\mu_3\text{-}O)$ (**42**) and $Cp^*Ir(CpCo)_2(\mu_3\text{-}CO)(\mu_3\text{-}O)$ (**43**) will be reported from reaction of the unsaturated cluster complexes **1** - **3** with dioxygen in the *solid state*.

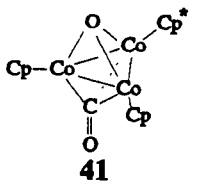

41

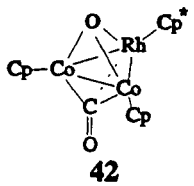

42

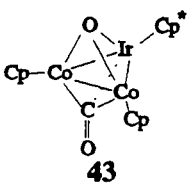

43

Our studies will be primarily be concerned with the characterization of the oxo containing products including their crystal structures.

5.2 Formation of Oxo Adducts

The first observation of the oxo adduct $Cp^*Ir(CpCo)_2(\mu_3\text{-}CO)(\mu_3\text{-}O)$ occurred in an attempt to recrystallize a sample of the unsaturated cluster complex $Cp^*Ir(CpCo)_2(\mu_3\text{-}CO)_2$ (1) which had been stored in a screw cap vial in an inert atmosphere glove box for several months. Further investigations indicated that the oxo adduct was already present in the mixture prior to recrystallization. Furthermore, fresh, microcrystalline samples of **1** and **2** showed partial conversion to the corresponding oxo adduct over a period of several weeks when stored as solids in the glove box. Trace amounts of dioxygen in the glove box are thought to be the source of the oxidant in these reactions. When the microcrystalline samples of the $46e^-$ complexes are stored outside the glove box in air with the exclusion of light, the conversion to oxo adduct proceeds within a few days as shown in Figure 5.2. We believe that CO_2 is formed as byproduct in this reaction, however, we have not studied this hypothesis in these investigations. In contrast to these findings, the reactivity reported for the Ir complex **1** towards dioxygen in *solution* involves cluster fragmentation forming the dinuclear complex $Cp^*Ir(\mu_2\text{-}CO)_2CpCo$.[4] This result was reproduced under mild conditions by adding the unsaturated trinuclear cluster complex at low temperature (-78 °C) to dry ether containing small amounts of oxygen. We believe that the difference in reactivity found for the solid state versus solution is caused by lattice effects. The molecules in the crystal lattice are less mobile making cluster fragmentation a less favored process. Since the oxo adducts themselves are very stable in solution, the

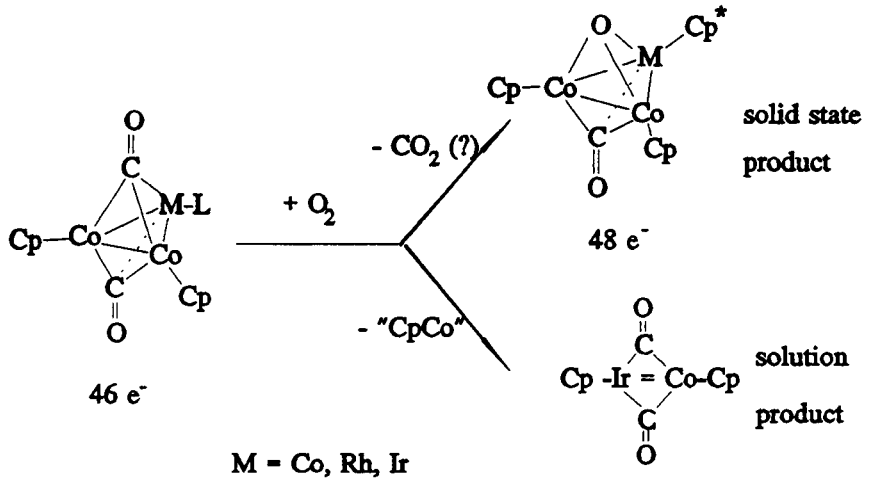

Figure 5.2: Formation of oxo-adducts **41**, **42** and **43** in the solid state (top) and fragmentation in solution (bottom).

fragmentation observed in solution has to proceed from an intermediate prior to loss of the carbonyl ligand. Formation of oxo adducts by solid state reaction has been observed for the entire series of heteronuclear cluster complexes $Cp^*M(CpCo)_2(\mu_3\text{-}CO)_2$ (M = Co, Rh, Ir), but not for the all-Cp cluster complex $(CpCo)_3(\mu_3\text{-}CO)_2$. On the other hand the all-Cp based cluster complex $(CpCo)_3(\mu_3\text{-}CO)(\mu_3\text{-}O)$ has been isolated by Dahl in very low yield by photolysis of a solution of the mononuclear complex $CpCo(CO)_2$ which presumably formed because of the presence of dioxygen in the reaction system.[5]

5.3. Spectroscopic Data

Table 5.1 lists the NMR, IR and MS data obtained for the oxo adducts. The proton NMR spectra exhibit a singlet for each the Cp and Cp^* protons with

Table 5.1: Spectroscopic data of the μ_3-oxo adducts **41** - **43**.

	Cp*Co (41)	Cp*Rh (42)	Cp*Ir (43)
^{1}H NMR (C_6D_6)	4.564 s, 10H 1.612 s, 15H	4.65 s, 10H 1.64 s, 15H	4.632 s, 10H 1.723 s, 15H
^{13}C NMR (C_6D_6)	-	-	257.4 (CO) 95.6 (Cp*-C) 82.7 (Cp) 9.9 (Cp*-CH_3)
IR	1681	-	1655
MS	-	530 (M^+) 502 (-CO) 303 ([Cp*RhCp]$^+$)	620 (M^+) 592 (-CO) 526 (-CO, - Cp-H) 393 ([Cp*IrCp]$^+$). HRMS: M^+ = 620.0198 (calc. 620.0147).

the relative intensities 10 : 15, consistent with two equivalent CpCo edges in the trinuclear cluster. In addition to the signals of these groups the ^{13}C NMR spectrum of the Ir containing complex **43** exhibits a signal due to the carbonyl ligand at 257.4 ppm consistent with a bridging bonding mode. The carbonyl stretching frequencies of 1681 and 1655 cm^{-1} observed in the IR spectrum of **41** and **43** strongly indicate the presence of a μ_3-bridging carbonyl ligand in each complex. The mass of the molecular ion peaks in **42** and **43** is consistent with a complex of the composition Cp*M$(CpCo)_2(CO)(O)$. High resolution mass spectrometry and an elemental analysis obtained for the Ir containing complex **43** confirm this formula. If the carbonyl ligand is bridging one face of the cluster as

indicated by the IR data, then the oxo ligand most likely bridges the opposite face rendering the two CpCo edges equivalent as suggested by the NMR data.

5.4 Crystal Structure

We were able to obtain crystals suitable for x-ray diffraction for both the Ir and Rh containing complexes. The two compounds are isomorphic and both crystallize in the orthorhombic space group $P2_12_12_1$ with similar unit cell dimensions. Different views of the Ir containing complex **43** are shown in Figure 5.3, and selected bond distances and -angles are listed in Table 5.2. In the side view at the top of Figure 5.3 the Cp^* ligand has been omitted for clarity. The structural features of both compounds are very similar. The three metal atoms are arranged in a triangle which is bridged by a carbonyl ligand on one side and by an oxygen atom on the opposite side consistent with the spectroscopic data obtained for these complexes in solution. The vertices of the metal triangle are capped by the Cp and Cp^* ligands perpendicular to the plane of the metals. The oxo ligand is not exactly above the center of the metal triangle but slightly displaced towards the Co-Co edge resulting in an Ir - oxygen bond which is 0.15 Å longer than the corresponding Co - oxygen bond. The distances between the carbonyl carbon and the metal atoms on the other hand differ only by half of that amount. The basic features of the structures of these two heteronuclear complexes resemble the ones reported by Dahl for the all-CpCo complex $(CpCo)_2(\mu_3\text{-}CO)(\mu_3\text{-}O)$.[5]

Side View

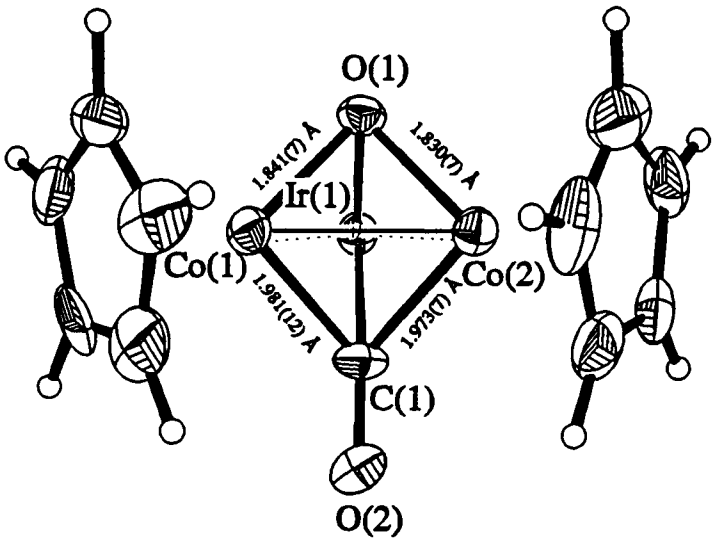

Top View

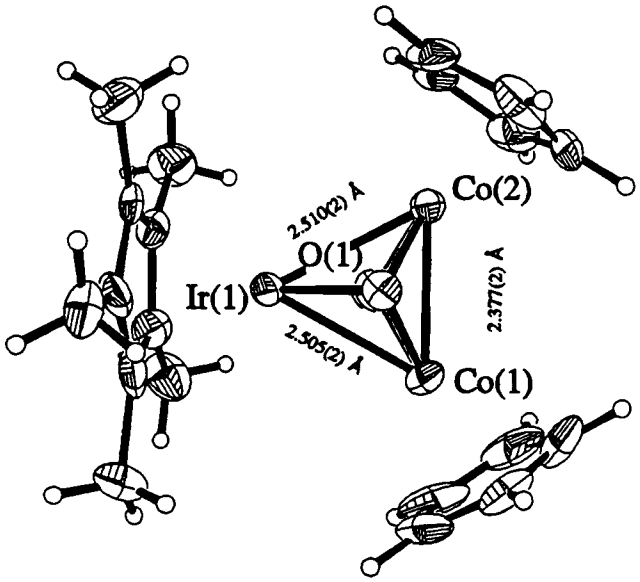

Figure 5.3: Crystal structure of $Cp^*Ir(CpCo)_2(\mu_3\text{-}CO)(\mu_3\text{-}O)$ (**43**). In the side view the Cp^* ligand is omitted for clarity.

Table 5.2: Selected bond distances in the oxo cluster complexes $Cp^*M(CpCo)_2(\mu_3\text{-}CO)(\mu_3\text{-}O)$, **42** and **43**.

M = Ir		M = Rh	
Unit Cell Dimensions a, b, c / Å			
9.371(2) 13.119(2) 16.239(3)		9.356(2) 13.076(3) 16.309(3)	
Bond distance / Å			
Ir1 O1	1.997(7)	Rh1 O2	1.984(4)
Ir1 C1	2.054(11)	Rh1 C1	2.086(5)
Ir1 Co1	2.505(2)	Rh1 Co1	2.4912(9)
Ir1 Co2	2.510(2)	Rh1 Co2	2.4986(9)
Co1 O1	1.841(7)	Co1 O2	1.832(4)
Co1 C1	1.981(12)	Co1 C1	1.964(5)
Co1 Co2	2.377(2)	Co1 Co2	2.3690(10)
Co2 O1	1.830(7)	Co2 O2	1.831(4)
Co2 C1	1.973(11)	Co2 C1	1.951(5)
Bond angle / °			
Co1 Ir1 Co2	56.58(5)	Co1 Rh1 Co2	56.69(2)
Co2 Co1 Ir1	61.81(5)	Co2 Co1 Rh1	61.81(3)
Co1 Co2 Ir1	61.61(5)	Co1 Co2 Rh1	61.50(3)
Co2 O1 Co1	80.7(3)	Co2 O2 Co1	80.60(15)
Co2 O1 Ir1	81.8(3)	Co2 O2 Rh1	81.72(14)
Co1 O1 Ir1	81.4(3)	Co1 O2 Rh1	81.40(14)
O2 C1 Co2	135.5(9)	O1 C1 Co2	137.4(4)
O2 C1 Co1	133.5(10)	O1 C1 Co1	135.8(4)
O2 C1 Ir1	135.2(9)	O1 C1 Rh1	131.6(4)

5.5. Summary

The oxo capped cluster complexes $Cp^*M(CpCo)_2(\mu_3\text{-}CO)(\mu_3\text{-}CO)$ (M = Ir, Rh, Co) were obtained by exposing microcrystalline samples of the corresponding unsaturated trinuclear dicarbonyl complexes to air. The reaction appears to be unique to the solid state, since exposure to oxygen in solution causes cluster fragmentation. Crystal structures were obtained for the Rh and Ir containing complexes and confirm the triply bridging bonding mode of the oxygen ligand.

5.6. References

1. Cole, A. A.; Gordon, J. C.; Kelland, M. A.; Poli, R.; Rheingold, A. L.; *Organometallics* **1992**, *11*, 1754-1757.

2. Beringhelli, T.; D'Alfonso, G.; Freni, M.; Ciani, G.; Molinari, H.; *J. Organomet. Chem.* **1986**, *311*, 177-188.

3. a) Lavigne, G.; Lugan, N.; Bonnet, J.-J.; *Nouv. J. Chimie* **1981**, *5*, 423-425. b) Colombie, A.; Bonnet, J.-J.; Fompeyrine, P.; Lavigne, G.; Sunshine, S.; *Organometallics* **1986**, *5*, 1154-1159.

4. Herrmann, W. A.; Barnes, C. E.; Zahn, T.; Ziegler, M. L.; *Organometallics* **1985**, *4*, 172-179.

5. Uchtman, V. A.; Dahl, L. F.; *J. Am. Chem. Soc.* **1968**, *91*, 3763-3769.

CHAPTER 6

Summary

In this dissertation, the addition of diazoalkanes and alkynes to a series of unsaturated heteronuclear metal cluster complexes of the general formula L-M$(CpCo)_2(\mu_3\text{-}CO)_2$ has been described. Of particular interest was hereby to study the kinetics and thermodynamics of ligand reorientation about the metal triangle. The nature of the metal fragment L-M influences both the rate of reorientation and the preference for a certain positional isomer. The differences in energy between the different metal-metal edges were found to be small and in many cases two or more isomers with ligands bridging different edges were observed in equilibrium with each other.

Reaction of the trinuclear complexes diazomethane resulted in two types of adduct as described in Chapter two. In the case of the Cp^*Co and $Cp^‡$ containing cluster complexes $Cp^*Co(CpCo)(\mu_3\text{-}CO)_2$ (**3**) and $Cp^‡Co(CpCo)(\mu_3\text{-}CO)_2$ (**4**) the diazomethane coordinates with its terminal nitrogen to the trinuclear cluster in a face bridging binding mode. Spectroscopic and crystallographic data suggest that the coordinated diazomethane is best described as a hydrazone containing a N-N

single and C=N double bond. The Cp^*Ir containing complex $Cp^*Ir(CpCo)(\mu_3\text{-}CO)_2$ (**1**) on the other hand reacts with diazomethane under loss of dinitrogen and formation of a carbene complex exclusively. The complexes $Cp^*Rh(CpCo)(\mu_3\text{-}CO)_2$ (**2**) and $(CpCo)_3(\mu_3\text{-}CO)_2$ (**5**) form a mixture containing both hydrazone and carbene adducts in comparable amounts. In the case of the heteronuclear carbene complexes **8** and **7** the kinetic isomer contains the carbene ligand bridging the LM-CoCp edge.

The carbene ligands are mobile about the different edges of the metal triangle. In the Cp^*Rh complex **7** interconversion between two different diastereomers takes is observed as the carbene ligand moves from a Rh-Co edge to the Co-Co edge. Furthermore, movement of the carbene ligand between the two Rh-Co edges leads results in interconversion of two enantiomers. The later process appears to proceed through an intermediate involving a triply bridging carbene ligand, a coordination mode which was not known for carbene ligands so far.

In the case of the Cp^*Ir complex **8** refluxing in toluene resulted in loss of a CO ligand. The new open coordination site is filled by incorporating one hydrogen of the carbene ligand into the cluster as a hydride ligand, resulting in the carbyne hydride complex **18**. The hydride ligand exchanges with the hydrogen of the carbyne ligand at a rate observable by magnetization transfer techniques.

Chapter three describes the addition of alkynes R-C≡C-R" to the unsaturated complexes $L\text{-}M(CpCo)_2(\mu_3\text{-}CO)_2$ which results in the formation of the

alkyne adducts L-M$(CpCo)_2(\mu_3\text{-}CO)(\eta^2,\mu_2\text{-}R\text{-}C{\equiv}C\text{-}R')$ (R = R′ = H, Tol, Ph; R = Tol, R′ = H). In all complexes, the alkyne coordinates in a μ_3-$\|$ fashion with the C≡C bond parallel to a metal edge. The preferred orientation was found to depend on both the nature of the fragment L-M and the alkyne. In the case of the acetylene and tolylacetylene adducts, the alkyne prefers to be parallel to a M-Co edge if the fragment L-M is Cp^*Ir or $Cp^‡Co$, but the orientation parallel to a Co-Co edge is preferred for L-M = Cp^*Rh or Cp^*Co. The differences in energy between the isomers are small and the less favored isomers are normally observed in small amounts. Fast interconversion of the different isomers takes place at room temperature, but at -100 °C the rate of interchange is slowed down sufficiently in order to observe separated signals in the NMR spectrum for the different positional isomers. In the case of the ditolyl- or diphenylacetylene acetylene adducts, on the other hand, only the isomer with the alkyne parallel to the CpCo-CoCp edge is observed. In addition, the rotation of the tolyl substituents of the alkynes is locked at low temperature due to steric interaction with the Cp^* and Cp ligands.

In Chapter four ^{13}C NMR relaxation times were used to study the rotational reorientation of phenyl substituents in several single and linked bis-carbyne cluster complexes of the general form $(CpCo)_3(\mu_3\text{-}CR)_2$. A phenyl ring linking two $(CpCo)_3$ units exhibited especially slowed reorientation. The rate of phenyl group rotation was found to be determined predominantly by steric interaction with the Cp ligands of the $(CpCo)_3$ units.

Finally, the formation of some μ_3-oxo containing complexes by exposure of the unsaturated complexes L-M$(CpCo)_2(\mu_3\text{-}CO)_2$ with oxygen in the *solid state* has been described in Chapter five.

CHAPTER 7

Experimental Part

7.1. Spectroscopic and Analytical Methods

Infrared (IR) spectra were taken as KBr pellet or hexane solution using a Bio-Lab FTS-7 fourier transform IR spectrometer. Nominal and high resolution mass spectra were taken with a VG ZAB-EQ hybrid high performance mass spectrometer using electron impact ionization. Elemental analyses were performed by Desert Analysis in Tucson, Arizona. Single crystal x-ray diffraction was done using a Nicolet R3 diffractometer. Structure solutions and refinements were performed either on a micro Vax using the SHELXTL program or on a PC using SHELX93.

Routine proton NMR spectra were recorded using a Bruker AC-250 spectrometer. Most carbon-13 as well as all variable temperature and two dimensional experiments were performed on a Bruker AMX-400WB spectrometer operating at 400.13 MHz for proton (100.62 MHz for carbon-13) using a 5 mm quadrunuclear probehead (QNP). ^{13}C T_1 relaxation times were obtained using either the QNP or a 10 mm broadband probehead.

Standard Bruker pulse programs were used for COSY, NOESY, heteronuclear correlation experiments, proton T_1 and NOE measurements. For selective inversion transfer, ^{13}C T_1 relaxation time measurements and kinetic experiments existing pulse programs were modified. The "attached proton test" experiment (APT) used to distinguish C and CH_2 from CH and CH_3 was adapted from the literature.[1] A listing of the pulse programs together with a brief description of the required parameters can be found in the appendix. Chemical shifts are reported relative to TMS using the residual solvent signal as reference. Temperatures in variable temperature NMR experiments were calibrated using methanol at low temperature or ethylene glycol at high temperature according to the procedure of Van Geet[2] and are accurate to at least ±2 °C. After reaching a set temperature at least ten minutes was waited before acquisition of data in order to allow for complete equilibration of the temperature within the sample. The probehead was retuned prior to each two dimensional experiment or when changing the temperature by more than 20 K. 90° pulses and decoupler power settings were determined by using standard methods.[3, 4] Chemical shifts are reported relative to tetramethylsilane (TMS) with a downfield shift having a positive sign. In ^1H NMR, the residual proton resonance of the deuterated solvent was used as reference; $CHCl_3$: δ_{1_H} = 7.24 ppm, C_6D_5H: δ_{1_H} = 7.15 ppm, $CHDCl_2$: δ_{1_H} = 5.32 ppm, CD_2H-C_6D_5: δ_{1_H} = 2.09 ppm. For ^{13}C NMR, the solvent signal was used: $CDCl_3$: δ_{13_H} = 77 ppm, C_6D_6: δ_{13_C}128 ppm, CD_2Cl_2: δ_{13_C} = 53.8 ppm, $C_6D_5CD_3$: 20.4 ppm.

7.2. Lineshape Analysis

Lineshape analysis was performed using the program DNMR5[5]. Input parameters included besides the rate constants of exchange the chemical shift of the exchanging sites, their populations and the natural linewidth. These values were normally obtained from spectra well below the coalescence temperature and extrapolated for higher temperatures. In the case of the alkyne adducts $Cp^*Rh(CpCo)_2(\mu_3\text{-}CO)(Tol\text{-}C{\equiv}CH)$, $Cp^*Co(CpCo)_2(\mu_3\text{-}CO)(Tol\text{-}C{\equiv}CH)$ and $(CpCo)_3(\mu_3\text{-}CO)(Ph\text{-}C{\equiv}CH)$ an automatic refinement of the parameters was performed with the simulation, whereas for all other cases parameters were adjusted manually by visually comparing calculated and experimental spectrum. A description of the input format for DNMR5 can be found in Appendix 2 together with two sample input files. For automatic refinement, the experimental spectra were transferred to a PC, read into WINNMR and saved as ASCII files. In order to match the DNMR input format, the files were then edited using a spreadsheet program, reducing the number of data points below 1024 and scaling the largest peak to a value of 999 or below.

7.3. General Techniques

Solvents were dried by refluxing over Na/K alloy (hexane, ether, toluene, THF) or calcium hydride (methylene chloride) and handled under nitrogen. THF was predried by refluxing over KOH. Air sensitive compounds were handled under nitrogen using Schlenk techniques or under helium in a glove box.

Nitrogen was purified by passing it through a column with manganese(II) oxide to remove oxygen followed by a column with molecular sieves to remove water.

Chromatography was performed using silica which had been degassed under dynamic vacuum over night and was stored under nitrogen. Elution was done with increasing polarity in the order hexane, methylene chloride/hexane, methylene chloride, ether/hexane, ether and thf.

NMR samples of air sensitive compounds were prepared by vacuum transfer of the deuterated solvent on a diffusion pump followed by flame sealing of the tube. Alternatively, deuterated solvent was added in the glove box using a Young® NMR tube with teflon stopcock.

7.4. Literature Procedures

The following compounds were synthesized according to literature procedures: pentamethylcyclopentadiene (Cp^*-H),[6] cyclopentadienyl-dicarbonyl-cobalt(I) ($CpCo(CO)_2$, pentamethylcyclopentadienyl-dicarbinyl-cobalt(I) ($Cp^*Co(CO)_2$),[7]cyclopentadienyl-sodium (NaCp), tetramethyl-trifluoromethyl-cyclopentadienyl-cobalt(I)dicarbonyl ($Cp^‡Co(CO)_2$)[8], bistolan[9].

7.5. Diazomethane

Caution: Pure Diazomethane is potentially explosive. It should therefore never be isolated as a pure substance but always kept diluted in ether solution.

In a 500 ml round bottom flask equipped with a dropping funnel and a distillation column with a long glass tubing on the other side 11 g of potassium hydroxide were dissolved in 9 ml of water. Then 60 ml of 2,2-methoxy-ethoxyethanol and 12 ml of diethylether ether were added. Then 32 g of N-methyl-N-nitroso-p-toluenesulfonamide (Diazald®) were dissolved in 200 ml of diethylether and placed in the dropping funnel. A receiving Schlenk containing potassium hydroxide pellets was connected to the other end of the distillation column such that the glass tubing at the end of the distillation column extended down to one inch above the bottom of the Schlenk. The receiver flask was then cooled with a NaCl/ice bath. The solution in the round bottom flask was then heated until reflux was observed at which point the diazald solution was dropwise added to the round bottom flask. The drop rate was adjusted such that a constant gas evolution took place and a constant overpressure was maintained in the round bottom flask. Adding all of the diazald solution normally took about one hour. If all diazald was added, heating was continued until no more ether distilled over. At that point the receiver Schlenk, in which a yellow solution of diazomethane in ether had been collected, was removed from the system and stored in the freezer over night.

The next morning the Schlenk with the diazomethane solution was connected to a distillation bridge with a Schlenk containing anhydrous ether and potassium hydroxide pellets, cooled with dry-ice/iso-propanol as receiving vessel. The diazomethane solution was then stirred and allowed to warm to room temperature. In the course of an hour the ether in the receiving Schlenk turned yellow as the diazomethane transferred into the cooled Schlenk. Pulling a slight vacuum on the receiving Schlenk speeds up the transfer process. The distilled diazomethane solution can then be stored at - 78°C for several weeks.

^{13}C labeled diazomethene was synthesized by the same procedure from 0.45 g of Diazald®-^{13}C using a smaller version of the apparatus described above.

7.6. Diazoethane

Caution: Pure diazoethane is potentially explosive. It should therefore never be isolated as a pure substance but always kept diluted in solution.

An amount of 6 g KOH was placed in a Schlenk vessel and dissolved in 10 ml distilled water. Then 50 ml of ether were added and the solution cooled to -8 °C using ice/NaCl. After saturating the solution with nitrogen by pulling a brief vacuum and refilling with nitrogen, 1 g of 1-ethyl-1-nitroso-3-nitro-guanidine was added and the solution stirred for 3 h, maintaining a temperature below 0 °C. The orange ether phase was then transferred with a pipet into another Schlenk containing 5 g of KOH pellets. After standing at -78 °C over night that solution was used without further purification.

7.7. Mono- and Dinuclear Precursors

7.7.1. Cobalt(II)-hexamine Chloride $[Co(NH_3)_6]Cl_2$

In a wide bottom Schlenk vessel 20 g of Hexaquo-cobalt(II)-chloride, $[Co(H_2O)_6]Cl_2$ were suspended in saturated aqueous ammonia and stirred under slight heating for 2 h. The color turned from pink to dark blue and back to pink again. The suspension was then allowed to settle down and the ammonia above the solid was removed with a pipet. The residue was then washed by stirring with degassed methanol. The solid was again allowed to settle down and the methanol was pipetted off. Washing with methanol was repeated for three times and the residue dried under vacuum over night. The yield was 18 g of pink powder (93 % yield).

7.7.2. Cobaltocene

In a glove box, 13.5 g of cobalt(II)-hexamine-chloride, $[Co(NH_3)_6]Cl_2$ (58.2 mmol) were mixed with 12 g of cyclopentadienyl-sodium, CpNa (166.8) in a Schlenk. The Schlenk was taken out of the box, evacuated and refilled with nitrogen. Then 150 ml of dry tetrahydrofurane were added, resulting in a immediate gas evolution. The mixture was heated to reflux for two hours after which the solvent was removed under vacuum. The remainder was taken into the glove box and transferred into a 250 ml round bottom flask which was then equipped with a condenser. The residue was then sublimed at 80 °C and $< 10^{-4}$

torr onto a condenser at −10 °C, yielding 8.15 g (43 mmol) of pure product (74% of theoretical yield).

^{1}H NMR (C_6D_6) : -50.5 (s)

7.7.3. Cyclopentadienyl-cobalt(I) Bis-ethylene, $CpCo(C_2H_4)_2$ [10]

In a jacketed Schlenk which was connected to an ethylene tank and a vacuum line, 7.45 g of cobaltocene were dissolved in 200 ml of dried ether. Then a brief vacuum was pulled and refilled with ethylene. The solution was then stirred and cooled to -10 °C, maintaining 1 atm overpressure of ethylene. Over a period of three days 3-4 g of potassium were added in 0.5 g portions. The color changed from a deep red to a bright orange. At that point stirring was stopped and the precipitate allowed to settle down. The solution was then cannulated into another Schlenk which was precooled to -78 °C. Two thirds of the solvent were removed under vacuum without heating. Then hexane was added and the remaining ether was pulled off until crystallization began. After storing in the refrigerator under ethylene gas over night the remaining solution was pipetted off the crystallized product, yielding 4.5 g of crystalline product (63% theoretical yield) which was stored in the refrigerator under ethylene atmosphere.

7.7.4. Bis(pentamethylcyclopentadienyl-rhodium(III) dichloride), $(Cp^*RhCl)_2Cl_2$

Rhodium(III)chloride hydrate, $RhCl_3 \cdot 3H_2O$ (3.2 g, 12.2 mmol) were dissolved in 50 ml methanol and the solution was degassed by pulling a brief vacuum

and refilling with nitrogen. Then 3.2 ml (20.4 mmol) of pentamethylcyclopentadiene, Cp^*-H, were added and the solution heated to reflux for 20 h. Then the methanol was removed under vacuum and the residue redissolved in just the necessary amount of methylene chloride. Three times the amount of hexane was added and the solvent removed under vacuum to one third of its initial volume. The precipitation was completed by keeping the Schlenk in the freezer over night. The precipitate was filtered over a medium frit and washed with hexane to yield 3.1 g of $[Cp^*RhCl]_2Cl_2$ (83 % of theoretical yield).

^{1}H NMR ($CDCl_3$): 1.623

7.7.5. Bis(pentamethylcyclopentadienyl-iridium(III) dichloride), $(Cp^*IrCl)_2Cl_2$

In a Schlenk vessel 2.7 g (7.67 mmol) of iridium(III)chloride trihydrate, $IrCl_3 \cdot 3H_2O$ were dissolved in 30 ml methanol. The solution was heated to reflux to complete dissolving and 2.8 ml (26 mmol) of pentamethylcyclopentadien Cp^*-H were added with a syringe. Reflux was continued for 14 h, after which an orange precipitate has formed. The solution is cooled in the freezer to -20 °C, filtered through a medium frit and the residue washed with cold methanol. After drying in a desiccator under vacuum 2.15 g of $[Cp^*IrCl]_2Cl_2$ (70.4 % of theoretical yield) were obtained.

^{1}H NMR ($CDCl_3$): 1.595

7.7.6. Activated Zinc

In an erlenmeyer flask 20 g of granulated zincum metal (30 mesh) were suspended in dilute hydrochloric acid for about 10 minutes after which the acid was then poured off. The residue was then washed three times with distilled water, two times with methanol and twice with ether. The final product was dried under vacuum and stored in a Schlenk under nitrogen.

7.7.7. Pentamethylcyclopentadienyl-rhodium(I) Dicarbonyl, $Cp^*Rh(CO)_2$

A Pyrex high pressure bottle was loaded with 3.1 g of $(Cp^*RhCl)_2Cl_2$ (5.0 mmol). Then 50 ml of methanol were added and the solid dissolved. The bottle was placed in a low pressure hydrogenator which was connected to a carbon monoxide tank. The solution was pressurized to 40 psi of carbon monoxide and stirred for 1 h at room temperature to saturate the solution. Then 1 g of activated zinc was added, the solution repressurized and stirring was continued. Three more additions of 1 g of Zn were made over the next 18 h. Then the methanol was removed under vacuum using a rotary evaporator. The residue was dissolved in methylene chloride and washed with distilled water to break up zinc adducts. The aqueous phase was then again extracted with methylene chloride. The organic phases were combined and the solvent removed under vacuum. The residue purified by column chromatography. Elution with hexane yielded 1.1 g of the desired dicarbonyl.

Subsequent elution with methylene chloride and then ether yielded some small amounts of di- and trinuclear side products. Further elution with methanol yielded 980 mg of starting material.

^{1}H NMR (C_6D_6): 1.735

7.7.8. Pentamethylcyclopentadienyl-iridium(I)-dicarbonyl, $Cp^*Ir(CO)_2$, Method 1

In a glove box, 1.35 g of $(Cp^*IrCl)_2Cl_2$ (1.69 mmol) were mixed with 2.4 g of triirondodecacarbonyl ($Fe_3(CO)_{12}$). The mixture was taken out of the box and dissolved in 20 ml of degassed benzene. The solution was heated to reflux for 22 h, after which a yellow color could be observed in the benzene condensing on the reflux condenser. An about equal amount of hexane was added and the solvent slowly removed under vacuum. Some product will be lost due to codistillation with the benzene. That amount can be minimized by adding the hexane and by not warming the solution while removing the solvent. The residue was sublimed onto a cold finger yielding 650 mg of yellow product (50 % yield).

^{1}H NMR (C_6D_6): 1.779

7.7.9. Pentamethylcyclopentadienyl-iridium(I)-dicarbonyl, $Cp^*Ir(CO)_2$, Method 2[11]

This procedure is similar to the one described above for $Cp^*Rh(CO)_2$. However, methylene chloride is used as solvent and an excess of 12 g of zinc metal were added in one portion.

7.7.10. Carbon-13 labled Pentamethylcyclopentadienyl-rhodium(I)dicarbonyl, $Cp^*Rh(^{13}CO)_2$

In a Schlenk vessel 400 mg of dicarbonyl were dissolved in methylene chloride. A flask containing 1 liter ^{13}CO gas was connected as shown below:

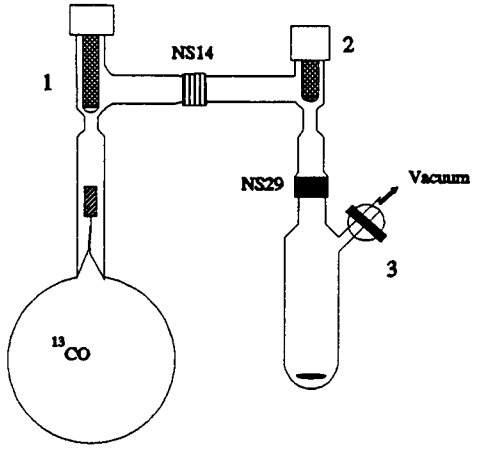

With valve 1 closed, the solution was frozen in liquid nitrogen and the system evacuated for five minutes. Then valve 3 was closed and the solution was allowed to warm to room temperature. The glass seal on the CO bulb was then shattered by lifting the metal weight with a magnet and allowing it to fall onto the tip of the seal. Then valve 1 was opened and the solution stirred under ^{13}CO atmosphere for 3 days. In 24h intervals samples were taken with a syringe through valve 3 (which was sealed with a septum) and analyzed by mass spectrometry to monitor the progress of the reaction. Eventually the bulb containing the ^{13}CO gas was cooled in liquid nitrogen to condense excess ^{13}CO from the Schlenk back into the bulb. Valve 1 was then closed and the Schlenk disconnected from the system.

The final enrichment was 81% (65% $Cp^*Rh(^{13}CO)_2$, 31.5% $Cp^*Rh(^{13}CO)(^{12}CO)$ and 3.4% $Cp^*Rh(^{12}CO)_2$).

7.8. Unsaturated Trinuclear 46e⁻ Complexes

7.8.1. Pentamethylcyclopentadienyl-rhodium(I)-bis(cyclopentadienyl-cobalt(I))-di-μ_3-carbonyl, $Cp^*Rh(CpCo)_2(\mu_3\text{-}CO)_2$ (2)

In a glove box 800 mg of pentamethyl-cyclopentadienyl-rhodium(I) dicarbonyl (2.72 mmol) were placed in a Schlenk vessel and dissolved in 20 ml of ether. Then 1100 mg of cyclopentadienyl-cobalt(I)-bisethylene (6.1 mmol) in 20 ml hexane were filtered through a pipette with cotton plug into the solution containing the dicarbonyl, resulting in immediate precipitation. The solution was stirred for about five minutes with repeatedly pulling a brief vacuum, until only $^1/_3$ of the initial solvent is left. The solution is filtered through a medium frit and the residue washed with hexane, resulting in 1200 mg of $Cp^*Rh(CpCo)_2(CO)_2$ (81% yield).

^1H NMR (C_6D_6): 3.67 (s, 10 H, Cp), 0.33 (s, 15 H, Cp^*).

7.8.2. Pentamethylcyclopentadienyl-iridium(I)-bis(cyclopentadienyl-cobalt(I))-di-μ_3-carbonyl, $Cp^*Ir(CpCo)_2(\mu_3\text{-}CO)_2$ (1)

In a glove box 740 mg of pentamethyl-cyclopentadienyl-iridium(I)-dicarbonyl were placed in a Schlenk vessel and dissolved in 20 ml of ether. Then

a solution of cyclopentadienyl-cobalt(I)bis-ethylene were filtered through a pipette with a cotton plug into the solution containing the dicarbonyl. A brief vacuum was pulled and the solution stirred for five minutes during which time a precipitate had formed. The solution was then concentrated to 1/3 of its original volume and filtered through a medium frit. After washing the precipitate with hexane 973 mg of trinuclear complex (73% yield) were obtained.

^{1}H-NMR (C_6D_6): -23, -46

7.8.3. Tris(cyclopentadienyl-cobalt(I))-di-μ_3-carbonyl, $(CpCo)_3(\mu_3\text{-}CO)_2$ (5)

In a glove box, 470 mg of cyclopentadienylcobalt(I)dicarbonyl ($CpCo(CO)_2$) (2.6 mmol) was dissolved in 10 ml of hexane. To that solution, 1000 mg of cyclopentadienylcobalt(I)bis-ethylene ($CpCo(C_2H_4)_2$) in 25 ml hexane were added by filtration through a pipet with cotton plug. Then a vacuum was pulled until only half of the solvent was left. The red-brown solution turned black and a precipitate was observed which was collected on a medium frit. After washing with hexane 1 g of product was obtained (90.5% yield).

7.8.4. (Trifluoromethyl-tetramethyl)-cyclopentadienyl-cobalt(I)-bis(cyclopentadienyl-cobalt(I))-di-μ_3-carbonyl, $Cp^{\ddagger}Co(CpCo)_2(\mu_3\text{-}CO)_2$, (4)

The procedure is analogous to the one described above for $(CpCo)_3(\mu_3\text{-}CO)_2$ was followed. 600 mg of $Cp^{\ddagger}Co(CO)_2$ (1.97 mmol) were reacted with

710 mg of $CpCo(C_2H_4)_2$ to yield 310 mg of a mixture of the desired product with dinuclear and tetranuclear cluster complexes.

^1H NMR (C_6D_6): 10.0 (6H, $Cp^{\ddagger}$-CH_3); -5.4 (6H, $Cp^{\ddagger}$-CH_3); -18.5 (10H, Cp).

7.9. General Procedures for Diazoalkane Reactions

7.9.1. Cp^* Containing Cluster Complexes

In the glove box, typically between 200-500 mg of cluster complex (Rh^*Co_2, Ir^*Co_2 or Co^*Co_2) were dissolved in ether, taken out of the box and hooked up to a vacuum/nitrogen line and to a bubbler. The solution was frozen in liquid nitrogen and the Schlenk evacuated and refilled with nitrogen. Then an ether solution of the diazoalkane at -78° C (dry ice/iso-propanol) was transferred onto the frozen solution with a teflon hose. Another brief vacuum was pulled and after refilling with nitrogen the valve to the bubbler was opened and the solution allowed to warm. After stirring for 5-10 min the solvent was removed under vacuum and the mixture separated by liquid chromatography unless stated differently.

7.9.2. All CpCo and $Cp^{\ddagger}$ Containing Cluster Complexes

The procedure for Co_3 and $Co^{\ddagger}Co_2$ is similar to the one described above, but the cluster complexes are not dissolved in ether prior to reaction but the diazoalkane solution is transferred directly onto the solid material kept at liquid nitrogen temperature.

7.9.3. Reaction of $Cp_3Co_3(\mu_3\text{-}CO)_2$ with Diazomethane

Two products were isolated from that reaction mixture in about equal amounts :

a) Tris-cyclopentadienyl-tri-cobalt(I)-bis(μ^2-carbonyl)-μ^2-carbene, $(CpCo)_3(\mu\text{-}CO)_2(\mu\text{-}CH_2)$, **6**: Elution with hexane/$MeCl_2$ 1:5 as a red-brown solution.

b) Tris-(cyclopentadienylcobalt(I))-(μ_3-carbonyl)-(μ_3-N-diazomethane) $(CpCo)_3(\mu_3\text{-}CO)(\mu_3\text{-}NNCH_2)$, **9**: Elution with hexane/ether yields a green-brown band.

Spectroscopic data for **6** and **9**: Table 2.2.

7.9.4. Reaction of $(CpCo)_3(\mu_3\text{-}CO)_2$ with Diazoethane:

Two identified products were isolated from that reaction:

a) Bis-cyclopentadienyl-dicobalt-di-μ_2-carbonyl-μ_2-ethylidene, $(CpCo)_2\text{-}(\mu_2\text{-}CO)_2(\mu_2\text{-}CHMe)$: Elution with methylene chloride/hexane yields a red brown band.

^{1}H-NMR (C_6D_6) : 8.27 (q, J_{HH} = 7.2 Hz, 1 H, CHMe), 4.615 (s, 10 H, Cp), 2.34 (d, J_{HH} = 7.2 Hz, 3 H, $CHCH_3$).

b) Tris-cyclopentadienyl-tris-cobalt(I)-(μ_3-carbonyl)-(μ_3-N-diazoethane), $(CpCo)_3(\mu_3\text{-}CO)(\mu_3\text{-}NNCHMe)$ **13**: The major product of this reaction is the hydrazone adduct which is eluted from the column with a mixture of ether and hexane. Spectroscopic data: see Table 2.5.

7.9.5. Reaction of $Cp^*Co(CpCo)_2(\mu_3\text{-}CO)_2$ (3) with Diazomethane

Three characterized fractions were obtained from this reaction :

a) Elution with methylene chloride yielded a yellow-brown band which was identified as the tricarbonyl $Cp^*Co(CpCo)_2(\mu\text{-}CO)_3$: ^{1}H-NMR (C_6D_6) : 4.62 (s, 10 H, Cp), 1.40 (s, 15 H, Cp^*); ^{13}C-NMR (C_6D_6) : 256 (CO), 101.7 (Cp^*-C), 87.7 (Cp), 8.1 (Cp^*-CH_3).

b) Elution with hexane/ether 4:1 yielded 60 mg of the hydrazone adduct $Cp^*Co(CpCo)_2(\mu_3\text{-}CO)(NNCH_2)$ as brown solution.

Spectroscopic data: Table 2.4.

c) Elution with hexane/ether 1:5 yielded a yellow-brown band which is the oxo adduct $Cp^*Co(CpCo)_2(\mu_3\text{-}CO)(\mu_3\text{-}O)$.

Spectroscopic data: Table 5.1.

7.9.6. Reaction of $Cp^‡Co(CpCo)_2(\mu_3\text{-}CO)_2$ (4) with Diazomethane

Several fractions were obtained after chromatography of the reaction mixture. The only identified product was the hydrazone adduct $Cp^‡Co(CpCo)_2(\mu_3\text{-}CO)(\mu_3\text{-}NNCH_2)$ (**12**).

Spectroscopic data: Table 2.4.

7.9.7. Reaction of $Cp^*Rh(CpCo)_2(\mu_3\text{-}CO)_2$ (2) with diazomethane

Two products were isolated from that reaction :

a) Pentamethylcyclopentadienylrhodium(I)-bis(cyclopentadienylcobalt(I)-μ_2-methylene-di(μ_2-carbonyl) ($Cp^*Rh(CpCo)_2(\mu_2\text{-}CO)_2(\mu_2\text{-}CH_2)$): From a 377 mg batch of $Cp^*Rh(CpCo)_2$ elution with CH_2Cl_2/hexane gave a reddish-brown band of containing 85 mg of the carbene adduct **7a.**
Elemental analysis: C: 49.63 % (calc. 49.66 %); H: 4.86 % (calc. 4.85 %).
Spectroscopic data: Table 2.4.

b) Pentamethylcyclopentadienylrhodium(I)-bis(cyclopentadienylcobalt(I)-μ_3-N-diazomethane-μ_3-carbonyl, $Cp^*Rh(CpCo)_2(\mu_3\text{-}CO)(\mu_3\text{-}NNCH_2)$: Elution with ether/hexane yielded 90 mg of the hydrazone adduct as a green-brown solution.
Elemental analysis: C 45.91 % (calc. 47.50 %); H: 4.78 % (calc. 4.89 %); N: 4.43 % (calc. 5.04 %).
Spectroscopic data: Table 2.4.

7.9.8. Reaction of $Cp^*Rh(CpCo)_2(\mu_3\text{-}CO)_2$ (2) with Diazoethane: $Cp^*Rh(CpCo)_2(\mu_3\text{-}CO)(\mu_3\text{-}NNCHCH_3)$

A reaction involving 300 mg of Rh^*Co_2 yielded exclusively the hydrazone adduct. After recrystalization 70 mg of pure product were isolated. Spectroscopic data: Table 2.5.

7.9.9. Reaction of $Cp^*Ir(CpCo)_2(\mu_3\text{-}CO)_2$ with Diazomethane : Pentamethyl-cyclopentadienyliridium(I)-bis(cyclopentacarbonylcobalt(I))μ-methylidene-bis(μ-carbonyl), $Cp^*Ir(CpCo)_2(\mu_2\text{-}CO)_2(\mu_2\text{-}CH_2)$

Elution with hexane/ether 1:1 as brown solution. A batch of 550 mg **1** typically yielded 200 mg of $Cp^*Ir(CpCo)_{2(\mu}2\text{-}CO)_2(\mu_2\text{-}CH_2)$ (36 % of theoretical yield).

Spectroscopic data: Table 2.4.

Elemental analysis : C: 42.72 % (calc. : 42.79 %); H: 4.27 % (calc. 4.22 %).

7.9.10. Reaction of $Cp^*Ir(CpCo)_2(\mu_3\text{-}CO)_2$ with Diazoethane

The presence of the hydrazone adduct in the reaction mixture compound was established by NMR spectroscopy. Purification by chromatography required polar solvent mixtures like thf/methanol in order to elute significant amounts of material. It appears that the hydrazone adduct decomposes under these conditions.

Spectroscopic data: Table 2.5.

7.10. Pentamethylcyclopentadienyl-iridium(I)-bis(cyclopentadienyl-cobalt(I))μ_3-(methylidyne)-(μ_3-carbonyl)(μ_2-hydride), $Cp^*Ir(CpCo)_2(\mu_3\text{-}CO)(\mu_3\text{-}CH)(\mu_2\text{-}H)$.

200 mg of the carbene complex **8** (0.31 mmol) were dissolved in toluene and heated under reflux for 2h. After removal of the solvent the resulting

product was purified by chromatography. Elution with ether/hexane yielded 141 mg of the carbyne-hydride complex (74% yield).

Spectroscopic data: Table 2.9.

Elemental analysis : C: 42.98 % (cal. 42.79 %); H: 4.50 % (calc. 4.22 %).

7.11. Reaction of $Cp^*Ir(CpCo)_2(\mu_3\text{-}CO)(\mu_3\text{-}CH)(\mu_2\text{-}H)$ (18) with Tolyacetylene: Formation of 1,3,4- and 1,3,5-Tristolylbenzene

In a Schlenk, 20 mg of carbyne-hydride complex **18** (0.03 mmol) were dissolved in toluene. 20 μl of tolylacetylene (0.17 mmol, 6-fold excess) were added and the solution heated to reflux. As soon as reflux was observed, heating was stopped immediately and the solution allowed to cool to room temperature. Chromatography yielded only tristolyl benzene, but no fraction containing any metal complex was eluted. However, there was a black residue left on top of the column which did not move even with the most polar solvent.

No attempt was made to further separate the 1,3,5 and 1,3,4 isomers of tristolylbenzene.

Spectroscopic data: ^{1}H NMR 7.758 (s), 7.65-7.55 (various m), 7.48 (d), 7.29 (m), 7.14-7.0 (m), 2.435 (s, Me-1,3,5), 2.42, 2.343, 2.340 (s, 1,3,4). ^{13}C: 142.2(s), 140.8(s), 140.0(s), 1392 (s), 138.8 (s), 138.4 (s), 138.3(s), 137.8 (s), 137.2 (s), 137.1 (s), 136.1 (s), 136.0 (s), 131.1 (d), 129.7 (d), 129.68 (d), 129.5 (d), 129.2 (d), 128.7 (d), 128.6 (d), 127.2 (d), 126.9 (d), 125.7 (d), 124.6 (d), 21.11 (q), 21.10 (q). MS (EI): 348 (100%, M^+, 333 (7%, -CH_3), 318 (8%, -2 CH_3), 030 (5%, -3 CH_3).

7.12. Reaction of $Cp_*Rh(CpCo)_2(\mu_3\text{-}CO)_2$ and $Cp^*Ir(CpCo)_2(\mu_3\text{-}CO)_2$ with Acetylene

In a glove box, the trinuclear cluster complex was placed in a Schlenk and dissolved in ether. The Schlenk was taken out of the box and connected to an acetylene tank and a vacuum line. A brief vacuum was pulled and the Schlenk refilled with acetylene. The solution was stirred for 5 minutes after which the solvent was removed under vacuum. The product was then purified by column chromatography.

7.12.1. Pentamethylcyclopentadienyl-iridium(I)-bis(cyclopentadienyl-cobalt(I))-(μ_3-carbonyl)-μ_3-acetylene, $Cp^*Ir(CpCo)_2(\mu_3\text{-}CO)\mu_3,\eta_2\text{-}(HC{\equiv}CH)$

a) Elution with ether/hexane yielded a red-brown band. A batch of 300 mg $Cp^*Ir(CpCo)_2(\mu_3\text{-}CO)_2$ yielded 50 mg of $Cp^*Ir(CpCo)_2(\mu_3\text{-}CO)(\mu_3\text{-}HCCH)$ after recrystallization.

Spectroscopic data: Table 3.1.

b) Minor amounts of a second compound were isolated from this column (ether/hexane) which is most likely a derivative of a dinuclear adduct:

Spectroscopic data: Table 3.3.

7.12.2. Pentamethylcyclopentadienyl-rhodium(I)-bis(cyclopentadienyl-cobalt(I))-(μ_3-carbonyl)-μ_3-acetylene, $Cp^*Rh(CpCo)_2$-(μ_3,η_2-HC≡CH)

Used: 300 mg of Rh^*Co_2. Elution with ether/hexane (40:60) yielded a green-brown fraction from which 152 mg of Rh*Co2(HCCH) were isolated. Elemental analysis: C 51.07% (calc. 51.16%); H 5.11% (calc. 5.00%). Spectroscopic data: Table 3.1.

7.13. Reaction of $Cp^*Rh(CpCo)_2(\mu_3\text{-}CO)_2$ (25), $Cp^*Rh(CpCo)_2(\mu_3\text{-}CO)_2$ (2) and $Cp^*Ir(CpCo)_2(\mu_3\text{-}CO)_2$ (1) with Tolylacetylene

Several hundred milligrams of cluster complex were dissolved in ether. The Schlenk was taken out of the box and the solution frozen in liquid nitrogen. A brief vacuum was pulled, and under nitrogen purge a fivefold excess of the alkyne added to the frozen solution with a syringe. After pulling another vacuum and refilling with nitrogen the solution was thawn and stirred for five minutes. The solvent was then removed under vacuum and the crude product purified by column chromatography. Typical yields were in the range of 50-70%.

7.13.1. Pentamethylcyclopentadienyl-iridium(I)-bis-(cyclopentadienyl-cobalt(I))-(μ_3-carbonyl)-μ_3-tolylacetylene, $Cp^*Ir(CpCo)_2$-(μ_3-CO)(μ_3,η^2-Tol-C≡CH) (23)

Used 560 mg 1. Elution with ether/hexane yielded 250 mg of green-brown product.

Elemental analysis: C 49.82% (calc. 50.07); H 4.57% (calc. 4.62%).

Spectroscopic data: Table 3.4.

7.13.2. Pentamethylcyclopentadienyl-rhodium(I)-bis(cyclopentadienyl-cobalt(I))-(μ_3-carbonyl)-(μ_3,η^2-tolylacetylene, $Cp^*Rh(CpCo)_2(\mu_3\text{-}CO)(\mu_3,\eta^2\text{-}Tol\text{-}C{\equiv}CH)$ (24)

Elution with ether/hexane yielded 108 mg green-brown product.

Elemental analysis: C 56.98% (calc. 57.19%); H 5.35% (calc. 5.24%).

Spectroscopic data: Table 3.4.

7.13.3. Pentamethylcyclopentadienyl-cobalt(I)-bis(cyclopentadienyl-cobalt(I))-(μ_3-carbonyl)-(μ_3,η^2-tolylacetylene, $Cp^*Co(CpCo)_2(\mu_3\text{-}CO)(\mu_3,\eta^2\text{-}Tol\text{-}C{\equiv}CH)$ (25)

Used 187 mg of Co^*Co_2. Elution with CH_2Cl_2/hexane yielded 40 mg of a brown band which was identified as $Cp^*Co(CpCo)_2(CO)_3$. Further elution with ether/hexane yielded a red-brown band from which 60 mg of desired alkyne adduct **25** were isolated.

Spectroscopic data: Table 3.4.

7.13.4. (Tetramethyl-trifluoromethyl)cyclopentadienyl-cobalt(I)-bis-(cyclopentadienyl-cobalt(I))-(μ_3-carbonyl)-(μ_3,η^2-tolylacetylene), $Cp^{\ddagger}Co(CpCo)_2(\mu_3\text{-}CO)(\mu_3,\eta^2\text{-}Tol\text{-}C{\equiv}CH)$ (27)

Separation with ether/hexane yielded the desired adduct and the tetranuclear complex $Cp^{\ddagger}(CpCo)_3(CO)_2$ which is already present in the starting material.

Spectroscopic data: Table 3.4.

7.14. Reaction of $Cp^*Rh(CpCo)_2(\mu_3\text{-}CO)_2$ (2) and $Cp^*Ir(CpCo)_2(\mu_3\text{-}CO)_2$ with Diphenylacetylene (Bistolan) and Bistolylacetylene

In a glove box the cluster complex was dissolved in ether. A solution of a three- to fivefold excess of the alkyne in ether was added and the solution stirred for several hours. The progress of the reaction was followed by periodically removing the solvent under vacuum and taking a NMR spectrum of the mixture. After six hours no starting material was left and the mixture was purified by chromatography. Typical yields in that reaction were around 10%.

7.14.1. Pentamethylcyclopentadienyl-iridium(I)-bis-(cyclopentadienyl-cobalt(I))-μ_3-carbonyl-μ_3-diphenylacetylene, $Cp^*Ir(CpCo)_2(\mu_3\text{-}CO)(\mu_3,\eta^2\text{-}PhC{\equiv}CPh)$ (29)

Spectroscopic data: Table 3.8.

7.14.2. Pentamethylcyclopentadienyl-iridium(I)-bis-(cyclopentadienyl-cobalt(I))-(μ_3-carbonyl)-μ_3,η^2-bistolylacetylene, $Cp^*Ir(CpCo)_2(\mu_3\text{-}CO)(\mu_3,\eta^2\text{-}TolC{\equiv}CTol)$ (30)

Spectroscopic data: Table 3.8.

7.14.3. Pentamethylcyclopentadienyl-rhodium(I)-bis-(cyclopentadienyl-cobalt(I))-(μ_3-carbonyl)-μ_3-diphenylacetylene, $Cp^*Rh(CpCo)_2(\mu_3\text{-}CO)(\mu_3,\eta^2\text{-}PhC{\equiv}CPh)$ (31)

a) The mixture contained alkyne adduct **31** and the tricarbonyl $Cp^*Rh(CpCo)_2(\mu_2\text{-}CO)_3$ in a ratio of about 2:1. 50 mg of adduct were isolated from a 300 mg batch of **2** by eluting with CH_2Cl_2.

Spectroscopic data: Table 3.8.

b) A minor side product was eluted with hexane/ether which is due to a species containing two Cp^*Rh fragments:

^1H NMR (C_6D_6): 7.50 (d, 2H); 7.42 (d, 2H); 7.28 (t, 2H); 7.08 (t, 1H); 6.93 (t, 2H); 6.85 (t, 1H); 1.52 (s, 15H); 1.42 (s, 15H). IR (KBr): MS (EI): 532 ($[Cp^*Rh(CO)]_2^{\cdot+}$); 373 ($[Cp^*RhCp^*]^{\cdot+}$.

7.14.4. Pentamethylcyclopentadienyl-rhodium(I)-bis-(cyclopentadienyl-cobalt(I))-(μ_3-carbonyl)-μ_3-bistolylacetylene, $Cp^*Rh(CpCo)_2(\mu_3\text{-}CO)(\mu_3,\eta^2\text{-}TolC{\equiv}CTol)$ (32)

A batch of 225 mg **2** yielded about 20 mg adduct.

Spectroscopic data: Table 3.8.

7.15. Formation of μ_3-oxo Adducts:

Microcrystalline samples of the trinuclear 46e$^-$ cluster complexes **1** and **2** were exposed to air at room temperature under the exclusion of light for a couple of weeks. After that time the starting material was gone and oxo adduct was observed as main product. The same reaction was observed in the glove box at a smaller rate over a period of several month indicating traces of oxygen present in the box atmosphere.

7.15.1. Pentamethylcyclopentadienyl-iridium(I)-bis(cyclopentadienyl-cobalt(I))(μ_3-carbonyl)(μ_3-oxo), $Cp^*Ir(CpCo)_2(\mu_3\text{-}CO)(\mu_3\text{-}O)$

Elemental analysis: C 40.60 % (calc. 40.72 %); H 3.97 % (calc. 4.04 %).

Spectroscopic data: Table 5.1.

7.15.2. Pentamethylcyclopentadienyl-rhodium(I)-bis(cyclopentadienyl-cobalt(I))(μ_3-carbonyl)(μ_3-oxo), $Cp^*Rh(CpCo)_2(\mu_3\text{-}CO)(\mu_3\text{-}O)$

Spectroscopic data: Table 5.1.

7.16. Scission Reactions

Around 200 mg of the alkyne adduct $Cp^*Ir(CpCo)_2(\mu_3\text{-}CO)(\mu_3\text{-}Tol\text{-}C{\equiv}CH)$ (**23**), $Cp^*Co(CpCo)_2(\mu_3\text{-}CO)(\mu_3\text{-}Tol\text{-}C{\equiv}CH)$ (**25**) or $(CpCo)_3(\mu_3\text{-}CO)(\mu_3\text{-}Ph\text{-}C{\equiv}CH)$ (**28**) were dissolved in decahydronaphtalene ("decalin") and heated under reflux for 30 (**28**) or 48 h (**23** and **25**). The reaction mixture was then separated

by chromatography. Only the all-CpCo complex **28** yielded a bis-carbyne complex, whereas for the Cp*M containing complexes only starting material was recovered.

7.16.1. Tris-(cyclopentadienyl-cobalt(I))-μ_3-methylidyne-μ_3-phenylmethylidyne, (μ_3-PhC)(CpCo)$_3$(μ_3-CH) (35).

A batch of 250 mg of tris-(cyclopentadienylcobalt(I))-phenylacetylene (CpCo)$_3$(μ_3-CO)(η^2,μ_3-Ph-C≡CH) (0.50 mmol) yielded 126 mg of product (53 % yield) after elution with hexane/ether 9:1. More product was eluted as a 3:1 mixture together with some tetranuclear alkyne adduct (CpCo)$_4$(μ-CO)(Ph-C≡CH) as a continuation of the this fraction. Final elution with ether/hexane 1:1 yielded a small amount of starting material.

Spectroscopic data for **35**:

^{1}H NMR (C_6D_6): 18.63 (s, 1H, μ_3-CH); 8.35 (d, J_{HH} = 7.3 Hz, 2H, o-Ph-H); 7.48 (t, J_{HH} = 7.3 Hz, 2H, m-Ph-H); 7.36 (t, J_{HH} = 7.3 Hz, 1H, p-Ph-H); 4.39 (s, 15H, Cp). ^{13}C NMR (CD_2Cl_2): 332.5 (s, μ_3-CPh); 326.5 (d, $^1J_{CH}$=169.4 Hz, μ_3-CH); 167.3 (s, ipso-Ph-C); 127.7 (d, $^1J_{CH}$ = 158.7 Hz, m-Ph-CH); 127.4 (d, $^1J_{CH}$ = 159.7 Hz, o-Ph-CH); 125.5 (d, $^1J_{CH}$ = 160.2 Hz, p-Ph-CH); 83.56 (d, Cp). MS: 474 (M^+); 189 ($Cp_2Co^{\cdot+}$).

Spectroscopic data for (CpCo)$_4$(CO)(Ph-C≡CH):

^{1}H NMR (C_6D_6): 10.84 (s, ≡CH), 7.2-6.8 (m, Ph), 4.32 (s, Cp). MS (EI): 598 (M^+)

7.17. References

1. Patt, S.; Shoolery, J. N.; *J. Magn. Res.* **1982**, *46*, 535-539.

2. a) Van Geet, A. L.; *Anal. Chem.* **1968**, *40*, 2227-2229. b) Van Get, A. L.; *Anal. Chem.* **1970**, *42*, 679-680.

3. Derome, A.; *Modern NMR Techniques in Chemistry Research*; First Edition, Pergamon Press, **1987.**

4. Braun, S.; Kalinowski, H.-O.; Berger, S.; *100 and More Basic NMR Experiments*, First Edition, Verlag Chemie **1996.**

5. Stephenson, D. S.; Binch, G.; *Quantum Chem. Progr. Exch.* **1978**, *32*, 145.

6. Threlkel, R. S.; Bercaw, J. E.; *J. Organomet. Chem.* **1977**, *136*, 1-5.

7. Beyers, L. R.; Uchtman, U. A.; Dahl, L. F.; *J. Am. Chem. Soc.* **1981**, *103*, 1942-51.

8. Vierkötter, S. A.; Ph. D. Thesis; Knoxville, May **1994.**

9. Nguyen, P.; Yuan, Z.; Agocs, L.; Lesley, G.; Marder, T. B.; *Inorg. Chim. Acta* **1994**, *220*, 289.

10. Jonas, K.; Deffense, E.; Habermann, D.; *Angew. Chem. Suppl.* **1983**, 1005-1016.

11. Ball, R. G.; Graham, W. A. G.; Heinekey, D. M.; Hoyano, J. K.; McMaster, A. D.; Mattson, B. M.; Michel, S. T.; *Inorg. Chem.* **1990**, *29*, 2023-2025.

APPENDIXES

APPENDIX 1:

Description of NMR Experiments

Carbon-13 T_1 measurements

The pulse program t1irdc.hf was used to measure ^{13}C NMR relaxation times :

```
;t1irdc.hf
;T1 measurement using inversion recovery
;decoupling during acquisition
;using average cycles

1 ze
  d11 s2 cpd
2 d1
3 p2 ph1
  vd
  p1 ph2
  go=2 ph31
  d1 iv wr #0  if #0 zd
  lo to 3 times l4
  d11 rf #0
  lo to 3 times l5
do
exit


ph1=0 2
ph2=0 0 2 2 1 1 3 3
ph31=0 0 2 2 1 1 3 3

;hl1: ecoupler high power level
;p1 :  90 degree transmitter high power pulse
;p2 : 180 degree transmitter high power pulse
;d1 : relaxation delay; 1-5 * T1
;d11: delay for disk I/O                              [30 msec]
;vd : variable delay, taken from vd-list
;l4 : number of values in vd list
;l5 : number of average cycles
;define VDLIST
;this pulse program produces a ser-file (PARMOD = 2D)
```

The standard inversion recovery pulse program was modified to allow to cycle through the vd list for several (l5) times in order to achieve a better long term stability of the experiment. A 180° pulse inverts all proton magnetization. During a variable delay vd the spins are relaxing back towards equilibrium. A 90° pulse then turns the remaining magnetization into observable magnetization in the x,y plane. Proton decoupling is employed throughout the experiment. The free induction decays obtained from that measurement are then stored in a serial file analogous to two dimensional data. A list containing the different delays (vd list)

can be created by typing **edlist vd** *name*. The parameter **vdlist** specifies the name used for the file containing the list with values of the delays vd. The delays in the vd-list were arranged randomly rather than increasing order to compensate for long term instabilities of the experiment. Relaxation delays were in the order of $2 \cdot T_1$ with vd ranging from 3 μs up to $5 \cdot T_1$, using one dummy scan per delay vd. Typical acquisition parameters :

	f2	f1
td	32k	12 (= l4 = number of variable delays)
sw (from 1D spectrum)	10 ppm	-
sfo1 (from 1D spectrum)	400.136245	-
d1	10s	-
ns	16	-
l4 (= td(f1))	12	-
p1	7.15 μs (90° ^{13}C)	-
p2	14.3 μs (180°^{13}C)	-
ds	1	
vdlist	*listname*	

For workup one fid is read from the serial file using the command **rser** *number*. After fourier transform the resulting spectrum a phase correction is performed like for a regular 1D spectrum and stored in the 2D spectrum using **[store 2D]**. Before processing the serial file the following processing parameters have to be set :

	f2	f1
mc2	-	QF
si	32k	16 (power of 2 ≥ td(f1))
lb	1	-
phmod	pk	no
sf	(from 1D spectrum)	-

The command **xf2** is the used to process the serial file with fourier transformation in only one dimension and **abs2** is used to perform an automatic baseline correction.

The resulting spectra are then evaluated using the t1-subroutine in UXNMR which is entered by clicking on **[T1/T2]**.

Type **edt1**, set number of experiments equal l4 (i.e. 12). Then the command **rspc** is used to read in the first one dimensional spectrum of the data set. The desired peaks are selected using the **[def. points]** option in the calibration menu and integration regions are defined as for a regular one dimensional spectrum. After returning to the T_1 window by clicking on **[T_1/T_2]**, peak picking and integration is performed on all spectra using the command **pd**. Finally, a three parameter fit is executed and the results printed by the command **dat1**.

Selective Inversion Transfer

Chemical exchange slow on the NMR chemical shift time scale was studied quantitatively with the selective inversion transfer recovery method using the pulse program irsel.hf :

```
;irsel.hf
;Selective inversion transfer recovery by using a selective
;low power decoupler pulse
; Frank-Holger Foersterling  Nov. 20 1992

hi2
1 ze
2 d1
  p2:d  ph1
  vd
  p1 ph2
  go=2 ph31
  d11 wr #0 if #0 iv
  lo to 1 times l4
exit
```

```
ph1=0 2
ph2=0 0 2 2 1 1 3 3
ph31=0 0 2 2 1 1 3 3

;hl1: ecoupler high power level
;dl0 : decoupler low power level
;p1 :  90 degree transmitter high power pulse
;p2 : selective 180 degree decoupler low power pulse
;d1 : relaxation delay; 1-5 * T1
;d11: delay for disk I/O                              [30 msec]
;vd : variable delay, taken from vd-list
;L4: l4 = number of experiments = number of delays in vd-list
;NS: 8 * n
;DS: 2 or 4
;td1: number of experiments
;define VDLIST
;this pulse program produces a ser-file (PARMOD = 2D)
```

A low power 180° pulse (dl0=30.5 dB, p2 = 5 ms on the QNP probe) is applied through the decoupler channel and selectively inverts one of the two exchanging resonances, in our case the carbyne or hydride resonance of **18.** During the variable delay vd chemical exchange causes the inversion to be transferred to the non irradiated resonance. Finally a high power 90° pulse is applied and the fid acquired.

Setup is similar to the T_1 experiments described above. Values of the variable delay ranged from 3 μs up to $5 \cdot T_1$. (l4=td[1]=12). The spectra were processed as described for T_1 measurements. However, output of the **dat1** command was directed into a text file by specifying a filename as current printer in the **edo** menu. That file was then transferred to a PC using ftp and data analysis was performed using nonlinear regression within Sigma Plot.

Kinetic Measurements

The pulse program kinet.hf was used to follow the course of a reaction by NMR :

```
;kinet.hf
;kinetic measurement without decoupling with constant delay between experiments.
```

```
1 ze
d11
2 d1
  p1 ph2
 go=2 ph31
  d11 wr #0 if #0
d5
lo to 1 times l4
d11
exit

ph1=0 2
ph2=0 0 2 2 1 1 3 3
ph31=0 0 2 2 1 1 3 3

;hl1: ecoupler high power level
;p1 :  90 degree transmitter high power pulse
;d1 : relaxation delay; 1-5 * T1
;d5 : delay between different experiments
;d11: delay for disk I/O                              [30 msec]
;l4 : number of experiments
;NS: 8 * n
;DS: 2 or 4
;td1: = l4 = number of experiments
;this pulse program produces a ser-file (PARMOD = 2D)
```

Setup of this experiment is analog to the selective inversion transfer experiment. No vd list is used but a fixed delay d5 is used. In order to use the t1 subroutine of UXNMR to process the data a variable delay list containing successive numbers from 0 to l4-1 was created and the status parameter **2s vdlist** was set to *vdlistname*. Workup and data transfer to a PC were then performed as described for the selective inversion transfer experiment. In Sigma Plot the time axis was then calculated according to $t = index\# \cdot (ns \cdot (d1 + aq) + d5)$.

Attached Proton Test (APT)

```
;apt.ta
;attached proton test
;using spin modulated spin echo

d20=1s/(cnst2)
d3=de


  d20 s2
1 ze
2 d1 cpd
  p1 ph1
```

```
  d20
  p2 ph2 do
  d20
  d3 cpd
  p2 ph3
 go=2 ph31
  wr #0
  d20 do

exit

ph1=0 2 2 0 1 3 3 1
ph2=1 3 3 1
ph3=1 3 1 3
ph31=0 2 2 0 1 3 3 1

;s2 : ecoupler power level for cpd decoupling
;p1 : 45(!) degree pulse
;p2 : 180 degree transmitter high power pulse
;p31 :90 degree pulse for cpd decoupling
;d1 : relaxation delay 1-2 T1
;d3 = de
;const2 = Jxh X, XH2 positive,  XH, XH3 negative
;ns : 4*n
;ds : 2 or 4
;cpd : cpd decoupling accourding to sequence defined by cpdprg
```

2-D NOE and exchange spectroscopy

```
;noesytp
;2D homonuclear correlation via dipolar coupling
;dipolar coupling may be due to noe or chemical exchange.
;phase sensitive using TPPI


;;d0=3u


1 ze
2 d1
3 p1 ph1
  d0
  p1 ph2
  d8
  p1 ph3
  go=2 ph31
  d1 wr #0 if #0 id0 ip1 zd
  lo to 3 times td1
exit

ph1=0 2
ph2=0 0 0 0 0 0 0 0
    2 2 2 2 2 2 2 2
ph3=0 0 2 2 1 1 3 3
ph31=0 2 2 0 1 3 3 1
     2 0 0 2 3 1 1 3


;hl1: ecoupler high power level
;p1 :  90 degree transmitter high power pulse
;d0 : incremented delay (2D)                          [3 usec]
```

```
;d1 : relaxation delay; 1-5 * T1
;d8 : mixing time
;in0: 1/(2 * SW) = DW
;nd0: 2
;NS: 8 * n
;DS: 2 or 4
;td1: number of experiments
;MC2:  TPPI
```

Typical acquisition parameters :

	f2	f1
td	2k	296
nd0	-	2
sw	9.612 ppm	9.612 ppm
sfo1	400.1368697	400.136897
d1	5s	-
d8	3s	-
ns	16	-
p1	7.7 μs (90° proton)	

The values for sw and sfo1 are obtained from a one dimensional spectrum. The mixing time d8 depends on the cross relaxation rate of the specific compound and can be in the range of 0.2 to 3 s.

Processing parameters:

	f2	f1
mc2	-	TPPI
si	1K	1K
wdw	qsine	qsine
ssb	2	2
phmod	pk	pk
sf		

xfb is used in order to execute a two dimensional fourier transform. An interactive phase correction in both dimensions is then performed such that the diagonal peaks appear positive. Cross peaks due to exchange then appear

positive, whereas cross peaks due to NOE are negative at room temperature and positive at 170 K. The commands **abs1** and **abs2** then are used for baseline correction. T_1 noise was reduced by saving a f2 partition (**[1D]** submenue, click with middle mouse button on **[f2-part]** and define a region along the entire f2-dimension of the spectrum with no signal in it) and subtracting it as baseline from the entire spectrum using the command **sub2**. Finally the spectrum was symmetrized using the command **syma**.

Inverse $^1H\{^{13}C\}$ correlation

```
;invbtp
;2D H-1/X correlation via heteronuclear zero and double quantum
;   coherence using BIRD sequence
;phase sensitive using TPPI
;with decoupling during acquisition
;A. Bax and S. Subramanian, J. Magn. Reson. 67, 565-569 (1986)


;;p2=p1*2
;;p4=p3*2
;;d0=3u
;;d2=1s/(cnst2*2)
;;d13=4u


1 ze
2 d1 do
3 p1 ph1
  d2 dhi
  (p2 ph1) (p4 ph4):d
  d2
  p1 ph2
  d7
  p3:d ph5
  p1 ph1
  d2
  p3:d ph6
  d0
  p2 ph3
  d0
  p3:d ph7
  d13
  d2 dlo
  go=2 ph31 cpd
  d1 do wr #0 if #0 id0 ip6 zd
  lo to 3 times td1
exit


ph1=0
ph2=2
```

```
ph3=0
ph4=0
ph5=0 0 0 0 2 2 2 2
ph6=0 2
ph7=0 0 2 2
ph31=0 2 2 0


;hl1: ecoupler high power level
;dl0: power level for dlo mode
;p1 :  90 degree transmitter high power pulse
;p2 : 180 degree transmitter high power pulse
;p3 :  90 degree decoupler high power pulse
;p4 : 180 degree decoupler high power pulse
;p31: 90 degree pulse for slave timer (cpd-sequence)
;d0 : incremented delay (2D)                    [3 usec]
;d1 : relaxation delay; 1-5 * T1
;d2 : 1/(2J)XH
;d7 : delay for inversion recovery
;     optimize to give null for protons bound to C-12
;d13: short delay (e.g. to compensate delay line)     [3 usec]
;in0: 1/(4 * SW(X)) = (1/2) DW(X)
;nd0: 4
;NS: 4 * n
;DS: 2 or 4
;td1: number of experiments
;MC2: TPPI
;cpd: cpd-decoupling according to sequence defined by cpdprg
```

APPENDIX 2:

Input format for DNMR5

```
C     INPUT IS AS FOLLOWS                                                DNMR  15
C     1.   TEXT                                              (8A10)      DNMR  16
C        PROBLEM NAME, IF FIRST FIELD BLANK THEN END OF RUN              DNMR
C     2.   N,NE,MU,NMES,NSYM                                 (5I2)       DNMR  18
C          N=NUMBER OF NUCLEI                                            DNMR  19
C          NE=NUMBER OF NUCLEAR CONFIGURATIONS                           DNMR  20
C          MU=1 FOR MUTUAL EXCHANGE,=0 OTHERWISE                         DNMR  21
C          NMES=NUMBER OF SETS OF MAGNETICALLY EQUIVALENT NUCLEI,        DNMR  22
C          NMES MUST INCLUDE ALL SETS OF MAGNETICALLY EQUIVALENT         DNMR  23
C          NUCLEI EVEN THE TRIVIAL SETS CONTAINING ONLY ONE NUCLEUS      DNMR  24
C          THUS IF THE OPTION IS NOT TO BE USED THEN NMES=N              DNMR  25
C          NSYM=NUMBER OF SYMMETRY PAIRS. A SYMMETRY PAIR IS DEFINED     DNMR  26
C          AS TWO NUCLEI RELATED BY PERMUTATION SYMMETRY.                DNMR  27
C          NSYM=0 IF NO SYMMETRY                                         DNMR  28
C          NOTE.  THE SYMMETRY AND MAGNETIC EQUIVALENCE OPTIONS          DNMR  29
C          CANNOT BE USED SIMULTANEOUSLY                                 DNMR  30
C     3.   ITMAX,SETOUT,SCAF                              (I5,2F10)      DNMR  31
C          ITMAX=MAXIMUM NUMBER OF ITERATIONS, IF BLANK THEN SET EQUAL   DNMR  32
C          TO 10. IF ITMAX.LT.0 THEN SIMULATION ONLY                     DNMR  33
C          SETOUT=RATIO(REDUCTION IN ERROR/ERROR) AT WHICH ITERATION     DNMR  34
C          IS TERMINATED                                                 DNMR  35
C          SCAF=STEP MULTIPLICATION FACTOR ( USUALLY=1.0 )               DNMR  36
C     4.   IDATA,IPRINT,IPLOT,IPUNCH,NO,SCAL,HEIGHT,SF(1),SF(NO)         DNMR  37
C          IDATA=0 IF SPECTRUM ON TAPE, OR 1 IF ON CARDS (4I1,I6,4F10)   DNMR  38
C          OR 2 IF USING THE TAPE SIMULATION TEST DECK                   DNMR  39
C          IPRINT=1 IF INPUT AND OUTPUT SPECTRA TO BE PRINTED, ELSE 0    DNMR  40
C          IPLOT=0 IF NO PLOT OUTPUT, =1 IF PLOT OF ORIGINAL SPECTRUM    DNMR  41
C          ONLY, =2 IF PLOT OF SMOOTHED SPECTRUM ONLY, =3 IF PLOT OF     DNMR  42
C          ORIGINAL AND SMOOTHED ON SEPARATE SHEETS, =4 IF PLOT OF       DNMR  43
C          SIMULATED SPECTRUM ONLY, =5 IF PLOT OF ORIGINAL AND           DNMR  44
C          SIMULATED ON SEPARATE SHEETS, =6 IF PLOT OF SMOOTHED AND      DNMR  45
C          SIMULATED ON SEPARATE SHEETS, =7 IF PLOT OF ORIGINAL, SMOOTHDNMR  46
C          AND SIMULATED ALL ON SEPARATE SHEETS, =8 IF PLOT OF SIMULATEDNMR  47
C          ON ORIGINAL, AND =9 IF PLOT OF SIMULATED ON SMOOTHED.         DNMR  48
C          IPUNCH=1 IF SPECTRAL OUTPUT ON CARDS, ELSE 0                  DNMR  49
C          NO=NUMBER OF SPECTRAL POINTS IN SIMULATION                    DNMR  50
C          SCAL=PLOT SCALING FACTOR IN HZ/MM                             DNMR  51
C          HEIGHT IS THE MAXIMUM SPECTRUM HEIGHT IN MM. FOR CARD         DNMR  52
C          INPUT OR SIMULATION THIS IS ONLY PERTINENT TO PLOT OR         DNMR  53
C          PUNCH OUTPUT. HOWEVER FOR TAPE INPUT, THE SPECTRUM            DNMR  54
C          INTENSITY VALUES ARE ALL SCALED SO THAT THE DIFFERENCE        DNMR  55
C          BETWEEN THE GREATEST AND LEAST IS EQUAL TO HEIGHT.            DNMR  56
C          THIS THEREFORE AFFECTS BALIC, BATILT, AND THE ERROR VALUE     DNMR  57
C          WHICH BECOME PROPORTIONAL TO HEIGHT.                          DNMR  58
C          SF(1)=FREQUENCY OF FIRST POINT IN SIMULATED SPECTRUM          DNMR  59
C          SF(NO)=FREQUENCY OF LAST POINT IN SIMULATED SPECTRUM          DNMR  60
C          NO,SF(1),SF(NO) BLANK IF ITMAX.GE.0                           DNMR  61
C          PRINT AND PUNCH OPTIONS ONLY APPLY WHEN ITMAX.LT.0            DNMR  62
C          OR IDATA.EQ.1                                                 DNMR  63
C          PLOT OPTIONS 1 TO 9 ARE EQUIVALENT FOR ITMAX.LT.0 AND         DNMR  64
C          FOR IDATA.EQ.1 AND ALL RESULT IN PLOT OF SIMULATED SPECTRUM   DNMR  65
C     5.   NNMES(I),I=1,NMES                                 (5I1)       DNMR  66
C          NUMBER OF NUCLEI IN MAGNETICALLY EQUIVALENT SET I             DNMR  67
C          OMIT IF NMES=N                                                DNMR  68
C     6.   W(I,J),J=1,NMES                                   (5F10)      DNMR  69
C          CHEMICAL SHIFTS IN HZ FOR NUCLEAR CONFIGURATION I,            DNMR  70
C          IF NSYM.NE.0 THE LABELING MUST BE CHOSEN SO THAT ALL          DNMR  71
C          SYMMETRY PAIRS PRECEDE THOSE SPINS NOT RELATED BY SYMMETRY    DNMR  72
C     7.   NEXT SET OF CARDS INPUT COUPLING CONSTANTS (HZ) FOR           DNMR  73
C          NUCLEAR CONFIGURATION I                                       DNMR  74
C          AJ(I,J,K),....                                 (4F10)         DNMR  75
C          FIRST CARD AJ(I,1,2),AJ(I,1,3),.....AJ(I,1,NMES)              DNMR  76
C          SECOND CARD AJ(I,2,3),AJ(I,2,4),.....AJ(I,2,NMES)             DNMR  77
C          ETC.                                                          DNMR  78
C          LAST CARD AJ(I,NMES-1,NMES)                                   DNMR  79
C          SKIP 7 IF NMES=1                                              DNMR  80
C     8.   IF MU=0 REPEAT 6 AND 7 FOR ALL NUCLEAR CONFIGURATIONS I       DNMR  81
C     9.   IF MU=1 READ IN EXCHANGE VECTORS FOR MUTUAL EXCHANGE          DNMR  82
C          ONE VECTOR PER CARD                                           DNMR  83
```

```
C          IE(I,K),K=1,NMES                                    (5I1) DNMR  84
C           FIRST CARD - SECOND EXCHANGE VECTOR                       DNMR  85
C           SECOND CARD - THIRD EXCHANGE VECTOR                       DNMR  86
C           ETC.                                                      DNMR  87
C           THE INTEGER ELEMENTS OF THE NTH EXCHANGE VECTOR REPRESENT DNMR  88
C           THE LABELING OF THE NUCLEI (OR THE LABELING OF THE SETS IF DNMR  89
C           EQUIVALENCE IS USED) IN THE NTH CONFIGURATION IN TERMS OF DNMR  90
C           THE CONSECUTIVE LABELING IN THE FIRST CONFIGURATION       DNMR  91
C     10.   IF MU=0 READ IN POPULATIONS OF NUCLEAR CONFIGURATIONS     DNMR  92
C          POP(I),I=1,NE                                      (4F10) DNMR  93
C     11.  T2(I),I=1,NE                                       (4F10) DNMR  94
C           THE RELAXATION TIMES OF THE INDIVIDUAL NUCLEAR CONFIGS.   DNMR  95
C     12.  RC(I,J)                                            (F10)  DNMR  96
C           RATE CONSTANTS IN 1/SEC ONE PER CARD                      DNMR  97
C           CARD SEQUENCE IS RC(1,2),RC(1,3),...RC(1,NE),RC(2,3),..   DNMR  98
C           IF MU=1 THIS SET CONSISTS OF SINGLE CARD RC(1,2) ONLY     DNMR  99
C           SKIP IF NE.EQ.1                                           DNMR 100
C     13.  BALIC,BATILT                                       (2F10) DNMR 101
C           BALIC=BASELINE INCREMENT                                  DNMR 102
C           BATILT=BASELINE TILT                                      DNMR 103
C     14.   IF ITMAX.LT.0 RETURN TO 1.                                DNMR 104
C     15.  XO,UM,SWEEPW                                       (3F10) DNMR 105
C           XO=FREQUENCY OF ORIGIN POINT, FOR CARD INPUT THIS IS      DNMR 106
C           EQUIVALENT TO THE "ZEROTH" POINT, FOR TAPE INPUT IT IS    DNMR 107
C           THE FREQUENCY OF THE FIRST POINT ON THE TAPE              DNMR 108
C           UM=CONVERTING FACTOR, I.E. FREQUENCY SEPARATION OF TWO    DNMR 109
C           ADJACENT SPECTRAL POINTS. POSITIVE IF POINT NUMBERING IS  DNMR 110
C           IN THE NEGATIVE FREQUENCY DIRECTION, NEGATIVE OTHERWISE   DNMR 111
C           LEAVE BLANK IF IDATA.EQ.0 OR IDATA.EQ.2                   DNMR 112
C           SWEEPW=FREQUENCY WIDTH OF SPECTRUM RECORDED ON TAPE       DNMR 113
C           LEAVE BLANK IF IDATA.EQ.1                                 DNMR 114
C     16.   IF IDATA.EQ.0 OR 2 READ IN SPECTRAL CONTROLS FOR TAPE     DNMR 115
C          NS,NOF,FSNOIS,FENOIS,FSTRUN,FETRUN              (2I5,4F10) DNMR 116
C           NS=SMOOTHING FACTOR, WHERE INITIAL SMOOTHING OCCURS       DNMR 117
C           OVER (2*NS+1) POINTS                                      DNMR 118
C           NOF=NUMBER OF FINAL SMOOTHED AND TRUNCATED POINTS         DNMR 119
C           REQUIRED (LESS THAN 1025)                                 DNMR 120
C           FSNOIS=FREQUENCY STARTING POINT FOR NOISE MEASUREMENT     DNMR 121
C           FENOIS=FREQUENCY ENDING POINT FOR NOISE MEASUREMENT       DNMR 122
C           FSTRUN=FREQUENCY STARTING POINT FOR PRETRUNCATION         DNMR 123
C           FETRUN=FREQUENCY ENDING POINT FOR PRETRUNCATION           DNMR 124
C     17.   IF IDATA.EQ.2 READ IN THE TAPE SIMULATION DECK (10200F5) OR DNMR 125
C           IF IDATA.EQ.1 READ AN EXPERIMENTAL SPECTRUM FROM CARDS. THISDNMR 126
C           CONSISTS OF UP TO 1024 POINTS IN ANY ORDER, BLANKS AND    DNMR 127
C           END OF CARDS ARE IGNORED. EACH PAIR IS III.NNN+ WHERE     DNMR 128
C           III IS A POINT NUMBER, AND NNN THE HEIGHT OF THE SPECTRUM DNMR 129
C           ABOVE THE BASELINE AT THAT POINT, III AND NNN UP TO THREE DNMR 130
C           DIGITS AND MAY BE NEGATIVE. SPECTRUM TERMINATED BY *.     DNMR 131
C     18.   IF IDATA.EQ.1 READ IN AN ESTIMATED SPECTRAL NOISE VALUE   DNMR 132
C          RNOIS                                              (F10)  DNMR 133
C     19.  NLL(I),I=1,16                                      (16I3) DNMR 134
C           THE NUMBERS OF THE PARAMETERS TO BE VARIED INDEPENDENTLY  DNMR 135
C           WHERE THE NUMBERING IS THAT SHOWN ON THE FIRST SIMULATION DNMR 136
C     20.  NSPL(I,J),J=1,10                                   (10I3) DNMR 137
C           THE NUMBERS OF THE PARAMETERS TO BE VARIED BUT KEPT EQUAL DNMR 138
C           TO AN INDEPENDENT PARAMETER IN LIST 19 ( IF NSPL NEGATIVE DNMR 139
C           THEN PARAMETER KEPT EQUAL BUT OF OPPOSITE SIGN )          DNMR 140
C           I.E. IF 4 AND 5 KEPT EQUAL TO 2 THEN CARD IS 002004005    DNMR 141
C           A BLANK CARD TERMINATES THIS SEQUENCE                     DNMR 142
C     21.  PLL(I),PUL(I)                                      (2F10) DNMR 143
C           LOWER AND UPPER LIMITS ON PARAMETERS. ONE CARD PER        DNMR 144
C           VARIED PARAMETER IN THE SAME ORDER AS IN LIST 19.         DNMR 145
      STOP
C**   THIS PROGRAM VALID ON FTN4 AND FTN5 **
      END
```

Input File to simulate coalescence of Cp signals in $(CpCo)_3(\mu_3\text{-}CO)(\mu_3\text{-}Ph\text{-}C{\equiv}CH)$ (with iterative refinement of parameters):

```
Co3-(Ph-CCH)  Cp signals
0103000100
  050 0.00001       1.
1101       1.5      960.      1600.0    2100.0
1763.2
1763.2
1897.4
0.333      0.333     0.333
0.06       0.06      0.06
0.1
0.1
0.1
0.0        0.0
1598.525   -1.4749
2.0
 01 07 10 13 14 15
 01 02
 07 08 09
 10 11 12

1700.      1800.
0.001      5.0
0.001      100000
1550.      1650.
-100.      100
-5.0       5.0
```

Input file to simulate coalescence of alkyne protons in $Cp^*Rh(CpCo)_2(\mu_3\text{-}CO)(\mu_3\text{-}HC{\equiv}CH)$ (bandshape calculation only):

```
Rh*Co2-(H-CC-H)   alkyne signals signals  T=170 K
0603000200
-1    400.        1.
1001  1024 0.01     600.      3300.0    4500.0
11
4382.5     3514.0
2.1
3514.0     4382.5
2.1
3777.8     3777.8
2.1
0.165      0.165     0.67
0.05       0.05      0.05
0.0
220.
220.
```

APPENDIX 3:

Relaxation Times of Bis-Carbyne Complexes 35 - 37 and Bistolan 38

Table A3-1: Carbon-13 relaxation times in **35**

T / K	$T_{1,meta}$/s	$T_{1,ortho}$/s	$T_{1,para}$/s	$T_{1,Cp}$/s	$T_1^{DD}{}_{,Cp}$/s
321	6.4	6.7	2.4	7.5	8.3
311	6.1	6.1	2.3	7.0	7.8
300	5.3	5.2	2.1	6.6	7.3
278.4	3.9	4.0	1.7	4.6	5.1
267.8	3.4	3.5	1.2	4.4	4.9

Table A3-2: Carbon-13 relaxation times in **36**

T / s	$T_{1,ortho}$/s	$T_{1,meta}$/s	$T_{1,middle}$/s	$T_{1,para}$/s	$T_{1,Cp}$/s	$T_{1,Cp}{}^{DD}$/s
300.[a]	-	2.5	1.6	0.37	1.7	2.5
318	3.5	3.4	2.3	0.59	3.1	4.3
308	3.3	3.0	2.0	0.46	2.7	3.8
302	3.0	3.0	2.0	0.48	2.6	3.6
290.2	2.3	2.3	1.6	0.36	2.0	2.9
274.6	1.7	1.8	1.1	0.33	1.6	2.3
268.5	1.7	1.6	1.0	0.30	1.4	2.0
249.7	1.2	1.2	0.81	0.23	1.2	1.7

a) 5 mm tube. All other measurements on this compound were performed in a 10 mm tube.

Table A3-3: C-13 relaxation times in **37**

T / K	carbyne phenyl			alkyne phenyl			
	$T_{1,para}$/s	$T_{1,meta}$/s	$T_{1,inner}$/s	$T_{1,para}$/s	$T_{1,ortho}$/s	$T_{1,meta}$/s	$T_{1,Cp}$/s
311	0.65	3.2	3.0	0.84	4.6	4.4	3.3
306	0.57	2.7	2.7	0.68	3.7	3.5	2.9
300	0.54	2.8	2.4	0.67	3.8	3.6	2.8
278	0.41	2.0	1.8	0.48	2.6	2.5	2.0
257	0.32	1.4	1.3	0.33	1.9	1.8	1.5

Table A3-4: C-13 relaxation times in **38**

T / K	$T_{1,para}$ / s	$T_{1,ortho}$ / s	$T_{1,meta}$ / s	$T_{1,inner}$ / s
300.0	0.83	4.8	4.6	3.9
289.2	0.75	4.1	4.0	3.6
278.4	0.59	3.6	3.5	3.0
267.7	0.57	3.2	3.1	2.7
256.9	0.47	2.6	2.7	2.4

APPENDIX 4

Crystal Structure of $(CpCo)_3(\mu_2\text{-}CO)_2(\mu_2\text{-}CH_2)$

Crystal data and structure refinement

Identification code	co3ch2pu
Empirical formula	$C_{18}H_{17}Co_3O_2$
Formula weight	442.11
Temperature	293(2) K
Wavelength	0.71073 Å
Crystal system	orthorhombic
Space group	Pnma
Unit cell dimensions	a = 14.868(3) Å α = 90° b = 12.197(3) Å β = 90° c = 8.786(3) Å γ = 90°
Volume, Z	1593.3(7) A^3, 4
Density (calculated)	1.843 Mg/m^3
Absorption coefficient	3.091 mm^{-1}
F(000)	888
Crystal size	? x ? x ? mm
Theta range for data collection	2.69 to 22.53 deg.
Limiting indices	-16<=h<=16, -13<=k<=5, -4<=l<=9
Reflections collected	2240
Independent reflections	1108 [R(int) = 0.0255]
Refinement method	Full-matrix least-squares on F^2
Data / restraints / parameters	1105 / 0 / 105
Goodness-of-fit on F^2	1.089
Final R indices [I>2sigma(I)]	R1 = 0.0877, wR2 = 0.2190
R indices (all data)	R1 = 0.1005, wR2 = 0.2356
Largest diff. peak and hole	2.831 and -0.992 $e.A^{-3}$

Atomic coordinates (x 10^4) and equivalent isotropic displacement parameters $Å^2$ x 10^3). U(eq) is defined as one third of the trace of the orthogonalized Uij tensor.

	x	y	z	U(eq)
Co(2)	797(2)	2500	850(2)	21(1)
Co(1)	1012(1)	3478(2)	3166(2)	38(1)
C(2)	242(13)	2500	4319(21)	31(4)
C(1)	70(11)	3549(12)	1790(15)	44(4)
O(1)	-595(13)	4000(16)	1529(17)	132(8)
C(15)	1339(17)	4524(17)	4938(20)	94(9)
C(12)	2218(12)	4344(15)	2800(19)	56(5)
C(14)	1138(25)	5086(23)	3865(32)	159(17)
C(22)	1012(25)	3361(18)	-1088(26)	146(17)
C(13)	1514(20)	5018(18)	2561(34)	112(10)
C(11)	2178(19)	3883(25)	4313(33)	120(9)
C(23)	1805(15)	3030(18)	-700(20)	89(8)
C(21)	538(22)	2500	-1359(30)	157(29)

Bond lengths [Å]

Co(2)-C(1)#1	1.867(14)
Co(2)-C(1)	1.867(14)
Co(2)-C(21)	1.98(3)
Co(2)-C(22)#1	2.03(2)
Co(2)-C(22)	2.03(2)
Co(2)-C(23)	2.13(2)
Co(2)-C(23)#1	2.13(2)
Co(2)-Co(1)	2.380(3)
Co(2)-Co(1)#1	2.380(3)
Co(1)-C(1)	1.85(2)
Co(1)-C(2)	1.94(2)
Co(1)-C(11)	2.06(3)
Co(1)-C(14)	2.06(2)
Co(1)-C(15)	2.07(2)
Co(1)-C(13)	2.09(2)
Co(1)-C(12)	2.11(2)
Co(1)-Co(1)#1	2.386(4)
C(2)-Co(1)#1	1.94(2)
C(1)-O(1)	1.15(2)
C(15)-C(14)	1.20(4)
C(15)-C(11)	1.57(4)
C(12)-C(13)	1.35(3)
C(12)-C(11)	1.44(3)
C(14)-C(13)	1.28(3)
C(22)-C(21)	1.29(4)
C(22)-C(23)	1.29(3)
C(23)-C(23)#1	1.29(4)
C(21)-C(22)#1	1.29(4)

Bond angles [°]

C(1)#1-Co(2)-C(1)	86.5(10)	C(11)-Co(1)-Co(1)#1	103.8(9)
C(1)#1-Co(2)-C(21)	108.8(8)	C(15)-Co(1)-C(12)	66.8(8)
C(1)-Co(2)-C(21)	108.8(8)	C(13)-Co(1)-C(12)	37.5(8)
C(1)#1-Co(2)-C(22)#1	96.2(7)	C(1)-Co(1)-Co(2)	50.5(4)
C(1)-Co(2)-C(22)#1	144.9(12)	C(2)-Co(1)-Co(2)	93.4(5)
C(21)-Co(2)-C(22)#1	37.5(11)	C(11)-Co(1)-Co(2)	130.5(8)
C(1)#1-Co(2)-C(22)	144.9(12)	C(14)-Co(1)-Co(2)	138.0(9)
C(1)-Co(2)-C(22)	96.2(7)	C(15)-Co(1)-Co(2)	169.4(5)
C(21)-Co(2)-C(22)	37.5(11)	C(13)-Co(1)-Co(2)	106.3(8)
C(22)#1-Co(2)-C(22)	62.4(14)	C(12)-Co(1)-Co(2)	103.6(5)
C(1)#1-Co(2)-C(23)	154.1(7)	C(1)-Co(1)-Co(1)#1	92.7(5)
C(1)-Co(2)-C(23)	118.9(8)	C(2)-Co(1)-Co(1)#1	52.0(4)
C(21)-Co(2)-C(23)	60.6(10)	C(14)-Co(1)-Co(1)#1	161.9(10)
C(22)#1-Co(2)-C(23)	60.5(8)	C(15)-Co(1)-Co(1)#1	128.0(6)
C(22)-Co(2)-C(23)	36.1(10)	C(13)-Co(1)-Co(1)#1	154.0(8)
C(1)#1-Co(2)-C(23)#1	118.9(8)	C(12)-Co(1)-Co(1)#1	120.1(6)
C(1)-Co(2)-C(23)#1	154.1(7)	Co(2)-Co(1)-Co(1)#1	59.92(5)
C(21)-Co(2)-C(23)#1	60.6(10)	Co(1)-C(2)-Co(1)#1	75.9(7)
C(22)#1-Co(2)-C(23)#1	36.1(10)	Co(1)-C(2)-H(2A)	115.9(5)
C(22)-Co(2)-C(23)#1	60.5(8)	Co(1)#1-C(2)-H(2A)	115.9(5)
C(23)-Co(2)-C(23)#1	35.4(12)	Co(1)-C(2)-H(2B)	115.6(5)
C(1)#1-Co(2)-Co(1)	92.5(4)	Co(1)#1-C(2)-H(2B)	115.6(5)
C(1)-Co(2)-Co(1)	49.9(5)	H(2A)-C(2)-H(2B)	113.1
C(21)-Co(2)-Co(1)	149.84(9)	O(1)-C(1)-Co(1)	143(2)
C(22)#1-Co(2)-Co(1)	163.1(11)	O(1)-C(1)-Co(2)	137.2(14)
C(22)-Co(2)-Co(1)	115.9(9)	Co(1)-C(1)-Co(2)	79.6(6)
C(23)-Co(2)-Co(1)	107.5(4)	C(14)-C(15)-C(11)	102(2)
C(23)#1-Co(2)-Co(1)	127.2(7)	C(14)-C(15)-Co(1)	72.8(12)
C(1)#1-Co(2)-Co(1)#1	49.9(5)	C(11)-C(15)-Co(1)	67.5(12)
C(1)-Co(2)-Co(1)#1	92.5(4)	C(13)-C(12)-C(11)	110(2)
C(21)-Co(2)-Co(1)#1	149.84(9)	C(13)-C(12)-Co(1)	70.6(11)
C(22)#1-Co(2)-Co(1)#1	115.9(9)	C(11)-C(12)-Co(1)	68.2(13)
C(22)-Co(2)-Co(1)#1	163.1(11)	C(15)-C(14)-C(13)	124(4)
C(23)-Co(2)-Co(1)#1	127.2(7)	C(15)-C(14)-Co(1)	73(2)
C(23)#1-Co(2)-Co(1)#1	107.5(4)	C(13)-C(14)-Co(1)	73.2(14)
Co(1)-Co(2)-Co(1)#1	60.16(11)	C(21)-C(22)-C(23)	107(2)
C(1)-Co(1)-C(2)	85.6(7)	C(21)-C(22)-Co(2)	69(2)
C(1)-Co(1)-C(11)	160.4(10)	C(23)-C(22)-Co(2)	76.2(13)
C(2)-Co(1)-C(11)	112.8(10)	C(14)-C(13)-C(12)	104(3)
C(1)-Co(1)-C(14)	102.6(13)	C(14)-C(13)-Co(1)	71.0(14)
C(2)-Co(1)-C(14)	118.8(8)	C(12)-C(13)-Co(1)	71.9(12)
C(11)-Co(1)-C(14)	63.3(14)	C(12)-C(11)-C(15)	99(2)
C(1)-Co(1)-C(15)	129.8(9)	C(12)-C(11)-Co(1)	71.3(13)
C(2)-Co(1)-C(15)	97.2(7)	C(15)-C(11)-Co(1)	67.9(12)
C(11)-Co(1)-C(15)	44.6(10)	C(22)-C(23)-C(23)#1	108(2)
C(14)-Co(1)-C(15)	33.8(11)	C(22)-C(23)-Co(2)	67.7(11)
C(1)-Co(1)-C(13)	93.6(10)	C(23)#1-C(23)-Co(2)	72.3(6)
C(2)-Co(1)-C(13)	153.7(8)	C(22)-C(21)-C(22)#1	109(3)
C(11)-Co(1)-C(13)	67.0(12)	C(22)-C(21)-Co(2)	73(2)
C(14)-Co(1)-C(13)	35.8(8)	C(22)#1-C(21)-Co(2)	73(2)
C(15)-Co(1)-C(13)	63.5(9)		
C(1)-Co(1)-C(12)	121.4(7)		
C(2)-Co(1)-C(12)	153.0(7)		
C(11)-Co(1)-C(12)	40.5(9)		
C(14)-Co(1)-C(12)	59.5(10)		

Symmetry transformations used to generate equivalent atoms:
#1 x,-y+1/2,z

Anisotropic displacement parameters ($Å^2$ x 10^3).
The anisotropic displacement factor exponent takes the form:
$-2\pi^2$ [$h^2 a^{*2}$ U11 + ... + 2 h k a* b* U12]

	U11	U22	U33	U23	U13	U12
Co(2)	22(1)	20(1)	21(1)	0	-5(1)	0
Co(1)	50(1)	32(1)	33(1)	-14(1)	5(1)	-19(1)
C(2)	46(11)	14(9)	34(10)	0	-12(9)	0
C(1)	62(10)	45(9)	27(7)	5(7)	-3(7)	26(8)
O(1)	158(16)	158(16)	78(10)	41(11)	25(10)	118(15)
C(15)	164(21)	98(15)	20(8)	-12(10)	2(11)	-110(16)
C(12)	58(10)	57(11)	53(10)	-1(9)	-10(9)	-40(9)
C(14)	264(39)	101(21)	112(21)	-73(19)	112(27)	-136(25)
C(22)	276(40)	78(17)	83(18)	81(15)	129(24)	129(23)
C(13)	162(27)	49(13)	126(21)	-14(15)	33(22)	-58(16)
C(23)	105(15)	110(18)	51(11)	-52(11)	27(11)	-70(13)
C(21)	50(18)	419(93)	1(11)	0	-6(12)	0

Hydrogen coordinates (x 10^4) and isotropic displacement parameters ($Å^2$ x 10^3)

	x	y	z	U(eq)
H(2A)	-382(13)	2500	4040(21)	80
H(2B)	335(13)	2500	5401(21)	80
H(15A)	1068(17)	4542(17)	5929(20)	80
H(12A)	2653(12)	4149(15)	2039(19)	80
H(14A)	607(25)	5534(23)	3895(32)	80
H(22A)	829(25)	4105(18)	-1261(26)	80
H(13A)	1392(20)	5403(18)	1631(34)	80
H(11A)	2591(19)	3430(25)	4869(33)	80
H(23A)	2306(15)	3495(18)	-458(20)	80
H(21A)	-54(22)	2500	-1795(30)	80

APPENDIX 5

Crystal Data of $(CpCo)_3(\mu_3\text{-}CO)(\mu_3\text{-}NNCH_2)$

Crystal data and structure refinement

Identification code	co3nnchf
Empirical formula	C17 H17 Co3 N2 O
Formula weight	442.12
Temperature	293(2) K
Wavelength	0.71073 A
Crystal system	Triclinic
Space group	P-1
Unit cell dimensions	a = 8.8960(10) Å alpha = 83.780(10)° b = 9.1020(10) Å beta = 88.670(10)° c = 11.074(2) Å gamma = 62.010(10)°
Volume, Z	786.7(2) $Å^3$, 2
Density (calculated)	1.866 Mg/m^3
Absorption coefficient	3.129 mm^{-1}
F(000)	444
Crystal size	? x ? x ? mm
Theta range for data collection	2.55 to 22.54°
Limiting indices	0<=h<=9, -8<=k<=9, -11<=l<=11
Reflections collected	2293
Independent reflections	2058 [R(int) = 0.0148]
Refinement method	Full-matrix least-squares on F^2
Data / restraints / parameters	2056 / 0 / 208
Goodness-of-fit on F^2	0.903
Final R indices [I>2sigma(I)]	R1 = 0.0347, wR2 = 0.0953
R indices (all data)	R1 = 0.0390, wR2 = 0.1026
Largest diff. peak and hole	0.622 and -0.827 $e.Å^{-3}$

Atomic coordinates (x 10^4) and equivalent isotropic displacement parameters ($Å^2$ x 10^3). U(eq) is defined as one third of the trace of the orthogonalized Uij tensor.

	x	y	z	U(eq)
Co(1)	411(1)	2912(1)	2649(1)	14(1)
Co(2)	2088(1)	-37(1)	2582(1)	14(1)
Co(3)	3343(1)	1811(1)	2157(1)	15(1)
C(1)	1514(5)	1716(5)	1239(4)	18(1)
C(2)	3394(6)	1835(6)	5182(5)	27(1)
O(1)	1114(4)	1909(4)	194(3)	22(1)
N(1)	2328(4)	1380(4)	3510(3)	15(1)
N(2)	2603(5)	1149(5)	4766(3)	23(1)
C(10)	-1328(6)	5192(6)	1776(5)	26(1)
C(11)	-2080(6)	4125(6)	2003(5)	24(1)
C(12)	-2033(6)	3711(6)	3290(4)	22(1)
C(13)	-1258(6)	4526(6)	3838(4)	23(1)
C(14)	-807(6)	5431(6)	2907(5)	30(1)
C(20)	771(7)	-1308(6)	2214(5)	28(1)
C(21)	2277(7)	-1911(6)	1565(5)	31(1)
C(22)	3659(7)	-2563(6)	2430(5)	29(1)
C(23)	2975(6)	-2375(6)	3594(5)	28(1)
C(24)	1186(6)	-1585(6)	3471(5)	27(1)
C(30)	5841(6)	791(7)	1521(5)	34(1)
C(31)	5734(6)	1591(6)	2585(4)	22(1)
C(32)	4517(6)	3284(6)	2339(5)	25(1)
C(33)	3870(7)	3541(7)	1130(5)	31(1)
C(34)	4681(7)	2018(7)	637(5)	32(1)

Bond lengths [Å]

Co(1)-N(1)	1.821(3)	C(1)-O(1)	1.189(5)
Co(1)-C(1)	1.970(5)	C(2)-N(2)	1.260(6)
Co(1)-C(10)	2.064(5)	N(1)-N(2)	1.394(5)
Co(1)-C(11)	2.061(4)	C(10)-C(14)	1.418(7)
Co(1)-C(14)	2.076(5)	C(10)-C(11)	1.416(7)
Co(1)-C(12)	2.077(4)	C(11)-C(12)	1.431(7)
Co(1)-C(13)	2.092(4)	C(12)-C(13)	1.410(7)
Co(1)-Co(3)	2.3879(8)	C(13)-C(14)	1.417(7)
Co(1)-Co(2)	2.3900(9)	C(20)-C(24)	1.414(7)
Co(2)-N(1)	1.822(3)	C(20)-C(21)	1.401(7)
Co(2)-C(1)	1.942(4)	C(21)-C(22)	1.424(8)
Co(2)-C(20)	2.067(5)	C(22)-C(23)	1.405(7)
Co(2)-C(24)	2.079(5)	C(23)-C(24)	1.408(7)
Co(2)-C(22)	2.080(5)	C(30)-C(34)	1.414(8)
Co(2)-C(23)	2.087(5)	C(30)-C(31)	1.429(7)
Co(2)-C(21)	2.085(5)	C(31)-C(32)	1.406(7)
Co(2)-Co(3)	2.4218(8)	C(32)-C(33)	1.422(7)
Co(3)-N(1)	1.832(4)	C(33)-C(34)	1.395(8)
Co(3)-C(1)	1.979(4)		
Co(3)-C(33)	2.067(5)		
Co(3)-C(32)	2.076(4)		
Co(3)-C(34)	2.082(5)		
Co(3)-C(31)	2.101(5)		
Co(3)-C(30)	2.105(5)		

Bond Angles [°]

N(1)-Co(1)-C(1)	85.6(2)	N(1)-Co(2)-Co(3)	48.65(11)
N(1)-Co(1)-C(10)	158.4(2)	C(1)-Co(2)-Co(3)	52.55(13)
C(1)-Co(1)-C(10)	100.3(2)	C(20)-Co(2)-Co(3)	157.0(2)
N(1)-Co(1)-C(11)	159.8(2)	C(24)-Co(2)-Co(3)	163.0(2)
C(1)-Co(1)-C(11)	99.3(2)	C(22)-Co(2)-Co(3)	116.69(14)
C(10)-Co(1)-C(11)	40.1(2)	C(23)-Co(2)-Co(3)	132.04(14)
N(1)-Co(1)-C(14)	122.8(2)	C(21)-Co(2)-Co(3)	127.36(14)
C(1)-Co(1)-C(14)	132.7(2)	Co(1)-Co(2)-Co(3)	59.50(2)
C(10)-Co(1)-C(14)	40.1(2)	N(1)-Co(3)-C(1)	85.1(2)
C(11)-Co(1)-C(14)	67.4(2)	N(1)-Co(3)-C(33)	146.4(2)
N(1)-Co(1)-C(12)	123.6(2)	C(1)-Co(3)-C(33)	105.5(2)
C(1)-Co(1)-C(12)	131.3(2)	N(1)-Co(3)-C(32)	116.3(2)
C(10)-Co(1)-C(12)	67.4(2)	C(1)-Co(3)-C(32)	142.7(2)
C(11)-Co(1)-C(12)	40.5(2)	C(33)-Co(3)-C(32)	40.1(2)
C(14)-Co(1)-C(12)	67.0(2)	N(1)-Co(3)-C(34)	173.7(2)
N(1)-Co(1)-C(13)	108.5(2)	C(1)-Co(3)-C(34)	95.6(2)
C(1)-Co(1)-C(13)	165.9(2)	C(33)-Co(3)-C(34)	39.3(2)
C(10)-Co(1)-C(13)	67.0(2)	C(32)-Co(3)-C(34)	66.5(2)
C(11)-Co(1)-C(13)	67.2(2)	N(1)-Co(3)-C(31)	111.8(2)
C(14)-Co(1)-C(13)	39.8(2)	C(1)-Co(3)-C(31)	160.1(2)
C(12)-Co(1)-C(13)	39.5(2)	C(33)-Co(3)-C(31)	66.6(2)
N(1)-Co(1)-Co(3)	49.37(11)	C(32)-Co(3)-C(31)	39.3(2)
C(1)-Co(1)-Co(3)	52.98(13)	C(34)-Co(3)-C(31)	66.4(2)
C(10)-Co(1)-Co(3)	118.83(13)	N(1)-Co(3)-C(30)	135.3(2)
C(11)-Co(1)-Co(3)	146.54(14)	C(1)-Co(3)-C(30)	120.5(2)
C(14)-Co(1)-Co(3)	115.04(14)	C(33)-Co(3)-C(30)	66.3(2)
C(12)-Co(1)-Co(3)	172.89(13)	C(32)-Co(3)-C(30)	66.4(2)
C(13)-Co(1)-Co(3)	137.70(13)	C(34)-Co(3)-C(30)	39.5(2)
N(1)-Co(1)-Co(2)	49.02(11)	C(31)-Co(3)-C(30)	39.7(2)
C(1)-Co(1)-Co(2)	51.82(13)	N(1)-Co(3)-Co(1)	48.97(11)
C(10)-Co(1)-Co(2)	147.7(2)	C(1)-Co(3)-Co(1)	52.61(13)
C(11)-Co(1)-Co(2)	120.13(14)	C(33)-Co(3)-Co(1)	113.0(2)
C(14)-Co(1)-Co(2)	171.8(2)	C(32)-Co(3)-Co(1)	117.91(14)
C(12)-Co(1)-Co(2)	116.11(13)	C(34)-Co(3)-Co(1)	135.7(2)
C(13)-Co(1)-Co(2)	137.79(14)	C(31)-Co(3)-Co(1)	146.99(13)
Co(3)-Co(1)-Co(2)	60.91(3)	C(30)-Co(3)-Co(1)	173.1(2)
N(1)-Co(2)-C(1)	86.4(2)	N(1)-Co(3)-Co(2)	48.32(11)
N(1)-Co(2)-C(20)	148.2(2)	C(1)-Co(3)-Co(2)	51.17(13)
C(1)-Co(2)-C(20)	105.6(2)	C(33)-Co(3)-Co(2)	156.2(2)
N(1)-Co(2)-C(24)	115.6(2)	C(32)-Co(3)-Co(2)	163.30(14)
C(1)-Co(2)-C(24)	141.3(2)	C(34)-Co(3)-Co(2)	127.97(14)
C(20)-Co(2)-C(24)	39.9(2)	C(31)-Co(3)-Co(2)	133.08(13)
N(1)-Co(2)-C(22)	130.7(2)	C(30)-Co(3)-Co(2)	118.0(2)
C(1)-Co(2)-C(22)	123.7(2)	Co(1)-Co(3)-Co(2)	59.59(2)
C(20)-Co(2)-C(22)	66.6(2)	O(1)-C(1)-Co(2)	136.4(3)
C(24)-Co(2)-C(22)	66.7(2)	O(1)-C(1)-Co(1)	133.9(3)
N(1)-Co(2)-C(23)	108.6(2)	Co(2)-C(1)-Co(1)	75.3(2)
C(1)-Co(2)-C(23)	162.6(2)	O(1)-C(1)-Co(3)	135.0(3)
C(20)-Co(2)-C(23)	66.2(2)	Co(2)-C(1)-Co(3)	76.3(2)
C(24)-Co(2)-C(23)	39.5(2)	Co(1)-C(1)-Co(3)	74.4(2)
C(22)-Co(2)-C(23)	39.4(2)	N(2)-N(1)-Co(1)	127.2(3)
N(1)-Co(2)-C(21)	169.9(2)	N(2)-N(1)-Co(2)	126.8(3)
C(1)-Co(2)-C(21)	97.3(2)	Co(1)-N(1)-Co(2)	82.01(14)
C(20)-Co(2)-C(21)	39.4(2)	N(2)-N(1)-Co(3)	137.2(3)
C(24)-Co(2)-C(21)	66.8(2)	Co(1)-N(1)-Co(3)	81.7(2)
C(22)-Co(2)-C(21)	40.0(2)	Co(2)-N(1)-Co(3)	83.0(2)
C(23)-Co(2)-C(21)	66.5(2)	C(2)-N(2)-N(1)	116.9(4)
N(1)-Co(2)-Co(1)	48.97(11)	C(14)-C(10)-C(11)	108.2(4)
C(1)-Co(2)-Co(1)	52.86(13)	C(14)-C(10)-Co(1)	70.4(3)
C(20)-Co(2)-Co(1)	116.1(2)	C(11)-C(10)-Co(1)	69.8(3)
C(24)-Co(2)-Co(1)	117.52(14)	C(10)-C(11)-C(12)	107.6(4)
C(22)-Co(2)-Co(1)	175.73(14)	C(10)-C(11)-Co(1)	70.0(3)
C(23)-Co(2)-Co(1)	144.3(2)	C(12)-C(11)-Co(1)	70.4(3)
C(21)-Co(2)-Co(1)	139.9(2)	C(13)-C(12)-C(11)	107.9(4)

C(13)-C(12)-Co(1)	70.8(3)
C(11)-C(12)-Co(1)	69.2(3)
C(12)-C(13)-C(14)	108.3(4)
C(12)-C(13)-Co(1)	69.7(3)
C(14)-C(13)-Co(1)	69.5(3)
C(10)-C(14)-C(13)	108.0(4)
C(10)-C(14)-Co(1)	69.5(3)
C(13)-C(14)-Co(1)	70.7(3)
C(24)-C(20)-C(21)	109.1(4)
C(24)-C(20)-Co(2)	70.5(3)
C(21)-C(20)-Co(2)	70.9(3)
C(20)-C(21)-C(22)	107.3(4)
C(20)-C(21)-Co(2)	69.6(3)
C(22)-C(21)-Co(2)	69.8(3)
C(23)-C(22)-C(21)	107.8(5)
C(23)-C(22)-Co(2)	70.6(3)
C(21)-C(22)-Co(2)	70.2(3)
C(24)-C(23)-C(22)	108.8(4)
C(24)-C(23)-Co(2)	69.9(3)
C(22)-C(23)-Co(2)	70.0(3)
C(20)-C(24)-C(23)	107.1(4)
C(20)-C(24)-Co(2)	69.6(3)
C(23)-C(24)-Co(2)	70.6(3)
C(34)-C(30)-C(31)	107.4(5)
C(34)-C(30)-Co(3)	69.4(3)
C(31)-C(30)-Co(3)	70.0(3)
C(32)-C(31)-C(30)	107.7(5)
C(32)-C(31)-Co(3)	69.4(3)
C(30)-C(31)-Co(3)	70.3(3)
C(31)-C(32)-C(33)	108.1(4)
C(31)-C(32)-Co(3)	71.3(3)
C(33)-C(32)-Co(3)	69.6(3)
C(34)-C(33)-C(32)	108.1(5)
C(34)-C(33)-Co(3)	70.9(3)
C(32)-C(33)-Co(3)	70.3(3)
C(33)-C(34)-C(30)	108.7(5)
C(33)-C(34)-Co(3)	69.8(3)
C(30)-C(34)-Co(3)	71.1(3)

Symmetry transformations used to generate equivalent atoms:

Anisotropic displacement parameters ($Å^2$ x 10^3)
The anisotropic displacement factor exponent takes the form:
$-2\pi^2$ [$h^2 a^2$ U11 + ... + 2 h k a* b* U12]

	U11	U22	U33	U23	U13	U12
Co(1)	12(1)	12(1)	18(1)	0(1)	0(1)	-5(1)
Co(2)	14(1)	12(1)	18(1)	-1(1)	2(1)	-7(1)
Co(3)	13(1)	16(1)	18(1)	-2(1)	2(1)	-9(1)
C(1)	16(2)	17(2)	24(3)	0(2)	1(2)	-12(2)
C(2)	28(3)	24(3)	24(3)	-5(2)	-4(2)	-8(2)
O(1)	28(2)	29(2)	13(2)	1(1)	-4(1)	-16(2)
N(1)	15(2)	16(2)	15(2)	-2(2)	0(2)	-8(2)
N(2)	22(2)	27(2)	15(2)	2(2)	-3(2)	-10(2)
C(10)	15(2)	16(2)	34(3)	6(2)	5(2)	1(2)
C(11)	10(2)	27(3)	31(3)	0(2)	-5(2)	-4(2)
C(12)	13(2)	17(2)	34(3)	0(2)	5(2)	-5(2)
C(13)	19(2)	16(2)	30(3)	-10(2)	6(2)	-4(2)
C(14)	21(3)	16(3)	49(4)	-5(2)	0(2)	-4(2)
C(20)	30(3)	24(3)	41(3)	-1(2)	-5(2)	-20(2)
C(21)	50(4)	22(3)	30(3)	-8(2)	9(3)	-24(3)
C(22)	28(3)	10(2)	43(3)	-3(2)	14(2)	-6(2)
C(23)	30(3)	17(3)	32(3)	7(2)	-3(2)	-11(2)
C(24)	32(3)	21(3)	34(3)	-3(2)	12(2)	-19(2)
C(30)	19(3)	43(3)	50(4)	-21(3)	17(3)	-21(3)
C(31)	19(2)	24(3)	30(3)	-4(2)	4(2)	-16(2)
C(32)	27(3)	25(3)	34(3)	0(2)	2(2)	-22(2)
C(33)	34(3)	39(3)	32(3)	9(3)	-3(2)	-29(3)
C(34)	36(3)	55(4)	24(3)	-9(3)	10(2)	-38(3)

Hydrogen coordinates (x 10^4) and isotropic
displacement parameters ($Å^2$ x 10^3)

	x	y	z	U(eq)
H(2A)	3775(6)	2477(6)	4637(5)	80
H(2B)	3615(6)	1719(6)	6041(5)	80
H(10A)	-1200(6)	5677(6)	991(5)	80
H(11)	-2681(6)	3955(6)	1369(5)	50
H(12)	-2412(6)	2954(6)	3679(4)	50
H(13A)	-1051(6)	4467(6)	4693(4)	80
H(14A)	-235(6)	6077(6)	3019(5)	80
H(20A)	-359(7)	-782(6)	1857(5)	80
H(21A)	2361(7)	-1902(6)	698(5)	80
H(22A)	4845(7)	-3043(6)	2245(5)	80
H(23)	3699(6)	-2707(6)	4308(5)	50
H(24A)	391(6)	-1299(6)	4116(5)	80
H(30A)	6551(6)	-372(7)	1432(5)	80
H(31)	6324(6)	1086(6)	3354(4)	50
H(32A)	4185(6)	4112(6)	2898(5)	80
H(33)	2987(7)	4561(7)	725(5)	50
H(34)	4340(7)	2021(7)	-180(5)	50

APPENDIX 6

Crystal Structure of $Cp^*Rh(CpCo)_2(\mu_2\text{-}CO)_2(\mu_2\text{-}CH_2)$ (7)

Crystal data and structure refinement

Identification code	rhch2fin
Empirical formula	$C_{23}H_{27}Co_2O_2Rh$
Formula weight	556.22
Temperature	293(2) K
Wavelength	0.71073 Å
Crystal system	Orthorhombic
Space group	Pbca
Unit cell dimensions	a = 15.499(4) Å α = 90° b = 15.936(4) Å β = 90° c = 16.819(4) Å γ = 90°
Volume, Z	4154(2) A^3, 8
Density (calculated)	1.779 Mg/m^3
Absorption coefficient	2.380 mm^{-1}
F(000)	2240
Crystal size	0.4 x 0.3 x 0.15 mm
Theta range for data collection	2.20 to 22.55°
Limiting indices	-16<=h<=0, -17<=k<=17, -18<=l<=18
Reflections collected	8421
Independent reflections	2730 [R(int) = 0.0346]
Refinement method	Full-matrix least-squares on F^2
Data / restraints / parameters	2730 / 0 / 263
Goodness-of-fit on F^2	1.060
Final R indices [I>2sigma(I)]	R1 = 0.0302, wR2 = 0.0675
R indices (all data)	R1 = 0.0434, wR2 = 0.0745
Largest diff. peak and hole	0.497 and -0.379 $e.Å^{-3}$

Atomic coordinates (x 10^4) and equivalent isotropic displacement parameters ($Å^2$ x 10^3). U(eq) is defined as one third of the trace of the orthogonalized Uij tensor.

	x	y	z	U(eq)
Rh(1)	1096(1)	7762(1)	1087(1)	26(1)
Co(1)	2262(1)	8602(1)	414(1)	29(1)
Co(2)	1856(1)	8946(1)	1771(1)	33(1)
C(33)	-104(3)	7216(3)	1597(3)	32(1)
C(34)	-408(3)	7912(3)	1141(3)	34(1)
C(35)	-177(3)	7773(3)	348(3)	36(1)
C(32)	276(3)	6622(3)	1075(3)	35(1)
C(1)	1800(4)	7789(4)	2095(4)	44(2)
C(2)	2198(4)	7431(4)	583(3)	39(1)
C(14)	1688(4)	9414(4)	-426(4)	56(2)
C(31)	266(3)	6988(3)	303(3)	38(1)
C(15)	1899(5)	8652(4)	-776(3)	58(2)
C(22)	907(4)	9425(4)	2512(4)	55(2)
C(21)	1706(5)	9468(4)	2892(4)	63(2)
C(13)	2438(6)	9764(4)	-144(4)	60(2)
C(12)	3114(4)	9241(5)	-332(4)	58(2)
C(11)	2793(5)	8556(5)	-724(4)	63(2)
O(1)	2515(3)	6799(3)	373(4)	38(2)
O(2)	3660(4)	8710(4)	1511(3)	87(2)
O(3)	1939(7)	7385(6)	2626(5)	37(4)
C(43)	-285(4)	7077(4)	2468(3)	50(2)
C(25)	2239(5)	9975(4)	2461(5)	69(2)
C(44)	-976(4)	8594(4)	1445(4)	55(2)
C(24)	1761(6)	10265(4)	1804(5)	72(2)
C(46)	-421(4)	8318(4)	-346(3)	55(2)
C(23)	935(5)	9924(4)	1832(4)	58(2)
C(41)	547(4)	6557(4)	-445(3)	53(2)
C(3)	2929(4)	8694(4)	1337(3)	38(1)
C(42)	597(4)	5759(3)	1292(4)	55(2)

Bond lengths [Å]

Rh(1)-C(2)	1.980(6)
Rh(1)-C(1)	2.017(6)
Rh(1)-C(32)	2.217(5)
Rh(1)-C(31)	2.217(5)
Rh(1)-C(33)	2.225(5)
Rh(1)-C(35)	2.331(5)
Rh(1)-C(34)	2.344(5)
Rh(1)-Co(2)	2.5042(9)
Rh(1)-Co(1)	2.5181(9)
Co(1)-C(3)	1.871(6)
Co(1)-C(2)	1.890(6)
Co(1)-C(15)	2.081(6)
Co(1)-C(11)	2.085(6)
Co(1)-C(12)	2.087(6)
Co(1)-C(13)	2.093(6)
Co(1)-C(14)	2.112(6)
Co(1)-Co(2)	2.4299(11)
Co(2)-C(3)	1.860(6)
Co(2)-C(1)	1.924(6)
Co(2)-C(22)	2.074(6)
Co(2)-C(21)	2.075(6)

Co(2)-C(25)	2.095(6)
Co(2)-C(24)	2.109(6)
Co(2)-C(23)	2.116(6)
C(33)-C(32)	1.419(7)
C(33)-C(34)	1.428(7)
C(33)-C(43)	1.508(8)
C(34)-C(35)	1.400(7)
C(34)-C(44)	1.490(7)
C(35)-C(31)	1.428(8)
C(35)-C(46)	1.502(8)
C(32)-C(31)	1.424(8)
C(32)-C(42)	1.507(7)
C(1)-O(3)	1.122(9)
C(1)-H(1A)	0.983(6)
C(1)-H(1B)	0.974(6)
C(2)-O(1)	1.174(7)
C(2)-H(2A)	0.967(6)
C(2)-H(2B)	0.969(6)
C(14)-C(13)	1.374(10)
C(14)-C(15)	1.390(9)
C(31)-C(41)	1.499(7)
C(15)-C(11)	1.397(10)
C(22)-C(23)	1.394(9)
C(22)-C(21)	1.396(10)
C(21)-C(25)	1.364(9)
C(13)-C(12)	1.375(10)
C(12)-C(11)	1.369(10)
O(2)-C(3)	1.171(7)
C(25)-C(24)	1.410(10)
C(24)-C(23)	1.391(10)

Bond Angles [°]

C(2)-Rh(1)-C(1)	84.2(2)	C(13)-Co(1)-Co(2)	104.8(2)
C(2)-Rh(1)-C(32)	105.8(2)	C(14)-Co(1)-Co(2)	112.4(2)
C(1)-Rh(1)-C(32)	109.6(2)	C(3)-Co(1)-Rh(1)	93.8(2)
C(2)-Rh(1)-C(31)	95.6(2)	C(2)-Co(1)-Rh(1)	51.0(2)
C(1)-Rh(1)-C(31)	145.7(2)	C(15)-Co(1)-Rh(1)	105.0(2)
C(32)-Rh(1)-C(31)	37.5(2)	C(11)-Co(1)-Rh(1)	132.7(2)
C(2)-Rh(1)-C(33)	141.5(2)	C(12)-Co(1)-Rh(1)	169.8(2)
C(1)-Rh(1)-C(33)	97.9(2)	C(13)-Co(1)-Rh(1)	139.9(2)
C(32)-Rh(1)-C(33)	37.3(2)	C(14)-Co(1)-Rh(1)	108.9(2)
C(31)-Rh(1)-C(33)	61.8(2)	Co(2)-Co(1)-Rh(1)	60.78(3)
C(2)-Rh(1)-C(35)	120.2(2)	C(3)-Co(2)-C(1)	86.8(2)
C(1)-Rh(1)-C(35)	155.0(2)	C(3)-Co(2)-C(22)	161.7(3)
C(32)-Rh(1)-C(35)	61.1(2)	C(1)-Co(2)-C(22)	98.6(3)
C(31)-Rh(1)-C(35)	36.5(2)	C(3)-Co(2)-C(21)	122.9(3)
C(33)-Rh(1)-C(35)	60.1(2)	C(1)-Co(2)-C(21)	97.0(3)
C(2)-Rh(1)-C(34)	154.4(2)	C(22)-Co(2)-C(21)	39.3(3)
C(1)-Rh(1)-C(34)	120.3(2)	C(3)-Co(2)-C(25)	97.6(3)
C(32)-Rh(1)-C(34)	60.9(2)	C(1)-Co(2)-C(25)	127.3(3)
C(31)-Rh(1)-C(34)	60.2(2)	C(22)-Co(2)-C(25)	65.2(3)
C(33)-Rh(1)-C(34)	36.3(2)	C(21)-Co(2)-C(25)	38.2(3)
C(35)-Rh(1)-C(34)	34.8(2)	C(3)-Co(2)-C(24)	106.7(3)
C(2)-Rh(1)-Co(2)	89.5(2)	C(1)-Co(2)-C(24)	160.9(3)
C(1)-Rh(1)-Co(2)	48.9(2)	C(22)-Co(2)-C(24)	64.4(3)
C(32)-Rh(1)-Co(2)	153.04(14)	C(21)-Co(2)-C(24)	64.4(3)
C(31)-Rh(1)-Co(2)	164.9(2)	C(25)-Co(2)-C(24)	39.2(3)
C(33)-Rh(1)-Co(2)	120.72(14)	C(3)-Co(2)-C(23)	141.3(3)
C(35)-Rh(1)-Co(2)	129.61(14)	C(1)-Co(2)-C(23)	131.4(3)
C(34)-Rh(1)-Co(2)	111.92(13)	C(22)-Co(2)-C(23)	38.9(3)
C(2)-Rh(1)-Co(1)	47.9(2)	C(21)-Co(2)-C(23)	65.5(3)
C(1)-Rh(1)-Co(1)	88.7(2)	C(25)-Co(2)-C(23)	65.7(3)
C(32)-Rh(1)-Co(1)	147.44(14)	C(24)-Co(2)-C(23)	38.5(3)
C(31)-Rh(1)-Co(1)	116.39(14)	C(3)-Co(2)-Co(1)	49.6(2)
C(33)-Rh(1)-Co(1)	168.82(13)	C(1)-Co(2)-Co(1)	93.5(2)
C(35)-Rh(1)-Co(1)	111.29(13)	C(22)-Co(2)-Co(1)	146.2(2)
C(34)-Rh(1)-Co(1)	132.58(13)	C(21)-Co(2)-Co(1)	166.7(2)
Co(2)-Rh(1)-Co(1)	57.87(3)	C(25)-Co(2)-Co(1)	128.6(2)
C(3)-Co(1)-C(2)	89.0(2)	C(24)-Co(2)-Co(1)	105.5(2)
C(3)-Co(1)-C(15)	160.8(3)	C(23)-Co(2)-Co(1)	112.7(2)
C(2)-Co(1)-C(15)	99.7(3)	C(3)-Co(2)-Rh(1)	94.5(2)
C(3)-Co(1)-C(11)	123.1(3)	C(1)-Co(2)-Rh(1)	52.2(2)
C(2)-Co(1)-C(11)	97.1(3)	C(22)-Co(2)-Rh(1)	102.7(2)
C(15)-Co(1)-C(11)	39.2(3)	C(21)-Co(2)-Rh(1)	131.8(2)
C(3)-Co(1)-C(12)	96.3(2)	C(25)-Co(2)-Rh(1)	167.8(2)
C(2)-Co(1)-C(12)	127.2(3)	C(24)-Co(2)-Rh(1)	136.9(3)
C(15)-Co(1)-C(12)	64.8(3)	C(23)-Co(2)-Rh(1)	105.1(2)
C(11)-Co(1)-C(12)	38.3(3)	Co(1)-Co(2)-Rh(1)	61.35(3)
C(3)-Co(1)-C(13)	103.3(3)	C(32)-C(33)-C(34)	108.8(5)
C(2)-Co(1)-C(13)	161.3(2)	C(32)-C(33)-C(43)	125.4(5)
C(15)-Co(1)-C(13)	64.6(3)	C(34)-C(33)-C(43)	125.1(5)
C(11)-Co(1)-C(13)	64.4(3)	C(32)-C(33)-Rh(1)	71.1(3)
C(12)-Co(1)-C(13)	38.4(3)	C(34)-C(33)-Rh(1)	76.4(3)
C(3)-Co(1)-C(14)	137.7(3)	C(43)-C(33)-Rh(1)	126.0(4)
C(2)-Co(1)-C(14)	133.1(3)	C(35)-C(34)-C(33)	107.8(5)
C(15)-Co(1)-C(14)	38.7(3)	C(35)-C(34)-C(44)	126.4(5)
C(11)-Co(1)-C(14)	64.8(3)	C(33)-C(34)-C(44)	125.3(5)
C(12)-Co(1)-C(14)	64.2(3)	C(35)-C(34)-Rh(1)	72.1(3)
C(13)-Co(1)-C(14)	38.1(3)	C(33)-C(34)-Rh(1)	67.3(3)
C(3)-Co(1)-Co(2)	49.2(2)	C(44)-C(34)-Rh(1)	132.5(4)
C(2)-Co(1)-Co(2)	93.9(2)	C(34)-C(35)-C(31)	108.2(5)
C(15)-Co(1)-Co(2)	145.6(2)	C(34)-C(35)-C(46)	125.7(5)
C(11)-Co(1)-Co(2)	166.5(2)	C(31)-C(35)-C(46)	125.9(5)
C(12)-Co(1)-Co(2)	128.2(2)	C(34)-C(35)-Rh(1)	73.1(3)
		C(31)-C(35)-Rh(1)	67.4(3)

C(46)-C(35)-Rh(1)	129.1(4)	C(25)-C(24)-Co(2)	69.9(4)
C(31)-C(32)-C(33)	106.6(5)	C(22)-C(23)-C(24)	106.3(7)
C(31)-C(32)-C(42)	126.7(5)	C(22)-C(23)-Co(2)	69.0(4)
C(33)-C(32)-C(42)	126.6(5)	O(2)-C(3)-Co(1)	138.2(5)
C(31)-C(32)-Rh(1)	71.3(3)	C(24)-C(23)-Co(2)	70.5(4)
C(33)-C(32)-Rh(1)	71.7(3)	O(2)-C(3)-Co(2)	139.6(5)
C(42)-C(32)-Rh(1)	123.8(4)	O(2)-C(3)-Co(1)	138.2(5)
O(3)-C(1)-Co(2)	140.0(7)	Co(2)-C(3)-Co(1)	81.3(2)
O(3)-C(1)-Rh(1)	139.5(7)		
Co(2)-C(1)-Rh(1)	78.9(2)		
O(3)-C(1)-H(1A)	63.7(7)		
Co(2)-C(1)-H(1A)	116.4(4)		
Rh(1)-C(1)-H(1A)	116.1(4)		
O(3)-C(1)-H(1B)	45.7(6)		
Co(2)-C(1)-H(1B)	116.9(5)		
Rh(1)-C(1)-H(1B)	116.6(4)		
H(1A)-C(1)-H(1B)	109.4(6)		
O(1)-C(2)-Co(1)	141.2(5)		
O(1)-C(2)-Rh(1)	135.9(5)		
Co(1)-C(2)-Rh(1)	81.1(2)		
O(1)-C(2)-H(2A)	46.2(4)		
Co(1)-C(2)-H(2A)	115.8(4)		
Rh(1)-C(2)-H(2A)	115.4(4)		
O(1)-C(2)-H(2B)	64.7(5)		
Co(1)-C(2)-H(2B)	115.7(4)		
Rh(1)-C(2)-H(2B)	115.3(4)		
H(2A)-C(2)-H(2B)	110.8(6)		
C(13)-C(14)-C(15)	107.6(6)		
C(13)-C(14)-Co(1)	70.2(4)		
C(15)-C(14)-Co(1)	69.4(3)		
C(32)-C(31)-C(35)	108.4(5)		
C(32)-C(31)-C(41)	125.1(5)		
C(35)-C(31)-C(41)	125.8(5)		
C(32)-C(31)-Rh(1)	71.3(3)		
C(35)-C(31)-Rh(1)	76.1(3)		
C(41)-C(31)-Rh(1)	125.8(4)		
C(14)-C(15)-C(11)	107.6(6)		
C(14)-C(15)-Co(1)	71.9(4)		
C(11)-C(15)-Co(1)	70.6(4)		
C(23)-C(22)-C(21)	108.6(6)		
C(23)-C(22)-Co(2)	72.2(4)		
C(21)-C(22)-Co(2)	70.4(4)		
C(25)-C(21)-C(22)	108.9(6)		
C(25)-C(21)-Co(2)	71.7(4)		
C(22)-C(21)-Co(2)	70.3(3)		
C(14)-C(13)-C(12)	108.7(6)		
C(14)-C(13)-Co(1)	71.7(4)		
C(12)-C(13)-Co(1)	70.6(4)		
C(11)-C(12)-C(13)	108.5(6)		
C(11)-C(12)-Co(1)	70.7(4)		
C(13)-C(12)-Co(1)	71.0(4)		
C(12)-C(11)-C(15)	107.7(6)		
C(12)-C(11)-Co(1)	70.9(4)		
C(15)-C(11)-Co(1)	70.3(4)		
C(2)-O(1)-H(2A)	54.2(4)		
C(2)-O(1)-H(2B)	49.1(4)		
H(2A)-O(1)-H(2B)	103.2(5)		
C(1)-O(3)-H(1A)	52.1(5)		
C(1)-O(3)-H(1B)	57.7(6)		
H(1A)-O(3)-H(1B)	109.7(8)		
C(21)-C(25)-C(24)	107.0(7)		
C(21)-C(25)-Co(2)	70.1(4)		
C(24)-C(25)-Co(2)	70.9(4)		
C(23)-C(24)-C(25)	109.2(6)		
C(23)-C(24)-Co(2)	71.0(3)		

Anisotropic displacement parameters ($Å^2 \times 10^3$)
The anisotropic displacement factor exponent takes the form:
$-2\pi^2 [h^2 a^{*2} U11 + ... + 2 h k a^* b^* U12]$

	U11	U22	U33	U23	U13	U12
Rh(1)	31(1)	25(1)	23(1)	2(1)	1(1)	1(1)
Co(1)	34(1)	28(1)	24(1)	2(1)	3(1)	1(1)
Co(2)	43(1)	34(1)	23(1)	-2(1)	1(1)	-4(1)
C(33)	29(3)	34(3)	34(3)	3(3)	6(2)	-3(2)
C(34)	28(3)	40(3)	35(3)	6(3)	0(3)	0(2)
C(35)	27(3)	48(3)	32(3)	2(3)	2(2)	-3(3)
C(32)	35(3)	27(3)	44(3)	-3(3)	3(3)	-4(2)
C(1)	45(3)	47(4)	39(3)	0(3)	-2(3)	-8(3)
C(2)	39(3)	40(4)	38(3)	6(3)	1(3)	-4(3)
C(14)	53(4)	62(4)	52(4)	29(4)	10(4)	16(4)
C(31)	39(3)	43(3)	31(3)	-7(3)	0(3)	-9(3)
C(15)	85(5)	68(5)	22(3)	8(3)	-6(3)	-28(4)
C(22)	61(4)	54(4)	51(4)	-18(4)	18(4)	-8(3)
C(21)	91(6)	72(5)	27(3)	-19(3)	7(4)	-12(4)
C(13)	109(6)	34(4)	38(3)	8(3)	16(4)	-17(4)
C(12)	48(4)	88(5)	40(4)	22(4)	5(3)	-14(4)
C(11)	88(6)	61(5)	38(4)	2(3)	29(4)	24(4)
O(1)	31(3)	16(3)	68(4)	-3(3)	9(3)	14(2)
O(2)	81(4)	108(5)	73(4)	9(3)	-10(3)	-6(3)
O(3)	56(7)	38(6)	17(6)	36(5)	-23(5)	-5(5)
C(43)	55(4)	53(4)	42(3)	7(3)	17(3)	2(3)
C(25)	74(5)	65(5)	67(5)	-37(4)	8(4)	-22(4)
C(44)	48(4)	57(4)	58(4)	-3(3)	3(3)	10(3)
C(24)	128(7)	26(3)	62(5)	-10(3)	36(5)	-10(4)
C(46)	45(4)	78(5)	41(3)	15(4)	-6(3)	0(3)
C(23)	72(5)	40(4)	61(4)	-18(3)	2(4)	18(4)
C(41)	53(4)	62(4)	43(3)	-22(3)	5(3)	-5(3)
C(3)	30(3)	46(3)	39(3)	6(3)	-7(3)	-5(3)
C(42)	62(4)	31(3)	72(4)	7(3)	7(4)	1(3)

Hydrogen coordinates (x 10^4) and isotropic displacement parameters (A^2 x 10^3)

	x	y	z	U(eq)
H(1A)	2346	7475	2085	0
H(1B)	1495	7669	2588	0
H(2A)	2145	7090	109	0
H(2B)	2627	7198	940	0
H(14A)	1110(4)	9660(4)	-391(4)	67
H(15A)	1498(5)	8269(4)	-1044(3)	70
H(22A)	401(4)	9117(4)	2706(4)	66
H(21A)	1854(5)	9195(4)	3396(4)	76
H(13A)	2486(6)	10306(4)	127(4)	72
H(12A)	3724(4)	9351(5)	-221(4)	70
H(11A)	3132(5)	8093(5)	-947(4)	75
H(43A)	-544(4)	7572(4)	2690(3)	75
H(43B)	245(4)	6958(4)	2741(3)	75
H(43C)	-673(4)	6611(4)	2529(3)	75
H(25A)	2833(5)	10130(4)	2598(5)	83
H(44A)	-1030(4)	8547(4)	2011(4)	82
H(44B)	-1536(4)	8547(4)	1205(4)	82
H(44C)	-730(4)	9129(4)	1313(4)	82
H(24A)	1975(6)	10649(4)	1393(5)	87
H(46A)	-182(4)	8087(4)	-825(3)	82
H(46B)	-198(4)	8873(4)	-265(3)	82
H(46C)	-1038(4)	8341(4)	-390(3)	82
H(23A)	462(5)	10029(4)	1459(4)	69
H(41A)	480(4)	6933(4)	-887(3)	79
H(41B)	200(4)	6067(4)	-529(3)	79
H(41C)	1142(4)	6396(4)	-398(3)	79
H(42A)	531(4)	5673(3)	1854(4)	83
H(42B)	1195(4)	5710(3)	1151(4)	83
H(42C)	269(4)	5345(3)	1009(4)	83

APPENDIX 7

Crystal Structure of $(Cp^*Ir(CpCo)_2(\mu_3\text{-}CO)(\mu_3\text{-}CH)(\mu_2\text{-}H)$

Crystal data and structure refinement

Identification code	irchhch
Empirical formula	$C_{22}H_{27}Co_2IrO$
Formula weight	617.50
Temperature	293(2) K
Wavelength	0.71073 Å
Crystal system	Monoclinic
Space group	P2(1)/c
Unit cell dimensions	a = 10.187(2) Å α = 90° b = 9.314(2) Å β = 96.56(2)° c = 20.900(6) Å gamma = 90°
Volume, Z	1970.0(8) A^3, 4
Density (calculated)	2.082 Mg/m^3
Absorption coefficient	8.410 mm^{-1}
F(000)	1192
Crystal size	? x ? x ? mm
Theta range for data collection	2.01 to 23.05°
Limiting indices	-5<=h<=11, -5<=k<=10, -23<=l<=22
Reflections collected	3203
Independent reflections	2760 [R(int) = 0.0209]
Refinement method	Full-matrix least-squares on F^2
Data / restraints / parameters	2755 / 0 / 238
Goodness-of-fit on F^2	1.165
Final R indices [I>2sigma(I)]	R1 = 0.0459, wR2 = 0.0923
R indices (all data)	R1 = 0.0601, wR2 = 0.1034
Largest diff. peak and hole	2.717 and -1.250 $e.Å^{-3}$

Atomic coordinates (x 10^4) and equivalent isotropic displacement parameters (A^2 x 10^3). U(eq) is defined as one third of the trace of the orthogonalized Uij tensor.

	x	y	z	U(eq)
Ir(1)	7294(1)	2310(1)	4149(1)	23(1)
Co(2)	7300(2)	4016(2)	3211(1)	23(1)
Co(1)	5365(2)	3969(2)	3770(1)	25(1)
C(14)	8713(11)	1788(12)	5045(6)	24(3)
C(13)	7672(12)	766(12)	4984(5)	24(3)
O(1)	7768(12)	5367(12)	4441(6)	70(3)
C(15)	9349(11)	1718(13)	4477(6)	29(3)
C(12)	7723(12)	-20(13)	4392(6)	28(3)
C(11)	8751(11)	599(13)	4070(6)	25(3)
C(42)	6839(14)	-1256(13)	4152(7)	38(3)
C(44)	9051(13)	2801(14)	5596(6)	38(3)
C(43)	6805(13)	426(15)	5496(7)	38(3)
C(41)	9189(15)	84(16)	3460(7)	45(4)
C(1)	7287(13)	4490(12)	4074(6)	27(3)
C(2)	6163(11)	2467(14)	3286(6)	28(3)
C(33)	4263(12)	5595(14)	4170(6)	34(3)
C(35)	3307(12)	3699(15)	3579(6)	35(3)
C(45)	10567(12)	2580(15)	4359(7)	42(4)
C(34)	3630(12)	4251(15)	4199(7)	38(3)
C(32)	4373(12)	5842(14)	3520(7)	36(3)
C(25)	7886(15)	3578(16)	2297(6)	41(4)
C(31)	3801(12)	4650(14)	3147(6)	31(3)
C(23)	7581(22)	5801(18)	2667(9)	62(5)
C(24)	7018(16)	4748(22)	2269(7)	60(5)
C(22)	8780(22)	5325(25)	2946(8)	80(7)
C(21)	8976(16)	3945(22)	2713(8)	59(5)

Bond lengths [Å]

Ir(1)-C(2)	2.031(12)	Co(1)-C(33)	2.114(12)
Ir(1)-C(1)	2.037(11)	Co(1)-H(1)	1.64(9)
Ir(1)-C(15)	2.197(12)	C(14)-C(15)	1.42(2)
Ir(1)-C(11)	2.197(11)	C(14)-C(13)	1.42(2)
Ir(1)-C(13)	2.260(11)	C(14)-C(44)	1.50(2)
Ir(1)-C(12)	2.260(12)	C(13)-C(12)	1.44(2)
Ir(1)-C(14)	2.284(11)	C(13)-C(43)	1.50(2)
Ir(1)-Co(2)	2.524(2)	O(1)-C(1)	1.19(2)
Ir(1)-Co(1)	2.554(2)	C(15)-C(11)	1.44(2)
Ir(1)-H(1)	1.44(9)	C(15)-C(45)	1.52(2)
Co(2)-C(2)	1.868(12)	C(12)-C(11)	1.43(2)
Co(2)-C(1)	1.859(12)	C(12)-C(42)	1.51(2)
Co(2)-C(23)	2.05(2)	C(11)-C(41)	1.48(2)
Co(2)-C(22)	2.063(14)	C(2)-H(2)	1.34(10)
Co(2)-C(24)	2.07(2)	C(33)-C(32)	1.40(2)
Co(2)-C(21)	2.099(14)	C(33)-C(34)	1.41(2)
Co(2)-C(25)	2.105(12)	C(35)-C(34)	1.40(2)
Co(2)-Co(1)	2.404(2)	C(35)-C(31)	1.40(2)
Co(1)-C(2)	1.957(12)	C(32)-C(31)	1.44(2)
Co(1)-C(31)	2.040(12)	C(25)-C(21)	1.37(2)
Co(1)-C(1)	2.047(13)	C(25)-C(24)	1.40(2)
Co(1)-C(32)	2.053(12)	C(23)-C(22)	1.37(3)
Co(1)-C(34)	2.087(12)	C(23)-C(24)	1.37(2)
Co(1)-C(35)	2.104(13)	C(22)-C(21)	1.40(3)

Bond Angles [°]

C(2)-Ir(1)-C(1)	82.1(5)	C(24)-Co(2)-C(25)	39.2(6)
C(2)-Ir(1)-C(15)	135.9(5)	C(21)-Co(2)-C(25)	38.1(6)
C(1)-Ir(1)-C(15)	105.6(5)	C(2)-Co(2)-Co(1)	52.7(4)
C(2)-Ir(1)-C(11)	107.8(5)	C(1)-Co(2)-Co(1)	55.6(4)
C(1)-Ir(1)-C(11)	135.6(5)	C(23)-Co(2)-Co(1)	117.2(5)
C(15)-Ir(1)-C(11)	38.2(5)	C(22)-Co(2)-Co(1)	143.7(7)
C(2)-Ir(1)-C(13)	139.5(5)	C(24)-Co(2)-Co(1)	115.8(4)
C(1)-Ir(1)-C(13)	133.8(4)	C(21)-Co(2)-Co(1)	177.1(6)
C(15)-Ir(1)-C(13)	61.8(4)	C(25)-Co(2)-Co(1)	140.4(4)
C(11)-Ir(1)-C(13)	62.6(4)	C(2)-Co(2)-Ir(1)	52.5(4)
C(2)-Ir(1)-C(12)	110.1(5)	C(1)-Co(2)-Ir(1)	52.8(3)
C(1)-Ir(1)-C(12)	166.8(5)	C(23)-Co(2)-Ir(1)	162.4(6)
C(15)-Ir(1)-C(12)	62.4(4)	C(22)-Co(2)-Ir(1)	130.3(7)
C(11)-Ir(1)-C(12)	37.4(4)	C(24)-Co(2)-Ir(1)	158.8(6)
C(13)-Ir(1)-C(12)	37.3(4)	C(21)-Co(2)-Ir(1)	116.1(5)
C(2)-Ir(1)-C(14)	170.1(5)	C(25)-Co(2)-Ir(1)	127.5(4)
C(1)-Ir(1)-C(14)	105.7(4)	Co(1)-Co(2)-Ir(1)	62.37(5)
C(15)-Ir(1)-C(14)	36.8(4)	C(2)-Co(1)-C(31)	103.5(5)
C(11)-Ir(1)-C(14)	62.4(4)	C(2)-Co(1)-C(1)	83.7(5)
C(13)-Ir(1)-C(14)	36.4(4)	C(31)-Co(1)-C(1)	140.7(5)
C(12)-Ir(1)-C(14)	61.5(4)	C(2)-Co(1)-C(32)	134.2(5)
C(2)-Ir(1)-Co(2)	46.9(3)	C(31)-Co(1)-C(32)	41.2(5)
C(1)-Ir(1)-Co(2)	46.6(3)	C(1)-Co(1)-C(32)	107.6(5)
C(15)-Ir(1)-Co(2)	108.3(3)	C(2)-Co(1)-C(34)	137.2(5)
C(11)-Ir(1)-Co(2)	109.7(3)	C(31)-Co(1)-C(34)	66.3(5)
C(13)-Ir(1)-Co(2)	170.0(3)	C(1)-Co(1)-C(34)	131.6(5)
C(12)-Ir(1)-Co(2)	139.6(3)	C(32)-Co(1)-C(34)	65.6(5)
C(14)-Ir(1)-Co(2)	135.5(3)	C(2)-Co(1)-C(35)	106.3(5)
C(2)-Ir(1)-Co(1)	48.9(3)	C(31)-Co(1)-C(35)	39.4(5)
C(1)-Ir(1)-Co(1)	51.5(4)	C(1)-Co(1)-C(35)	169.9(5)
C(15)-Ir(1)-Co(1)	157.0(3)	C(32)-Co(1)-C(35)	66.6(5)
C(11)-Ir(1)-Co(1)	156.7(3)	C(34)-Co(1)-C(35)	39.0(5)
C(13)-Ir(1)-Co(1)	133.0(3)	C(2)-Co(1)-C(33)	171.0(5)
C(12)-Ir(1)-Co(1)	140.6(3)	C(31)-Co(1)-C(33)	67.5(5)
C(14)-Ir(1)-Co(1)	140.9(3)	C(1)-Co(1)-C(33)	103.9(5)
Co(2)-Ir(1)-Co(1)	56.52(5)	C(32)-Co(1)-C(33)	39.1(5)
C(2)-Ir(1)-H(1)	72(4)	C(34)-Co(1)-C(33)	39.3(5)
C(1)-Ir(1)-H(1)	76(4)	C(35)-Co(1)-C(33)	66.3(5)
C(15)-Ir(1)-H(1)	152(4)	C(2)-Co(1)-Co(2)	49.4(3)
C(11)-Ir(1)-H(1)	148(4)	C(31)-Co(1)-Co(2)	108.0(4)
C(13)-Ir(1)-H(1)	96(4)	C(1)-Co(1)-Co(2)	48.5(3)
C(12)-Ir(1)-H(1)	112(4)	C(32)-Co(1)-Co(2)	105.5(4)
C(14)-Ir(1)-H(1)	116(4)	C(34)-Co(1)-Co(2)	171.1(4)
Co(2)-Ir(1)-H(1)	93(4)	C(35)-Co(1)-Co(2)	139.9(4)
Co(1)-Ir(1)-H(1)	37(4)	C(33)-Co(1)-Co(2)	132.9(4)
C(2)-Co(2)-C(1)	91.6(5)	C(2)-Co(1)-Ir(1)	51.5(4)
C(2)-Co(2)-C(23)	143.0(8)	C(31)-Co(1)-Ir(1)	154.6(4)
C(1)-Co(2)-C(23)	111.2(6)	C(1)-Co(1)-Ir(1)	51.1(3)
C(2)-Co(2)-C(22)	163.4(7)	C(32)-Co(1)-Ir(1)	158.7(4)
C(1)-Co(2)-C(22)	101.9(6)	C(34)-Co(1)-Ir(1)	127.0(4)
C(23)-Co(2)-C(22)	38.8(8)	C(35)-Co(1)-Ir(1)	134.5(4)
C(2)-Co(2)-C(24)	108.3(7)	C(33)-Co(1)-Ir(1)	137.4(4)
C(1)-Co(2)-C(24)	145.9(7)	Co(2)-Co(1)-Ir(1)	61.11(5)
C(23)-Co(2)-C(24)	38.8(7)	C(2)-Co(1)-H(1)	70(3)
C(22)-Co(2)-C(24)	65.0(7)	C(31)-Co(1)-H(1)	147(3)
C(2)-Co(2)-C(21)	124.4(7)	C(1)-Co(1)-H(1)	72(3)
C(1)-Co(2)-C(21)	125.8(7)	C(32)-Co(1)-H(1)	156(3)
C(23)-Co(2)-C(21)	65.1(7)	C(34)-Co(1)-H(1)	96(3)
C(22)-Co(2)-C(21)	39.2(7)	C(35)-Co(1)-H(1)	109(3)
C(24)-Co(2)-C(21)	64.7(6)	C(33)-Co(1)-H(1)	117(3)
C(2)-Co(2)-C(25)	99.7(5)	Co(2)-Co(1)-H(1)	93(3)
C(1)-Co(2)-C(25)	163.9(6) 1	Ir(1)-Co(1)-H(1)	31(3)
C(23)-Co(2)-C(25)	65.3(6)		
C(22)-Co(2)-C(25)	65.1(6)		

C(15)-C(14)-C(13)	107.5(10)
C(15)-C(14)-C(44)	125.9(11)
C(13)-C(14)-C(44)	126.5(11)
C(15)-C(14)-Ir(1)	68.3(7)
C(13)-C(14)-Ir(1)	70.9(6)
C(44)-C(14)-Ir(1)	124.4(8)
C(14)-C(13)-C(12)	108.5(10)
C(14)-C(13)-C(43)	125.0(11)
C(12)-C(13)-C(43)	125.9(12)
C(14)-C(13)-Ir(1)	72.7(6)
C(12)-C(13)-Ir(1)	71.4(6)
C(43)-C(13)-Ir(1)	128.6(8)
C(14)-C(15)-C(11)	109.0(10)
C(14)-C(15)-C(45)	124.8(12)
C(11)-C(15)-C(45)	125.9(11)
C(14)-C(15)-Ir(1)	74.9(7)
C(11)-C(15)-Ir(1)	70.9(6)
C(45)-C(15)-Ir(1)	125.6(9)
C(11)-C(12)-C(13)	107.4(10)
C(11)-C(12)-C(42)	126.3(12)
C(13)-C(12)-C(42)	126.3(11)
C(11)-C(12)-Ir(1)	68.9(7)
C(13)-C(12)-Ir(1)	71.4(6)
C(42)-C(12)-Ir(1)	124.3(9)
C(12)-C(11)-C(15)	107.4(10)
C(12)-C(11)-C(41)	125.8(12)
C(15)-C(11)-C(41)	126.6(11)
C(12)-C(11)-Ir(1)	73.7(7)
C(15)-C(11)-Ir(1)	71.0(7)
C(41)-C(11)-Ir(1)	124.9(9)
C(12)-C(42)-H(42A)	110.0(7)
C(12)-C(42)-H(42B)	109.2(7)
H(42A)-C(42)-H(42B)	109.5
C(12)-C(42)-H(42C)	109.2(7)
H(42A)-C(42)-H(42C)	109.5
H(42B)-C(42)-H(42C)	109.5
C(14)-C(44)-H(44A)	109.6(7)
C(14)-C(44)-H(44B)	109.3(7)
H(44A)-C(44)-H(44B)	109.5
C(14)-C(44)-H(44C)	109.6(7)
H(44A)-C(44)-H(44C)	109.5
H(44B)-C(44)-H(44C)	109.5
C(13)-C(43)-H(43A)	109.2(7)
C(13)-C(43)-H(43B)	110.1(7)
H(43A)-C(43)-H(43B)	109.5
C(13)-C(43)-H(43C)	109.1(7)
H(43A)-C(43)-H(43C)	109.5
H(43B)-C(43)-H(43C)	109.5
C(11)-C(41)-H(41A)	110.2(7)
C(11)-C(41)-H(41B)	109.1(8)
H(41A)-C(41)-H(41B)	109.5
C(11)-C(41)-H(41C)	109.1(8)
H(41A)-C(41)-H(41C)	109.5
H(41B)-C(41)-H(41C)	109.5
O(1)-C(1)-Co(2)	137.8(11)
O(1)-C(1)-Ir(1)	129.8(10)
Co(2)-C(1)-Ir(1)	80.6(4)
O(1)-C(1)-Co(1)	132.3(11)
Co(2)-C(1)-Co(1)	75.8(4)
Ir(1)-C(1)-Co(1)	77.4(4)
Co(2)-C(2)-Co(1)	77.8(5)
Co(2)-C(2)-Ir(1)	80.6(5)
Co(1)-C(2)-Ir(1)	79.6(4)
Co(2)-C(2)-H(2)	140(4)
Co(1)-C(2)-H(2)	131(4)
Ir(1)-C(2)-H(2)	125(4)
C(32)-C(33)-C(34)	106.0(12)
C(32)-C(33)-Co(1)	68.1(7)
C(34)-C(33)-Co(1)	69.4(7)
C(32)-C(33)-H(33A)	125.6(8)
C(34)-C(33)-H(33A)	128.4(8)
Co(1)-C(33)-H(33A)	126.3(4)
C(34)-C(35)-C(31)	107.5(12)
C(34)-C(35)-Co(1)	69.9(7)
C(31)-C(35)-Co(1)	67.8(7)
C(34)-C(35)-H(35A)	127.2(8)
C(31)-C(35)-H(35A)	125.2(8)
Co(1)-C(35)-H(35A)	125.4(4)
C(15)-C(45)-H(45A)	109.1(7)
C(15)-C(45)-H(45B)	110.2(7)
H(45A)-C(45)-H(45B)	109.5
C(15)-C(45)-H(45C)	109.2(7)
H(45A)-C(45)-H(45C)	109.5
H(45B)-C(45)-H(45C)	109.5
C(35)-C(34)-C(33)	110.3(12)
C(35)-C(34)-Co(1)	71.2(7)
C(33)-C(34)-Co(1)	71.4(7)
C(35)-C(34)-H(34A)	125.1(8)
C(33)-C(34)-H(34A)	124.7(8)
Co(1)-C(34)-H(34A)	125.0(4)
C(33)-C(32)-C(31)	109.1(12)
C(33)-C(32)-Co(1)	72.8(7)
C(31)-C(32)-Co(1)	68.9(7)
C(33)-C(32)-H(32A)	125.4(8)
C(31)-C(32)-H(32A)	125.5(7)
Co(1)-C(32)-H(32A)	124.7(4)
C(21)-C(25)-C(24)	107(2)
C(21)-C(25)-Co(2)	70.7(8)
C(24)-C(25)-Co(2)	69.2(8)
C(21)-C(25)-H(25A)	125.0(11)
C(24)-C(25)-H(25A)	127.9(10)
Co(2)-C(25)-H(25A)	124.9(4)
C(35)-C(31)-C(32)	107.0(11)
C(35)-C(31)-Co(1)	72.7(7)
C(32)-C(31)-Co(1)	69.9(7)
C(35)-C(31)-H(31A)	127.0(8)
C(32)-C(31)-H(31A)	125.8(7)
Co(1)-C(31)-H(31A)	126.4(4)
C(22)-C(23)-C(24)	109(2)
C(22)-C(23)-Co(2)	71.1(10)
C(24)-C(23)-Co(2)	71.4(9)
C(22)-C(23)-H(23A)	128.4(12)
C(24)-C(23)-H(23A)	123.0(11)
Co(2)-C(23)-H(23A)	124.6(5)
C(23)-C(24)-C(25)	108(2)
C(23)-C(24)-Co(2)	69.8(9)
C(25)-C(24)-Co(2)	71.6(8)
C(23)-C(24)-H(24A)	128.0(11)
C(25)-C(24)-H(24A)	123.8(10)
Co(2)-C(24)-H(24A)	124.9(5)
C(23)-C(22)-C(21)	108(2)
C(23)-C(22)-Co(2)	70.2(9)
C(21)-C(22)-Co(2)	71.8(9)
C(23)-C(22)-H(22A)	124.4(12)
C(21)-C(22)-H(22A)	127.7(13)
Co(2)-C(22)-H(22A)	126.3(5)
C(25)-C(21)-C(22)	108(2)
C(25)-C(21)-Co(2)	71.2(8)
C(22)-C(21)-Co(2)	69.0(9)
C(25)-C(21)-H(21A)	126.3(11)
C(22)-C(21)-H(21A)	125.5(13)
Co(2)-C(21)-H(21A)	125.4(5)

Anisotropic displacement parameters ($Å^2$ x 10^3)
The anisotropic displacement factor exponent takes the form:
$-2\pi^2$ [h^2 a^{*2} U11 + ... + 2 h k a* b* U12]

	U11	U22	U33	U23	U13	U12
Ir(1)	22(1)	24(1)	26(1)	7(1)	8(1)	5(1)
Co(2)	27(1)	24(1)	19(1)	2(1)	7(1)	-1(1)
Co(1)	22(1)	28(1)	27(1)	8(1)	6(1)	5(1)
C(14)	25(7)	13(6)	31(7)	5(5)	-5(5)	3(5)
C(13)	44(8)	21(6)	9(6)	3(5)	9(5)	19(6)
O(1)	78(9)	52(7)	80(9)	2(7)	7(7)	-2(6)
C(15)	19(6)	29(7)	39(8)	9(6)	6(6)	2(5)
C(12)	26(7)	23(7)	34(8)	5(6)	-3(6)	-3(5)
C(11)	22(6)	32(7)	23(7)	7(6)	6(5)	11(5)
C(42)	52(9)	23(7)	40(8)	-2(6)	2(7)	4(6)
C(44)	37(7)	35(8)	38(8)	-6(6)	-9(6)	-2(6)
C(43)	32(7)	40(8)	45(9)	12(7)	15(6)	10(6)
C(41)	56(9)	42(8)	40(9)	-3(7)	19(7)	14(7)
C(1)	52(8)	7(5)	20(7)	-8(5)	-9(6)	-8(6)
C(2)	26(6)	36(7)	25(6)	6(6)	12(5)	-2(6)
C(33)	35(8)	31(7)	34(8)	-3(6)	-1(6)	13(6)
C(35)	27(7)	43(8)	36(8)	-9(7)	10(6)	0(6)
C(45)	20(7)	51(9)	55(9)	16(8)	1(6)	1(7)
C(34)	22(7)	44(9)	50(9)	4(7)	17(6)	10(6)
C(32)	28(7)	30(7)	50(9)	6(7)	8(6)	16(6)
C(25)	56(10)	46(9)	25(7)	-7(7)	25(7)	-7(8)
C(31)	27(7)	43(8)	21(7)	2(6)	-6(6)	13(6)
C(23)	97(15)	42(10)	56(12)	7(9)	42(11)	-1(10)
C(24)	47(10)	108(15)	30(9)	18(10)	16(8)	11(10)
C(22)	102(16)	108(17)	36(10)	-14(11)	31(11)	-92(15)
C(21)	41(10)	97(15)	44(10)	27(10)	22(8)	-3(9)

Hydrogen coordinates (x 10^4) and isotropic
displacement parameters ($Å^2$ x 10^3)

	x	y	z	U(eq)
H(42A)	7216(14)	-2147(13)	4314(7)	80
H(42B)	5986(14)	-1131(13)	4298(7)	80
H(42C)	6747(14)	-1267(13)	3690(7)	80
H(44A)	9655(13)	2345(14)	5920(6)	80
H(44B)	9454(13)	3647(14)	5443(6)	80
H(44C)	8261(13)	3063(14)	5778(6)	80
H(43A)	7238(13)	-267(15)	5787(7)	80
H(43B)	6633(13)	1281(15)	5729(7)	80
H(43C)	5985(13)	36(15)	5297(7)	80
H(41A)	9832(15)	-666(16)	3544(7)	80
H(41B)	8439(15)	-277(16)	3187(7)	80
H(41C)	9573(15)	870(16)	3249(7)	80
H(33A)	4576(12)	6223(14)	4519(6)	80
H(35A)	2865(12)	2810(15)	3464(6)	80
H(45A)	11341(12)	2089(15)	4552(7)	80
H(45B)	10612(12)	2685(15)	3905(7)	80
H(45C)	10520(12)	3512(15)	4552(7)	80
H(34A)	3438(12)	3793(15)	4589(7)	80
H(32A)	4764(12)	6676(14)	3349(7)	80
H(25A)	7764(15)	2677(16)	2076(6)	80
H(31A)	3713(12)	4573(14)	2686(6)	80
H(23A)	7169(22)	6715(18)	2718(9)	80
H(24A)	6183(16)	4771(22)	2005(7)	80
H(22A)	9383(22)	5887(25)	3231(8)	80
H(21A)	9742(16)	3359(22)	2827(8)	80
H(1)	5979(92)	2701(104)	4264(46)	50
H(2)	5627(92)	1361(104)	2944(46)	50

APPENDIX 8

Crystal Structure of $Cp^*Rh(CpCo)_2(\mu_3\text{-}CO)(\mu_3\text{-}HC{\equiv}CH)$

Crystal data and structure refinement

Identification code	rhhchfin
Empirical formula	$C_{23}H_{27}Co_2ORh$
Formula weight	540.22
Temperature	293(2) K
Wavelength	0.71073 Å
Crystal system	Monoclinic
Space group	P2(1)/c
Unit cell dimensions	a = 14.539(3) Å α = 90° b = 10.707(2) Å β = 115.17(2)° c = 14.581(3) Å γ = 90°
Volume, Z	2054.3(7) $Å^3$, 4
Density (calculated)	1.747 Mg/m^3
Absorption coefficient	2.400 mm^{-1}
F(000)	1088
Crystal size	? x ? x ? mm
Theta range for data collection	2.45 to 22.55°
Limiting indices	-15<=h<=5, -5<=k<=11, -14<=l<=13
Reflections collected	2853
Independent reflections	2635 [R(int) = 0.0098]
Refinement method	Full-matrix least-squares on F^2
Data / restraints / parameters	2635 / 0 / 250
Goodness-of-fit on F^2	1.122
Final R indices [I>2sigma(I)]	R1 = 0.0291, wR2 = 0.0679
R indices (all data)	R1 = 0.0371, wR2 = 0.0720
Largest diff. peak and hole	0.407 and -0.493 $e.A^{-3}$

Atomic coordinates (x 10^4) and equivalent isotropic displacement parameters (A^2 x 10^3) U(eq) is defined as one third of the trace of the orthogonalized Uij tensor.

	x	y	z	U(eq)
Rh(1)	7309(1)	1325(1)	3381(1)	25(1)
Co(2)	8096(1)	3480(1)	3723(1)	29(1)
Co(1)	9074(1)	1803(1)	3416(1)	28(1)
O(1)	7367(2)	2549(3)	1593(2)	41(1)
C(3)	9136(4)	2356(4)	4674(4)	32(1)
C(15)	6734(3)	-621(4)	3153(4)	36(1)
C(12)	5678(3)	1013(4)	2314(3)	33(1)
C(11)	6256(3)	15(4)	2197(4)	34(1)
C(13)	5785(3)	993(4)	3346(4)	34(1)
C(2)	8230(4)	2079(4)	4695(4)	31(1)
C(14)	6417(3)	-27(4)	3847(4)	34(1)
C(1)	7769(3)	2313(4)	2476(4)	31(1)
C(32)	10559(4)	1962(6)	3570(6)	63(2)
C(44)	6670(4)	-429(6)	4914(4)	53(2)
C(34)	9369(5)	802(7)	2365(5)	70(2)
C(45)	7356(4)	-1791(5)	3347(5)	55(2)
C(24)	6953(5)	4763(6)	3335(9)	86(3)
C(35)	9731(5)	141(6)	3262(6)	67(2)
C(43)	5263(4)	1857(6)	3777(5)	57(2)
C(33)	9885(5)	1930(7)	2540(5)	62(2)
C(31)	10449(4)	834(6)		

Bond lengths [Å]

Rh(1)-C(2)	1.983(5)	O(1)-C(1)	1.193(5)
Rh(1)-C(1)	2.015(5)	C(3)-C(2)	1.364(7)
Rh(1)-C(15)	2.218(5)	C(3)-H(3A)	1.03(6)
Rh(1)-C(13)	2.223(4)	C(15)-C(14)	1.427(7)
Rh(1)-C(14)	2.234(4)	C(15)-C(11)	1.437(7)
Rh(1)-C(12)	2.241(4)	C(15)-C(45)	1.500(7)
Rh(1)-C(11)	2.246(4)	C(12)-C(11)	1.413(7)
Rh(1)-Co(2)	2.5288(8)	C(12)-C(13)	1.446(7)
Rh(1)-Co(1)	2.5954(8)	C(12)-C(42)	1.490(7)
Co(2)-C(3)	1.969(5)	C(11)-C(41)	1.495(7)
Co(2)-C(2)	2.016(5)	C(13)-C(14)	1.414(7)
Co(2)-C(23)	2.034(6)	C(13)-C(43)	1.495(7)
Co(2)-C(25)	2.037(6)	C(2)-H(2A)	0.95(6)
Co(2)-C(24)	2.041(6)	C(14)-C(44)	1.502(7)
Co(2)-C(22)	2.042(6)	C(32)-C(31)	1.400(9)
Co(2)-C(21)	2.046(6)	C(32)-C(33)	1.401(9)
Co(2)-C(1)	2.088(5)	C(34)-C(35)	1.380(9)
Co(2)-Co(1)	2.4475(9)	C(34)-C(33)	1.387(9)
Co(1)-C(1)	1.888(5)	C(24)-C(25)	1.319(11)
Co(1)-C(3)	1.892(5)	C(24)-C(23)	1.425(13)
Co(1)-C(34)	2.060(6)	C(35)-C(31)	1.356(9)
Co(1)-C(35)	2.076(6)	C(23)-C(22)	1.407(13)
Co(1)-C(33)	2.079(5)	C(25)-C(21)	1.292(10)
Co(1)-C(32)	2.080(5)	C(22)-C(21)	1.303(11)
Co(1)-C(31)	2.085(5)		

C(2)-Rh(1)-C(1)	98.3(2)	C(21)-Co(2)-C(1)	151.2(3)
C(2)-Rh(1)-C(15)	125.7(2)	C(3)-Co(2)-Co(1)	49.27(14)
C(1)-Rh(1)-C(15)	127.2(2)	C(2)-Co(2)-Co(1)	72.08(14)
C(2)-Rh(1)-C(13)	110.1(2)	C(23)-Co(2)-Co(1)	123.0(3)
C(1)-Rh(1)-C(13)	132.4(2)	C(25)-Co(2)-Co(1)	166.4(3)
C(15)-Rh(1)-C(13)	62.4(2)	C(24)-Co(2)-Co(1)	155.7(3)
C(2)-Rh(1)-C(14)	102.2(2)	C(22)-Co(2)-Co(1)	115.3(2)
C(1)-Rh(1)-C(14)	159.5(2)	C(21)-Co(2)-Co(1)	133.4(3)
C(15)-Rh(1)-C(14)	37.4(2)	C(1)-Co(2)-Co(1)	48.41(13)
C(13)-Rh(1)-C(14)	37.0(2)	C(3)-Co(2)-Rh(1)	74.24(14)
C(2)-Rh(1)-C(12)	144.3(2)	C(2)-Co(2)-Rh(1)	50.19(13)
C(1)-Rh(1)-C(12)	99.9(2)	C(23)-Co(2)-Rh(1)	124.4(4)
C(15)-Rh(1)-C(12)	62.3(2)	C(25)-Co(2)-Rh(1)	123.2(2)
C(13)-Rh(1)-C(12)	37.8(2)	C(24)-Co(2)-Rh(1)	108.2(2)
C(14)-Rh(1)-C(12)	62.3(2)	C(22)-Co(2)-Rh(1)	162.7(4)
C(2)-Rh(1)-C(11)	163.0(2)	C(21)-Co(2)-Rh(1)	156.7(3)
C(1)-Rh(1)-C(11)	97.6(2)	C(1)-Co(2)-Rh(1)	50.65(13)
C(15)-Rh(1)-C(11)	37.5(2)	Co(1)-Co(2)-Rh(1)	62.85(2)
C(13)-Rh(1)-C(11)	62.3(2)	C(1)-Co(1)-C(3)	103.4(2)
C(14)-Rh(1)-C(11)	62.2(2)	C(1)-Co(1)-C(34)	94.2(2)
C(12)-Rh(1)-C(11)	36.7(2)	C(3)-Co(1)-C(34)	160.9(3)
C(2)-Rh(1)-Co(2)	51.37(14)	C(1)-Co(1)-C(35)	122.4(3)
C(1)-Rh(1)-Co(2)	53.26(13)	C(3)-Co(1)-C(35)	122.6(3)
C(15)-Rh(1)-Co(2)	175.75(12)	C(34)-Co(1)-C(35)	39.0(3)
C(13)-Rh(1)-Co(2)	120.89(13)	C(1)-Co(1)-C(33)	101.1(2)
C(14)-Rh(1)-Co(2)	143.52(13)	C(3)-Co(1)-C(33)	140.3(3)
C(12)-Rh(1)-Co(2)	121.95(12)	C(34)-Co(1)-C(33)	39.2(3)
C(11)-Rh(1)-Co(2)	145.55(12)	C(35)-Co(1)-C(33)	65.3(3)
C(2)-Rh(1)-Co(1)	69.23(14)	C(1)-Co(1)-C(32)	136.9(3)
C(1)-Rh(1)-Co(1)	46.26(13)	C(3)-Co(1)-C(32)	104.5(2)
C(15)-Rh(1)-Co(1)	119.67(12)	C(34)-Co(1)-C(32)	65.6(2)
C(13)-Rh(1)-Co(1)	177.85(13)	C(35)-Co(1)-C(32)	65.0(2)
C(14)-Rh(1)-Co(1)	144.97(13)	C(33)-Co(1)-C(32)	39.4(2)
C(12)-Rh(1)-Co(1)	142.06(12)	C(1)-Co(1)-C(31)	158.8(2)
C(11)-Rh(1)-Co(1)	118.93(12)	C(3)-Co(1)-C(31)	96.8(2)
Co(2)-Rh(1)-Co(1)	57.04(2)	C(34)-Co(1)-C(31)	65.0(3)
C(3)-Co(2)-C(2)	40.0(2)	C(35)-Co(1)-C(31)	38.0(2)
C(3)-Co(2)-C(23)	157.0(5)	C(33)-Co(1)-C(31)	65.6(2)
C(2)-Co(2)-C(23)	161.9(5)	C(32)-Co(1)-C(31)	39.3(2)
C(3)-Co(2)-C(25)	118.4(3)	C(1)-Co(1)-Co(2)	55.79(14)
C(2)-Co(2)-C(25)	102.0(3)	C(3)-Co(1)-Co(2)	52.08(14)
C(23)-Co(2)-C(25)	65.5(3)	C(34)-Co(1)-Co(2)	147.0(2)
C(3)-Co(2)-C(24)	153.8(4)	C(35)-Co(1)-Co(2)	168.1(2)
C(2)-Co(2)-C(24)	121.3(4)	C(33)-Co(1)-Co(2)	126.1(2)
C(23)-Co(2)-C(24)	40.9(4)	C(32)-Co(1)-Co(2)	125.3(2)
C(25)-Co(2)-C(24)	37.7(3)	C(31)-Co(1)-Co(2)	145.3(2)
C(3)-Co(2)-C(22)	118.6(4)	C(1)-Co(1)-Rh(1)	50.44(14)
C(2)-Co(2)-C(22)	147.1(4)	C(3)-Co(1)-Rh(1)	73.75(14)
C(23)-Co(2)-C(22)	40.4(4)	C(34)-Co(1)-Rh(1)	113.6(2)
C(25)-Co(2)-C(22)	63.0(3)	C(35)-Co(1)-Rh(1)	109.0(2)
C(24)-Co(2)-C(22)	65.9(3)	C(33)-Co(1)-Rh(1)	144.6(2)
C(3)-Co(2)-C(21)	103.5(3)	C(32)-Co(1)-Rh(1)	171.9(2)
C(2)-Co(2)-C(21)	113.3(3)	C(31)-Co(1)-Rh(1)	132.7(2)
C(23)-Co(2)-C(21)	65.2(3)	Co(2)-Co(1)-Rh(1)	60.11(2)
C(25)-Co(2)-C(21)	36.9(3)	C(2)-C(3)-Co(1)	107.8(3)
C(24)-Co(2)-C(21)	63.6(3)	C(2)-C(3)-Co(2)	71.8(3)
C(22)-Co(2)-C(21)	37.2(3)	Co(1)-C(3)-Co(2)	78.6(2)
C(3)-Co(2)-C(1)	94.0(2)	C(2)-C(3)-H(3A)	125(3)
C(2)-Co(2)-C(1)	94.9(2)	Co(1)-C(3)-H(3A)	126(3)
C(23)-Co(2)-C(1)	90.0(2)	Co(2)-C(3)-H(3A)	127(4)
C(25)-Co(2)-C(1)	145.2(3)	C(14)-C(15)-C(11)	107.9(4)
C(24)-Co(2)-C(1)	107.8(3)	C(14)-C(15)-C(45)	126.1(5)
C(22)-Co(2)-C(1)	114.1(4)	C(11)-C(15)-C(45)	125.7(5)
		C(14)-C(15)-Rh(1)	71.9(3)

C(11)-C(15)-Rh(1)	72.3(3)	C(23)-C(24)-Co(2)	69.3(4)
C(45)-C(15)-Rh(1)	126.7(3)	C(25)-C(24)-H(24A)	127.0(6)
C(11)-C(12)-C(13)	107.9(4)	C(23)-C(24)-H(24A)	126.3(7)
C(11)-C(12)-C(42)	125.5(5)	Co(2)-C(24)-H(24A)	126.5(2)
C(13)-C(12)-C(42)	126.6(5)	C(31)-C(35)-C(34)	109.0(6)
C(11)-C(12)-Rh(1)	71.9(2)	C(31)-C(35)-Co(1)	71.3(3)
C(13)-C(12)-Rh(1)	70.4(2)	C(34)-C(35)-Co(1)	69.9(3)
C(42)-C(12)-Rh(1)	123.7(3)	C(31)-C(35)-H(35A)	125.7(4)
C(12)-C(11)-C(15)	108.0(4)	C(34)-C(35)-H(35A)	125.3(4)
C(12)-C(11)-C(41)	126.2(5)	Co(1)-C(35)-H(35A)	125.4(2)
C(15)-C(11)-C(41)	125.8(5)	C(13)-C(43)-H(43A)	110.2(3)
C(12)-C(11)-Rh(1)	71.4(3)	C(13)-C(43)-H(43B)	108.9(3)
C(15)-C(11)-Rh(1)	70.1(3)	H(43A)-C(43)-H(43B)	109.5
C(41)-C(11)-Rh(1)	124.1(3)	C(13)-C(43)-H(43C)	109.3(3)
C(14)-C(13)-C(12)	108.0(4)	H(43A)-C(43)-H(43C)	109.5
C(14)-C(13)-C(43)	126.6(5)	H(43B)-C(43)-H(43C)	109.5
C(12)-C(13)-C(43)	125.4(5)	C(34)-C(33)-C(32)	107.2(6)
C(14)-C(13)-Rh(1)	71.9(2)	C(34)-C(33)-Co(1)	69.7(3)
C(12)-C(13)-Rh(1)	71.8(2)	C(32)-C(33)-Co(1)	70.4(3)
C(43)-C(13)-Rh(1)	124.8(3)	C(34)-C(33)-H(33A)	126.2(4)
C(3)-C(2)-Rh(1)	109.1(4)	C(32)-C(33)-H(33A)	126.6(4)
C(3)-C(2)-Co(2)	68.1(3)	Co(1)-C(33)-H(33A)	126.4(2)
Rh(1)-C(2)-Co(2)	78.4(2)	C(35)-C(31)-C(32)	108.3(6)
C(3)-C(2)-H(2A)	129(4)	C(35)-C(31)-Co(1)	70.6(3)
Rh(1)-C(2)-H(2A)	121(4)	C(32)-C(31)-Co(1)	70.2(3)
Co(2)-C(2)-H(2A)	128(4)	C(35)-C(31)-H(31A)	126.0(4)
C(13)-C(14)-C(15)	108.2(4)	C(32)-C(31)-H(31A)	125.7(4)
C(13)-C(14)-C(44)	125.2(5)	Co(1)-C(31)-H(31A)	125.8(2)
C(15)-C(14)-C(44)	126.6(5)	C(12)-C(42)-H(42A)	109.4(3)
C(13)-C(14)-Rh(1)	71.1(3)	C(12)-C(42)-H(42B)	109.7(3)
C(15)-C(14)-Rh(1)	70.7(3)	H(42A)-C(42)-H(42B)	109.5
C(44)-C(14)-Rh(1)	125.6(3)	C(12)-C(42)-H(42C)	109.3(3)
O(1)-C(1)-Co(1)	136.5(4)	H(42A)-C(42)-H(42C)	109.5
O(1)-C(1)-Rh(1)	132.1(4)	H(42B)-C(42)-H(42C)	109.5
Co(1)-C(1)-Rh(1)	83.3(2)	C(11)-C(41)-H(41A)	109.3(3)
O(1)-C(1)-Co(2)	129.7(4)	C(11)-C(41)-H(41B)	110.0(3)
Co(1)-C(1)-Co(2)	75.8(2)	H(41A)-C(41)-H(41B)	109.5
Rh(1)-C(1)-Co(2)	76.1(2)	C(11)-C(41)-H(41C)	109.1(3)
C(31)-C(32)-C(33)	107.3(6)	H(41A)-C(41)-H(41C)	109.5
C(31)-C(32)-Co(1)	70.5(3)	H(41B)-C(41)-H(41C)	109.5
C(33)-C(32)-Co(1)	70.3(3)	C(22)-C(23)-C(24)	103.4(6)
C(31)-C(32)-H(32A)	126.4(4)	C(22)-C(23)-Co(2)	70.1(4)
C(33)-C(32)-H(32A)	126.3(4)	C(24)-C(23)-Co(2)	69.8(4)
Co(1)-C(32)-H(32A)	126.0(2)	C(22)-C(23)-H(23A)	126.8(7)
C(14)-C(44)-H(44A)	109.5(3)	C(24)-C(23)-H(23A)	129.6(7)
C(14)-C(44)-H(44B)	109.7(3)	Co(2)-C(23)-H(23A)	128.4(2)
H(44A)-C(44)-H(44B)	109.5	C(21)-C(25)-C(24)	111.1(8)
C(14)-C(44)-H(44C)	109.3(3)	C(21)-C(25)-Co(2)	71.9(4)
H(44A)-C(44)-H(44C)	109.5	C(24)-C(25)-Co(2)	71.3(4)
H(44B)-C(44)-H(44C)	109.5	C(21)-C(25)-H(25A)	124.4(6)
C(35)-C(34)-C(33)	108.2(6)	C(24)-C(25)-H(25A)	124.5(6)
C(35)-C(34)-Co(1)	71.2(4)	Co(2)-C(25)-H(25A)	123.5(2)
C(33)-C(34)-Co(1)	71.2(3)	C(21)-C(22)-C(23)	108.4(8)
C(35)-C(34)-H(34A)	125.7(4)	C(21)-C(22)-Co(2)	71.6(4)
C(33)-C(34)-H(34A)	126.0(4)	C(23)-C(22)-Co(2)	69.5(4)
Co(1)-C(34)-H(34A)	125.3(2)	C(21)-C(22)-H(22A)	124.1(6)
C(15)-C(45)-H(45A)	109.7(3)	C(23)-C(22)-H(22A)	127.4(7)
C(15)-C(45)-H(45B)	109.1(3)	Co(2)-C(22)-H(22A)	125.3(2)
H(45A)-C(45)-H(45B)	109.5	C(25)-C(21)-C(22)	110.4(8)
C(15)-C(45)-H(45C)	109.6(3)	C(25)-C(21)-Co(2)	71.2(4)
H(45A)-C(45)-H(45C)	109.5	C(22)-C(21)-Co(2)	71.2(4)
H(45B)-C(45)-H(45C)	109.5	C(25)-C(21)-H(21A)	124.1(6)
C(25)-C(24)-C(23)	106.7(7)	C(22)-C(21)-H(21A)	125.5(6)
C(25)-C(24)-Co(2)	71.0(4)	Co(2)-C(21)-H(21A)	123.8(2)

Anisotropic displacement parameters (A^2 x 10^3). The anisotropic displacement factor exponent takes the form: $-2\pi^2$ [h^2 a^{*2} U11 + ... + 2 h k a* b* U12]

	U11	U22	U33	U23	U13	U12
Rh(1)	26(1)	23(1)	26(1)	-1(1)	12(1)	-1(1)
Co(2)	34(1)	21(1)	36(1)	0(1)	19(1)	1(1)
Co(1)	28(1)	26(1)	33(1)	0(1)	16(1)	2(1)
O(1)	45(2)	50(2)	26(2)	6(2)	14(2)	3(2)
C(3)	35(3)	28(3)	27(3)	-3(2)	9(2)	-4(2)
C(15)	32(3)	25(3)	49(3)	-3(2)	16(2)	-7(2)
C(12)	25(2)	38(3)	31(3)	2(2)	7(2)	-3(2)
C(11)	33(3)	34(3)	32(3)	-6(2)	11(2)	-11(2)
C(13)	26(2)	39(3)	40(3)	-3(2)	16(2)	-4(2)
C(2)	38(3)	27(3)	30(3)	-2(2)	17(2)	-1(2)
C(14)	30(3)	37(3)	38(3)	0(2)	16(2)	-12(2)
C(1)	34(3)	28(3)	35(3)	-2(2)	19(2)	-2(2)
C(32)	36(3)	56(4)	108(6)	-20(4)	41(4)	-9(3)
C(44)	56(3)	66(4)	36(3)	7(3)	19(3)	-16(3)
C(34)	49(4)	100(6)	69(5)	-43(4)	33(4)	3(4)
C(45)	51(3)	30(3)	79(4)	-5(3)	24(3)	-4(3)
C(24)	41(4)	32(4)	140(8)	-4(4)	-7(5)	11(3)
C(35)	66(4)	41(4)	113(6)	-4(4)	58(5)	12(3)
C(43)	50(3)	65(4)	71(4)	-5(3)	40(3)	3(3)
C(33)	61(4)	83(5)	68(5)	24(4)	54(4)	23(4)
C(31)	41(3)	73(5)	59(4)	15(3)	24(3)	27(3)
C(42)	38(3)	57(4)	48(3)	8(3)	8(3)	-3(3)
C(41)	63(4)	60(4)	39(3)	-16(3)	24(3)	-15(3)
C(23)	287(15)	33(4)	26(4)	18(3)	45(6)	66(7)
C(25)	120(7)	45(4)	108(7)	12(4)	87(6)	33(4)
C(22)	136(8)	26(4)	196(11)	22(5)	140(9)	9(4)
C(21)	75(5)	32(4)	112(7)	-21(4)	15(5)	1(4)

Hydrogen coordinates (x 10^4) and isotropic displacement parameters (A^2 x 10^3)

	x	y	z	U(eq)
H(3A)	9785(44)	2612(59)	5299(47)	80
H(2A)	8057(44)	2095(58)	5256(48)	80
H(32A)	11025(4)	2623(6)	3912(6)	80
H(44A)	6172(4)	-1017(6)	4913(4)	80
H(44B)	7330(4)	-812(6)	5204(4)	80
H(44C)	6670(4)	289(6)	5309(4)	80
H(34A)	8866(5)	514(7)	1724(5)	80
H(45A)	6919(4)	-2507(5)	3189(5)	80
H(45B)	7717(4)	-1789(5)	2928(5)	80
H(45C)	7834(4)	-1821(5)	4047(5)	80
H(24A)	6238(5)	4590(6)	3057(9)	80
H(35A)	9514(5)	-680(6)	3347(6)	80
H(43A)	4613(4)	1523(6)	3673(5)	80
H(43B)	5678(4)	1955(6)	4489(5)	80
H(43C)	5171(4)	2655(6)	3449(5)	80
H(33A)	9806(5)	2560(7)	2043(5)	80
H(31A)	10826(4)	589(6)	4693(5)	80
H(42A)	4389(4)	1589(5)	1141(4)	80
H(42B)	5032(4)	2701(5)	1804(4)	80
H(42C)	5374(4)	2025(5)	1046(4)	80
H(41A)	5819(4)	-891(6)	857(4)	80
H(41B)	6310(4)	413(6)	857(4)	80
H(41C)	7000(4)	-720(6)	1425(4)	80
H(23A)	7326(12)	4999(7)	2057(5)	80
H(25A)	7382(8)	4804(6)	4849(7)	80
H(22A)	9109(8)	5462(6)	3440(10)	80
H(21A)	9046(6)	5323(6)	5055(7)	80

APPENDIX 9
Crystal Structure of $Cp^*Rh(CpCo)_2(\mu_3\text{-}CO)(\mu_3\text{-}Tol\text{-}C{\equiv}CH)$

Crystal data and structure refinement for 1.

Identification code	rhtolpub
Empirical formula	C30 H33 Co2 O Rh
Formula weight	630.33
Temperature	100(2) K
Wavelength	0.71073 Å
Crystal system	Monoclinic
Space group	#14 : P2(1)/n
Unit cell dimensions	a = 9.232(2) Å α = 90° b = 16.507(3) Å β = 90.99(2)° c = 17.050(3) Å γ = 90°
Volume, Z	2597.9(9) $Å^3$, 4
Density (calculated)	1.612 Mg/m^3
Absorption coefficient	1.910 mm^{-1}
F(000)	1280
Crystal size	0.5 x 0.3 x 0.2 mm
Theta range for data collection	2.39 to 22.55°
Limiting indices	-9<=h<=0, 0<=k<=17, -18<=l<=18
Reflections collected	4072
Independent reflections	3410 [R(int) = 0.0147]
Absorption correction	Ellipsoidal
Refinement method	Full-matrix least-squares on F^2
Data / restraints / parameters	3409 / 0 / 307
Goodness-of-fit on F^2	1.071
Final R indices [I>2sigma(I)]	R1 = 0.0278, wR2 = 0.0614
R indices (all data)	R1 = 0.0365, wR2 = 0.0664
Largest diff. peak and hole	0.320 and -0.282 $e.A^{-3}$

Atomic coordinates (x 10^4) and equivalent isotropic displacement parameters (A^2 x 10^3). U(eq) is defined as one third of the trace of the orthogonalized Uij tensor.

	x	y	z	U(eq)
Rh(1)	2648(1)	3164(1)	5685(1)	20(1)
Co(2)	1241(1)	1973(1)	6264(1)	28(1)
Co(1)	888(1)	2344(1)	4866(1)	30(1)
O(1)	3511(3)	1459(2)	5243(2)	34(1)
C(4)	232(4)	3597(2)	6950(2)	25(1)
C(12)	3521(4)	4394(2)	5754(2)	28(1)
C(3)	657(4)	3094(2)	6275(2)	26(1)
C(14)	4710(4)	3389(2)	5088(2)	32(1)
C(1)	2547(4)	1902(2)	5412(2)	27(1)
C(15)	5033(4)	3291(2)	5908(2)	30(1)
C(5)	1000(4)	3583(2)	7662(2)	31(1)
C(2)	405(4)	3253(2)	5490(2)	29(1)
C(13)	3790(4)	4070(2)	4993(2)	30(1)
C(11)	4307(4)	3913(2)	6316(2)	26(1)
C(6)	-943(4)	4125(2)	6889(2)	33(1)
C(8)	-1324(4)	4615(3)	7513(2)	37(1)
C(45)	5997(5)	2654(3)	6259(3)	48(1)
C(7)	620(4)	4076(2)	8279(2)	32(1)
C(41)	4453(5)	4101(3)	7174(2)	45(1)
C(9)	-548(4)	4600(2)	8214(2)	30(1)
C(43)	3219(5)	4417(3)	4230(3)	51(1)
C(10)	-960(5)	5125(3)	8901(3)	44(1)
C(44)	5306(5)	2857(3)	4453(3)	53(1)
C(33)	1424(6)	1867(4)	3767(3)	59(2)
C(24)	1391(6)	1543(3)	7424(3)	48(1)
C(42)	2628(5)	5129(3)	5926(3)	45(1)
C(35)	-626(6)	2563(4)	3968(3)	59(2)
C(34)	732(6)	2606(3)	3658(3)	57(1)
C(23)	2116(6)	1017(3)	6932(3)	54(1)
C(25)	-56(6)	1583(3)	7167(4)	68(2)
C(32)	487(7)	1350(3)	4153(3)	65(2)
C(22)	1172(8)	719(3)	6377(3)	72(2)
C(31)	-814(6)	1781(4)	4282(3)	69(2)
C(21)	-201(8)	1060(4)	6518(4)	82(2)

Bond lengths [Å]

Rh(1)-C(2)	2.097(4)
Rh(1)-C(3)	2.114(4)
Rh(1)-C(1)	2.136(4)
Rh(1)-C(12)	2.186(4)
Rh(1)-C(13)	2.187(4)
Rh(1)-C(14)	2.205(4)
Rh(1)-C(11)	2.230(4)
Rh(1)-C(15)	2.237(4)
Rh(1)-Co(1)	2.5191(7)
Rh(1)-Co(2)	2.5644(7)
Co(2)-C(1)	1.908(4)
Co(2)-C(3)	1.928(4)
Co(2)-C(21)	2.061(5)
Co(2)-C(25)	2.069(5)
Co(2)-C(22)	2.080(5)
Co(2)-C(23)	2.099(5)
Co(2)-C(24)	2.103(4)
Co(2)-Co(1)	2.4775(9)
Co(1)-C(2)	1.897(4)
Co(1)-C(1)	1.922(4)
Co(1)-C(31)	2.067(5)
Co(1)-C(32)	2.073(5)
Co(1)-C(35)	2.087(5)
Co(1)-C(33)	2.100(5)
Co(1)-C(34)	2.106(5)
O(1)-C(1)	1.191(5)
C(4)-C(6)	1.394(5)
C(4)-C(5)	1.396(5)
C(4)-C(3)	1.478(5)
C(12)-C(13)	1.430(5)
C(12)-C(11)	1.432(5)
C(12)-C(42)	1.499(6)
C(3)-C(2)	1.379(5)
C(14)-C(13)	1.417(6)
C(14)-C(15)	1.432(6)
C(14)-C(44)	1.505(6)
C(15)-C(11)	1.415(6)
C(15)-C(45)	1.496(6)
C(5)-C(7)	1.380(6)
C(2)-H(2)	1.194(8)
C(13)-C(43)	1.508(5)
C(11)-C(41)	1.499(5)
C(6)-C(8)	1.387(6)
C(8)-C(9)	1.383(6)
C(7)-C(9)	1.385(6)
C(9)-C(10)	1.512(6)
C(33)-C(34)	1.388(7)
C(33)-C(32)	1.389(8)
C(24)-C(23)	1.387(7)
C(24)-C(25)	1.401(7)
C(35)-C(34)	1.371(7)
C(35)-C(31)	1.409(8)
C(23)-C(22)	1.367(8)
C(25)-C(21)	1.408(9)
C(32)-C(31)	1.417(8)
C(22)-C(21)	1.412(9)

Bond Angles [°]

C(2)-Rh(1)-C(3)	38.2(2)	C(22)-Co(2)-C(24)	65.1(2)
C(2)-Rh(1)-C(1)	89.7(2)	C(23)-Co(2)-C(24)	38.5(2)
C(3)-Rh(1)-C(1)	90.9(2)	C(1)-Co(2)-Co(1)	49.95(12)
C(2)-Rh(1)-C(12)	107.8(2)	C(3)-Co(2)-Co(1)	74.88(12)
C(3)-Rh(1)-C(12)	110.36(14)	C(21)-Co(2)-Co(1)	108.0(2)
C(1)-Rh(1)-C(12)	158.7(2)	C(25)-Co(2)-Co(1)	136.4(2)
C(2)-Rh(1)-C(13)	110.5(2)	C(22)-Co(2)-Co(1)	109.4(2)
C(3)-Rh(1)-C(13)	136.5(2)	C(23)-Co(2)-Co(1)	138.7(2)
C(1)-Rh(1)-C(13)	124.6(2)	C(24)-Co(2)-Co(1)	173.53(14)
C(12)-Rh(1)-C(13)	38.18(14)	C(1)-Co(2)-Rh(1)	54.72(11)
C(2)-Rh(1)-C(14)	140.6(2)	C(3)-Co(2)-Rh(1)	53.90(11)
C(3)-Rh(1)-C(14)	173.5(2)	C(21)-Co(2)-Rh(1)	167.1(2)
C(1)-Rh(1)-C(14)	95.6(2)	C(25)-Co(2)-Rh(1)	145.9(2)
C(12)-Rh(1)-C(14)	63.2(2)	C(22)-Co(2)-Rh(1)	144.6(2)
C(13)-Rh(1)-C(14)	37.6(2)	C(23)-Co(2)-Rh(1)	126.3(2)
C(2)-Rh(1)-C(11)	134.9(2)	C(24)-Co(2)-Rh(1)	126.51(14)
C(3)-Rh(1)-C(11)	113.36(14)	Co(1)-Co(2)-Rh(1)	59.92(2)
C(1)-Rh(1)-C(11)	132.3(2)	C(2)-Co(1)-C(1)	102.8(2)
C(12)-Rh(1)-C(11)	37.84(14)	C(2)-Co(1)-C(31)	116.2(2)
C(13)-Rh(1)-C(11)	63.16(14)	C(1)-Co(1)-C(31)	130.9(2)
C(14)-Rh(1)-C(11)	62.53(14)	C(2)-Co(1)-C(32)	156.1(2)
C(2)-Rh(1)-C(15)	170.6(2)	C(1)-Co(1)-C(32)	96.7(2)
C(3)-Rh(1)-C(15)	141.8(2)	C(31)-Co(1)-C(32)	40.0(2)
C(1)-Rh(1)-C(15)	99.6(2)	C(2)-Co(1)-C(35)	96.5(2)
C(12)-Rh(1)-C(15)	62.83(14)	C(1)-Co(1)-C(35)	159.9(2)
C(13)-Rh(1)-C(15)	62.96(14)	C(31)-Co(1)-C(35)	39.7(2)
C(14)-Rh(1)-C(15)	37.6(2)	C(32)-Co(1)-C(35)	66.2(2)
C(11)-Rh(1)-C(15)	36.94(14)	C(2)-Co(1)-C(33)	149.2(2)
C(2)-Rh(1)-Co(1)	47.45(11)	C(1)-Co(1)-C(33)	95.2(2)
C(3)-Rh(1)-Co(1)	71.11(11)	C(31)-Co(1)-C(33)	65.8(2)
C(1)-Rh(1)-Co(1)	47.91(10)	C(32)-Co(1)-C(33)	38.9(2)
C(12)-Rh(1)-Co(1)	139.67(10)	C(35)-Co(1)-C(33)	64.9(2)
C(13)-Rh(1)-Co(1)	112.35(10)	C(2)-Co(1)-C(34)	111.9(2)
C(14)-Rh(1)-Co(1)	112.83(11)	C(1)-Co(1)-C(34)	126.3(2)
C(11)-Rh(1)-Co(1)	175.11(10)	C(31)-Co(1)-C(34)	65.3(2)
C(15)-Rh(1)-Co(1)	140.16(11)	C(32)-Co(1)-C(34)	65.2(2)
C(2)-Rh(1)-Co(2)	66.99(11)	C(35)-Co(1)-C(34)	38.2(2)
C(3)-Rh(1)-Co(2)	47.49(10)	C(33)-Co(1)-C(34)	38.5(2)
C(1)-Rh(1)-Co(2)	46.81(11)	C(2)-Co(1)-Co(2)	71.61(12)
C(12)-Rh(1)-Co(2)	151.66(11)	C(1)-Co(1)-Co(2)	49.45(12)
C(13)-Rh(1)-Co(2)	169.81(10)	C(31)-Co(1)-Co(2)	116.0(2)
C(14)-Rh(1)-Co(2)	138.89(11)	C(32)-Co(1)-Co(2)	112.8(2)
C(11)-Rh(1)-Co(2)	125.98(10)	C(35)-Co(1)-Co(2)	145.5(2)
C(15)-Rh(1)-Co(2)	120.68(10)	C(33)-Co(1)-Co(2)	137.4(2)
Co(1)-Rh(1)-Co(2)	58.33(2)	C(34)-Co(1)-Co(2)	175.5(2)
C(1)-Co(2)-C(3)	104.2(2)	C(2)-Co(1)-Rh(1)	54.53(12)
C(1)-Co(2)-C(21)	122.3(3)	C(1)-Co(1)-Rh(1)	55.57(11)
C(3)-Co(2)-C(21)	121.2(3)	C(31)-Co(1)-Rh(1)	170.7(2)
C(1)-Co(2)-C(25)	158.4(2)	C(32)-Co(1)-Rh(1)	149.1(2)
C(3)-Co(2)-C(25)	97.2(2)	C(35)-Co(1)-Rh(1)	137.0(2)
C(21)-Co(2)-C(25)	39.9(2)	C(33)-Co(1)-Rh(1)	122.5(2)
C(1)-Co(2)-C(22)	91.8(2)	C(34)-Co(1)-Rh(1)	117.7(2)
C(3)-Co(2)-C(22)	161.0(2)	Co(2)-Co(1)-Rh(1)	61.75(2)
C(21)-Co(2)-C(22)	39.9(3)	C(6)-C(4)-C(5)	117.3(4)
C(25)-Co(2)-C(22)	66.6(2)	C(6)-C(4)-C(3)	120.7(4)
C(1)-Co(2)-C(23)	97.2(2)	C(5)-C(4)-C(3)	122.0(3)
C(3)-Co(2)-C(23)	145.2(2)	C(13)-C(12)-C(11)	107.8(3)
C(21)-Co(2)-C(23)	65.2(2)	C(13)-C(12)-C(42)	125.8(4)
C(25)-Co(2)-C(23)	65.5(2)	C(11)-C(12)-C(42)	126.3(4)
C(22)-Co(2)-C(23)	38.2(2)	C(13)-C(12)-Rh(1)	71.0(2)
C(1)-Co(2)-C(24)	131.6(2)	C(11)-C(12)-Rh(1)	72.7(2)
C(3)-Co(2)-C(24)	109.2(2)	C(42)-C(12)-Rh(1)	124.0(3)
C(21)-Co(2)-C(24)	65.7(2)	C(2)-C(3)-C(4)	127.3(3)
C(25)-Co(2)-C(24)	39.2(2)	C(2)-C(3)-Co(2)	102.5(3)

C(4)-C(3)-Co(2)	128.7(3)	C(35)-C(34)-C(33)	109.0(5)
C(2)-C(3)-Rh(1)	70.2(2)	C(35)-C(34)-Co(1)	70.2(3)
C(4)-C(3)-Rh(1)	125.8(3)	C(33)-C(34)-Co(1)	70.5(3)
Co(2)-C(3)-Rh(1)	78.61(14)	C(22)-C(23)-C(24)	109.6(5)
C(13)-C(14)-C(15)	108.4(3)	C(22)-C(23)-Co(2)	70.1(3)
C(13)-C(14)-C(44)	127.2(4)	C(24)-C(23)-Co(2)	70.9(3)
C(15)-C(14)-C(44)	124.4(4)	C(24)-C(25)-C(21)	107.1(5)
C(13)-C(14)-Rh(1)	70.5(2)	C(24)-C(25)-Co(2)	71.7(3)
C(15)-C(14)-Rh(1)	72.4(2)	C(21)-C(25)-Co(2)	69.8(3)
C(44)-C(14)-Rh(1)	124.3(3)	C(33)-C(32)-C(31)	107.6(5)
O(1)-C(1)-Co(2)	134.9(3)	C(33)-C(32)-Co(1)	71.6(3)
O(1)-C(1)-Co(1)	135.1(3)	C(31)-C(32)-Co(1)	69.8(3)
Co(2)-C(1)-Co(1)	80.6(2)	C(23)-C(22)-C(21)	107.6(5)
O(1)-C(1)-Rh(1)	128.4(3)	C(23)-C(22)-Co(2)	71.7(3)
Co(2)-C(1)-Rh(1)	78.5(2)	C(21)-C(22)-Co(2)	69.4(3)
Co(1)-C(1)-Rh(1)	76.53(14)	C(35)-C(31)-C(32)	106.9(5)
C(11)-C(15)-C(14)	107.9(3)	C(35)-C(31)-Co(1)	70.9(3)
C(11)-C(15)-C(45)	126.6(4)	C(32)-C(31)-Co(1)	70.2(3)
C(14)-C(15)-C(45)	125.5(4)	C(22)-C(21)-C(25)	107.8(5)
C(11)-C(15)-Rh(1)	71.2(2)	C(22)-C(21)-Co(2)	70.8(3)
C(14)-C(15)-Rh(1)	70.0(2)	C(25)-C(21)-Co(2)	70.4(3)
C(45)-C(15)-Rh(1)	125.4(3)		
C(7)-C(5)-C(4)	121.4(4)		
C(7)-C(5)-H(5A)	119.7(2)		
C(4)-C(5)-H(5A)	118.9(2)		
C(3)-C(2)-Co(1)	110.9(3)		
C(3)-C(2)-Rh(1)	71.5(2)		
Co(1)-C(2)-Rh(1)	78.02(14)		
C(3)-C(2)-H(2)	128.4(5)		
Co(1)-C(2)-H(2)	120.7(5)		
Rh(1)-C(2)-H(2)	119.8(4)		
C(14)-C(13)-C(12)	107.8(3)		
C(14)-C(13)-C(43)	126.9(4)		
C(12)-C(13)-C(43)	125.3(4)		
C(14)-C(13)-Rh(1)	71.9(2)		
C(12)-C(13)-Rh(1)	70.9(2)		
C(43)-C(13)-Rh(1)	124.1(3)		
C(15)-C(11)-C(12)	108.1(3)		
C(15)-C(11)-C(41)	126.5(4)		
C(12)-C(11)-C(41)	125.0(4)		
C(15)-C(11)-Rh(1)	71.8(2)		
C(12)-C(11)-Rh(1)	69.4(2)		
C(41)-C(11)-Rh(1)	129.4(3)		
C(8)-C(6)-C(4)	121.0(4)		
C(8)-C(6)-H(6A)	119.8(2)		
C(4)-C(6)-H(6A)	119.3(2)		
C(9)-C(8)-C(6)	121.2(4)		
C(9)-C(8)-H(8A)	119.1(2)		
C(6)-C(8)-H(8A)	119.7(2)		
C(5)-C(7)-C(9)	121.0(4)		
C(5)-C(7)-H(7A)	119.5(2)		
C(9)-C(7)-H(7A)	119.5(2)		
C(8)-C(9)-C(7)	118.1(4)		
C(8)-C(9)-C(10)	121.7(4)		
C(7)-C(9)-C(10)	120.2(4)		
C(34)-C(33)-C(32)	108.3(5)		
C(34)-C(33)-Co(1)	71.0(3)		
C(32)-C(33)-Co(1)	69.5(3)		
C(23)-C(24)-C(25)	108.0(5)		
C(23)-C(24)-Co(2)	70.6(3)		
C(25)-C(24)-Co(2)	69.1(3)		
C(34)-C(35)-C(31)	108.3(5)		
C(34)-C(35)-Co(1)	71.7(3)		
C(31)-C(35)-Co(1)	69.4(3)		

Anisotropic displacement parameters ($A^2 \times 10^3$).
The anisotropic displacement factor exponent takes the form:
$-2\pi^2 [h^2 a^{*2} U11 + ... + 2 h k a^* b^* U12]$

	U11	U22	U33	U23	U13	U12
Rh(1)	24(1)	18(1)	18(1)	1(1)	-3(1)	-1(1)
Co(2)	32(1)	22(1)	29(1)	3(1)	-1(1)	-6(1)
Co(1)	31(1)	31(1)	27(1)	-6(1)	-10(1)	-1(1)
O(1)	39(2)	25(2)	37(2)	-6(1)	-4(1)	7(1)
C(4)	23(2)	26(2)	27(2)	1(2)	2(2)	-4(2)
C(12)	24(2)	18(2)	40(2)	0(2)	-1(2)	-6(2)
C(3)	20(2)	27(2)	32(2)	3(2)	-1(2)	-6(2)
C(14)	30(2)	31(2)	35(2)	-2(2)	11(2)	-8(2)
C(1)	34(2)	20(2)	27(2)	3(2)	-6(2)	-2(2)
C(15)	22(2)	30(2)	38(2)	4(2)	1(2)	-6(2)
C(5)	31(2)	32(2)	31(2)	3(2)	0(2)	2(2)
C(2)	25(2)	30(2)	33(2)	-3(2)	-4(2)	-2(2)
C(13)	35(2)	30(2)	26(2)	7(2)	0(2)	-10(2)
C(11)	27(2)	22(2)	28(2)	-1(2)	-3(2)	-10(2)
C(6)	26(2)	36(2)	36(2)	-3(2)	-3(2)	1(2)
C(8)	28(2)	38(2)	44(3)	-3(2)	-1(2)	5(2)
C(45)	33(3)	36(3)	74(4)	5(2)	-12(2)	5(2)
C(7)	35(2)	30(2)	30(2)	1(2)	-3(2)	-3(2)
C(41)	52(3)	49(3)	35(3)	-4(2)	-7(2)	-18(2)
C(9)	29(2)	27(2)	35(2)	-2(2)	7(2)	-7(2)
C(43)	59(3)	49(3)	43(3)	23(2)	-9(2)	-17(2)
C(10)	48(3)	42(3)	44(3)	-10(2)	1(2)	0(2)
C(44)	59(3)	48(3)	54(3)	-13(3)	27(3)	-9(3)
C(33)	60(3)	80(4)	36(3)	-32(3)	-15(3)	12(3)
C(24)	73(4)	37(3)	33(3)	13(2)	9(2)	-1(2)
C(42)	47(3)	27(2)	62(3)	-5(2)	-1(2)	3(2)
C(35)	61(4)	71(4)	44(3)	-24(3)	-36(3)	19(3)
C(34)	74(4)	70(4)	26(3)	-8(2)	-17(3)	-6(3)
C(23)	72(4)	37(3)	53(3)	21(3)	10(3)	7(3)
C(25)	61(4)	58(4)	86(4)	40(3)	39(3)	8(3)
C(32)	94(5)	43(3)	57(3)	-25(3)	-43(3)	0(3)
C(22)	124(6)	23(3)	69(4)	5(3)	25(4)	-19(3)
C(31)	48(3)	106(5)	54(3)	-25(3)	-18(3)	-30(4)
C(21)	83(5)	77(5)	84(5)	39(4)	-21(4)	-61(4)

Hydrogen coordinates (x 10^4) and isotropic displacement parameters (A^2 x 10^3).

	x	y	z	U(eq)
H(5A)	1812(4)	3223(2)	7720(2)	80
H(6A)	-1499(4)	4145(2)	6408(2)	80
H(8A)	-2129(4)	4980(3)	7457(2)	80
H(45A)	6972(5)	2854(3)	6291(3)	80
H(45B)	5672(5)	2521(3)	6775(3)	80
H(45C)	5965(5)	2178(3)	5935(3)	80
H(7A)	1172(4)	4055(2)	8761(2)	80
H(41A)	5280(5)	4444(3)	7264(2)	80
H(41B)	3596(5)	4372(3)	7347(2)	80
H(41C)	4578(5)	3605(3)	7461(2)	80
H(43A)	3904(5)	4800(3)	4031(3)	80
H(43B)	3077(5)	3989(3)	3855(3)	80
H(43C)	2313(5)	4685(3)	4318(3)	80
H(10A)	-1786(5)	5450(3)	8760(3)	80
H(10B)	-1192(5)	4786(3)	9339(3)	80
H(10C)	-162(5)	5472(3)	9043(3)	80
H(44A)	6214(5)	3070(3)	4280(3)	80
H(44B)	5447(5)	2319(3)	4652(3)	80
H(44C)	4628(5)	2844(3)	4020(3)	80
H(33A)	2390(6)	1743(4)	3605(3)	80
H(24A)	1812(6)	1836(3)	7857(3)	80
H(42A)	3239(5)	5600(3)	5929(3)	80
H(42B)	1888(5)	5188(3)	5528(3)	80
H(42C)	2187(5)	5071(3)	6429(3)	80
H(35A)	-1333(6)	2989(4)	3964(3)	80
H(34A)	1145(6)	3073(3)	3412(3)	80
H(23A)	3128(6)	887(3)	6972(3)	80
H(25A)	-812(6)	1892(3)	7405(4)	80
H(32A)	688(7)	795(3)	4284(3)	80
H(22A)	1395(8)	339(3)	5970(3)	80
H(31A)	-1671(6)	1569(4)	4518(3)	80
H(21A)	-1081(8)	947(4)	6230(4)	80
H(2)	-94(8)	3850(4)	5196(4)	50

APPENDIX 10

Crystal Structure of $Cp^*Ir(CpCo)_2(\mu_3\text{-}CO)(\mu_3\text{-}Tol\text{-}C{\equiv}CH)$

Crystal data and structure refinement.

Identification code	Ir*Co2(Tol-CCH)
Empirical formula	C30 H33 Co2 Ir O
Formula weight	719.62
Temperature	293(2) K
Wavelength	0.71073 Å
Crystal system	Orthorhombic
Space group	P2(1)2(1)2(1)
Unit cell dimensions	a = 11.151(3) Å α = 90° b = 14.168(3) Å β = 90° c = 17.040(3) Å γ = 90°
Volume, Z	2692.1(10) $Å^3$, 4
Density (calculated)	1.776 Mg/m^3
Absorption coefficient	6.169 mm^{-1}
F(000)	1408
Crystal size	0.35 x 0.30 x 0.10 mm
Theta range for data collection	2.18 to 22.56°
Limiting indices	-3<=h<=12, -2<=k<=15, -18<=l<=18
Reflections collected	3550
Independent reflections	2938 [R(int) = 0.0350]
Absorption correction	Ellipsoidal
Refinement method	Full-matrix least-squares on F^2
Data / restraints / parameters	2938 / 0 / 302
Goodness-of-fit on F^2	1.261
Final R indices [I>2sigma(I)]	R1 = 0.0455, wR2 = 0.1012
R indices (all data)	R1 = 0.0681, wR2 = 0.1130
Absolute structure parameter	0.00(2)
Largest diff. peak and hole	0.498 and -0.705 $e.A^{-3}$

Atomic coordinates (x 10^4) and equivalent isotropic displacement parameters (A^2 x 10^3)
U(eq) is defined as one third of the trace of the orthogonalized Uij tensor.

	x	y	z	U(eq)
Ir(1)	-8210(1)	-1192(1)	-8056(1)	48(1)
Co(1)	-7354(3)	243(2)	-7334(1)	54(1)
Co(2)	-6196(3)	-403(2)	-8425(1)	52(1)
C(30)	-6689(21)	-1110(12)	-7479(11)	60(6)
O(1)	-6124(14)	-1614(9)	-7042(8)	76(5)
C(9)	-9126(31)	-2344(22)	-7414(18)	96(10)
C(26)	-7021(22)	3313(13)	-9540(10)	59(6)
C(22)	-7326(17)	626(11)	-8460(9)	38(4)
C(23)	-7210(18)	1550(11)	-8821(9)	46(5)
C(27)	-6904(27)	4260(13)	-9952(12)	106(10)
C(8)	-8446(28)	-2751(15)	-7988(22)	95(9)
C(24)	-8007(19)	1836(11)	-9408(9)	53(5)
C(25)	-7933(22)	2692(14)	-9759(10)	69(7)
C(21)	-8388(29)	157(15)	-8328(12)	96(10)
C(10)	-9882(27)	-1798(18)	-7830(18)	101(10)
C(6)	-9734(27)	-1911(15)	-8636(12)	69(6)
C(7)	-8750(29)	-2481(18)	-8711(18)	92(9)
C(1)	-10480(25)	-1485(17)	-9289(16)	162(17)
C(13)	-5526(24)	-946(20)	-9459(12)	89(8)
C(28)	-6240(25)	3023(15)	-8987(12)	91(10)
C(29)	-6317(22)	2184(13)	-8615(11)	70(7)
C(2)	-8272(35)	-2809(21)	-9446(18)	165(18)
C(12)	-5068(34)	-1465(21)	-8852(17)	119(11)
C(14)	-5138(22)	13(19)	-9381(13)	84(7)
C(4)	-9138(38)	-2438(28)	-6535(15)	242(34)
C(15)	-4442(29)	103(29)	-8684(18)	130(12)
C(5)	-10870(33)	-1395(27)	-7519(26)	228(22)
C(11)	-4469(33)	-903(38)	-8388(19)	168(18)
C(3)	-7523(29)	-3372(17)	-7740(26)	241(28)
C(18)	-6682(53)	1302(37)	-6653(22)	151(22)
C(17)	-6549(51)	457(44)	-6301(18)	171(22)
C(16)	-7621(71)	174(27)	-6141(20)	164(36)
C(19)	-7728(73)	1491(31)	-6789(20)	231(33)
C(20)	-8256(54)	810(54)	-6480(26)	191(23)

Bond lengths [A] and angles [deg] for 1.

Ir(1)-C(30)	1.96(2)
Ir(1)-C(21)	1.98(2)
Ir(1)-C(10)	2.09(3)
Ir(1)-C(6)	2.21(3)
Ir(1)-C(7)	2.22(2)
Ir(1)-C(9)	2.21(2)
Ir(1)-C(8)	2.23(2)
Ir(1)-Co(1)	2.561(3)
Ir(1)-Co(2)	2.586(3)
Co(1)-C(20)	1.94(4)
Co(1)-C(22)	1.99(2)
Co(1)-C(17)	2.00(3)
Co(1)-C(19)	2.04(3)
Co(1)-C(18)	2.04(2)
Co(1)-C(30)	2.07(2)
Co(1)-C(21)	2.05(2)
Co(1)-C(16)	2.06(3)
Co(1)-Co(2)	2.441(4)
Co(2)-C(22)	1.93(2)
Co(2)-C(30)	1.98(2)
Co(2)-C(11)	2.05(4)
Co(2)-C(13)	2.06(2)
Co(2)-C(12)	2.09(3)
Co(2)-C(14)	2.10(2)
Co(2)-C(15)	2.13(3)
C(30)-O(1)	1.21(2)
C(9)-C(8)	1.36(4)
C(9)-C(10)	1.35(4)
C(9)-C(4)	1.50(3)
C(26)-C(28)	1.35(3)
C(26)-C(25)	1.39(3)
C(26)-C(27)	1.52(2)
C(22)-C(21)	1.38(3)
C(22)-C(23)	1.45(2)
C(23)-C(24)	1.40(2)
C(23)-C(29)	1.39(2)
C(8)-C(7)	1.33(3)
C(8)-C(3)	1.42(3)
C(24)-C(25)	1.36(2)
C(10)-C(6)	1.39(3)
C(10)-C(5)	1.35(4)
C(6)-C(7)	1.37(4)
C(6)-C(1)	1.51(3)
C(7)-C(2)	1.44(3)
C(13)-C(14)	1.43(3)
C(13)-C(12)	1.37(3)
C(28)-C(29)	1.35(2)
C(12)-C(11)	1.31(4)
C(14)-C(15)	1.42(3)
C(15)-C(11)	1.51(4)
C(18)-C(19)	1.22(5)
C(18)-C(17)	1.35(5)
C(18)-C(20)	1.91(7)
C(17)-C(16)	1.29(7)
C(17)-C(20)	1.99(7)
C(16)-C(20)	1.28(7)
C(19)-C(20)	1.25(5)

Bond Angles [°]

C(30)-Ir(1)-C(21)	98.4(10)	C(20)-Co(1)-Co(2)	178(2)
C(30)-Ir(1)-C(10)	134.7(11)	C(22)-Co(1)-Co(2)	50.3(5)
C(21)-Ir(1)-C(10)	110.5(13)	C(17)-Co(1)-Co(2)	119.3(12)
C(30)-Ir(1)-C(6)	156.0(8)	C(19)-Co(1)-Co(2)	141(2)
C(21)-Ir(1)-C(6)	105.2(10)	C(18)-Co(1)-Co(2)	121.0(12)
C(10)-Ir(1)-C(6)	37.6(9)	C(30)-Co(1)-Co(2)	51.2(5)
C(30)-Ir(1)-C(7)	122.3(10)	C(21)-Co(1)-Co(2)	69.3(8)
C(21)-Ir(1)-C(7)	130.5(11)	C(16)-Co(1)-Co(2)	144(2)
C(10)-Ir(1)-C(7)	60.9(10)	C(20)-Co(1)-Ir(1)	120(2)
C(6)-Ir(1)-C(7)	35.9(9)	C(22)-Co(1)-Ir(1)	76.1(5)
C(30)-Ir(1)-C(9)	101.2(9)	C(17)-Co(1)-Ir(1)	135(2)
C(21)-Ir(1)-C(9)	141.5(14)	C(19)-Co(1)-Ir(1)	146(2)
C(10)-Ir(1)-C(9)	36.3(10)	C(18)-Co(1)-Ir(1)	174(2)
C(6)-Ir(1)-C(9)	61.8(9)	C(30)-Co(1)-Ir(1)	48.8(6)
C(7)-Ir(1)-C(9)	61.1(10)	C(21)-Co(1)-Ir(1)	49.3(6)
C(30)-Ir(1)-C(8)	97.7(9)	C(16)-Co(1)-Ir(1)	113(2)
C(21)-Ir(1)-C(8)	163.6(11)	Co(2)-Co(1)-Ir(1)	62.20(9)
C(10)-Ir(1)-C(8)	58.5(11)	C(22)-Co(2)-C(30)	103.1(8)
C(6)-Ir(1)-C(8)	58.4(9)	C(22)-Co(2)-C(11)	151(2)
C(7)-Ir(1)-C(8)	34.9(9)	C(30)-Co(2)-C(11)	93.5(12)
C(9)-Ir(1)-C(8)	35.8(10)	C(22)-Co(2)-C(13)	119.5(9)
C(30)-Ir(1)-Co(1)	52.4(5)	C(30)-Co(2)-C(13)	127.5(9)
C(21)-Ir(1)-Co(1)	51.9(7)	C(11)-Co(2)-C(13)	63.7(12)
C(10)-Ir(1)-Co(1)	124.8(7)	C(22)-Co(2)-C(12)	157.8(10)
C(6)-Ir(1)-Co(1)	149.9(7)	C(30)-Co(2)-C(12)	95.0(10)
C(7)-Ir(1)-Co(1)	173.8(8)	C(11)-Co(2)-C(12)	36.7(13)
C(9)-Ir(1)-Co(1)	121.3(9)	C(13)-Co(2)-C(12)	38.4(9)
C(8)-Ir(1)-Co(1)	143.7(8)	C(22)-Co(2)-C(14)	97.5(9)
C(30)-Ir(1)-Co(2)	49.2(6)	C(30)-Co(2)-C(14)	159.0(10)
C(21)-Ir(1)-Co(2)	67.2(9)	C(11)-Co(2)-C(14)	66.0(11)
C(10)-Ir(1)-Co(2)	176.2(9)	C(13)-Co(2)-C(14)	40.3(8)
C(6)-Ir(1)-Co(2)	139.2(6)	C(12)-Co(2)-C(14)	66.0(11)
C(7)-Ir(1)-Co(2)	117.9(8)	C(22)-Co(2)-C(15)	109.8(12)
C(9)-Ir(1)-Co(2)	147.0(9)	C(30)-Co(2)-C(15)	126.6(12)
C(8)-Ir(1)-Co(2)	123.0(9)	C(11)-Co(2)-C(15)	42.3(12)
Co(1)-Ir(1)-Co(2)	56.62(8)	C(13)-Co(2)-C(15)	67.4(11)
C(20)-Co(1)-C(22)	128(3)	C(12)-Co(2)-C(15)	67.5(13)
C(20)-Co(1)-C(17)	61(2)	C(14)-Co(2)-C(15)	39.4(9)
C(22)-Co(1)-C(17)	143(2)	C(22)-Co(2)-Co(1)	52.7(5)
C(20)-Co(1)-C(19)	36(2)	C(30)-Co(2)-Co(1)	54.7(6)
C(22)-Co(1)-C(19)	101.8(12)	C(11)-Co(2)-Co(1)	127.1(11)
C(17)-Co(1)-C(19)	64(2)	C(13)-Co(2)-Co(1)	169.0(8)
C(20)-Co(1)-C(18)	57(2)	C(12)-Co(2)-Co(1)	148.5(8)
C(22)-Co(1)-C(18)	110(2)	C(14)-Co(2)-Co(1)	141.6(8)
C(17)-Co(1)-C(18)	39.0(14)	C(15)-Co(2)-Co(1)	121.2(7)
C(19)-Co(1)-C(18)	35(2)	C(22)-Co(2)-Ir(1)	76.5(5)
C(20)-Co(1)-C(30)	131(3)	C(30)-Co(2)-Ir(1)	48.8(6)
C(22)-Co(1)-C(30)	97.6(7)	C(11)-Co(2)-Ir(1)	131.2(14)
C(17)-Co(1)-C(30)	94.8(14)	C(13)-Co(2)-Ir(1)	111.1(9)
C(19)-Co(1)-C(30)	158.4(12)	C(12)-Co(2)-Ir(1)	107.2(10)
C(18)-Co(1)-C(30)	128(2)	C(14)-Co(2)-Ir(1)	143.0(7)
C(20)-Co(1)-C(21)	111(2)	C(15)-Co(2)-Ir(1)	173.5(12)
C(22)-Co(1)-C(21)	39.7(8)	Co(1)-Co(2)-Ir(1)	61.18(10)
C(17)-Co(1)-C(21)	171.1(13)	O(1)-C(30)-Co(2)	131(2)
C(19)-Co(1)-C(21)	108(2)	O(1)-C(30)-Ir(1)	136(2)
C(18)-Co(1)-C(21)	136(2)	Co(2)-C(30)-Ir(1)	82.0(7)
C(30)-Co(1)-C(21)	92.8(9)	O(1)-C(30)-Co(1)	131.3(14)
C(20)-Co(1)-C(16)	37(2)	Co(2)-C(30)-Co(1)	74.2(6)
C(22)-Co(1)-C(16)	165.0(13)	Ir(1)-C(30)-Co(1)	78.8(8)
C(17)-Co(1)-C(16)	37(2)	C(8)-C(9)-C(10)	102(2)
C(19)-Co(1)-C(16)	64.0(14)	C(8)-C(9)-C(4)	133(4)
C(18)-Co(1)-C(16)	62(2)	C(10)-C(9)-C(4)	125(4)
C(30)-Co(1)-C(16)	97.2(12)	C(8)-C(9)-Ir(1)	73(2)
C(21)-Co(1)-C(16)	137(2)	C(10)-C(9)-Ir(1)	66.7(14)

C(4)-C(9)-Ir(1)	124(2)	Co(1)-C(18)-C(20)	58.8(13)
C(28)-C(26)-C(25)	118(2)	C(16)-C(17)-C(18)	106(4)
C(28)-C(26)-C(27)	122(2)	C(16)-C(17)-C(20)	39(2)
C(25)-C(26)-C(27)	120(2)	C(18)-C(17)-C(20)	67(3)
C(21)-C(22)-C(23)	126(2)	C(16)-C(17)-Co(1)	74(3)
C(21)-C(22)-Co(2)	101.1(14)	C(18)-C(17)-Co(1)	72(2)
C(23)-C(22)-Co(2)	129.5(14)	C(20)-C(17)-Co(1)	58.3(14)
C(21)-C(22)-Co(1)	72.4(11)	C(20)-C(16)-C(17)	101(4)
C(23)-C(22)-Co(1)	130.9(12)	C(20)-C(16)-Co(1)	67(2)
Co(2)-C(22)-Co(1)	76.9(6)	C(17)-C(16)-Co(1)	69(2)
C(24)-C(23)-C(29)	117(2)	C(20)-C(19)-C(18)	102(4)
C(24)-C(23)-C(22)	121(2)	C(20)-C(19)-Co(1)	68(2)
C(29)-C(23)-C(22)	123(2)	C(18)-C(19)-Co(1)	73(2)
C(7)-C(8)-C(9)	114(3)	C(16)-C(20)-C(19)	118(7)
C(7)-C(8)-C(3)	130(4)	C(16)-C(20)-C(17)	39(4)
C(9)-C(8)-C(3)	117(4)	C(19)-C(20)-C(17)	79(4)
C(7)-C(8)-Ir(1)	72.4(13)	C(16)-C(20)-Co(1)	76(3)
C(9)-C(8)-Ir(1)	71.6(14)	C(19)-C(20)-Co(1)	76(2)
C(3)-C(8)-Ir(1)	123(2)	C(17)-C(20)-Co(1)	61(2)
C(25)-C(24)-C(23)	123(2)	C(16)-C(20)-C(18)	80(5)
C(24)-C(25)-C(26)	119(2)	C(19)-C(20)-C(18)	39(3)
C(22)-C(21)-Ir(1)	115(2)	C(17)-C(20)-C(18)	40(2)
C(22)-C(21)-Co(1)	67.9(13)	Co(1)-C(20)-C(18)	64(2)
Ir(1)-C(21)-Co(1)	78.9(8)		
C(9)-C(10)-C(6)	112(3)		
C(9)-C(10)-C(5)	123(4)		
C(6)-C(10)-C(5)	122(4)		
C(9)-C(10)-Ir(1)	77(2)		
C(6)-C(10)-Ir(1)	76(2)		
C(5)-C(10)-Ir(1)	129(2)		
C(7)-C(6)-C(10)	105(3)		
C(7)-C(6)-C(1)	127(3)		
C(10)-C(6)-C(1)	128(3)		
C(7)-C(6)-Ir(1)	72(2)		
C(10)-C(6)-Ir(1)	66(2)		
C(1)-C(6)-Ir(1)	125(2)		
C(8)-C(7)-C(6)	107(3)		
C(8)-C(7)-C(2)	128(3)		
C(6)-C(7)-C(2)	125(3)		
C(8)-C(7)-Ir(1)	72.7(13)		
C(6)-C(7)-Ir(1)	71.7(14)		
C(2)-C(7)-Ir(1)	127(2)		
C(14)-C(13)-C(12)	109(3)		
C(14)-C(13)-Co(2)	71.1(12)		
C(12)-C(13)-Co(2)	72.0(14)		
C(26)-C(28)-C(29)	124(2)		
C(28)-C(29)-C(23)	120(2)		
C(11)-C(12)-C(13)	109(3)		
C(11)-C(12)-Co(2)	70(2)		
C(13)-C(12)-Co(2)	70(2)		
C(13)-C(14)-C(15)	109(3)		
C(13)-C(14)-Co(2)	68.6(11)		
C(15)-C(14)-Co(2)	72(2)		
C(11)-C(15)-C(14)	101(3)		
C(11)-C(15)-Co(2)	66(2)		
C(14)-C(15)-Co(2)	69(2)		
C(12)-C(11)-C(15)	113(3)		
C(12)-C(11)-Co(2)	73(2)		
C(15)-C(11)-Co(2)	72(2)		
C(19)-C(18)-C(17)	113(4)		
C(19)-C(18)-Co(1)	73(2)		
C(17)-C(18)-Co(1)	69(2)		
C(19)-C(18)-C(20)	40(3)		
C(17)-C(18)-C(20)	73(3)		

Anisotropic displacement parameters ($A^2 \times 10^3$).
The anisotropic displacement factor exponent takes the form:
$-2\pi^2 [h^2 a^{*2} U11 + ... + 2 h k a^* b^* U12]$

	U11	U22	U33	U23	U13	U12
Ir(1)	44(1)	47(1)	53(1)	8(1)	-11(1)	-3(1)
Co(1)	63(3)	54(2)	46(1)	-5(1)	-2(1)	1(1)
Co(2)	39(2)	65(2)	52(1)	0(1)	-2(1)	4(1)
C(30)	49(17)	55(10)	76(12)	12(9)	-22(13)	-24(13)
O(1)	71(14)	81(8)	76(9)	5(8)	-21(9)	10(8)
C(9)	74(26)	84(19)	129(21)	63(17)	-29(19)	-38(18)
C(26)	35(20)	68(12)	73(11)	19(9)	-15(11)	-18(12)
C(22)	26(11)	47(10)	42(8)	4(8)	-3(8)	-8(9)
C(23)	36(13)	55(10)	48(9)	15(8)	-3(9)	-7(9)
C(27)	127(29)	76(13)	114(16)	44(12)	-49(19)	-42(17)
C(8)	77(27)	48(13)	158(24)	10(17)	-41(23)	-9(14)
C(24)	47(17)	56(10)	56(9)	4(8)	-21(10)	-8(10)
C(25)	61(21)	79(14)	68(12)	24(10)	-16(12)	-18(13)
C(21)	70(29)	98(15)	121(18)	59(13)	-18(18)	-8(16)
C(10)	24(19)	62(15)	218(29)	-32(17)	48(19)	-7(13)
C(7)	90(24)	72(16)	113(19)	-31(15)	-16(17)	-1(15)
C(1)	129(34)	113(21)	244(33)	82(21)	-160(29)	-58(20)
C(13)	71(21)	137(24)	59(13)	-11(14)	25(13)	32(18)
C(28)	104(29)	71(15)	98(15)	8(12)	-58(17)	-36(15)
C(29)	64(18)	57(12)	90(13)	33(11)	-33(12)	-23(12)
C(2)	144(45)	138(29)	213(35)	-73(28)	41(35)	-68(32)
C(12)	151(35)	131(22)	75(21)	-6(17)	3(19)	31(20)
C(14)	33(20)	141(20)	77(15)	11(14)	34(13)	-18(15)
C(4)	314(79)	292(54)	119(24)	120(32)	-54(33)	-201(55)
C(15)	66(31)	232(35)	92(20)	-84(22)	19(21)	-21(26)
C(5)	151(44)	187(38)	345(63)	19(42)	-15(43)	-121(36)
C(11)	62(32)	333(56)	107(24)	106(31)	35(20)	70(33)
C(3)	180(44)	59(16)	483(79)	19(29)	-161(49)	-10(20)
C(18)	267(65)	91(28)	97(26)	-63(26)	21(28)	-101(36)
C(17)	111(49)	351(62)	49(15)	-111(26)	-34(20)	120(40)
C(16)	355(104)	94(23)	43(22)	13(16)	64(36)	56(41)
C(19)	420(93)	155(25)	120(24)	-40(20)	-34(40)	202(43)
C(20)	72(51)	395(68)	108(37)	-116(39)	22(37)	0(55)

Hydrogen coordinates (x 10^4) and isotropic displacement parameters ($Å^2$ x 10^3)

	x	y	z	U(eq)
H(27A)	-6233(27)	4591(13)	-9731(12)	80
H(27B)	-6784(27)	4181(13)	-10506(12)	80
H(27C)	-7624(27)	4616(13)	-9863(12)	80
H(24A)	-8632(19)	1413(11)	-9570(9)	80
H(25A)	-8501(22)	2880(14)	-10152(10)	80
H(21A)	-9150(29)	468(15)	-8374(12)	80
H(1A)	-11097(25)	-1920(17)	-9442(16)	80
H(1B)	-10839(25)	-901(17)	-9126(16)	80
H(1C)	-9955(25)	-1371(17)	-9725(16)	80
H(13A)	-5998(24)	-1204(20)	-9878(12)	80
H(28A)	-5638(25)	3465(15)	-8824(12)	80
H(29A)	-5741(22)	2025(13)	-8218(11)	80
H(2A)	-8685(35)	-3373(21)	-9602(18)	80
H(2B)	-8343(35)	-2343(21)	-9851(18)	80
H(2C)	-7440(35)	-2950(21)	-9360(18)	80
H(12A)	-5140(34)	-2128(21)	-8747(17)	80
H(14A)	-5385(22)	512(19)	-9726(13)	80
H(4A)	-9569(38)	-2978(28)	-6344(15)	80
H(4B)	-8327(38)	-2458(28)	-6346(15)	80
H(4C)	-9520(38)	-1872(28)	-6350(15)	80
H(15A)	-4070(29)	667(29)	-8489(18)	80
H(5A)	-11509(33)	-1846(27)	-7467(26)	80
H(5B)	-10672(33)	-1146(27)	-7011(26)	80
H(5C)	-11122(33)	-890(27)	-7856(26)	80
H(11A)	-4071(33)	-1063(38)	-7907(19)	80
H(3A)	-7832(29)	-4005(17)	-7753(26)	80
H(3B)	-6850(29)	-3323(17)	-8088(26)	80
H(3C)	-7275(29)	-3221(17)	-7216(26)	80
H(18A)	-5978(53)	1667(37)	-6769(22)	80
H(17A)	-5878(51)	98(44)	-6111(18)	80
H(16A)	-7898(71)	-398(27)	-5899(20)	80
H(19A)	-8001(73)	2069(31)	-7022(20)	80
H(20A)	-9116(54)	791(54)	-6471(26)	80

APPENDIX 11

Crystal Structre of $Cp^*Rh(CpCo)2(\mu_3\text{-}CO)(\mu_3\text{-}O)$

Crystal data and structure refinement

Identification code	rhoxopub
Empirical formula	$C_{21}H_{25}Co_2O_2Rh$
Formula weight	530.18
Temperature	293(2) K
Wavelength	0.71073 Å
Crystal system	Orthorhombic
Space group	P2(1)2(1)2(1)
Unit cell dimensions	a = 9.356(2) Å α = 90° b = 13.076(3) Å β = 90° c = 16.309(3) Å γ = 90°
Volume, Z	1995.2(7) A^3, 4
Density (calculated)	1.765 Mg/m^3
Absorption coefficient	2.472 mm^{-1}
F(000)	1064
Theta range for data collection	2.00 to 25.06°
Limiting indices	-11<=h<=2, -15<=k<=0, -19<=l<=19
Reflections collected	4089
Independent reflections	3452 [R(int) = 0.2186]
Refinement method	Full-matrix least-squares on F^2
Data / restraints / parameters	3449 / 0 / 235
Goodness-of-fit on F^2	1.114
Final R indices [I>2sigma(I)]	R1 = 0.0335, wR2 = 0.0792
R indices (all data)	R1 = 0.0370, wR2 = 0.0828
Absolute structure parameter	-0.05(3)
Largest diff. peak and hole	0.401 and -0.517 $e.Å^{-3}$

Atomic coordinates (x 10^4) and equivalent isotropic displacement parameters ($Å^2$ x 10^3). U(eq) is defined as one third of the trace of the orthogonalized Uij tensor.

	x	y	z	U(eq)
Rh(1)	972(1)	9623(1)	5409(1)	26(1)
Co(1)	-915(1)	8767(1)	6240(1)	28(1)
Co(2)	1460(1)	8154(1)	6347(1)	26(1)
O(2)	255(3)	8196(3)	5464(2)	28(1)
O(1)	963(5)	10090(3)	7213(2)	41(1)
C(44)	927(7)	9689(5)	3341(4)	47(1)
C(1)	754(5)	9496(4)	6677(3)	30(1)
C(21)	-2594(7)	9642(7)	6656(5)	61(2)
C(35)	2628(6)	10189(4)	4546(4)	35(1)
C(15)	3483(6)	8025(5)	6858(4)	42(1)
C(34)	1290(6)	10224(4)	4128(3)	35(1)
C(45)	3935(6)	9622(6)	4266(4)	51(2)
C(33)	361(6)	10875(4)	4576(4)	38(1)
C(32)	1132(6)	11285(4)	5266(4)	39(1)
C(43)	-1147(7)	11142(5)	4329(5)	54(2)
C(31)	2527(6)	10838(4)	5257(4)	36(1)
C(12)	2265(7)	6660(5)	6366(5)	51(2)
C(13)	1684(7)	6904(5)	7123(4)	49(2)
C(11)	3379(6)	7362(5)	6184(4)	43(1)
C(41)	3701(7)	11026(5)	5861(4)	47(2)
C(42)	583(8)	12037(5)	5868(5)	53(2)
C(25)	-2218(7)	8894(7)	7248(5)	64(2)
C(23)	-2920(6)	8067(6)	6089(4)	51(2)
C(24)	-2426(7)	7922(7)	6909(5)	57(2)
C(14)	2422(7)	7753(6)	7432(4)	47(2)
C(22)	-3032(6)	9125(6)	5949(5)	53(2)

Bond lengths [Å]

Rh(1)-O(2)	1.984(4)	Co(2)-C(12)	2.094(6)
Rh(1)-C(1)	2.086(5)	O(1)-C(1)	1.185(7)
Rh(1)-C(31)	2.168(6)	C(44)-C(34)	1.502(8)
Rh(1)-C(32)	2.190(6)	C(21)-C(22)	1.399(11)
Rh(1)-C(33)	2.202(6)	C(21)-C(25)	1.418(12)
Rh(1)-C(35)	2.220(5)	C(35)-C(34)	1.426(8)
Rh(1)-C(34)	2.251(5)	C(35)-C(31)	1.441(9)
Rh(1)-Co(1)	2.4912(9)	C(35)-C(45)	1.501(8)
Rh(1)-Co(2)	2.4986(9)	C(15)-C(11)	1.403(10)
Co(1)-O(2)	1.832(4)	C(15)-C(14)	1.410(9)
Co(1)-C(1)	1.964(5)	C(34)-C(33)	1.418(9)
Co(1)-C(25)	2.053(6)	C(33)-C(32)	1.440(9)
Co(1)-C(21)	2.059(7)	C(33)-C(43)	1.508(9)
Co(1)-C(22)	2.090(6)	C(32)-C(31)	1.430(8)
Co(1)-C(24)	2.101(7)	C(32)-C(42)	1.482(9)
Co(1)-C(23)	2.102(6)	C(31)-C(41)	1.495(8)
Co(1)-Co(2)	2.3690(10)	C(12)-C(13)	1.386(10)
Co(2)-O(2)	1.831(4)	C(12)-C(11)	1.420(10)
Co(2)-C(1)	1.951(5)	C(13)-C(14)	1.401(10)
Co(2)-C(14)	2.053(6)	C(25)-C(24)	1.400(12)
Co(2)-C(15)	2.074(6)	C(23)-C(22)	1.406(11)
Co(2)-C(13)	2.078(6)	C(23)-C(24)	1.428(10)
Co(2)-C(11)	2.089(6)		

Bond Angles [°]

O(2)-Rh(1)-C(1)	81.2(2)	O(2)-Co(1)-Rh(1)	51.96(12)
O(2)-Rh(1)-C(31)	157.0(2)	C(1)-Co(1)-Rh(1)	54.3(2)
C(1)-Rh(1)-C(31)	103.7(2)	C(25)-Co(1)-Rh(1)	145.1(2)
O(2)-Rh(1)-C(32)	163.8(2)	C(21)-Co(1)-Rh(1)	118.1(3)
C(1)-Rh(1)-C(32)	101.0(2)	C(22)-Co(1)-Rh(1)	116.6(2)
C(31)-Rh(1)-C(32)	38.3(2)	C(24)-Co(1)-Rh(1)	174.9(2)
O(2)-Rh(1)-C(33)	129.7(2)	C(23)-Co(1)-Rh(1)	139.8(2)
C(1)-Rh(1)-C(33)	130.2(2)	Co(2)-Co(1)-Rh(1)	61.81(3)
C(31)-Rh(1)-C(33)	63.9(2)	O(2)-Co(2)-C(1)	88.9(2)
C(32)-Rh(1)-C(33)	38.3(2)	O(2)-Co(2)-C(14)	162.9(2)
O(2)-Rh(1)-C(35)	125.3(2)	C(1)-Co(2)-C(14)	98.1(3)
C(1)-Rh(1)-C(35)	136.3(2)	O(2)-Co(2)-C(15)	151.7(2)
C(31)-Rh(1)-C(35)	38.3(2)	C(1)-Co(2)-C(15)	105.7(2)
C(32)-Rh(1)-C(35)	63.5(2)	C(14)-Co(2)-C(15)	39.9(3)
C(33)-Rh(1)-C(35)	62.8(2)	O(2)-Co(2)-C(13)	124.4(2)
O(2)-Rh(1)-C(34)	114.5(2)	C(1)-Co(2)-C(13)	125.0(3)
C(1)-Rh(1)-C(34)	163.9(2)	C(14)-Co(2)-C(13)	39.7(3)
C(31)-Rh(1)-C(34)	63.2(2)	C(15)-Co(2)-C(13)	66.4(3)
C(32)-Rh(1)-C(34)	63.0(2)	O(2)-Co(2)-C(11)	116.4(2)
C(33)-Rh(1)-C(34)	37.1(2)	C(1)-Co(2)-C(11)	140.5(2)
C(35)-Rh(1)-C(34)	37.2(2)	C(14)-Co(2)-C(11)	66.8(3)
O(2)-Rh(1)-Co(1)	46.64(10)	C(15)-Co(2)-C(11)	39.4(3)
C(1)-Rh(1)-Co(1)	49.8(2)	C(13)-Co(2)-C(11)	66.5(3)
C(31)-Rh(1)-Co(1)	150.0(2)	O(2)-Co(2)-C(12)	105.1(2)
C(32)-Rh(1)-Co(1)	123.5(2)	C(1)-Co(2)-C(12)	163.2(3)
C(33)-Rh(1)-Co(1)	119.1(2)	C(14)-Co(2)-C(12)	65.9(3)
C(35)-Rh(1)-Co(1)	171.6(2)	C(15)-Co(2)-C(12)	65.8(3)
C(34)-Rh(1)-Co(1)	139.1(2)	C(13)-Co(2)-C(12)	38.8(3)
O(2)-Rh(1)-Co(2)	46.48(10)	C(11)-Co(2)-C(12)	39.7(3)
C(1)-Rh(1)-Co(2)	49.4(2)	O(2)-Co(2)-Co(1)	49.72(11)
C(31)-Rh(1)-Co(2)	120.7(2)	C(1)-Co(2)-Co(1)	53.0(2)
C(32)-Rh(1)-Co(2)	144.6(2)	C(14)-Co(2)-Co(1)	124.2(2)
C(33)-Rh(1)-Co(2)	175.4(2)	C(15)-Co(2)-Co(1)	155.9(2)
C(35)-Rh(1)-Co(2)	121.1(2)	C(13)-Co(2)-Co(1)	113.9(2)
C(34)-Rh(1)-Co(2)	144.4(2)	C(11)-Co(2)-Co(1)	164.6(2)
Co(1)-Rh(1)-Co(2)	56.69(2)	C(12)-Co(2)-Co(1)	130.8(2)
O(2)-Co(1)-C(1)	88.5(2)	O(2)-Co(2)-Rh(1)	51.81(12)
O(2)-Co(1)-C(25)	160.2(3)	C(1)-Co(2)-Rh(1)	54.2(2)
C(1)-Co(1)-C(25)	98.2(3)	C(14)-Co(2)-Rh(1)	143.6(2)
O(2)-Co(1)-C(21)	155.5(3)	C(15)-Co(2)-Rh(1)	118.4(2)
C(1)-Co(1)-C(21)	102.5(3)	C(13)-Co(2)-Rh(1)	175.2(2)
C(25)-Co(1)-C(21)	40.3(3)	C(11)-Co(2)-Rh(1)	117.4(2)
O(2)-Co(1)-C(22)	120.0(2)	C(12)-Co(2)-Rh(1)	142.4(2)
C(1)-Co(1)-C(22)	136.7(3)	Co(1)-Co(2)-Rh(1)	61.50(3)
C(25)-Co(1)-C(22)	66.5(3)	Co(2)-O(2)-Co(1)	80.6(2)
C(21)-Co(1)-C(22)	39.4(3)	Co(2)-O(2)-Rh(1)	81.72(14)
O(2)-Co(1)-C(24)	123.1(3)	Co(1)-O(2)-Rh(1)	81.40(14)
C(1)-Co(1)-C(24)	127.0(3)	O(1)-C(1)-Co(2)	137.4(4)
C(25)-Co(1)-C(24)	39.4(3)	O(1)-C(1)-Co(1)	135.8(4)
C(21)-Co(1)-C(24)	66.9(3)	Co(2)-C(1)-Co(1)	74.5(2)
C(22)-Co(1)-C(24)	66.3(3)	O(1)-C(1)-Rh(1)	131.6(4)
O(2)-Co(1)-C(23)	105.9(2)	Co(2)-C(1)-Rh(1)	76.4(2)
C(1)-Co(1)-C(23)	164.5(2)	Co(1)-C(1)-Rh(1)	75.9(2)
C(25)-Co(1)-C(23)	66.4(3)	C(22)-C(21)-C(25)	107.5(7)
C(21)-Co(1)-C(23)	66.4(3)	C(22)-C(21)-Co(1)	71.5(4)
C(22)-Co(1)-C(23)	39.2(3)	C(25)-C(21)-Co(1)	69.6(4)
C(24)-Co(1)-C(23)	39.7(3)	C(34)-C(35)-C(31)	107.9(5)
O(2)-Co(1)-Co(2)	49.68(11)	C(34)-C(35)-C(45)	125.9(6)
C(1)-Co(1)-Co(2)	52.5(2)	C(31)-C(35)-C(45)	126.1(5)
C(25)-Co(1)-Co(2)	121.7(3)	C(34)-C(35)-Rh(1)	72.6(3)
C(21)-Co(1)-Co(2)	151.6(2)	C(31)-C(35)-Rh(1)	68.9(3)
C(22)-Co(1)-Co(2)	169.0(2)	C(45)-C(35)-Rh(1)	126.7(4)
C(24)-Co(1)-Co(2)	114.5(2)	C(11)-C(15)-C(14)	108.3(6)
C(23)-Co(1)-Co(2)	134.3(2)	C(11)-C(15)-Co(2)	70.9(3)

C(14)-C(15)-Co(2)	69.2(3)
C(33)-C(34)-C(35)	108.2(5)
C(33)-C(34)-C(44)	125.5(6)
C(35)-C(34)-C(44)	126.3(6)
C(33)-C(34)-Rh(1)	69.6(3)
C(35)-C(34)-Rh(1)	70.2(3)
C(44)-C(34)-Rh(1)	126.9(4)
C(34)-C(33)-C(32)	108.6(5)
C(34)-C(33)-C(43)	125.1(6)
C(32)-C(33)-C(43)	126.2(6)
C(34)-C(33)-Rh(1)	73.3(3)
C(32)-C(33)-Rh(1)	70.4(3)
C(43)-C(33)-Rh(1)	125.4(4)
C(31)-C(32)-C(33)	107.3(5)
C(31)-C(32)-C(42)	126.4(6)
C(33)-C(32)-C(42)	126.3(6)
C(31)-C(32)-Rh(1)	70.0(3)
C(33)-C(32)-Rh(1)	71.3(3)
C(42)-C(32)-Rh(1)	124.3(4)
C(32)-C(31)-C(35)	108.0(5)
C(32)-C(31)-C(41)	126.6(6)
C(35)-C(31)-C(41)	125.4(5)
C(32)-C(31)-Rh(1)	71.7(3)
C(35)-C(31)-Rh(1)	72.8(3)
C(41)-C(31)-Rh(1)	122.6(4)
C(13)-C(12)-C(11)	108.9(6)
C(13)-C(12)-Co(2)	70.0(4)
C(11)-C(12)-Co(2)	70.0(3)
C(12)-C(13)-C(14)	108.0(6)
C(12)-C(13)-Co(2)	71.2(4)
C(14)-C(13)-Co(2)	69.2(4)
C(15)-C(11)-C(12)	106.7(6)
C(15)-C(11)-Co(2)	69.7(3)
C(12)-C(11)-Co(2)	70.3(3)
C(24)-C(25)-C(21)	108.9(7)
C(24)-C(25)-Co(1)	72.1(4)
C(21)-C(25)-Co(1)	70.1(4)
C(22)-C(23)-C(24)	107.9(7)
C(22)-C(23)-Co(1)	69.9(4)
C(24)-C(23)-Co(1)	70.1(4)
C(25)-C(24)-C(23)	107.1(8)
C(25)-C(24)-Co(1)	68.5(4)
C(23)-C(24)-Co(1)	70.2(4)
C(13)-C(14)-C(15)	108.0(6)
C(13)-C(14)-Co(2)	71.1(4)
C(15)-C(14)-Co(2)	70.8(3)
C(21)-C(22)-C(23)	108.6(7)
C(21)-C(22)-Co(1)	69.1(4)
C(23)-C(22)-Co(1)	70.9(4)

Anisotropic displacement parameters ($Å^2$ x 10^3). The anisotropic displacement factor exponent takes the form $-2\pi^2$ [$h^2 a^{*2}$ U11 + ... + 2 h k a* b* U12]

	U11	U22	U33	U23	U13	U12
Rh(1)	24(1)	30(1)	24(1)	2(1)	0(1)	2(1)
Co(1)	21(1)	38(1)	26(1)	-3(1)	2(1)	-1(1)
Co(2)	23(1)	32(1)	24(1)	2(1)	0(1)	2(1)
O(2)	27(2)	32(2)	25(2)	0(2)	-1(2)	0(1)
O(1)	45(2)	44(2)	36(2)	-14(2)	-5(2)	2(2)
C(44)	50(3)	54(4)	35(3)	5(3)	1(3)	-6(4)
C(1)	25(3)	38(3)	26(3)	2(2)	-3(2)	2(2)
C(21)	34(3)	66(5)	84(6)	-27(5)	10(3)	6(3)
C(35)	32(3)	39(3)	34(3)	9(3)	5(2)	-4(2)
C(15)	31(3)	46(4)	48(4)	9(3)	-13(3)	1(3)
C(34)	39(3)	40(3)	27(3)	11(2)	1(2)	-4(2)
C(45)	38(3)	71(4)	43(3)	3(3)	8(3)	5(4)
C(33)	42(3)	31(3)	39(3)	13(3)	0(3)	-1(2)
C(32)	39(3)	36(3)	42(3)	5(2)	-3(3)	1(2)
C(43)	51(4)	49(4)	64(4)	14(3)	-13(3)	4(3)
C(31)	36(3)	34(3)	37(3)	9(2)	3(2)	-6(2)
C(12)	50(4)	39(4)	64(5)	-2(3)	-17(4)	15(3)
C(13)	45(4)	43(4)	60(4)	22(3)	1(3)	3(3)
C(11)	30(3)	49(4)	48(4)	0(3)	2(3)	13(3)
C(41)	44(4)	53(4)	44(4)	4(3)	-9(3)	-10(3)
C(42)	55(4)	42(4)	62(5)	-4(3)	-1(3)	5(3)
C(25)	35(3)	115(7)	42(4)	-23(4)	21(3)	-20(4)
C(23)	23(3)	83(5)	46(4)	-16(4)	6(3)	-16(3)
C(24)	39(4)	76(5)	56(4)	1(4)	15(3)	-16(3)
C(14)	46(4)	64(4)	30(3)	9(3)	-4(3)	15(3)
C(22)	20(3)	72(5)	67(5)	1(4)	-4(3)	11(3)

Hydrogen coordinates (x 10^4) and isotropic displacement parameters ($Å^2$ x 10^3)

	x	y	z	U(eq)
H(44A)	1168(7)	10118(5)	2884(4)	80
H(44B)	1467(7)	9066(5)	3311(4)	80
H(44C)	-76(7)	9533(5)	3325(4)	80
H(21A)	-2559(7)	10367(7)	6747(5)	80
H(15A)	4157(6)	8573(5)	6921(4)	80
H(45A)	4471(6)	10041(6)	3893(4)	80
H(45B)	4518(6)	9457(6)	4732(4)	80
H(45C)	3651(6)	9004(6)	3994(4)	80
H(43A)	-1109(7)	11712(5)	3958(5)	80
H(43B)	-1588(7)	10570(5)	4061(5)	80
H(43C)	-1696(7)	11327(5)	4804(5)	80
H(12A)	1942(7)	6105(5)	6028(5)	80
H(13A)	904(7)	6564(5)	7391(4)	80
H(11A)	3971(6)	7361(5)	5704(4)	80
H(41A)	4286(7)	11590(5)	5689(4)	80
H(41B)	3267(7)	11185(5)	6379(4)	80
H(41C)	4281(7)	10425(5)	5916(4)	80
H(42A)	768(8)	12715(5)	5670(5)	80
H(42B)	-426(8)	11949(5)	5947(5)	80
H(42C)	1070(8)	11936(5)	6380(5)	80
H(25A)	-1881(7)	9030(7)	7793(5)	80
H(23A)	-3147(6)	7530(6)	5709(4)	80
H(24A)	-2233(7)	7287(7)	7184(5)	80
H(14A)	2251(7)	8070(6)	7953(4)	80
H(22A)	-3345(6)	9458(6)	5456(5)	80

APPENDIX 12

Crystal Structure of $Cp^*Ir(CpCo)_2(\mu_3\text{-}CO)(\mu_3\text{-}O)$

Crystal data and structure refinement

Identification code	irco2oxo
Empirical formula	$C_{21}H_{25}Co_2IrO_2$
Formula weight	619.47
Temperature	293(2) K
Wavelength	0.71073 Å
Crystal system	Orthorhombic
Space group	P2(1)2(1)2(1)
Unit cell dimensions	a = 9.371(2) Å α = 90° b = 13.119(2) Å β = 90° c = 16.239(3) Å γ = 90°
Volume, Z	1996.4(6) A^3, 4
Density (calculated)	2.061 Mg/m^3
Absorption coefficient	8.303 mm^{-1}
F(000)	1192
Theta range for data collection	2.51 to 22.55°
Limiting indices	0<=h<=10, 0<=k<=14, 0<=l<=17
Reflections collected	1578
Independent reflections	1527 [R(int) = 0.0107]
Refinement method	Full-matrix least-squares on F^2
Data / restraints / parameters	1524 / 0 / 236
Goodness-of-fit on F^2	1.087
Final R indices [I>2sigma(I)]	R1 = 0.0252, wR2 = 0.0618
R indices (all data)	R1 = 0.0281, wR2 = 0.0699
Absolute structure parameter	0.003(14)
Largest diff. peak and hole	0.628 and -0.867 $e.A^{-3}$

Atomic coordinates (x 10^4) and equivalent isotropic displacement parameters ($Å^2$ x 10^3)
U(eq) is defined as one third of the trace of the orthogonalized Uij tensor.

	x	y	z	U(eq)
Ir(1)	987(1)	9631(1)	9595(1)	23(1)
Co(1)	-909(2)	8771(1)	8759(1)	26(1)
Co(2)	1469(2)	8155(1)	8652(1)	24(1)
O(1)	268(7)	8199(5)	9540(4)	25(2)
O(2)	957(9)	10075(6)	7781(5)	39(2)
C(1)	775(12)	9521(9)	8339(6)	27(3)
C(10)	-3039(13)	9090(12)	9031(8)	46(4)
C(11)	-2599(13)	9585(16)	8320(11)	63(5)
C(12)	-2168(14)	8883(15)	7732(9)	62(4)
C(13)	-2388(14)	7925(12)	8073(8)	48(4)
C(14)	-2915(13)	8063(10)	8890(8)	41(3)
C(20)	2407(14)	7751(11)	7549(8)	48(4)
C(21)	1653(14)	6910(11)	7853(9)	48(4)
C(22)	2247(15)	6652(10)	8642(9)	50(4)
C(23)	3400(13)	7377(10)	8801(8)	44(3)
C(24)	3476(12)	8012(10)	8133(8)	38(3)
C(30)	2559(11)	10826(9)	9758(7)	33(3)
C(31)	2655(12)	10157(9)	10469(7)	31(3)
C(32)	1315(13)	10203(9)	10898(7)	33(3)
C(33)	374(14)	10871(9)	10430(8)	41(3)
C(34)	1149(14)	11287(8)	9750(8)	35(3)
C(35)	3713(14)	11021(11)	9128(8)	47(3)
C(36)	3947(13)	9607(11)	10741(8)	50(3)
C(37)	941(14)	9685(10)	11672(7)	44(3)
C(38)	-1145(13)	11129(10)	10711(8)	47(3)
C(39)	602(16)	12027(10)	9134(8)	50(4)

Bond lengths [Å]

Ir(1)-O(1)	1.997(7)	Co(2)-C(21)	2.093(12)
Ir(1)-C(1)	2.054(11)	Co(2)-C(22)	2.102(13)
Ir(1)-C(30)	2.168(11)	O(2)-C(1)	1.174(13)
Ir(1)-C(33)	2.195(11)	C(10)-C(14)	1.37(2)
Ir(1)-C(34)	2.193(11)	C(10)-C(11)	1.39(2)
Ir(1)-C(31)	2.221(10)	C(11)-C(12)	1.39(2)
Ir(1)-C(32)	2.267(11)	C(12)-C(13)	1.39(2)
Ir(1)-Co(1)	2.505(2)	C(13)-C(14)	1.43(2)
Ir(1)-Co(2)	2.510(2)	C(20)-C(21)	1.40(2)
Co(1)-O(1)	1.841(7)	C(20)-C(24)	1.42(2)
Co(1)-C(1)	1.981(12)	C(21)-C(22)	1.44(2)
Co(1)-C(11)	2.039(13)	C(22)-C(23)	1.46(2)
Co(1)-C(12)	2.048(13)	C(23)-C(24)	1.37(2)
Co(1)-C(10)	2.087(12)	C(30)-C(31)	1.45(2)
Co(1)-C(13)	2.095(13)	C(30)-C(34)	1.45(2)
Co(1)-C(14)	2.108(12)	C(30)-C(35)	1.51(2)
Co(1)-Co(2)	2.377(2)	C(31)-C(32)	1.44(2)
Co(2)-O(1)	1.830(7)	C(31)-C(36)	1.48(2)
Co(2)-C(1)	1.973(11)	C(32)-C(37)	1.47(2)
Co(2)-C(24)	2.070(11)	C(32)-C(33)	1.46(2)
Co(2)-C(20)	2.065(12)	C(33)-C(34)	1.43(2)
Co(2)-C(23)	2.092(11)	C(33)-C(38)	1.53(2)
		C(34)-C(39)	1.49(2)

Bond Angles [°]

O(1)-Ir(1)-C(1)	81.8(4)	O(1)-Co(1)-Ir(1)	52.0(2)
O(1)-Ir(1)-C(30)	156.2(4)	C(1)-Co(1)-Ir(1)	52.9(3)
C(1)-Ir(1)-C(30)	103.7(4)	C(11)-Co(1)-Ir(1)	120.3(6)
O(1)-Ir(1)-C(33)	129.5(4)	C(12)-Co(1)-Ir(1)	144.9(5)
C(1)-Ir(1)-C(33)	129.8(5)	C(10)-Co(1)-Ir(1)	118.2(4)
C(30)-Ir(1)-C(33)	64.3(5)	C(13)-Co(1)-Ir(1)	174.6(4)
O(1)-Ir(1)-C(34)	163.8(4)	C(14)-Co(1)-Ir(1)	140.9(4)
C(1)-Ir(1)-C(34)	100.9(5)	Co(2)-Co(1)-Ir(1)	61.81(5)
C(30)-Ir(1)-C(34)	38.9(5)	O(1)-Co(2)-C(1)	88.4(4)
C(33)-Ir(1)-C(34)	38.1(5)	O(1)-Co(2)-C(24)	152.0(4)
O(1)-Ir(1)-C(31)	123.9(4)	C(1)-Co(2)-C(24)	106.1(5)
C(1)-Ir(1)-C(31)	136.4(4)	O(1)-Co(2)-C(20)	162.5(5)
C(30)-Ir(1)-C(31)	38.6(4)	C(1)-Co(2)-C(20)	98.6(5)
C(33)-Ir(1)-C(31)	63.8(4)	C(24)-Co(2)-C(20)	40.2(5)
C(34)-Ir(1)-C(31)	64.5(5)	O(1)-Co(2)-C(23)	117.1(4)
O(1)-Ir(1)-C(32)	113.5(4)	C(1)-Co(2)-C(23)	139.3(5)
C(1)-Ir(1)-C(32)	164.4(4)	C(24)-Co(2)-C(23)	38.4(5)
C(30)-Ir(1)-C(32)	63.5(4)	C(20)-Co(2)-C(23)	66.8(5)
C(33)-Ir(1)-C(32)	38.1(5)	O(1)-Co(2)-C(21)	124.3(5)
C(34)-Ir(1)-C(32)	63.6(4)	C(1)-Co(2)-C(21)	125.2(6)
C(31)-Ir(1)-C(32)	37.4(4)	C(24)-Co(2)-C(21)	66.5(5)
O(1)-Ir(1)-Co(1)	46.6(2)	C(20)-Co(2)-C(21)	39.3(6)
C(1)-Ir(1)-Co(1)	50.3(3)	C(23)-Co(2)-C(21)	67.7(5)
C(30)-Ir(1)-Co(1)	150.9(3)	O(1)-Co(2)-C(22)	104.4(4)
C(33)-Ir(1)-Co(1)	118.9(3)	C(1)-Co(2)-C(22)	164.6(5)
C(34)-Ir(1)-Co(1)	123.9(3)	C(24)-Co(2)-C(22)	66.2(5)
C(31)-Ir(1)-Co(1)	170.3(3)	C(20)-Co(2)-C(22)	66.7(5)
C(32)-Ir(1)-Co(1)	138.7(3)	C(23)-Co(2)-C(22)	40.8(5)
O(1)-Ir(1)-Co(2)	46.2(2)	C(21)-Co(2)-C(22)	40.1(5)
C(1)-Ir(1)-Co(2)	50.0(3)	O(1)-Co(2)-Co(1)	49.9(2)
C(30)-Ir(1)-Co(2)	120.7(3)	C(1)-Co(2)-Co(1)	53.2(3)
C(33)-Ir(1)-Co(2)	175.0(4)	C(24)-Co(2)-Co(1)	155.9(4)
C(34)-Ir(1)-Co(2)	145.3(3)	C(20)-Co(2)-Co(1)	123.4(4)
C(31)-Ir(1)-Co(2)	120.2(3)	C(23)-Co(2)-Co(1)	165.6(4)
C(32)-Ir(1)-Co(2)	143.2(3)	C(21)-Co(2)-Co(1)	112.8(4)
Co(1)-Ir(1)-Co(2)	56.58(5)	C(22)-Co(2)-Co(1)	130.2(4)
O(1)-Co(1)-C(1)	87.8(4)	O(1)-Co(2)-Ir(1)	52.0(2)
O(1)-Co(1)-C(11)	156.9(6)	C(1)-Co(2)-Ir(1)	52.9(3)
C(1)-Co(1)-C(11)	103.8(5)	C(24)-Co(2)-Ir(1)	118.8(4)
O(1)-Co(1)-C(12)	159.3(6)	C(20)-Co(2)-Ir(1)	143.5(4)
C(1)-Co(1)-C(12)	98.3(5)	C(23)-Co(2)-Ir(1)	117.5(4)
C(11)-Co(1)-C(12)	39.6(7)	C(21)-Co(2)-Ir(1)	174.4(4)
O(1)-Co(1)-C(10)	120.6(4)	C(22)-Co(2)-Ir(1)	142.3(4)
C(1)-Co(1)-C(10)	137.3(5)	Co(1)-Co(2)-Ir(1)	61.61(5)
C(11)-Co(1)-C(10)	39.3(6)	Co(2)-O(1)-Co(1)	80.7(3)
C(12)-Co(1)-C(10)	66.9(6)	Co(2)-O(1)-Ir(1)	81.8(3)
O(1)-Co(1)-C(13)	123.1(5)	Co(1)-O(1)-Ir(1)	81.4(3)
C(1)-Co(1)-C(13)	127.4(5)	O(2)-C(1)-Co(2)	135.5(9)
C(11)-Co(1)-C(13)	65.0(7)	O(2)-C(1)-Co(1)	133.5(10)
C(12)-Co(1)-C(13)	39.2(6)	Co(2)-C(1)-Co(1)	73.9(4)
C(10)-Co(1)-C(13)	65.6(6)	O(2)-C(1)-Ir(1)	135.2(9)
O(1)-Co(1)-C(14)	106.6(4)	Co(2)-C(1)-Ir(1)	77.1(4)
C(1)-Co(1)-C(14)	164.7(5)	Co(1)-C(1)-Ir(1)	76.7(4)
C(11)-Co(1)-C(14)	64.7(6)	C(14)-C(10)-C(11)	107.1(14)
C(12)-Co(1)-C(14)	66.4(6)	C(14)-C(10)-Co(1)	71.7(7)
C(10)-Co(1)-C(14)	38.2(5)	C(11)-C(10)-Co(1)	68.5(7)
C(13)-Co(1)-C(14)	39.7(5)	C(12)-C(11)-C(10)	110(2)
O(1)-Co(1)-Co(2)	49.5(2)	C(12)-C(11)-Co(1)	70.5(8)
C(1)-Co(1)-Co(2)	52.9(3)	C(10)-C(11)-Co(1)	72.2(8)
C(11)-Co(1)-Co(2)	151.7(5)	C(11)-C(12)-C(13)	106.5(14)
C(12)-Co(1)-Co(2)	120.3(5)	C(11)-C(12)-Co(1)	69.8(8)
C(10)-Co(1)-Co(2)	168.6(4)	C(13)-C(12)-Co(1)	72.3(8)
C(13)-Co(1)-Co(2)	113.6(4)	C(12)-C(13)-C(14)	107.9(13)
C(14)-Co(1)-Co(2)	133.9(4)	C(12)-C(13)-Co(1)	68.6(8)

C(14)-C(13)-Co(1)	70.6(7)
C(10)-C(14)-C(13)	108.1(12)
C(10)-C(14)-Co(1)	70.1(7)
C(13)-C(14)-Co(1)	69.7(7)
C(21)-C(20)-C(24)	108.1(12)
C(21)-C(20)-Co(2)	71.4(7)
C(24)-C(20)-Co(2)	70.1(7)
C(20)-C(21)-C(22)	107.7(12)
C(20)-C(21)-Co(2)	69.3(7)
C(22)-C(21)-Co(2)	70.3(7)
C(21)-C(22)-C(23)	106.9(12)
C(21)-C(22)-Co(2)	69.6(7)
C(23)-C(22)-Co(2)	69.2(7)
C(24)-C(23)-C(22)	107.1(11)
C(24)-C(23)-Co(2)	69.9(7)
C(22)-C(23)-Co(2)	70.0(7)
C(23)-C(24)-C(20)	110.2(12)
C(23)-C(24)-Co(2)	71.7(7)
C(20)-C(24)-Co(2)	69.7(7)
C(31)-C(30)-C(34)	108.4(10)
C(31)-C(30)-C(35)	126.6(10)
C(34)-C(30)-C(35)	125.0(11)
C(31)-C(30)-Ir(1)	72.7(6)
C(34)-C(30)-Ir(1)	71.5(6)
C(35)-C(30)-Ir(1)	121.8(8)
C(32)-C(31)-C(30)	107.8(10)
C(32)-C(31)-C(36)	126.2(11)
C(30)-C(31)-C(36)	125.7(10)
C(32)-C(31)-Ir(1)	73.0(6)
C(30)-C(31)-Ir(1)	68.7(6)
C(36)-C(31)-Ir(1)	128.1(8)
C(31)-C(32)-C(37)	127.1(12)
C(31)-C(32)-C(33)	107.5(11)
C(37)-C(32)-C(33)	125.4(11)
C(31)-C(32)-Ir(1)	69.6(5)
C(37)-C(32)-Ir(1)	127.8(8)
C(33)-C(32)-Ir(1)	68.3(6)
C(34)-C(33)-C(32)	109.0(11)
C(34)-C(33)-C(38)	128.1(12)
C(32)-C(33)-C(38)	122.7(12)
C(34)-C(33)-Ir(1)	70.9(6)
C(32)-C(33)-Ir(1)	73.6(6)
C(38)-C(33)-Ir(1)	126.2(8)
C(33)-C(34)-C(30)	107.2(10)
C(33)-C(34)-C(39)	126.5(12)
C(30)-C(34)-C(39)	126.3(12)
C(33)-C(34)-Ir(1)	71.0(6)
C(30)-C(34)-Ir(1)	69.6(6)
C(39)-C(34)-Ir(1)	123.1(9)

Anisotropic displacement parameters ($Å^2$ x 10^3). The anisotropic displacement factor exponent takes the form: $-2\pi^2$ [$h^2 a^{*2}$ U11 + ... + 2 h k a* b* U12]

	U11	U22	U33	U23	U13	U12
Ir(1)	23(1)	26(1)	21(1)	-2(1)	0(1)	1(1)
Co(1)	20(1)	34(1)	23(1)	2(1)	-2(1)	-2(1)
Co(2)	23(1)	29(1)	21(1)	-2(1)	0(1)	1(1)
O(1)	29(4)	27(4)	19(3)	5(4)	0(4)	1(3)
O(2)	38(5)	45(5)	33(4)	5(4)	10(4)	-1(4)
C(1)	40(7)	23(6)	19(5)	5(5)	3(5)	0(6)
C(10)	19(7)	73(10)	45(8)	4(7)	6(6)	8(7)
C(11)	21(7)	79(12)	90(14)	36(13)	-17(8)	13(8)
C(12)	27(7)	118(14)	42(8)	14(10)	-16(7)	-4(9)
C(13)	38(8)	64(9)	44(8)	-3(7)	-14(7)	-22(7)
C(14)	25(6)	45(7)	54(8)	23(7)	-15(6)	-13(6)
C(20)	40(8)	69(10)	35(7)	-3(7)	12(6)	16(8)
C(21)	34(7)	56(8)	55(10)	-41(8)	3(7)	5(7)
C(22)	60(9)	32(7)	57(9)	-3(7)	26(8)	5(7)
C(23)	33(6)	68(9)	30(7)	-2(7)	-8(6)	24(7)
C(24)	21(6)	41(7)	53(8)	-6(7)	5(6)	8(6)
C(30)	28(6)	36(6)	35(7)	-10(6)	-1(5)	-7(5)
C(31)	33(6)	40(7)	21(5)	-16(6)	-7(5)	-1(5)
C(32)	40(7)	35(7)	24(6)	-12(6)	9(5)	-2(6)
C(33)	54(8)	37(6)	33(6)	-19(7)	-7(7)	0(6)
C(34)	35(7)	26(6)	45(8)	1(5)	-4(7)	-1(6)
C(35)	39(8)	61(8)	41(7)	4(7)	10(6)	-2(7)
C(36)	36(7)	69(9)	46(7)	-2(7)	-10(6)	2(9)
C(37)	51(7)	45(7)	36(7)	-8(6)	-11(7)	-6(9)
C(38)	36(7)	47(7)	56(8)	-2(7)	10(7)	15(7)
C(39)	65(10)	36(8)	49(7)	3(7)	-2(7)	15(8)

Hydrogen coordinates (x 10^4) and isotropic displacement parameters ($Å^2$ x 10^3)

	x	y	z	U(eq)
H(10A)	-3356(13)	9429(12)	9522(8)	80
H(11A)	-2625(13)	10305(16)	8213(11)	80
H(12A)	-1770(14)	9030(15)	7201(9)	80
H(13A)	-2203(14)	7282(12)	7813(8)	80
H(14A)	-3148(13)	7528(10)	9270(8)	80
H(20A)	2206(14)	8094(11)	7040(8)	80
H(21A)	882(14)	6570(11)	7577(9)	80
H(22A)	1944(15)	6104(10)	8993(9)	80
H(23A)	4001(13)	7393(10)	9280(8)	80
H(24A)	4149(12)	8558(10)	8067(8)	80
H(35A)	4534(14)	10616(11)	9262(8)	80
H(35B)	3375(14)	10839(11)	8590(8)	80
H(35C)	3968(14)	11730(11)	9135(8)	80
H(36A)	3758(13)	9234(11)	11237(8)	80
H(36B)	4234(13)	9143(11)	10315(8)	80
H(36C)	4697(13)	10091(11)	10839(8)	80
H(37A)	1730(14)	9275(10)	11853(7)	80
H(37B)	730(14)	10190(10)	12083(7)	80
H(37C)	121(14)	9259(10)	11590(7)	80
H(38A)	-1581(13)	11587(10)	10325(8)	80
H(38B)	-1703(13)	10517(10)	10748(8)	80
H(38C)	-1097(13)	11447(10)	11242(8)	80
H(39A)	-351(16)	12222(10)	9283(8)	80
H(39B)	1199(16)	12621(10)	9115(8)	80
H(39C)	591(16)	11707(10)	8602(8)	80

VITA

Frank Holger Försterling was born in Marburg, Hessen, Germany in 1967. He graduated from the Martin Luther Gymnasium with the Abitur, the highest German high school diploma. In October 1986 he entered the chemistry program at the Philipps Universität Marburg and obtained his prediploma in the Summer of 1988. He continued his studies at the Philipps Universität at the graduate level and passed the final examinations in December 1990. He conducted the research for his thesis in the research group of Dr. Stefan Berger on rapid injection NMR studies on the Wittig reaction and obtained the "Diplomchemiker" degree in chemistry from the Philipps Universität Marburg in October 1991. It was during this time that he got introduced into the exiting field of NMR spectroscopy.

In Spring 1992 he was accepted at the University of Tennessee, to continue his studies towards a doctoral degree in chemistry. He joined the research group of Dr. Craig Barnes an conducted research in organometallic cluster chemistry combined with NMR spectroscopy. From May 1992 until June 1996 he also was the student operator in charge of the departmental AMX400 NMR spectrometer. On June 21, 1996 he successfully defended his dissertation "Synthesis and Fluxional Behavior of Mixed Metal Trinuclear Cluster Complexes of the Cobalt Group Containing Carbene, Carbyne and Alkyne Ligands" and received the Doctor of Philosophy degree in chemistry. Subsequently he accepted a postdoctoral position with Prof. Christian Griesinger at the Wolfgang von Goethe

Universität in Frankfurt, Germany where he will pursue NMR spectroscopic studies on biomolecular systems.